

University of Southampton Research Repository

Copyright © and Moral Rights for this thesis and, where applicable, any accompanying data are retained by the author and/or other copyright owners. A copy can be downloaded for personal non-commercial research or study, without prior permission or charge. This thesis and the accompanying data cannot be reproduced or quoted extensively from without first obtaining permission in writing from the copyright holder/s. The content of the thesis and accompanying research data (where applicable) must not be changed in any way or sold commercially in any format or medium without the formal permission of the copyright holder/s.

When referring to this thesis and any accompanying data, full bibliographic details must be given, e.g.

Thesis: Author (Year of Submission) "Full thesis title", University of Southampton, name of the University Faculty or School or Department, PhD Thesis, pagination.

Data: Author (Year) Title. URI [dataset]

University of Southampton

Faculty of Engineering and Physical Sciences

School of Chemistry

**Synthesis of Functional Polyaromatic Heterocycles and their Material and Medicinal
Applications**

by

Ashley David Shiels

ORCID ID 0009-0006-5101-077X

Thesis for the degree of Doctor of Philosophy

April 2025

University of Southampton

Abstract

Faculty of Engineering and Physical Sciences

School of Chemistry

Thesis for the degree of Doctor of Philosophy

Synthesis of Functional Polyaromatic Heterocycles and their Material and Medicinal Applications

by

Ashley David Shiels

Polyaromatic heterocycles can be found in almost all areas of chemistry being a highly versatile class of compounds. From materials to therapeutic agents, the extensive applications make them the targets of many research pursuits. Carbazole derived compounds have seen applications in OLEDs and LECs in the form of highly novel TADF emitters, then also appear in the anti-cancer and anti-fungal research centred around the indolocarbazole alkaloids.

Chapters 1 and 2 of this thesis describe the synthetic approaches utilised to access novel ionic salts combining fluorescent heterocyclic cations with polyoxometalate anions. A series of 7 novel polyoxometalate containing salts are isolated and their physical and optical properties examined. In this work we demonstrate the ability of polyoxometalate anions to enhance the solid-state photoluminescence of associated emissive heterocyclic cations. Furthermore, we have investigated the potential of these salts in the active layer of LECs, demonstrating the limited hole transporting ability of the materials.

Chapter 3 of this research endeavour displays the synthetic advances towards carbazole-based TADF emitters. The ability to control sequential S_NAr reactions on polyfluorinated aromatic systems, hexafluorobenzene and tetrafluoroisophthalonitrile, is explored. The capability to limit the substitution of carbazole to 2 positions with hexafluorobenzene and 3 positions with tetrafluoroisophthalonitrile was determined and further substitution with derivatised carbazole compounds scrutinised. The inability to substitute these final positions efficiently leads to a new approach targeting a difluoro-diiodo aromatic system that provides orthogonal opportunities for functionalisation. This system was successfully accessed in 2 steps with a 22% yield.

The final part of this thesis, Chapters 4 and 5, outline the refinement of the Brown group's approach to a reduced form of the staurosporine aglycone which presents as an indole-indoline system then investigates its regioselective functionalisation. Successful selective glycosylation of the indoline moiety allowed for the total synthesis of K252d as well as its β -anomer in a 4% yield over 6 steps. Furthermore, glycosylation with D-glucose and D-galactose yielded two previously unknown glycosidic analogues. The nature of the glycosylation step is studied, and the limitations of this approach made clear in the form of an equilibrium that limits the conversion to the initial glycosylated intermediate to approximately 40%.

Table of Contents

Table of Contents.....	3
Table of Tables.....	7
Table of Schemes	9
Table of Figures	11
Research Thesis: Declaration of Authorship.....	15
Acknowledgements	17
Definitions and Abbreviations	19
Chapter 1 Introduction	25
1.1 Smart Materials and E-textiles	25
1.2 Luminescent Materials	26
1.3 Luminescence.....	26
1.3.1 Fluorescence and Phosphorescence	26
1.3.2 Metal-organic Phosphorescence	28
1.3.3 Delayed Fluorescence.....	28
1.3.4 Aggregation Induced Emission.....	29
1.4 Organic Light-emitting Diodes (OLEDs)	30
1.4.1 OLED Device Structure.....	30
1.4.2 Brief History of OLED development	31
1.5 Light-emitting electrochemical cells (LECs).....	31
1.5.1 LEC Device Structure	31
1.5.2 Types of LEC Active Materials	32
1.6 The Challenges of Luminescence and Degradation mechanisms	33
1.6.1 Wide Band-gap Instability.....	34
1.6.2 Concentration Quenching	35
1.7 Active Layer and Molecular Design	35
1.7.1 Doped and Non-doped Layers	36

1.7.2	Charge Carrier Ability	37
1.7.3	Wavelength Tuning.....	37
1.8	Small Molecules and Their Use in LECs.....	38
1.8.1	Non-ionic Small Molecule LECs.....	38
1.8.2	Ionic Small Molecule LECs	46
1.8.3	Host-Guest Small Molecule LECs	57
1.9	Conclusions and Future Perspectives	60
Chapter 2	Polyoxometalate Anions in LECs	61
2.1	Background.....	61
2.1.1	The Effect of Polyoxometalate Anions on Solid-State Photoluminescence .	61
2.1.2	LEC Fabrication and Application to Textiles.....	61
2.1.3	Aims.....	62
2.2	Phenanthroimidazole-Polyoxometalate Emitters	63
2.2.1	Synthesis.....	63
2.2.2	Optical Properties	66
2.2.3	Electrochemical Properties	68
2.2.4	Solid-state Photoluminescent Properties	70
2.2.5	LEC Fabrication and Testing	74
2.2.6	Doped Layer Formulation	75
2.3	BODIPY-Polyoxometalate Emitters.....	77
2.3.1	Synthesis.....	77
2.3.2	Optical Properties	79
2.3.3	Photoluminescent Properties	80
2.3.4	LEC Fabrication and Testing	82
2.4	Conclusions and Future Perspectives	84
Chapter 3	Carbazole-Based TADF Emitters.....	85
3.1	Background.....	85
3.1.1	4CzIPN	85

3.1.2	S_NAr Reactions on Polyfluorinated Aromatics	86
3.1.3	Aims.....	88
3.2	S_NAr of Hexafluorobenzene Towards Ionic Carbazole-Based Emitters	88
3.3	S_NAr of Tetrafluoroisophthalonitrile Towards Ionic Carbazole-Based Emitters	91
3.4	A New Approach	93
3.5	Conclusions and Future Perspectives	95
 Chapter 4 Introduction to the Indolocarbazole Alkaloids and their Synthesis		
	97
4.1	Indolocarbazole Alkaloids	97
4.1.1	Discovery and Interest.....	97
4.1.2	PKC Inhibition	98
4.2	Indolocarbazole Alkaloids and Their Anti-cancer and Antifungal Properties	100
4.2.1	Anti-cancer Activity	100
4.2.2	Antifungal Activity	101
4.3	Synthesis of the Staurosporine Aglycone	102
4.4	Synthesis of Staurosporine	107
4.5	Glycosylation of Indolocarbazole Alkaloids	112
4.6	Conclusions and Future Perspectives	115
 Chapter 5 Regioselective Functionalisation of the Staurosporine Aglycone		
	117
5.1	Background.....	117
5.1.1	Indoline Glycosylation.....	117
5.1.2	Previous Work in the Brown Group	118
5.1.3	Aims and Conclusions	1200
5.2	Consolidation of the Brown Group's Approach to a Useful Indole-Indoline System.....	121

5.3	Synthesis of K252d and Related Staurosporine Aglycone Glycosidic Analogues	125
5.4	Conclusions and Future Perspectives	129
Chapter 6	Experimental.....	131
6.1	General Procedures.....	131
6.2	Procedures and Characterisation Data	133

Table of Tables

Table 1: Doped active layer formulations.	76
Table 2: Conditions for attempted SNAr reactions of tetra-carbazolyl 3.04	89
Table 3: Conditions tried for diiodination of 3.27	94
Table 4: Glycosylation 2,2'-Indolyindoline 5.01 by Chisolm and co-workers.	117
Table 5: Some of the attempted glycosylation conditions by Chambers.	120
Table 6: Attempted conditions for the deoxygenation of hydroxy lactam 5.14	123
Table 7: Attempted conditions for the deprotonation of TFA salt 5.19	124
Table 8: Conditions for N-glycosylation of indoline 5.16	126

Table of Schemes

Scheme 1: Costa and co-workers' synthesis of imidazo-pyridine based emitter.	44
Scheme 2: Chen H. F. and co-workers' synthesis of terfluorene derivative 1.45	47
Scheme 3: Synthesis of ionic phenanthroimidazole emitter 2.12	64
Scheme 4: Anion exchange reactions.	65
Scheme 5: Synthesis of electron transport material for host-guest active layer formulation.	75
Scheme 6: Synthesis of BODIPY 2.32	78
Scheme 7: Synthesis of BODIPY-triflate emitters (2.34 and 2.38) and BODIPY-polyoxometalate emitters (2.35 and 2.36).....	79
Scheme 8: Adachi and co-workers' synthesis of 4CzIPN.....	86
Scheme 9: SNAr reactions with carbazole and hexafluorobenzene (3.03).....	87
Scheme 10: Selective deprotection of phenol by Jarman and McCague.	88
Scheme 11: SNAr reactions of hexafluorobenzene with carbazole.	89
Scheme 12: Attempted SNAr reactions of tetra-carbazolyl 3.04	89
Scheme 13: Attempted introduction of charge via pendant alkyl chains.	90
Scheme 14: Attempted SNAr of our di-carbazolyl product 3.09	91
Scheme 15: SNAr reactions of tetrafluoroisophthalonitrile (3.02) with carbazole (3.09) and α - carboline (3.20) and the examination of their reactivity.	92
Scheme 16: SNAr reaction of tri-carbazolyl compound 3.21	93
Scheme 17: Synthesis of diiodo-difluoro target 3.29	94
Scheme 18: Attempted SNAr cross-coupling approach.	94
Scheme 19: Unsuccessful SNAr attempts.	95
Scheme 20: Proposed method to access derivatised carbazole-based TADF emitters....	96
Scheme 21: Synthesis of the staurosporine aglycone by Winterfeldt and co-workers' ...	103
Scheme 22: Synthesis of the staurosporine aglycone by Hill and co-workers'.	104

Scheme 23: Synthesis of the staurosporine aglycone by Faul and co-workers'.	105
Scheme 24: Synthesis of the staurosporine aglycone by Pabbaraja and co-workers'. ...	106
Scheme 25: Total synthesis of staurosporine (4.01) by Danishefsky and co-workers. ...	108
Scheme 26: Preparation of the requisite sugar in Danishefsky and co-workers' approach to the synthesis of staurosporine (4.01).	109
Scheme 27: Total synthesis of the staurosporine (4.01) by Wood and co-workers'.	110
Scheme 28: Wood and co-workers' preparation of furanose 4.60	111
Scheme 29: Formal synthesis of the staurosporine (4.01) by Seo and co-workers'.	112
Scheme 30: a) Synthesis of the rebeccamycin (4.07) by Clardy and co-workers', b) Synthesis of the rebeccamycin (4.07) by Danishefsky and co-workers'	113
Scheme 31: Regioselective glycosylation in the total synthesis of K252a (4.02) by Fukuyama and co-workers'	114
Scheme 32: Investigation of the glycosylation of 2,2'-indolylindolines by Chisolm and co-workers'	117
Scheme 33: Faul and co-workers' efforts to prepare indolocarbazole glycoside analogues of acryriaflavin A.	118
Scheme 34: Chambers' route towards successful glycosylation indolylindoline 5.16 and ultimately total synthesis of K252d (5.17).	119
Scheme 35: Preparation of bisindolylmaleimide 4.28	121
Scheme 36: Preparation of TFA salt 5.19	122
Scheme 37: Deoxygenation of hydroxy lactam 5.14	123
Scheme 38: Deprotonation of TFA salt 5.19	124
Scheme 39: N-glycosylation of indoline 5.16 with L-rhamnose.	126
Scheme 40: Glycosylation of indoline 5.16 with different sugars.	128
Scheme 41: Evaluation of DDQ oxidation of indoline glycoside intermediates 5.23-5.25	129
Scheme 42: Cyclisation, glycosylation, and oxidation to regioselectively functionalise the staurosporine aglycone.	130

Table of Figures

Figure 1: Multidisciplinary nature of e-textiles.	25
Figure 2: Jablonski diagram of electron excitation leading to fluorescence and phosphorescent emission.	26
Figure 3: Hole electron recombination in a light emitting diode.	27
Figure 4: Thermally activated delayed fluorescence process represented on a Jablonski diagram.	29
Figure 5: Representation of RIR and RIV behaviour upon aggregation.	30
Figure 6: OLED general structure.	31
Figure 7: General LEC structure. Indium tin oxide anode (blue), active layer (green), aluminium cathode (grey).	31
Figure 8: Illustration of a) electrodynamic model and b) electrochemical doping model for LEC operating mechanism.....	32
Figure 9: Examples of the constituents of a) iTC active layer, b) conjugated polymer active layer, c) small molecule active layer.....	33
Figure 10: Effect of derivatisation on bond dissociation energy.	34
Figure 11: Components of a doped LEC active layer.	36
Figure 12: HOMO LUMO energy levels of PVK, OXD-7 and 4CzIPN.....	37
Figure 13: Derivatisation of 4CzIPN to achieve a range of emission wavelengths.	38
Figure 14: Red emitting perylene derivative utilised by Hill and co-workers’.....	39
Figure 15: Structure of small molecule emitters referred to as red (1.12) and green (1.13).40	
Figure 16: Structure of bilayer LEC device fabricated in the work of Edman and co-workers’.	40
Figure 17: Blue emitting borazine derived fluorophores implemented by Kervyn and co-workers’.	41
Figure 18: Synthesis and derivatisation of phenanthroimidazole based targets by Choe and co-workers’.....	42

Figure 19: Pentacene based emitter 1.21 and pseudo-host dimers used by Costa and co-workers'	42
Figure 20: Neutral porphyrin emitters applied to LEC devices by Costa and co-workers'. 43	
Figure 21: Metal-organic emitters investigated by Costa and co-workers'.	44
Figure 22: Bithiazole emitters tested by Chen D. and co-workers'.	45
Figure 23: Porphyrin BODIPY dyad emitters investigated by Costa and co-workers'.	46
Figure 24: 2,2'-Bifluorene emitter studied by Chen H. F. and co-workers'.	48
Figure 25: Triarylamine HTM and triazine ETM implemented by Chen H. F. and co-workers'.	49
Figure 26: Structures of fluorene-based emitters used in the work of Choe and co-workers'.	50
Figure 27: Novel TADF emitters synthesised and tested by Wong and co-workers'	50
Figure 28: Ionic phenanthroimidazole derived emitters from the work of Choe and co-workers'.	51
Figure 29: Phenothiazine emitter 1.56 and its sulfone analogue 1.57 studied by Choe and co-workers'	52
Figure 30: Diphenylsulfone TADF emitters analysed by Wong and co-workers'.	52
Figure 31: Phenanthroimidazole and pyrene-imidazole derived emitters studied by Choe and co-workers'	53
Figure 32: The next generation of phenothiazine emitters studied by Choe and co-workers'.	54
Figure 33: Tetraphenylethene bearing AIE compounds analysed by Choe and co-workers'. 55	
Figure 34: Triazine donor-acceptor emitters reviewed by Choe and co-workers'.	55
Figure 35: Thenil based emitters examined by Choe and co-workers'	56
Figure 36: Red emitting benzothiadiazole compounds presented by Choe and co-workers'.	57
Figure 37: V-shaped acceptor-donor-acceptor emitters investigated by Choe and co-workers'.	57

Figure 38: Guest ionic iridium complex (1.81) and host ionic NIR dye (1.82) introduced by Su and co-workers'	58
Figure 39: Structures of host materials, poly(9-vinylcarbazole) (1.07), OXD-7 (1.09), and carbazole-based TADF emitter presented in the work of Niu and co-workers'.	59
Figure 40: Carbazole-based TADF emitter and diphenylsulfone TADF sensitizer described in the work of Yao and co-workers.	59
Figure 41: Emissive BODIPY cation and polyoxometalate anion used to enhance solid-state emission performance by Dessapt and co-workers'.	61
Figure 42: Structures of PEDOT:PSS (2.03) and superyellow (2.04) implemented in the work of Beeby and co-workers'.	62
Figure 43: a) Structure of ionic phenanthrimidazole based salts, b) Molar absorbance of 2.14 – 2.16 and 2.19 in DMF, c) Molar absorption of 2.17 – 2.19 in DMF.	66
Figure 44: a) Structure of ionic phenanthrimidazole based salts, b) Relative fluorescence intensities of 2.14 – 2.16 and 2.19 in DMF. c) Relative fluorescence intensities of 2.17 – 2.19 in DMF.	67
Figure 45: Cyclic voltammogram of 2.14	68
Figure 46: Cyclic voltammogram of 2.15	69
Figure 47: Cyclic voltammogram of 2.16	69
Figure 48: Cyclic voltammogram of 2.19	69
Figure 49: a) Structure of ionic phenanthroimidazole based salts, b) solid-state absorption of 2.14 – 2.16 and 2.19	70
Figure 50: Structure of ionic phenanthrimidazole based salts, b) solid-state photoluminescence of 2.19 , c) solid-state photoluminescence of 2.14 – 2.16	71
Figure 51: Potential conformer of compound 2.19 in solid-state.	72
Figure 52: Non-radiative decay pathways that may influence the emissive character of molybdenum containing salts 2.15 and 2.16	73
Figure 53: SEM imaging of uneven doped active layers. Left - entry 1. Right - entry 2.....	77
Figure 54: SEM imaging of a uniform active layer.	77

Figure 55: a) Structure of emissive pyridine containing BODIPY salts, b) absorbance of salts 2.34 - 2.36 and 2.38 in DMSO, c) structure of emissive phosphine containing BODIPY salts, d) emission of salts 2.34 - 2.36 and 2.38 in DMSO. ^a Phosphine-BODIPY cation.	80
Figure 56: a) Structure of emissive pyridine containing BODIPY salts, b) solid-state photoluminescence of salts 2.34 and 2.35 , c) structure of emissive phosphine containing BODIPY salts, d) solid-state photoluminescence of salts 2.36 and 2.38 . ^a Phosphine-BODIPY cation	82
Figure 57: SEM cross-section analysis of active layers. Left – BODIPY-triflate salt 2.34 . Right – BODIPY-hexatungstate 2.35	83
Figure 58: Electroluminescence of BODIPY triflate 2.34	83
Figure 59: Structure of redox active vanadium polyoxometalate cluster.	84
Figure 60: Structures of staurosporine (4.01), K252a (4.02), K252b (4.03), staurosporine aglycone (4.04), holyrine (4.05), rebeccamycin Aglycone (4.06), rebeccamycin (4.07), 7-hydroxy-K252c (4.08), acryiaflavin A (4.09), UCN-01 (4.10) and UCN-02 (4.11).....	98
Figure 61: Structures of IP ₃ (4.12), PIP ₂ (4.13), ATP (4.14), DAG (4.15) and ADP (4.16).....	99
Figure 62: Protein kinase C-mediated signal transduction.	100
Figure 63: Structures of Imatinib/Glivec® (4.16) and Midostaurin/Rydapt® (4.17).	101
Figure 64: Structure of recently published staurosporine derivative (4.18).....	102

Research Thesis: Declaration of Authorship

Print name: Ashley David Shiels

Title of thesis: Synthesis of Functional Polyaromatic Heterocycles and their Material and Medicinal Applications

I declare that this thesis and the work presented in it are my own and has been generated by me as the result of my own original research.

I confirm that:

1. This work was done wholly or mainly while in candidature for a research degree at this University;
2. Where any part of this thesis has previously been submitted for a degree or any other qualification at this University or any other institution, this has been clearly stated;
3. Where I have consulted the published work of others, this is always clearly attributed;
4. Where I have quoted from the work of others, the source is always given. With the exception of such quotations, this thesis is entirely my own work;
5. I have acknowledged all main sources of help;
6. Where the thesis is based on work done by myself jointly with others, I have made clear exactly what was done by others and what I have contributed myself;
7. None of this work has been published before submission

Signature: Date:.....

Acknowledgements

First, I would like to thank my supervisor Professor Richard Brown, and the person he took over from Dr Lynda Brown, for providing me the opportunity to undertake this PhD. Early in my time at Southampton you both gave me support but also the freedom to pursue my own ideas and interests, this gave me the chance to build confidence in my own ability and make this PhD one I could enjoy. You also provided all the input and suggestions I could hope for, helping me learn a lot in my time with you.

A huge thank you to Professor David Harrowven and SmartT Interreg for providing the funding for this research. Also, to our collaborators in ECS, Katie Court, Yi Li, Sasikumar Arumugam and their supervisor Professor Stephen Beeby for their role in this project and for dealing with us chemists, who at times could be quite demanding. I would like to thank Julie, Jon, and Neil for always helping whenever I had issues identifying or characterising my compounds. Additionally, thank you to the store's guys, Mark, and Keith who we all rely on to keep our work going.

A big thank you to the entire Brown group for all the help you have given me throughout these 4 years. Specifically, Nikita for always trying to help whenever she could, even if I was not always equally as useful, and for supporting me and sharing the burden when the jobs piled up as we became more experienced. Jack for always helping me tackle my synthetic challenges and for livening up the lab with your music. And George for being one of the only people I could talk about football with.

Finally, thank you to my family for supporting me through this journey especially my brother for providing his unique insight into my challenges with his inferior inorganic chemistry mind. Also, for providing me with my polyoxometalate materials even if you were really just hoping for your name on a paper.

Definitions and Abbreviations

°C – Degrees Celsius

4CzIPN – 1,2,3,5-Tetrakis(carbazol-9-yl)-4,6-dicyanobenzene

Ac – Acetyl

AcOH – Acetic acid

ADP – Adenosine diphosphate

AIE – Aggregation-induced emission

Aq – Aqueous

atm – Atmosphere

ATP – Adenosine triphosphate

BDE – Bond dissociation energy

Bn – Benzyl

Boc – *tert*-butyloxycarbonyl

BODIPY – Boron-dipyrromethene

BOM – Benzyloxymethyl

br – Broad

Brsm – Based on recovered starting material

Bu – Butyl

Calcd – Calculated

Cbz – Benzyloxycarbonyl

Conc. – Concentrated

CR – Charge recombination

CSA – Camphor sulfonic acid

CT – Charge transfer

d - Doublet

d.r. – Diastereomeric ratio

DAG – 1,2-Diacylglycerol

DBU – 1,8-Diazabicyclo[5.4.0]undec-7-ene

DCC – *N,N'*-Dicyclohexylcarbodiimide

DDQ – 2,3-Dichloro-5,6-dicyano-1,4-benzoquinone

DEAD – Diethyl azodicarboxylate

DET – Dexter energy transfer

DIBAL-H – Diisobutylaluminium hydride

DMAP – 4-(Dimethylamino)-pyridine

DMF – Dimethylformamide

DMSO – Dimethylsulfoxide

e.e. – Enantiomeric excess

ED – Electrodynamic

EI – Electron ionisation

Equiv. – Equivalents

ESI – Electrospray ionisation

Et – Ethyl

E-textiles – Electronic textiles

FLT3 – FMS-like tyrosine kinase 3

FMS – Feline McDonough Sarcoma

FRET - Förster resonance energy transfer

FT-IR – Fourier-transform infrared

g – Gram

GC – Gas chromatography

h – Hour(s)

HOMO – Highest occupied molecular orbital

HRMS – High-resolution mass spectrometry

IP₃ – Inositol triphosphate

ISC – Inter-system crossing

iTMC – Ionic transition metal complex

ITO – Indium tin oxide

J – Coupling constant

K – Kelvin

LDA – Lithium diisopropylamide

LEC – Light-emitting electrochemical cell

LiTMP – Lithium tetramethylpiperidide

LRMS – Low-resolution mass spectrometry

LUMO – Lowest unoccupied molecular orbital

m – Multiplet

mCPBA – *meta*-Chloroperoxybenzoic acid

Me – Methyl

mg – Milligram

min – Minute(s)

mmol – Millimole(s)

MS – Mass spectrometry

Ms – Mesyl

MW – Molecular weight

NBS – *N*-Bromosuccinimide

***n*-BuLi** – *n*-Butyllithium

NMR – Nuclear-magnetic resonance

NR – Non-radiative decay

OLED – Organic light-emitting diode

OXD-7 – 1,3-bis[2-(4-tert-butylphenyl)-1,3,4-oxadiazol-5-yl]benzene

p – Para

PEO – Polyethylene oxide

Ph – Phenyl

PIP₂ – Phosphatidylinositol-4,5-bisphosphate

PKC – Protein kinase C

PMMA – Polymethyl methacrylate

ppm – Parts per million

Pr – Propyl

PTSA – para-Toluenesulfonic acid

PVK – Poly(9-vinylcarbazole)

q – Quartet

RCM – Ring-closing metathesis

RIM – Restricted intermolecular motion

RIR – Restricted intermolecular rotation

RISC – Reverse inter-system crossing

RIV – Restricted intermolecular vibration

rt – Room temperature

s – Singlet

S₀ – Ground state

S₁ – Singlet state

sat. – Saturated

SEM – 2-(Trimethylsilyl)ethoxymethyl

SSA – Singlet-singlet annihilation

T – Temperature

t – Tertiary

t – Triplet

T₁ – Triplet state

TADF – Thermally activated delayed fluorescence

TBA – Tetrabutylammonium

TBAF – Tetrabutylammonium fluoride

TBDMS – Tetrabutyltrimethylsilyl

THBA – Tetrahydrodibenzosilole

THF – Tetrahydrofuran

TICT – Twisted intermolecular charge transfer

TLC – Thin-layer chromatography

TMS – Trimethylsilyl

TOF – Time of flight

TPE – Tetraphenylethene

Ts – Tosyl

TTA – Triplet-triplet annihilation

UCN-01 – 7-Hydroxystaurosporine

UV – Ultraviolet

WSCD – 1-Ethyl-3-(3-dimethylaminopropyl)carbodiimide

Δ – Heating to reflux

Chapter 1 Introduction

This thesis explores two independent bodies of work. The first body of work explores the synthesis of ionic fluorescent materials for application to light-emitting electrochemical cells. Chapter 1 will introduce this area giving relevant and contextual background information then Chapters 2 and 3 go on to outline my work in this area. Chapters 4 and 5 move away from this topic with Chapter 4 introducing the relevant and contextual background for my second body of work and Chapter 5 describes this work.

1.1 Smart Materials and E-textiles

Smart materials are defined as materials that can interact with the environment around us or a user. This broad definition encompasses numerous different types of materials with applications to various fields. Electronic textiles (e-textiles) are a type of material that come under this definition of smart materials. E-textiles are textiles that incorporate an electronic component, these can be wearable textiles, but any textile that has an electronic component is part of this field. This is a highly multidisciplinary area due to the numerous applications of these technologies as well as the wide range of skills required to create these textiles.^{1,2} Enforcing this point, a review from Ruckdashel and co-workers examined 300 publications in this field between 2017 and 2022 and found that approximately 25% of publications were achieved by collaboration of researchers in two or more countries.³

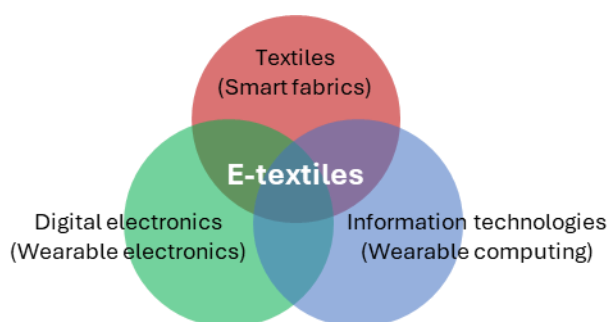


Figure 1: Multidisciplinary nature of e-textiles.

Some of the applications of e-textiles include; temperature sensing and control⁴, power generation and storage^{5, 6}, sensing modules for blood oxygen levels, respiration, electrocardiogram and sweat levels⁷, proximity sensing⁸ and luminescent materials.^{9,10} This vast array of applications means the potential for growth in this market is significant, the growth of the e-wearables market between 2014 and 2020 has been explosive as the abundant ways that E-textiles can enhance a person's life are exploited.¹¹ The e-wearables market covers all

electronically wearable products, including e-textiles, the e-textile market itself is expected to grow from approximately €100 million to over €2 billion in the next decade.¹²

1.2 Luminescent Materials

As has been mentioned, one of the applications of e-textiles is luminescent materials. To develop such materials there is a need for development of molecules that emit light upon electrical stimulation as well as appropriate devices that utilise such molecules and are suitable for integration into textiles. However, to do this a comprehensive understanding of the process of luminescence, the factors that hinder luminescence and the appropriate devices is a necessity, as well as this it is important to address how problems in a device's performance can be addressed through modification to emissive molecule or layer.

1.3 Luminescence

1.3.1 Fluorescence and Phosphorescence

For a molecule to be emissive it must first be electronically excited in some way. One method to achieve this is irradiation with light to give the molecule enough energy for an electron to transition from the ground state (S_0) to the first excited state (S_1) or a higher energy excited state (Figure 2). An electron from the HOMO is excited to the LUMO retaining its spin creating a singlet exciton. When excitation energy is converted to motion energy of nucleus oscillation, the molecule quickly relaxes to the state of lowest oscillation in the excited state. This means that excited states above S_1 quickly decay non-radiatively to S_1 . The singlet excited state is generally short-lived (a few nanoseconds) before returning to the ground state through fluorescent emission or a non-radiative decay process (Figure 2, red box).^{13, 14}

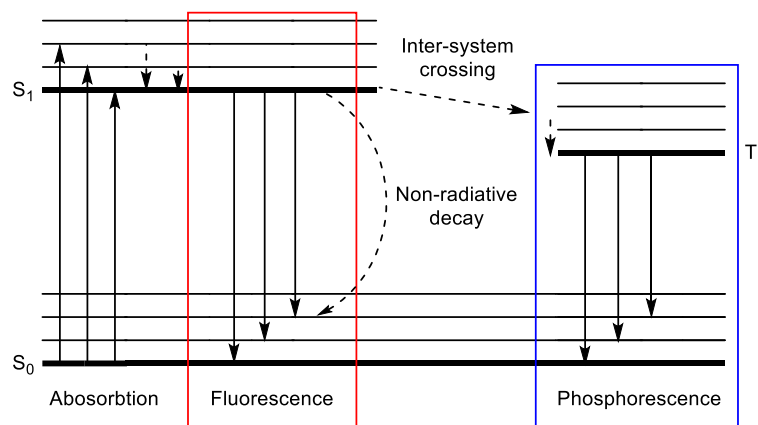


Figure 2: Jablonski diagram of electron excitation leading to fluorescence and phosphorescent emission.

Another method of excitation is the combination of negatively charged electrons and positively charged holes to form an excited state and this is how electro-luminescence is achieved (Figure 3).¹⁵ A semiconductor material capable of losing an electron from its HOMO, creating a positively charged hole, and capable of accepting an electron into its LUMO is employed. Electrons and holes move away from areas of high concentration, eventually meet, and can combine to produce an excited state.

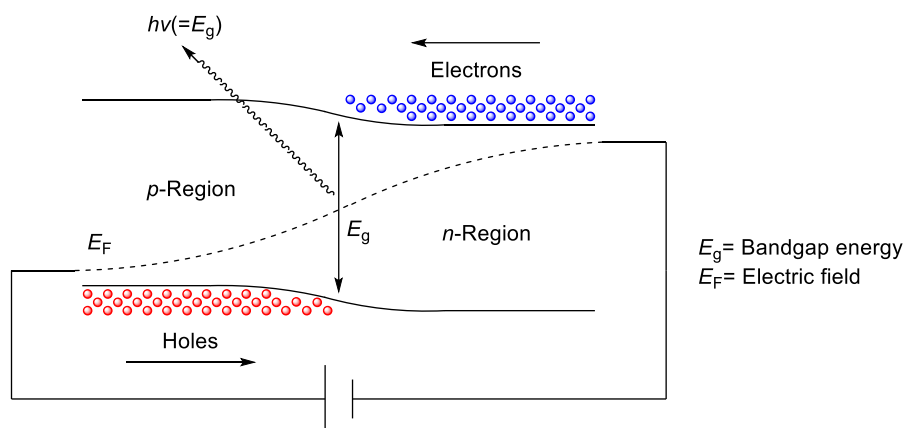


Figure 3: Hole electron recombination in a light emitting diode.

Phosphorescence occurs upon emissive relaxation of the triplet state to the ground state, $T_1 \rightarrow S_0$ (Figure 2, blue box). This process is incredibly low probability and generally does not occur at ambient temperatures in typical organic molecules excited by UV light. This is because an inter-system crossing (ISC) required between singlet and triplet state to form a triplet exciton, the rate of which is generally slow (0.1 to 1 μ s)¹³ due to the spin-forbidden nature of the process. Even when triplet excitons form, their long-lived nature tends to result in non-radiative decay and rarely leads to phosphorescence such that standard luminescent molecules are often treated as being incapable of phosphorescence. However, phosphorescence can occur when thermal non-radiative decay pathways (such as molecular vibration) are reduced at very low temperatures (cryogenic temperatures). In electro-luminescence negatively charged electrons and positively charged holes combine to form excitons thus the singlet or triplet nature of an exciton is dictated by spin statistics. There are four ways a hole and an electron can recombine defined by equation 1 where s_1 and s_2 are the spins associated to the electron and hole and m_1 and m_2 are their projections onto the z-axis.

$$1. |s, m\rangle = \sum_{m_1+m_2=m} C_{m_1 m_2 m}^{s_1 s_2 s} |s_1, m_1\rangle |s_2, m_2\rangle$$

The four combinations of spin and z-axis projection give equations 2 to 5.

$$2. \left| \frac{1}{2}, +\frac{1}{2} \right\rangle \otimes \left| \frac{1}{2}, +\frac{1}{2} \right\rangle \text{ by } (\uparrow\uparrow)$$

$$3. \left| \frac{1}{2}, +\frac{1}{2} \right\rangle \otimes \left| \frac{1}{2}, -\frac{1}{2} \right\rangle \text{ by } (\uparrow\downarrow)$$

$$4. \left| \frac{1}{2}, -\frac{1}{2} \right\rangle \otimes \left| \frac{1}{2}, +\frac{1}{2} \right\rangle \text{ by } (\uparrow\uparrow)$$

$$5. \left| \frac{1}{2}, -\frac{1}{2} \right\rangle \otimes \left| \frac{1}{2}, -\frac{1}{2} \right\rangle \text{ by } (\downarrow\downarrow)$$

These equations return values for the total spin of a state. There are three states with a total spin angular momentum of 1 and one with a total spin angular momentum of 0.^{16, 17}

$$\left. \begin{array}{l} |1, 1\rangle = \uparrow\uparrow \\ |1, 0\rangle = \frac{1}{\sqrt{2}}(\uparrow\downarrow + \downarrow\uparrow) \\ |1, -1\rangle = \downarrow\downarrow \end{array} \right\} s = 1 \text{ (triplet)}$$

And,

$$|0, 0\rangle = \frac{1}{\sqrt{2}}(\uparrow\downarrow - \downarrow\uparrow) \quad s = 0 \text{ (singlet)}$$

This means that 75% of excitons formed are triplet and 25% are singlet.¹⁸ The result is that a standard fluorescent molecule is limited to a total quantum yield of 25% as only singlet excited states can be harvested radiatively.

1.3.2 Metal-organic Phosphorescence

Room temperature phosphorescence in organic molecules is rare as but, in metal-organic complexes, phosphorescence becomes a viable route of radiative decay and even out-competes fluorescence. The coupling of heavy metals (such as Pt, Ir, Cu etc) gives rise to spin-orbit coupling between the metal and ligand. This reduces phosphorescence lifetime, increases rates of ISC and triplet states gain additional singlet character.¹⁹ The result is radiative decay from T_1 to S_0 in reasonable rates at room temperature which results in emissive complexes that can achieve 100% internal quantum efficiency by being able to harvest all excited states radiatively.²⁰

1.3.3 Delayed Fluorescence

As has been discussed a key drawback of traditional fluorescent emitters, when applied to electro-luminescence, is their inability to utilise triplet excitons for emission. However, this is not the case for all fluorescent emitters as there are some examples where specific organic molecules have harnessed triplet excitons for emission through processes commonly referred to as delayed fluorescence. The first type of delayed fluorescence discovered was p-type delayed fluorescence (also known as triplet-triplet annihilation). This is a process whereby two triplet

states on separate molecules interact to leave one molecule in the ground state and the other in an excited singlet state. This process in theory means that two excited triplet states can lead to an fluorescence thereby bringing the total maximum quantum yield (the ratio of photons emitted to photons absorbed), of a molecule that shows this process, up to 62.5%.²¹ This process was first seen in pyrene hence the name p-type delayed fluorescence.²²

The other type of delayed fluorescence is commonly referred to as thermally activated delayed fluorescence (TADF). In this process, a very narrow energy gap (<0.2 eV) between S_1 and T_1 allows for a reverse inter-system crossing (RISC) process to occur. This means that triplet excitons, with a small amount of energy (induced by heat), can cross to singlet excitons and decay to the ground state radiatively. A fluorescent molecule that displays this process could show enhanced performance by radiative triplet harvesting (Figure 4).²³

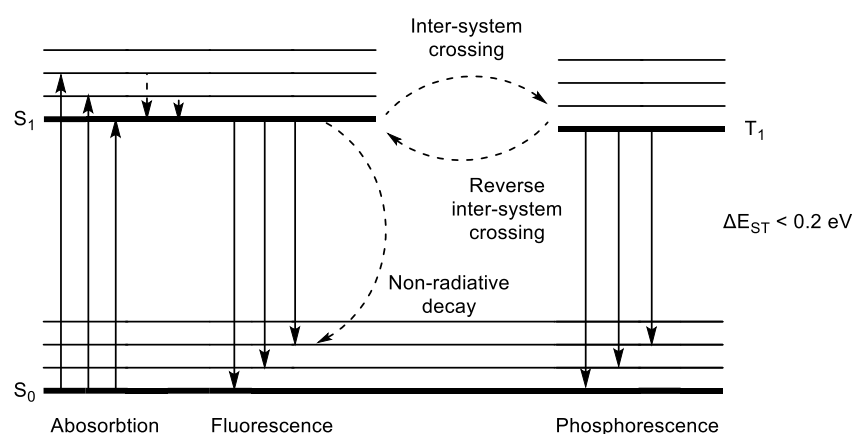


Figure 4: Thermally activated delayed fluorescence process represented on a Jablonski diagram.

1.3.4 Aggregation Induced Emission

Aggregation induced emission (AIE) is a process whereby a molecule that is not emissive in solution becomes emissive in solid-state.^{24, 25} Initially, there was a variety of proposed mechanisms for this process; restriction of intramolecular rotation (RIR), J-aggregation, molecular planarization, and twisted intramolecular charge transfer (TICT).²⁴⁻²⁶ RIR seemed to be the mechanism that could best explain the rise of this process in most molecules. This theory suggests that, in solution, free rotation of certain groups consumes exciton energy and provides a pathway of non-radiative decay. However, upon the formation of a solid film, free rotation is restricted, and the pathway of non-radiative decay is hindered which leads to emission upon aggregation but not in solution. This theory is commonly represented using tetraphenylethene (TPE) as an example (Figure 5). TPE in solution has free rotation of the phenyl groups however upon aggregation this movement is hindered, and emissive behaviour is induced. THBA was used to test this mechanism as the fusing of the phenyl groups should reduce rotation in solution and

lead to emissive behaviour in solution, however again AIE behaviour was observed so suggested that not only rotation, but intermolecular vibration can consume exciton energy. This theory has since been expanded to include restriction of intermolecular vibration (RIV) to give an overall mechanism referred to as restriction of intermolecular motion (RIM).²⁷

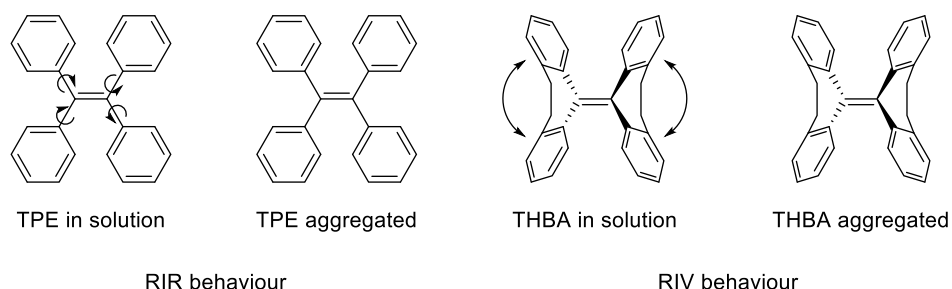


Figure 5: Representation of RIR and RIV behaviour upon aggregation.

1.4 Organic Light-emitting Diodes (OLEDs)

1.4.1 OLED Device Structure

To create luminescent materials there is a need for devices that incorporate organic emissive molecules and can electrically stimulate them. One such device is an organic light-emitting diode (OLED). These types of devices have seen much interest over the last 20 years,^{28, 29} mainly due to their applications to display technologies. The general structure of a multi-layer OLED device is represented below (Figure 6). OLEDs in general do not necessarily need to contain as many layers, as shown in Figure 6, a single emitting layer between an anode and a cathode would still class as an OLED. However, multi-layer devices are commonplace today usually adding hole transport, hole injection, electron transport and electron injection layers to the device. These layers aid in charge carrying through the device. A single-layer setup would mean one layer is responsible for having good photoluminescence and external quantum efficiency (EQE, the ratio of photons that are emitted from the device to the number of electrons injected into it) properties as well as being a good hole and electron transport material. This puts a lot of demand on a single molecule/layer however, by adding more layers to do specific jobs, molecules can be designed to be good at their role and work well with the other layers. This leads to a reduction in exciton quenching and charge carrier leakage, improving the device's performance.¹⁴

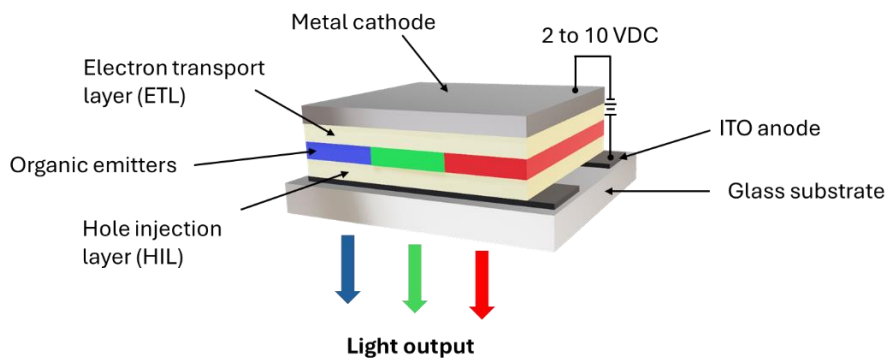


Figure 6: OLED general structure.

1.4.2 Brief History of OLED development

OLEDs have seen continuous development since they first were constructed in 1987.³⁰ The general history of the development of these devices can be split into three major sections. First-generation OLEDs that employ a fluorescent emitter and are limited to 25% internal quantum efficiency. Second-generation OLEDs, first reported in 1998, that utilised a metal-organic complex in the emissive layer to enable up to 100% internal quantum efficiency through phosphorescence emission.^{19, 31} Then finally third-generation, reported in 2009, use TADF type emitters to maintain the potential 100% internal quantum efficiency but move away from the use of rare, non-sustainable, earth metals in devices.³²

1.5 Light-emitting electrochemical cells (LECs)

1.5.1 LEC Device Structure

The general structure of a LEC device differs in one significant way from that of an OLED. That major difference is the presence of mobile ions in the devices active layer (emissive layer). Further to this LECs tend to have a much more simplified device structure having only three key layers, a transparent anode, air-stable cathode and an active layer responsible for emission.³³

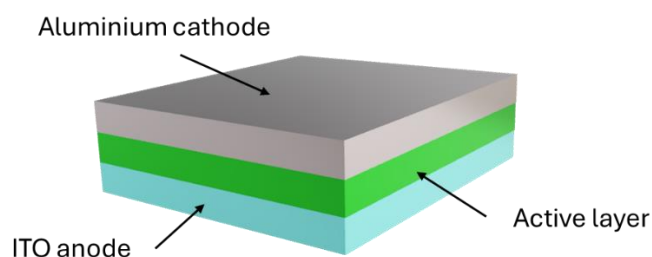


Figure 7: General LEC structure. Indium tin oxide anode (blue), active layer (green), aluminium cathode (grey).

The operating mechanism of these types of devices has been a topic of debate since their discovery. There are two generally accepted models: the electrodynamic model (ED)³⁴ and the electrochemical doping model.^{35,36} LECs usually operate under a constant applied voltage due to the migration of mobile ions in the active layer. When an external bias is applied mobile ions move towards the electrodes facilitating the injection of holes and electrons. In both models, the injection barrier is reduced due to the rearrangement of mobile ions under an applied bias (Figure 8).³⁷ Holes and electrons can then migrate towards a recombination zone and form excited states ultimately leading to the possibility of radiative recombination.

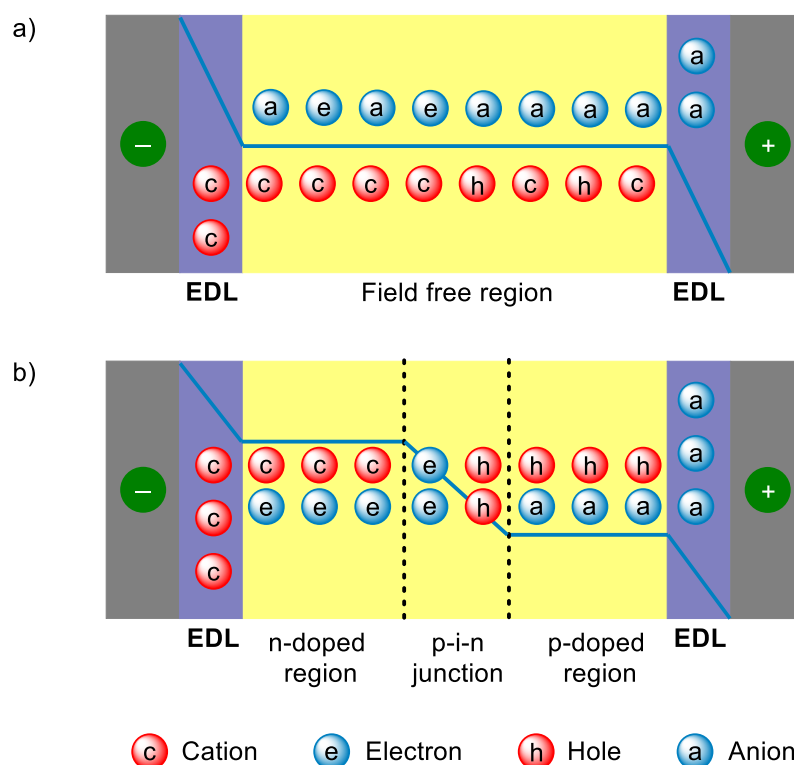


Figure 8: Illustration of a) electrodynamic model and b) electrochemical doping model for LEC operating mechanism.

1.5.2 Types of LEC Active Materials

Various types of active layer are employed in LEC devices and generally differ by the type of emissive molecule they utilise. There are three major categories that have received the bulk of development, these are polymer LECs, ionic transition metal complex (iTMC) LECs and small molecule LECs.

Polymer-based active layers contain fluorescent conjugated polymers as their emissive molecule, the active layer may also contain p and n-doping materials to assist with charge carrying as well as a solid electrolyte material (Figure 9, b). iTMC LECs use charged phosphorescent metal-ligand complexes with an associated counter ion for emission and

charge-carrying (Figure 9, a).³⁷ Small molecule LECs utilise a small molecule emitter and, like polymer LECs, they often see the addition of p and n-doping materials as well as solid electrolytes (Figure 9, c). However, it is also possible to employ ionic small molecules to alleviate the need for additional compounds. It is worth noting that these are the basic formulations of these types of active layer. Host-guest type setups are very common where a host material in high concentration is used that essentially works to funnel excited states onto an emissive guest material. In these types of setups, mixtures of all of these types of material have been fabricated.³⁸

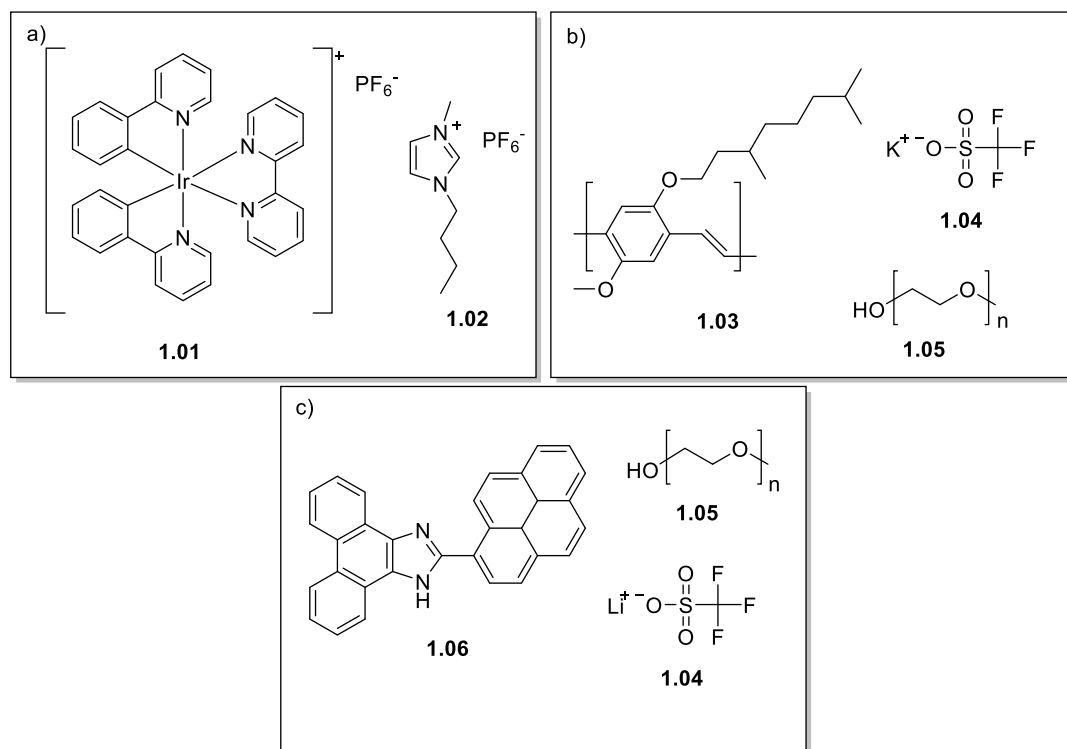


Figure 9: Examples of the constituents of a) iTMC active layer, b) conjugated polymer active layer, c) small molecule active layer.

1.6 The Challenges of Luminescence and Degradation mechanisms

The general mechanisms by which a molecule comes to show emission and the device setups that can bring about such emission by electrical stimulation have been introduced. However, there is a large gap between understanding these fundamental principles and being able to design effective working devices. This is because there are also many challenges that can be encountered that limit a devices or molecules performance. These problems differ depending on the wavelength of emission of the molecule, the type of device being fabricated and the mechanisms by which the molecule shows emission.

1.6.1 Wide Band-gap Instability

The first major challenge to address is wide band-gap instability. This is a problem for molecules showing emission in the blue to UV region of the electromagnetic spectrum. Inherently, molecules that emit in this region have a wide energy gap between the ground and excited state as this large energy gap is what gives rise to blue or UV emission. However, because of this there is a requirement for significantly higher power to achieve the same luminance intensity as green or red emission. This leads to much more heat generation in blue and UV devices leading to reduced stability of these devices due to morphological changes in the emissive layer.³⁹

Further to this, high levels of energy present in these devices is expected to lead to direct degradation of the organic molecules in the emissive layers.⁴⁰ For example, the S_1 (first singlet excited state) energy for a blue emitter can exceed 3.1 eV, this is approximately the same as C-N bond energy. As a result, homolysis of C-X bonds ($X = N, S, P$ etc) can occur and the generated free radicals can further quench emission.⁴¹ The ability to address this problem in molecular design has been explored in the work of Wang and co-workers'. Substitution of donating and withdrawing groups onto the degraded molecule can have significant effects on bond dissociation energies (Figure 10),⁴² however it is worth noting that these substitutions will also impact the wavelength of emission. Some substitutions can improve bond stability making emissive molecules more robust under these high energy conditions.

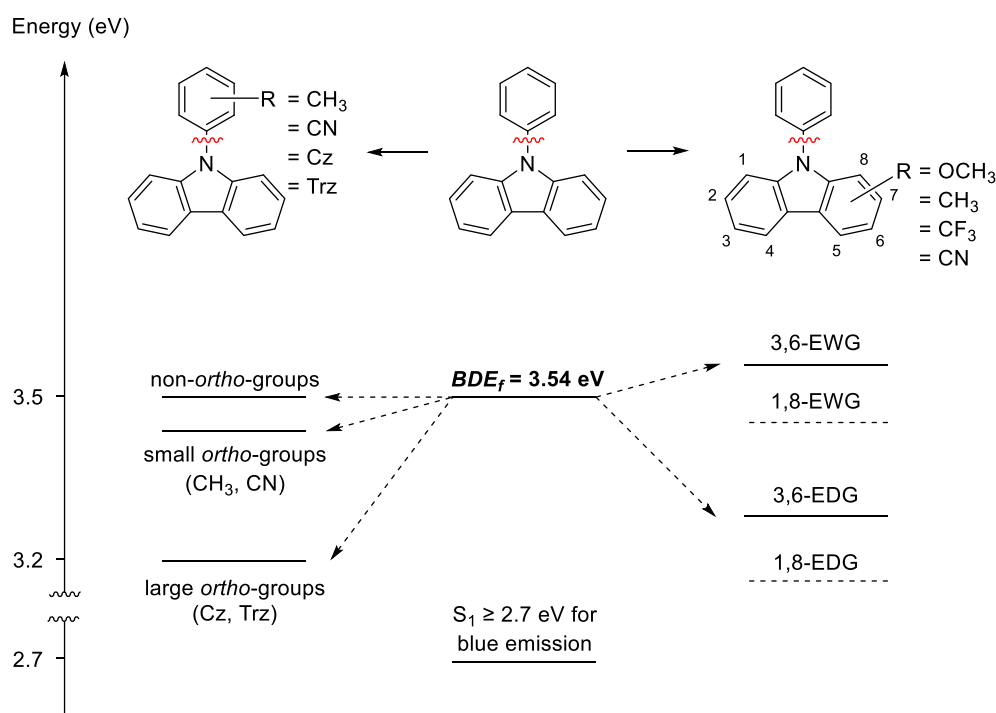


Figure 10: Effect of derivatisation on bond dissociation energy.

1.6.2 Concentration Quenching

Concentration quenching is another challenge that has been encountered, primarily during the fabrication of OLEDs. Unlike other problems, concentration quenching has appeared when using various types of emissive molecule however, the mechanism by which it occurs seems to differ depending on the class of emissive molecule. For example, traditional fluorescent emitters are expected to experience fluorescence quenching at higher concentrations due to Förster resonance energy transfer (FRET). This process is a classical long-range dipole-dipole interaction where one excited molecule can transfer energy, non-radiatively to another non-excited molecule returning to the ground state and exciting the other molecule,⁴³ multiple energy transfers dampen radiative excitons.⁴⁴ This can also occur between two singlet excited states that can annihilate (singlet-singlet annihilation (SSA)) leaving one molecule in the ground state and the other in a higher level singlet excited state.⁴⁵ This applies to a large amount of fluorescent molecules but will not be prevalent in molecules that contain little to no dipole moment.

Concentration quenching also appears when utilising metal-organic phosphorescent emitters. In this case, again a FRET process is responsible but between triplet states. A single-step bimolecular combination of two triplet states results in one molecule left in the ground state and the other in a higher-level triplet state (TTA).⁴⁵ In a standard fluorescent emitter this helps break through the 25% limit for exciton harvesting but in a phosphorescent emitter, the high energy triplet exciton is expected to lead to degradation.⁴⁶ These annihilations can also occur with polarons which is the general name for the species with an electron or a hole that recombine to give an excited state.

In TADF type emitters concentration quenching is again encountered however, the mechanism by which it occurs is expected to be slightly different. In this case, the non-radiative pathways such as ISC or non-radiative decay are preferable when the concentration of emissive molecule is increased. This is due to increased electronic stabilisation of excited states in higher concentrations meaning the rate of ISC depends on concentration. The mechanism by which the stabilisation occurs is known as the Dexter energy transfer (DET) model.⁴⁷ This process decreases exponentially with distance.

1.7 Active Layer and Molecular Design

Now most relevant areas of background information have been introduced, understanding these core concepts is key to begin to be able to think about how to pull together the information to utilise the best device and emitter for a given application. In this section, some of the major design points of an emissive molecule or layer will be discussed.

1.7.1 Doped and Non-doped Layers

Concentration quenching is a big problem that reduces a device's performance. This issue is facilitated by energy transfer between excited states or polarons and the extent to which this occurs is directly related to the distance between molecules. LECs and OLEDs are both solid-state devices therefore the best way to increase the distance between emissive molecules is to add another component to the layer reducing the concentration of emitter in the emissive layer. These types of devices have been previously introduced as host-guest devices. Using a host material in high concentrations alleviates degradation mechanisms and you can also add other components to aid with charge mobility. The major drawback of this is it adds more complexity to the fabrication of the emissive layer. Furthermore, the selection of materials to add to a layer needs to be given great consideration, materials need to be able to suitably trap excited states on the emitter molecule, avoid quenching and have suitable stability.⁴⁸ The work of Lundberg and co-workers' outlines the components of a doped layer utilising a TADF emitter **1.09** commonly referred to as 4CzIPN, with polymer host polyvinyl carbazole (PVK, **1.06**), n-doping material commonly referred to as OXD-7 (**1.08**) and an ionic liquid **1.07** as a source of mobile ions in an LEC device (Figure 11). These components have been carefully chosen to trap electrons on 4CzIPN due to its lower LUMO energy as well as aid in charge carrying due to the reversible oxidation and reduction nature of p and n-doping materials (Figure 12).⁴⁹

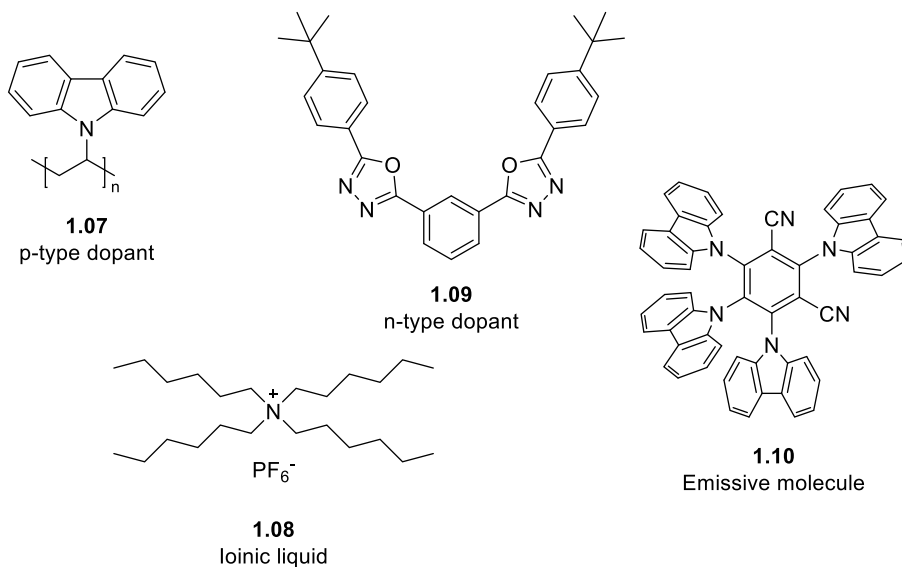


Figure 11: Components of a doped LEC active layer.

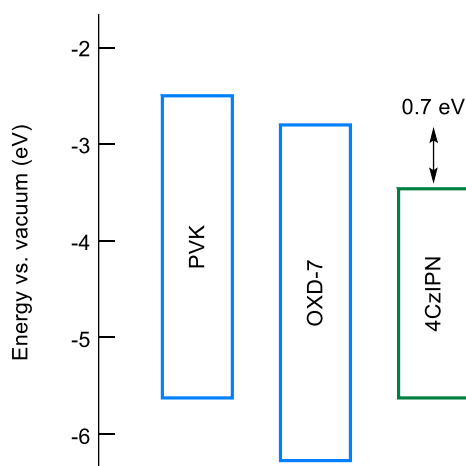


Figure 12: HOMO LUMO energy levels of PVK, OXD-7 and 4CzIPN.

Non-doped layers in LECs are much simpler employing only an ionic emitter in the emissive layer however, this requires much more careful design of the molecule as it needs to be able to resist degradation mechanisms as well as perform well as an emitter and charge carrier.

1.7.2 Charge Carrier Ability

A concept that has been mentioned extensively so far is charge carrier ability. This is necessary for electrically stimulated fluorescence as excitation is not done by simply exciting an electron from the ground state to an excited state. An excited state is achieved by the combination of polarons (holes and electrons) therefore there is a need for the emissive molecule, and other charge carriers, to be able to gain and lose an electron (be oxidised or reduced) in a reversible manner. This allows holes and electrons to move through the solid layer and combine to form an excited state. This is a feature that needs to be designed into emissive molecules. The simplest way this is done is to have both donor and acceptor moieties present in the emitter which usually results in a spatial separation of the HOMO and LUMO on the molecule.⁵⁰ The donor-acceptor design of emissive molecules is incredibly popular and successful in LECs and OLEDs however, non-donor acceptor structures can also work as long as reversible reduction and oxidation ability is present.⁵¹

1.7.3 Wavelength Tuning

One subject that has not been discussed in detail so far is emission wavelength despite it being a key feature that is one of the largest contributors to the design of an emitter. Every organic molecule will have an associated absorption and emission but the factors that affect whether a molecule will be a good emitter are extensive. Some examples of these may be the extent of conjugation, aromaticity, heteroatoms, and intermolecular motion. These all contribute to the rates of non-radiative and radiative decay which ultimately govern a molecules ability to be

emissive. Each molecule has an associated emission wavelength but one strategy to achieve the desired wavelength is to adjust the wavelength of a good performing emitter by derivatisation. This is generally done by substituting electron-donating or withdrawing groups onto certain positions to adjust HOMO or LUMO energy levels. For example, stabilization of the HOMO or destabilization of the LUMO increases the HOMO-LUMO energy gap resulting in a wavelength shift towards the blue region.⁵² This type of wavelength tuning has been conducted on metal-organic complexes⁵³ as well as fluorescent organic molecules (Figure 13).⁵⁴

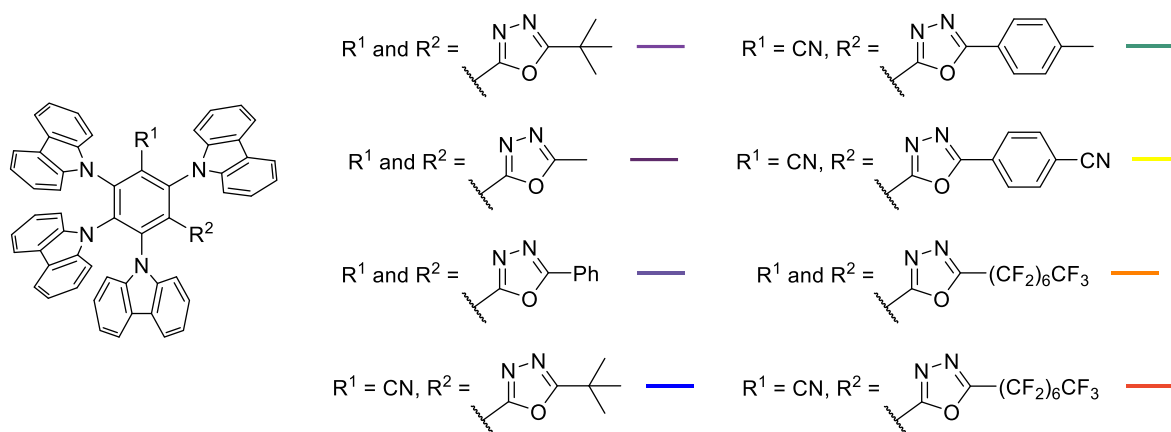


Figure 13: Derivatisation of 4CzIPN to achieve a range of emission wavelengths.

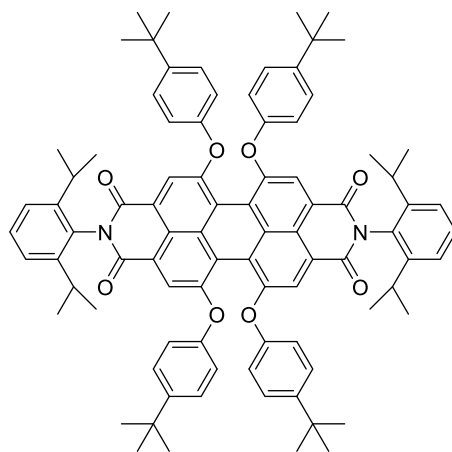
1.8 Small Molecules and Their Use in LECs

The reviewed material so far, has covered various fundamental principles and introduced the main points of consideration needed to understand the function of a fluorophore within an electroluminescent device. We have established the working principal of an LEC device and some of the factors that contribute to a successful luminescent device. Here in we will explore how small molecules have been applied to LEC devices previously, evaluating attempts to develop a comprehensive understanding of the technology and improve its performance. It is worth noting a large amount of the initial development of LECs was conducted utilising conjugated polymers which will not be covered here however, a comprehensive review of the use of polymers in light emitting technologies can be found in the review of Leni Akcelrud⁵⁵ and their application to LECs is covered in the review of Youssef and collaborators.⁵⁶

1.8.1 Non-ionic Small Molecule LECs

The first group to utilise a small molecule as an emitter in a LEC device was Hill and co-workers' in 2008.⁵⁷ A device was fabricated employing perylene derivative **1.11** (Figure 14) as the fluorescent emitter along with polyethylene oxide (PEO, **1.05**) and lithium triflate (**1.04**) in a 5:1:1 ratio respectively (by weight) as the active layer. Electroluminescence was generated at 622 nm

and the group reported a visibly red emission. The neutral perylene derivative **1.11** was selected for various reasons including high thermal, chemical, and photostability⁵⁸⁻⁶⁰ as well as easy potential derivatisation at the imide and phenol ether positions. To add to this at this time the use of n-type materials that are more easily and reversibly reduced could be beneficial in balancing doping effects in this type of device.



1.11

Figure 14: Red emitting perylene derivative utilised by Hill and co-workers’.

In 2013, Edman and co-workers’ made great progress in understanding the operating mechanism of LEC devices.³⁵ The group employed two small molecule emitters, referred to as red (**1.12**) and green (**1.13**) due to their emission colours, in two different types of LEC device (Figure 15). One of these devices employed a very standard setup (Figure 8) and the other was a bilayer device with a top layer consisting of the small molecule emitter and the bottom comprised of solid potassium triflate in PEO electrolyte (Figure 16). The result was that the bilayer device showed in-situ electrochemical doping and p-n junction formation demonstrating the ability of non-ionic small molecules to fulfil the role of both electrochemical doping and emission. This work gave unambiguous evidence for the electrochemical doping mechanism previously introduced (Figure 8b). The formulated devices also showed low turn on voltages of approximately 4.0 V and devices utilising red (**1.12**) and green (**1.13**) reported maximum brightness of 3700 and 750 cd m⁻² respectively. Maximum efficiency was measured at 2.25 and 1.05 cd A⁻¹ and the red device showed emission at 618 nm with CIE colour coordinates of (0.65, 0.36) which is close to the ideal red point for displays.

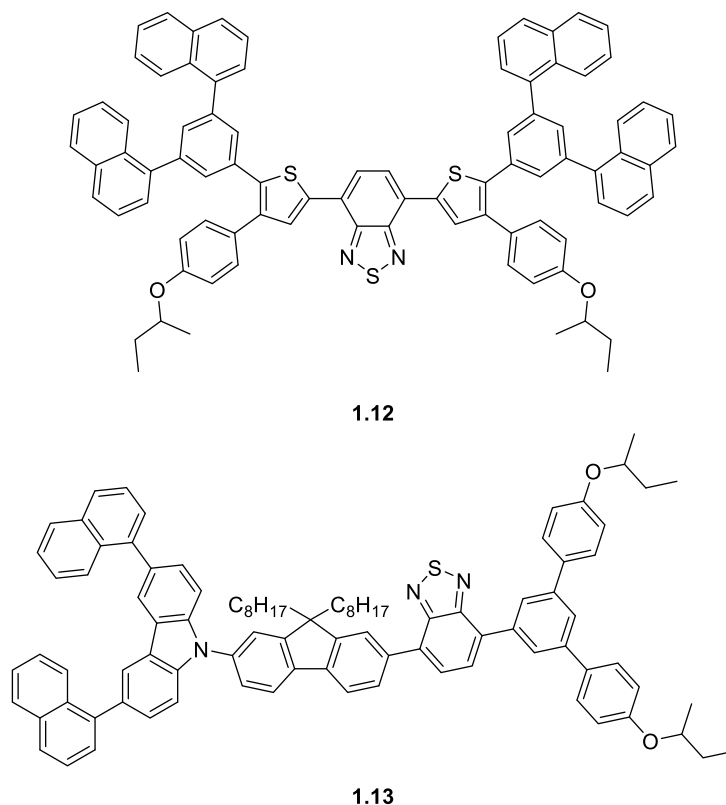


Figure 15: Structure of small molecule emitters referred to as red (**1.12**) and green (**1.13**).

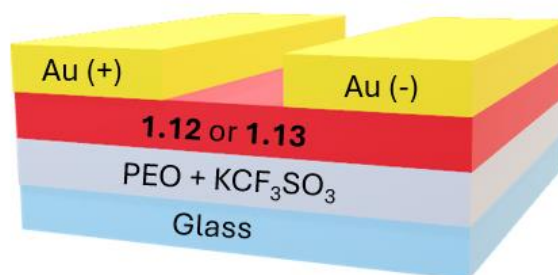
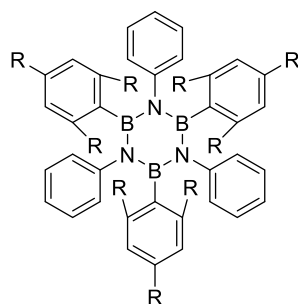


Figure 16: Structure of bilayer LEC device fabricated in the work of Edman and co-workers'.

In the same year, Kervyn and co-workers' attempted the implementation of a blue emitting borazine based small molecule into an LEC device.⁶¹ Borazine derivatives **1.14** and **1.15** (Figure 17) were tested for this role with initial photoluminescent data showing an interesting deviation of the emission profile depending on the obtained polymorph of the emitter. The range of polymorphs showed photoluminescence in the deep-blue and UV region between 300-375 nm varying with the polymorph. Such molecules rarely see application in luminescent devices due to the moisture sensitivity of B-N bonds, undergoing hydrolysis readily in the presence of moisture.⁶² However, the use of mesityl groups in **1.15** was expected to improve the resistance of the compound towards hydrolysis. For application of these borazine derivatives to a device, a low work function cathode of LiF (6 nm)/Ca (30 nm)/Al (150 nm) was fabricated to facilitate electron injection however, this created a device bearing more similarity to a simple OLED. The resulting

devices showed poor performance with high turn on voltages of approximately 9.5 V and low EQE of $<10^{-4}$ %.



1.14 R = H
1.15 R = Me

Figure 17: Blue emitting borazine derived fluorophores implemented by Kervyn and co-workers’.

Choe and co-workers’ were next to take up the mantle, attempting to expand the range of easily accessible small molecule blue emitters applied to LECs.⁶³ In 2015, the group synthesised a phenanthroimidazole based target (**1.18**) utilizing the one-pot Debus–Radziszewski imidazole synthesis (Figure 18).⁶⁴ The aim was to access a class of emitter that showed good solubility in common solvents, strong luminescence, and good thermal stabilities. **1.18** showed emission at 428 nm in solution with a good quantum yield of 0.6 and thus was applied to an LEC device being part of a 3-component active layer consisting of **1.18**, lithium triflate and PEO in a 1:0.18:0.1 mass ratio. The resulting device showed a low turn on voltage of 4.3 V with a maximum luminance of 125 cd m⁻², the cause of low luminance at high current densities was expected to be a consequence of aggregation in the solid state. To add to this a large undesirable redshift was observed between photo and electroluminescence expected to have been caused by interaction of the imidazole NH and the salt added to the active layer. This was addressed when the group later published investigation into **1.19** and **1.20** which contained alkyl substitution on the imidazole ring. The modified targets showed maximum brightness of 49 and 278 cd m⁻² respectively. Compared to the parent compound **1.18** the butyl containing derivative **1.19** showed diminished performance expected to be the result of challenges in thin film formation but the hexyl containing derivative **1.20** saw a two-fold improvement in performance. The hexyl chain is thought to have disrupted aggregation and eliminated interaction with the salt as intended.

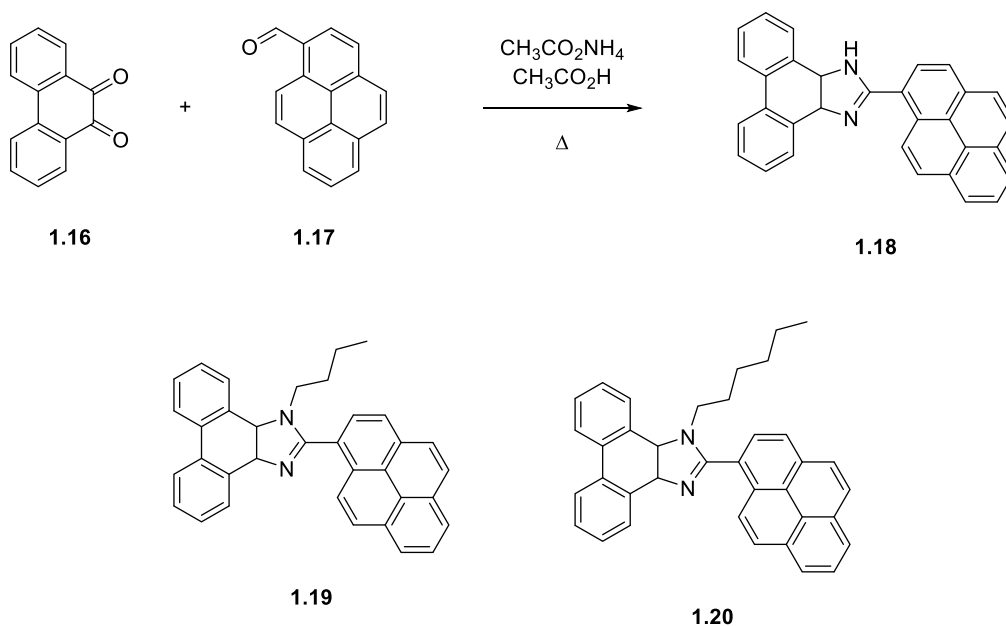


Figure 18: Synthesis and derivatisation of phenanthroimidazole based targets by Choe and co-workers’.

Introducing a new family of small molecules emitters to the field, Costa and co-workers in 2015 pioneered the use of pentacene based emitters (Figure 19).⁶⁵ Linearly fused benzene rings called acenes have outstanding features like ease of energy bandgap tuning by increasing number of benzene rings, and stability. The group studied a rather unique approach to the formulation of an active layer to apply to an LEC in which pentacene **1.21** was subjected to a photoinduced cycloaddition producing mixtures of **1.21**, **1.22** and **1.23**. 3-, 7- and 10-day aged solutions were mixed with lithium triflate and trimethylolpropane ethoxylate used to fabricate LEC devices, and the best performance was observed with the 10-day aged solution which was the only solution that contained the dimeric species. Stable white light devices featuring a maximum brightness of 10 cd m^{-2} were formed. The groups rationale for the improved performance with the presence of dimers **1.22** and **1.23** is that the dimers were acting as a high band-gap host with residual **1.21** acting as a low band-gap guest, giving a host-guest type active layer.

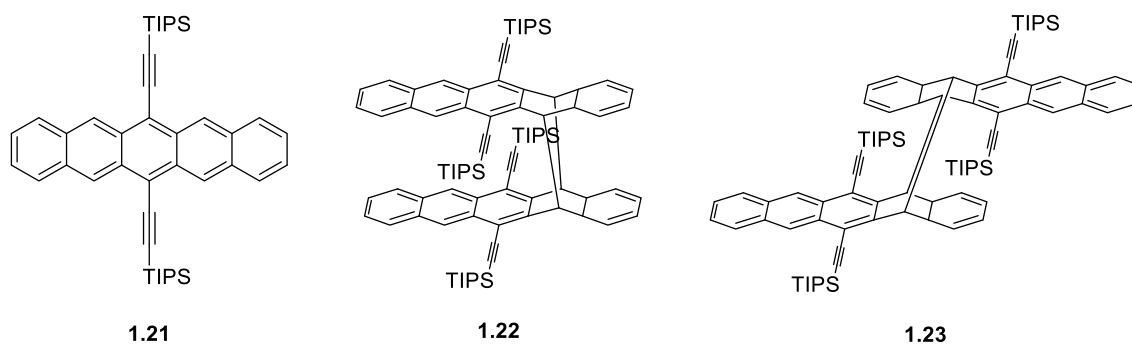


Figure 19: Pentacene based emitter **1.21** and pseudo-host dimers used by Costa and co-workers’.

Looking to investigate the relationship between molecular design and electroluminescence behaviour Costa and co-workers' continued their work with LEC devices as the suitable medium for such exploration.⁶⁶ This is due to the requirement of the emitter to perform the roles charge injection, charge transport, electron-hole recombination, and emission. The group examined the use of two porphyrin derived emitters, the free base **1.24** and the neutral metal organic complex **1.25** (Figure 20). Initial photoluminescence studies revealed the free base **1.24** had superior performance and was expected to produce better electroluminescence when applied to an LEC. Devices were fabricated with lithium triflate, trimethylolpropane ethoxylate, and porphyrins in the mass ratio of 0.06:0.15:1. Zn-porphyrin **1.25** produced a deep red emitting LEC with CIE colour coordinates of (0.68, 0.30) whilst the free base showed yellow/white emission with CIE of (0.44, 0.43).

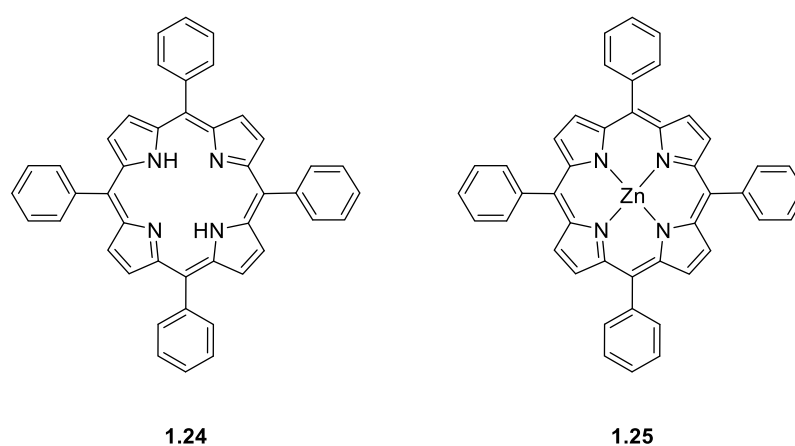


Figure 20: Neutral porphyrin emitters applied to LEC devices by Costa and co-workers'.

Costa and co-workers' furthered this work with their other publication in 2016 exploring the use of other metal centres with similar porphyrin scaffolds (Figure 21).⁶⁷ Interestingly initial scrutiny of the characteristic photoluminescence of the emitters revealed differing modes of luminescence depending on the metal centre. The Zn-porphyrin **1.28** produced fluorescence at 600 and 650 nm with a 3.8% quantum yield. Pt-porphyrin **1.27** showed phosphorescence at 695 and 730 nm with a 0.095% quantum yield. Pd-porphyrin **1.26** had a dual emission character producing both fluorescence and phosphorescence at 565-610 nm and 700 nm respectively with quantum yields of 0.047% and 0.0013%. Finally, Sn-porphyrin **1.29** displayed TADF at 610 and 665 nm with a quantum yield of 1.2%. LECs were fabricated with lithium triflate, trimethylolpropane ethoxylate, and the porphyrins in a 0.06:0.15:1 mass ratio. All devices produced deep red emission with Pt-porphyrin **1.27** being the standout performer boasting a EQE of 0.16%.

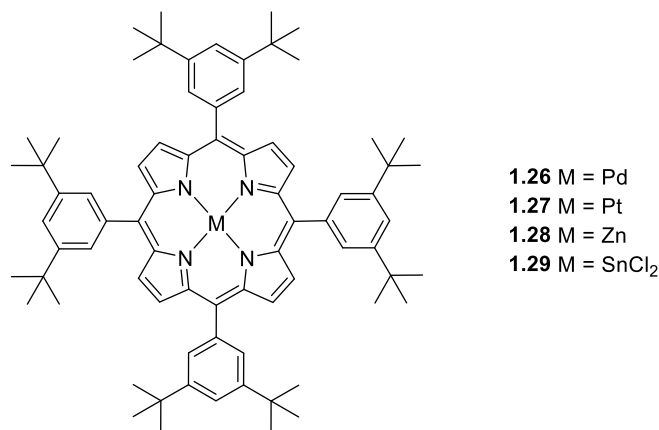
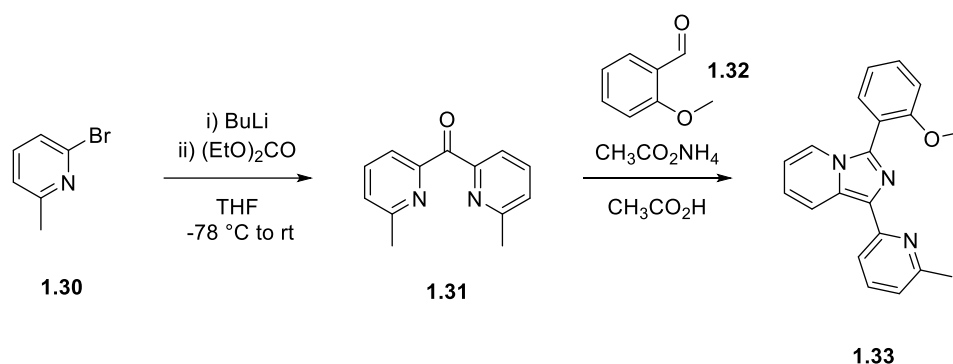


Figure 21: Metal-organic emitters investigated by Costa and co-workers’.

Maintaining their interest in this field, in 2018, Costa and co-workers provided a facile, low-cost synthesis of an imidazo-pyridine emitter with excellent redox properties to be applied to LECs (Scheme 1). The approach used double substitution on diethyl carbonate with the lithiated form of pyridine **1.30** to give ketone **1.31** which could undergo a cyclization with aldehyde **1.32** to form imidazo-pyridine **1.33** in the presence of ammonium acetate and acetic acid. The isolated emitter showed blue photoluminescence at 436 nm with a quantum yield of 0.4. An LEC device was fabricated using imidazo-pyridine **1.33**, trimethylolpropane ethoxylate, lithium triflate in the mass ratio 1:0.15:0.06. The device showed electroluminescent emission at 560 nm with CIE colour coordinates of (0.42, 0.50) indicating orange emission with a maximum luminance of 2.5 cd m⁻². Further to this the authors also tried doping the material with poly(methyl methacrylate) to try and reduce aggregation in the solid state which they suggested was causing a red-shift in emission. With 20% by weight presence of poly(methyl methacrylate) electroluminescence was observed at 480 nm confirming the groups suspicions. To add to this the synthesised emitter was also used as a ligand to create metal-organic complexes to be used as emitters however, devices fabricated with these complexes showed no improvement on their initial device.



Scheme 1: Costa and co-workers’ synthesis of imidazo-pyridine based emitter.

A major step forward in the work on neutral small molecule LECs was achieved in the work of Chen D. and co-workers’ when, in 2019, they reported devices utilising a series of bithiazole

derived emitters (Figure 22).⁶⁸ The groups work focused on their unique approach in applying inkjet printing to the fabrication of the LEC devices. The standout performing emitter was bithiazole **1.36** producing a yellow/green electroluminescence with CIE of (0.28, 0.42). The LEC device exploiting this emitter gave a maximum luminance of 18 000 cd m⁻² and an EQE of 12.8% which represents, by far, the best performing non-ionic small molecule LEC to date.

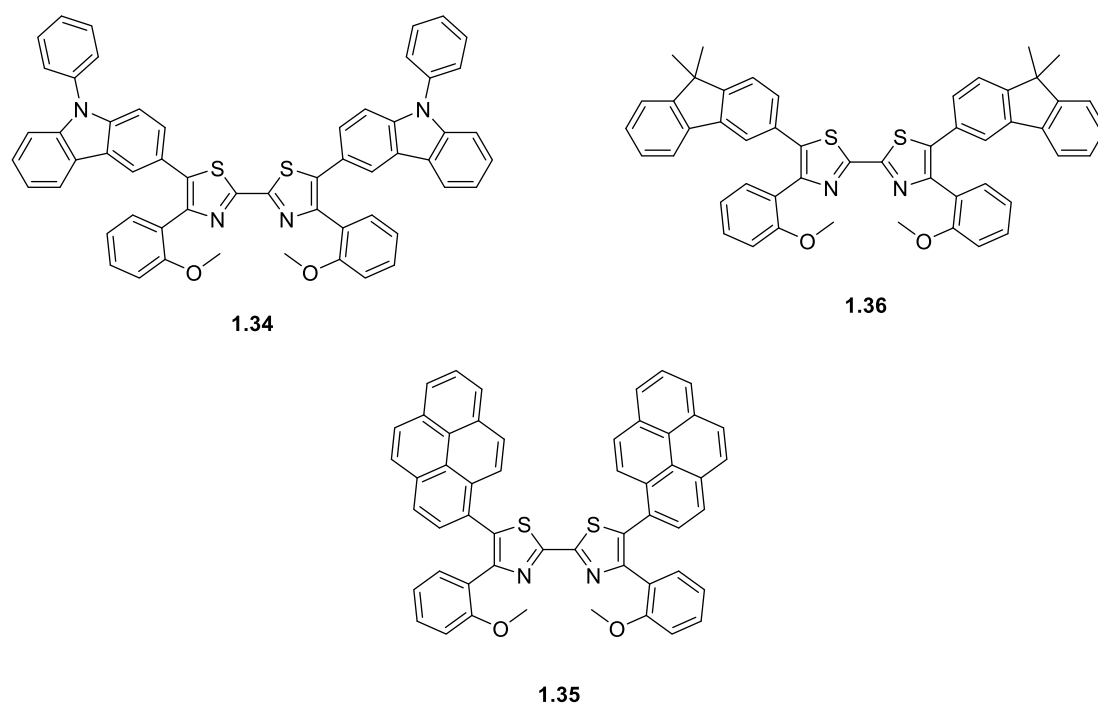
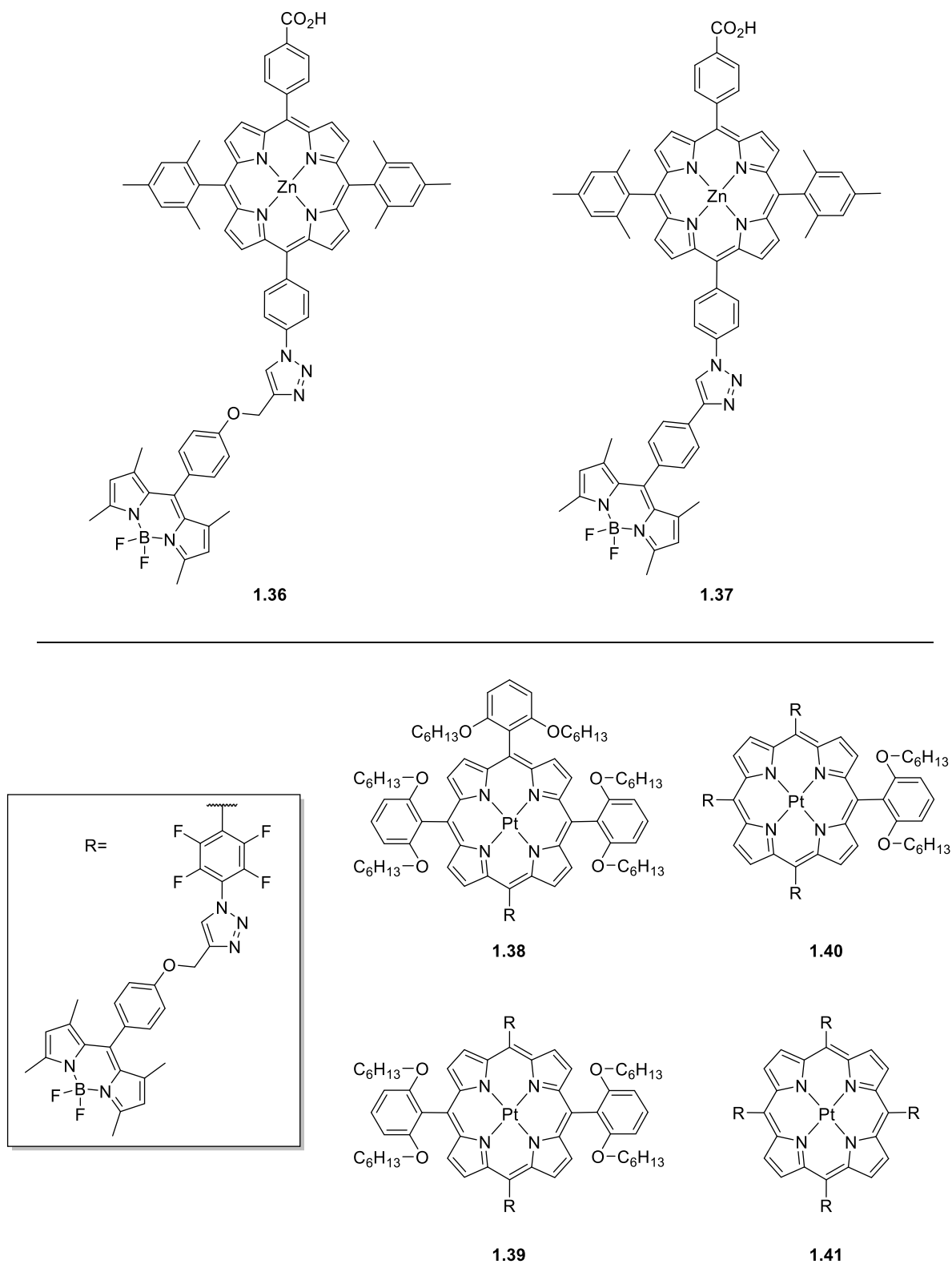


Figure 22: Bithiazole emitters tested by Chen D. and co-workers’.

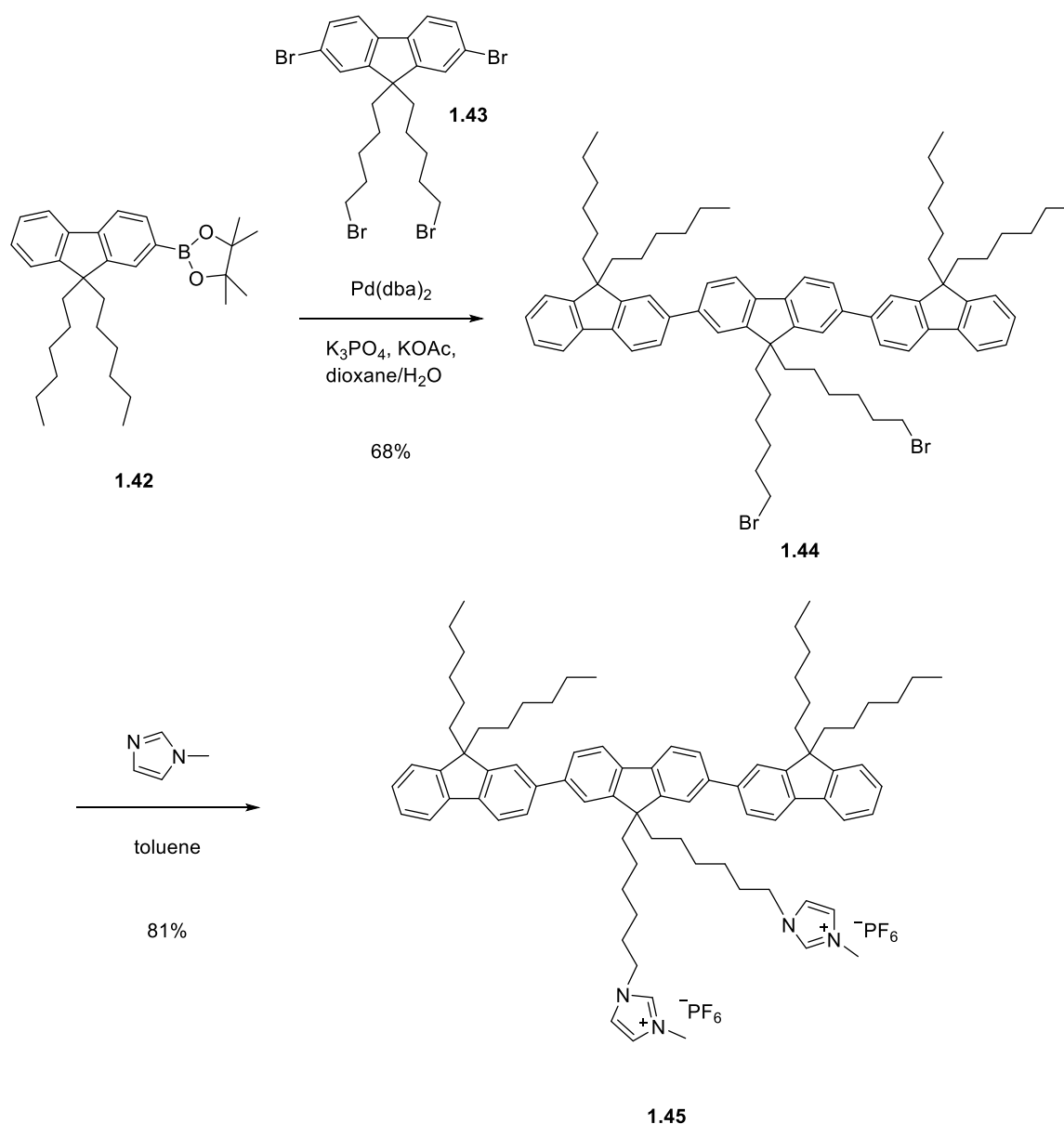
Costa and co-workers’ final contribution to date to the area of applying neutral small molecule emitters to LECs came in the form of investigation of so-called dyad small molecules in pursuit of efficient near-infrared (NIR) emission. This was work started in 2016 with scrutiny of porphyrin dyads **1.36** and **1.37** then more recently, in 2021, continued with modified dyads **1.38** to **1.41** (Figure 23). This work was a development of their initial investigation of porphyrin metal complexes **1.26** to **1.29** (Figure 22) where the group noted achieving either high efficiency but low stability with Pt-porphyrin **1.27** or high stability but low efficiency with Zn-porphyrin **1.28**. To improve upon this work dyad type molecules that covalently combine host type unit, in this case a boron dipyrromethene (BODIPY) with their guest emitter, the porphyrin metal complex. Their preliminary study with Zn-porphyrin dyads **1.36** and **1.37** produced devices that achieved lifetimes of >1000 hours which was a 10-fold improvement on the stability of their non-dyad devices.⁶⁹ The group followed up with analysis of Pt-porphyrin dyad where they saw a similar improvements performance with the outstanding results being obtained when incorporating 2 BODIPY (**1.39**) units into their dyad system.⁷⁰



1.8.2 Ionic Small Molecule LECs

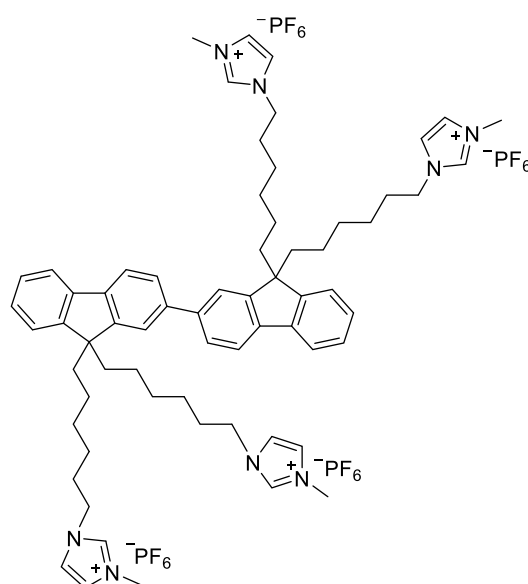
Ionic small molecule emitters provide an opportunity to simplify the LEC fabrication process providing the opportunity to forego the addition of solid electrolyte as mobile ions. The first implementation of an ionic small molecule emitter in an LEC was published in 2008 by Chen. H.

F. and co-workers'.⁷¹ They put to work a terfluorene derivative **1.45** which they prepared via a Suzuki coupling of boronate ester **1.42** with dibromo fluorene derivative **1.43**. This furnished the terfluorene core and subsequent substitution with 1-methylimidazole on the pendant alkyl bromide chains afforded the desired ionic emitter **1.45** (Scheme 2).⁷¹ LEC devices were fabricated and evaluation of whether an added ionic liquid would improve performance was conducted. One device exploited only terfluorene **1.45** and the other was doped with an added 10% 1-Butyl-3-methylimidazolium hexafluorophosphate ([BMIM][PF₆]) by weight. The devices boasted similar performance producing blue electroluminescence (424 nm) with an EQE of 1.04% for the non-doped device and an EQE of 1.14% for the device doped with the ionic liquid. However, the doped device did boast a significantly higher power efficiency expected to be a result greater accumulation of mobile ions and accelerated formation of doped regions.



Scheme 2: Chen H. F. and co-workers' synthesis of terfluorene derivative **1.45**.

Chen H. F. and co-workers' continued this work moving to the use of a 2,2'-bifluorene **1.46** derivative to attempt to achieve a UV emitting LEC. In a similar approach to their previous work, in this investigation the group investigated the effect of doping their active layer with 10% by weight polymethyl methacrylate (PMMA). This additive was not added to improve charge injection or mobility as it is a neutral additive. The expected role of PMMA is to disrupt aggregates in the solid phase and improve power efficiency. However, the group interestingly noted that the electroluminescent properties of devices fabricate with and without PMMA were almost entirely unchanged with similar emission wavelength of 386 nm observed. This suggests PMMA does not completely disrupt aggregation as a shift in wavelength would be expected, instead it is expected that smaller aggregates are formed. The doping with PMMA saw significant improvement in the performance of the device with EQE of 1.06% with PMMA compared to EQE of 0.15% without PMMA reported. Further to this, a seven-fold improvement in power efficiency was noted.



1.46

Figure 24: 2,2'-Bifluorene emitter studied by Chen H. F. and co-workers'.

The next contribution to the implementation of ionic small molecule emitters in LECs by Chen H. F. and co-workers' came in 2013.⁷² The authors move in a new direction with an interesting approach that looked to use a mixture of two ionic small molecules in one active layer. Their premise was the use of one small molecule as a hole transport material (HTM) and another as the electron transport material (ETM). The two could then combine to form an exciplex capable of emission. This type of setup would benefit from efficient and balanced charge transport. To achieve this triarylamine **1.47** as the HTM and triazine **1.48** as the ETM were used (Figure 25). Mixtures of the ETM and HTM produced a broad green emission which changed slightly dependent on the ratio of HTM and ETM used. To further confirm the formation of the exciplex, thin films were doped with PMMA which disrupted exciplex formation and suppressed emission. An LEC device

with optimal ratio of HTM and ETM produced green emission at 550 nm with EQE of 3.04%. The mixing ratio proved pivotal to device performance as other devices showed significantly worse results.

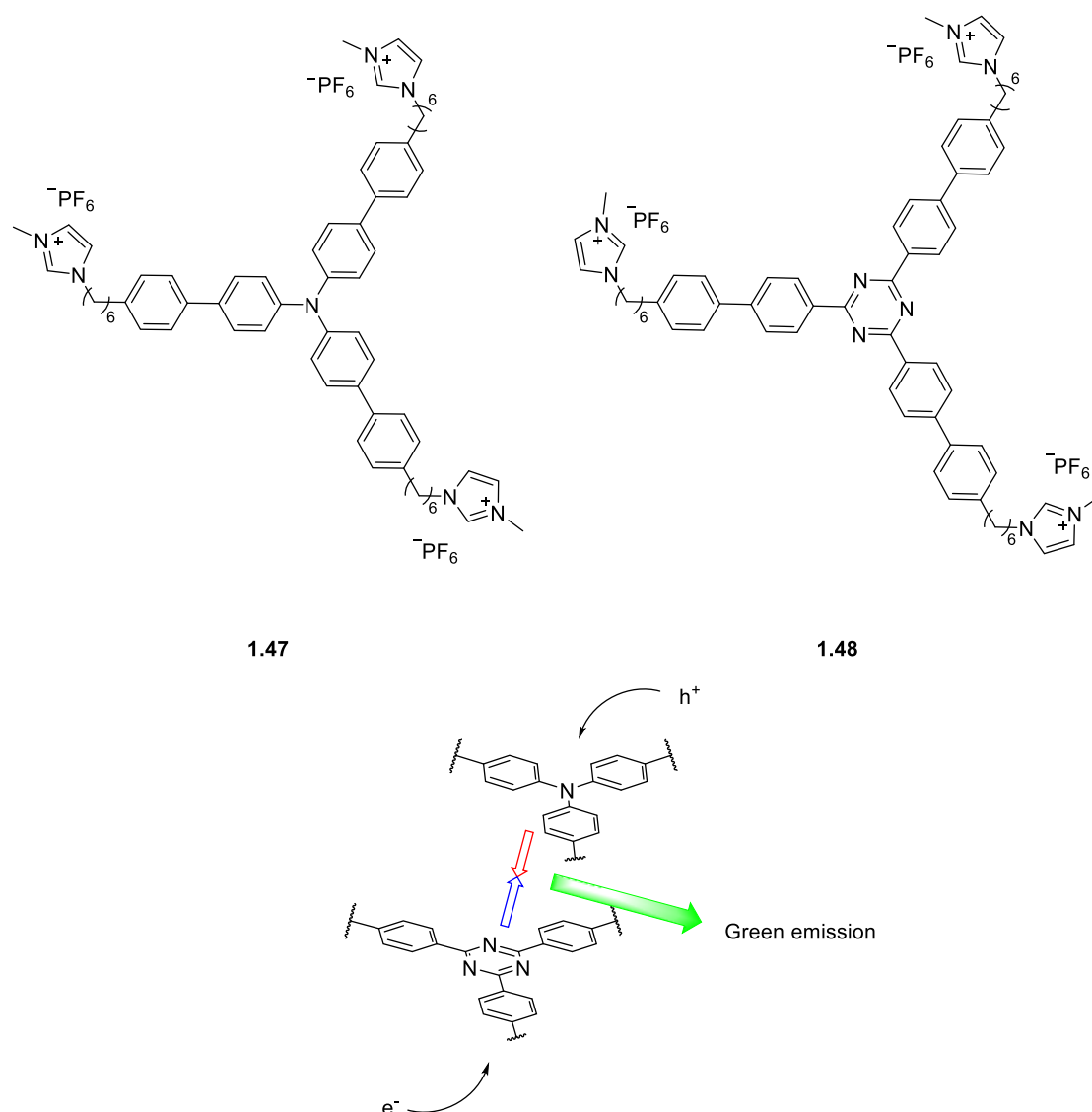


Figure 25: Triarylamine HTM and triazine ETM implemented by Chen H. F. and co-workers’.

Continuing with the exploration of the use of fluorene based emissive small molecules in LECs, Choe and co-workers’ published work, in 2015, researching blue emitting fluorene derivative **1.49** (Figure 26).⁷³ In a very similar study to Chen. H. F. and co-workers’ with **1.45**, the authors again wanted to examine the influence of doping with ionic liquid $[\text{BMIM}][\text{PF}_6]$. Devices were fabricated with and without the ionic liquid present (10% by weight ionic liquid was added) producing blue electroluminescence at 454 nm with impressive maximum luminance’s of 1105 cd m^{-2} without ionic liquid addition and 1247 cd m^{-2} with addition. Encouraged by these results the group went on to publish a study of fluorene derivatives **1.50** and **1.51** in 2016.⁷⁴ However, sadly devices fabricated incorporating these emissive fluorene derivatives saw drastically reduced maximum

luminance's of 120 and 136 cd m^{-2} respectively. The authors suggest that the reason for this is higher rates of nonradiative decay such as quenching of excitons in the active layer.

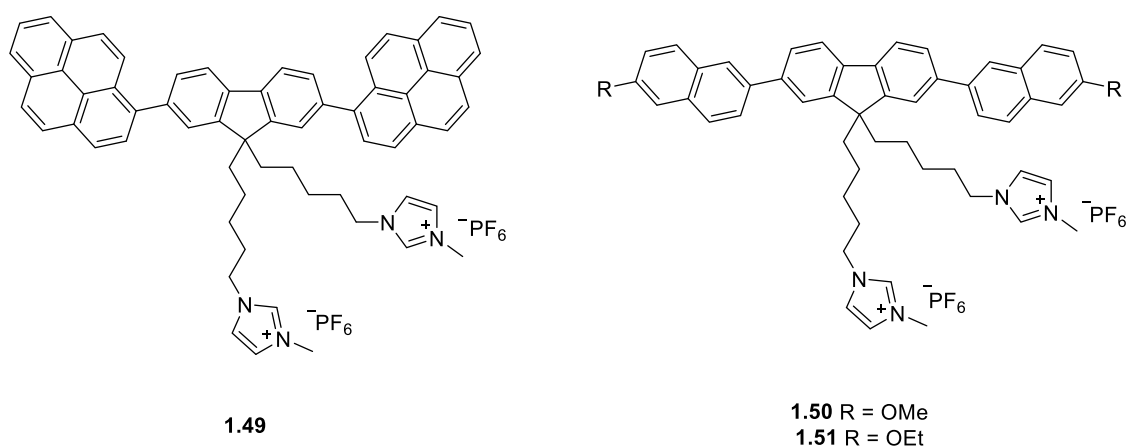


Figure 26: Structures of fluorene-based emitters used in the work of Choe and co-workers'.

Pushing the field of ionic small molecule emitters applied to LECs in a new direction Wong and co-workers' looked to be the first to apply TADF emitters. In 2015, the group synthesised two novel N-carbazoyl-dicyano benzene targets (**1.52** and **1.53**) and analysed their photoluminescence properties.⁷⁵ The resulting study showed long (microsecond) average lifetime and the shortening of the lifetime in air suggesting a triplet derived TADF process was occurring. With this conclusion application of the TADF emitters to LEC devices was the next task, devices were fabricated with either the emitter alone or doped with [Bmim][PF₆] at a molar ratio of 4:1 (4 parts emitter). Unfortunately, no emission was observed with devices fabricated with N-carbazoyl-dicyano benzene **1.52**. The devices fabricated with emitter **1.53** showed green emission at 538 nm with the best performance being obtained in the use of the doped active layer. A maximum luminance of 24 cd m^{-2} and an EQE of 0.29% were recorded. The authors suggested that generation of a more polar environment and widening of the singlet-triplet energy gap inhibited the TADF phenomenon resulting in poor performance.

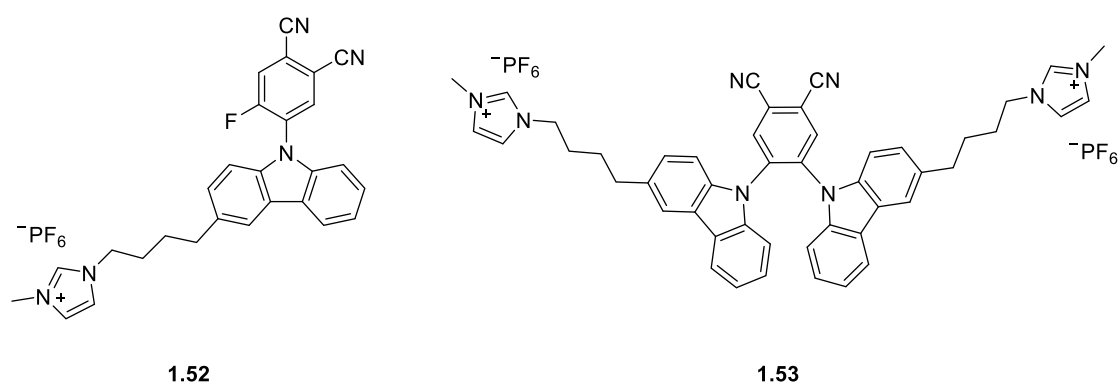


Figure 27: Novel TADF emitters synthesised and tested by Wong and co-workers'.

Phenanthroimidazole based emitters **1.19** and **1.20** (Figure 18) were introduced by Choe and co-workers' as neutral small molecule emitters to be applied to LECs. Later they continued this work wanting to compare the performance of structurally similar ionic and non-ionic targets. Thus, ionic phenanthroimidazole compounds **1.54** and **1.55** were produced (Figure 28).⁷⁶ Electroluminescent devices were fabricated without addition of any other components and produced blue emission at 484 nm for emitter **1.54** and 487 nm for emitter **1.55**. Superior device performance was reported with the use of the hexyl chain spacer (**1.55**) with a maximum luminance of 711 cd m⁻² observed, this is nearly 3 times better than the performance of the neutral analogue.

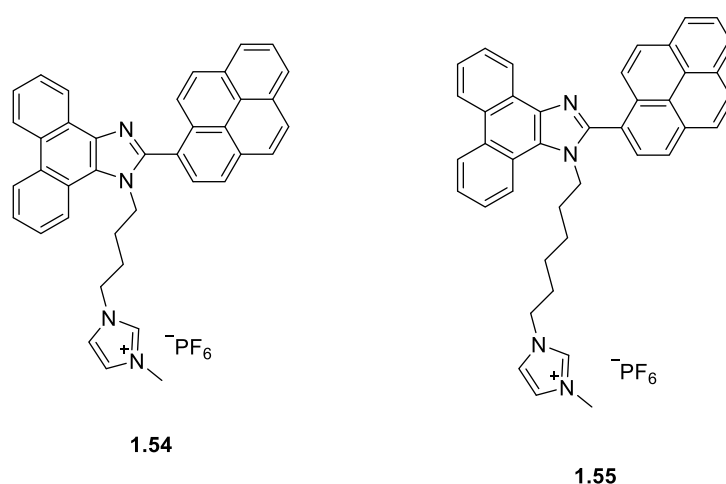


Figure 28: Ionic phenanthroimidazole derived emitters from the work of Choe and co-workers'.

Choe and co-workers' continued to expand their influence on the field of small molecule LECs, in 2016, with the development of green phenothiazine emitter **1.56** (Figure 29).⁷⁷ The emitter bore structural similarities with their earlier successful fluorene-based emitter **1.49** (Figure 27). Electroluminescent devices operated at low turn-on voltages exhibiting emission at 530 nm with the phenothiazine emitter and offering maximum brightness of 499 cd m⁻². In a following study the group looked to evaluate the effect on device performance of changing the oxidation on sulphur.⁷⁸ The sulfone analogue **1.57** was prepared and LECs fabricated. Interestingly an electroluminescence emission of 498 nm with maximum luminance of 509 cd m⁻² was reported indicating that oxidation provided a relatively simple way to tune emission wavelength with little no influence on the device's performance.

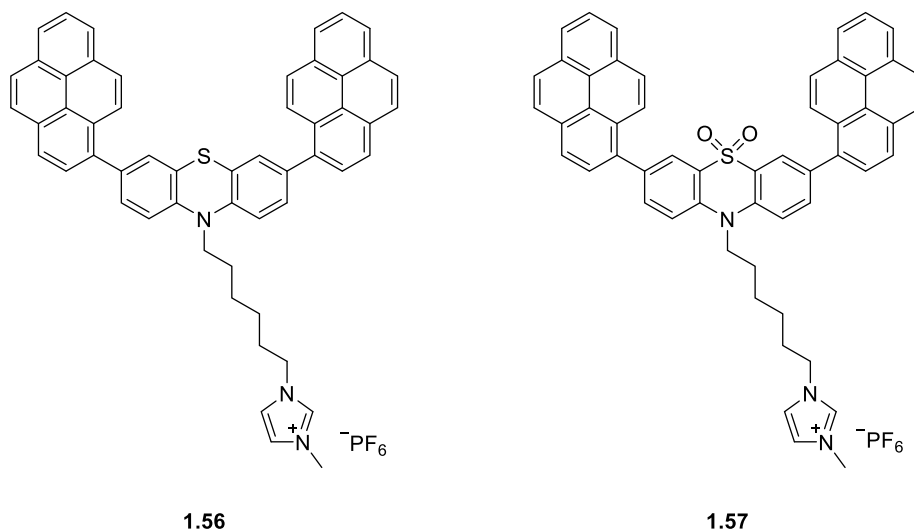


Figure 29: Phenothiazine emitter **1.56** and its sulfone analogue **1.57** studied by Choe and co-workers’.

The inquiry into the use of ionic TADF emitters in LECs was picked up by Wong and co-workers’ in 2017, looking to also fill an apparent absence of effective deep-blue emitters applied to LECs.⁷⁹ The authors reported the use of two diphenylsulfone emitters (**1.58** and **1.59**) based on TADF emitters that had previously been applied to OLEDs.^{80, 81} Thin-film photoluminescence measurements showed emission at 414 nm for target **1.58** and at 409 nm for emitter **1.59**. The group reported high photoluminescence quantum yields of 0.44 and 0.49 respectively making the emitters promising candidates for high performing devices. Disappointingly, electrochemical instability of the diphenylsulfone emitters in the LEC devices resulted in only one functional device, employing emitter **1.58**. Deep blue emission was achieved however, with low luminance of 2.5 cd m⁻². Evidence of the electrochemical instability was the observation of an additional emission peak at 550 nm in the electroluminescence spectra.

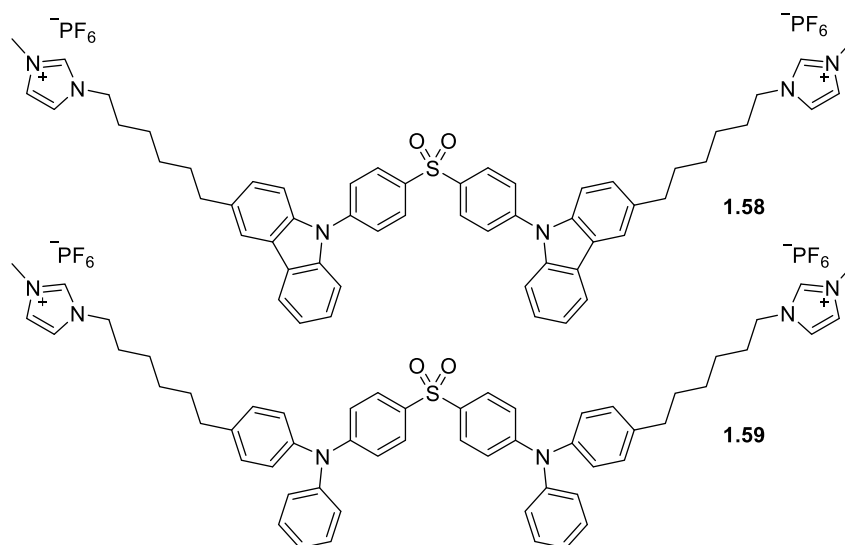


Figure 30: Diphenylsulfone TADF emitters analysed by Wong and co-workers’.

Choe and co-workers' returned to their inspection of phenanthroimidazole based emitters in 2017 with the publication of four novel pyrene or anthracene bearing compounds (**1.60** to **1.63**).⁸² The pyrene and anthracene units were bound in either an ortho or meta position and the group looked to evaluate the effect of such a difference. The authors report significantly worse solubility with the ortho linked emitters **1.62** and **1.63** to the extent that the group were unable to successfully fabricate LECs with these emitters. LECs fabricated with the meta linked emitters **1.60** and **1.61** showed blue electroluminescence at 485 and 474 nm respectively with maximum luminance of 179 and 26 cd m⁻² noted. An interesting experiment followed this in which the effect of doping the active layer with lithium triflate was examined. Three devices were manufactured using meta-pyrene emitter **1.60** and differing concentrations of lithium triflate (5%, 10% and 15% by weight). Pleasingly, the devices reported improved maximum luminance of 465, 440, and 585 cd m⁻² respectively demonstrating the utility of this approach. The group followed up this work with the analysis of the, less-fused, pyrene imidazole emitters **1.64** and **1.65**.⁸³ The aim of this work was to achieve a blue-shifted emission due to the reduced conjugation. This premise was successful with electroluminescence at 451 nm being reported when using emitter **1.64**.

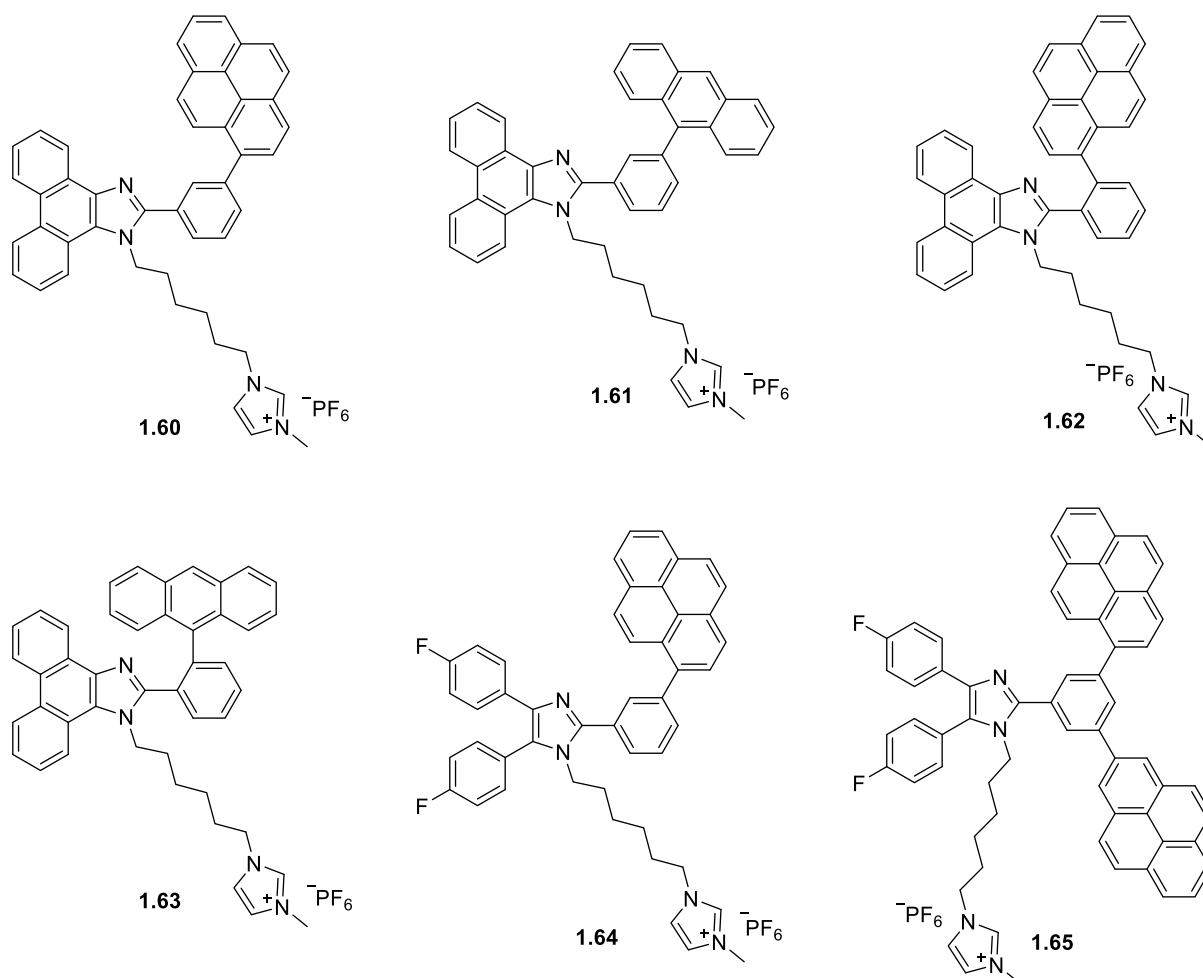


Figure 31: Phenanthroimidazole and pyrene-imidazole derived emitters studied by Choe and co-workers'.

Revisiting their work on phenothiazine emitters, in 2018, Choe and co-workers' developed two new emissive compounds, **1.66** and **1.67**.⁸⁴ These emitters incorporated naphthalene and phenanthrene units as opposed to their previously successful parent emitter that incorporated pyrene (**1.56**, Figure 29). Unfortunately, these new derivatives did not boast the same levels of performance with low luminance of 129 and 59 cd m⁻² at 499 and 505 nm reported respectively. The authors disclosed issues with stability and lifetime of the molecules, as well as the absence of n-doping. With this result in mind, structure **1.68** bearing carbazole moieties was later published with the group noting its improved thermal and electrochemical stability.⁸⁵ Devices fabricated with this emitter electroluminescence at 485 nm with a maximum brightness of 454 cd m⁻² and EQE of 1.76%. This performance was analogous to the parent compound **1.56**.

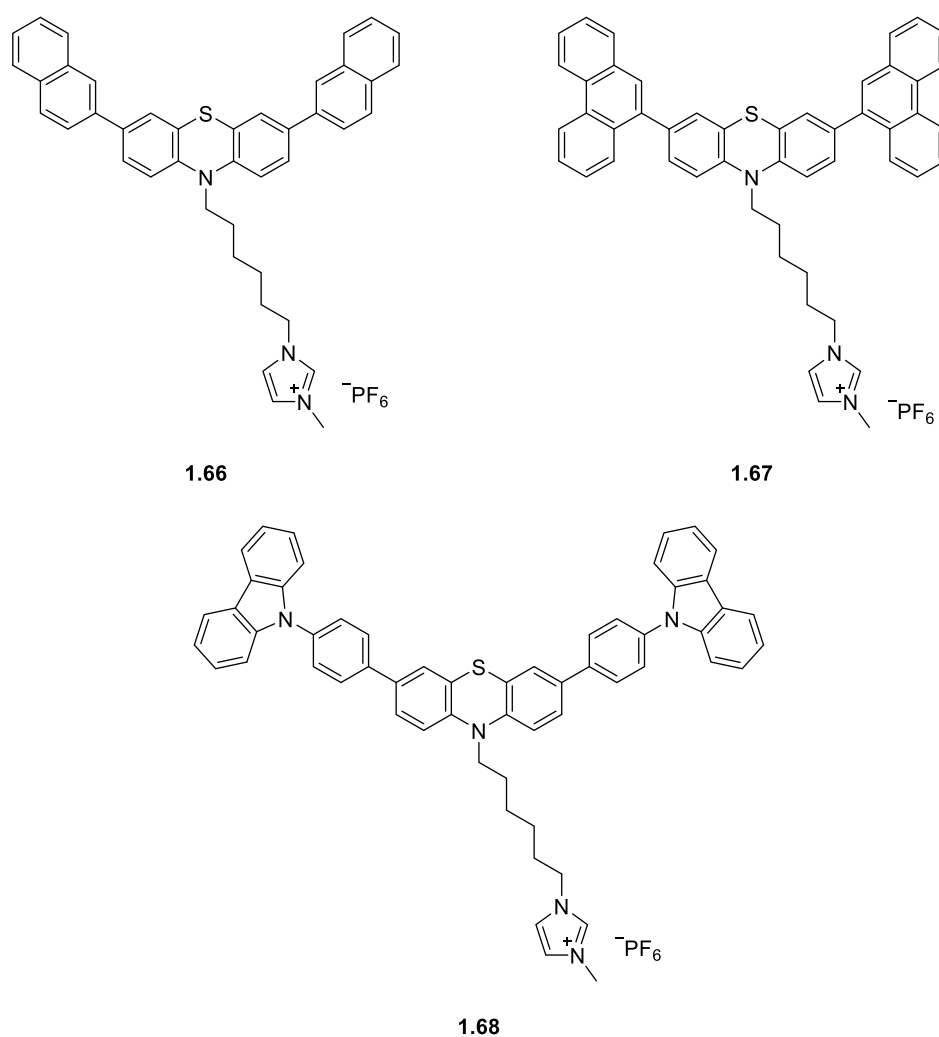


Figure 32: The next generation of phenothiazine emitters studied by Choe and co-workers'.

In a new direction Choe and co-workers' next considered the application of AIE to LECs.⁸⁶ With this goal they synthesised tetraphenylethene bearing emitters **1.67** and **1.68** and began photoluminescence investigations. As desired the emitters produced no fluorescence in solution but in thin film emission at 475 nm was observed. Devices were fabricated with only the emissive molecules present in the active layer and the result was blue electroluminescence at 474 nm for

both compounds. The para compound **1.67** displayed good performance with a maximum brightness value of 644 cd m^{-2} and an EQE of 2.63%. However, this was overshadowed by the performance of meta emitter **1.68**, producing a maximum brightness value of 1466 cd m^{-2} with an EQE of 2.95%.

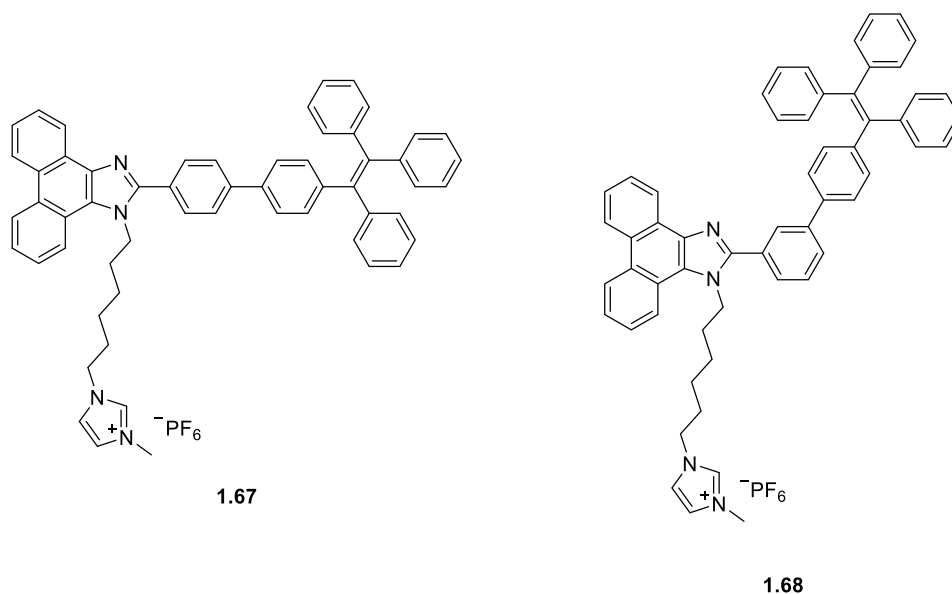


Figure 33: Tetraphenylethene bearing AIE compounds analysed by Choe and co-workers’.

Establishing themselves as the main force in the field of ionic small molecules LECs, Choe and co-workers’ continued their high publication output with their next study of green triazine based emitters **1.69** and **1.70** (Figure 34) in 2020.⁸⁷ These emitters fit the description of so-called donor-acceptor type emitters, which employ a donor unit with conjugated connectivity to an acceptor unit to allow intramolecular charge transfer (ICT) lowering the energy of molecular orbitals.⁸⁸ LEC devices fabricated with these emitters showed a sharp green emission at 505 nm with triazine **1.69** and 499 nm with triazine **1.70**. The phenanthroimidazole derived target **1.69** disclosed superior device performance with a maximum brightness of 1453 cd m^{-2} and an EQE of 1.65% compared to 1048 cd m^{-2} and 1.23% with diphenylimidazole **1.70**.

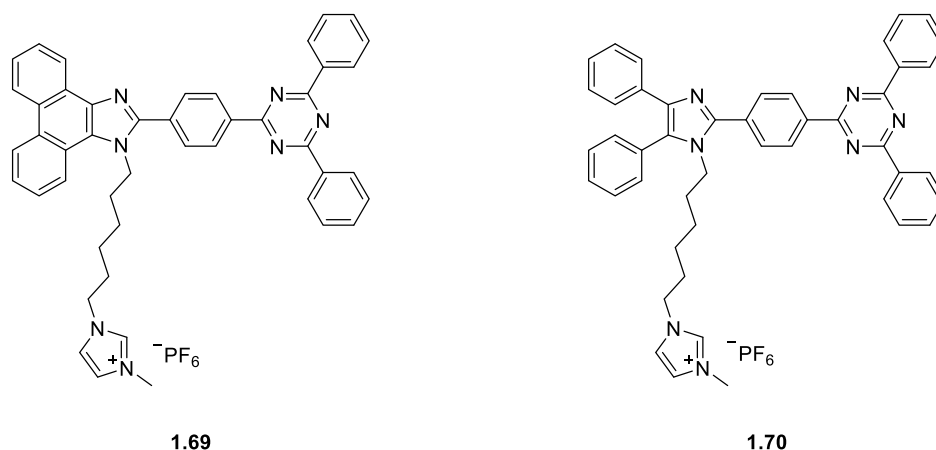


Figure 34: Triazine donor-acceptor emitters reviewed by Choe and co-workers’.

Looking to investigate new donor-acceptor type emitters, in 2021, Choe and co-workers were the first to introduce a thenil based small molecule into an LEC device.⁸⁹ This step came in the form of thenil-pyrene emitters **1.71** and **1.72** (Figure 35). Devices created incorporating these emitters showed ‘ultra-pure’ green electroluminescence at 521 and 525 nm respectively and enjoyed high maximum brightness values of 2307 cd m⁻² and 2479 cd m⁻². EQE of 3.47% was reported with emitter **1.71** and a similar 3.71% recorded with emitter **1.72**. These results were particularly pleasing as the reported CIE colour coordinates of (0.21, 0.65) and (0.19, 0.70) respectively were very close to ultrapure green emission in accordance with the recommendation ITU-R BT.2020. The ITU-R Recommendation BT.2020, defines various ideal aspects of ultra-high-definition television (UHDTV) including colour primaries (the ideal CIE coordinates of red, green and blue emission).⁹⁰

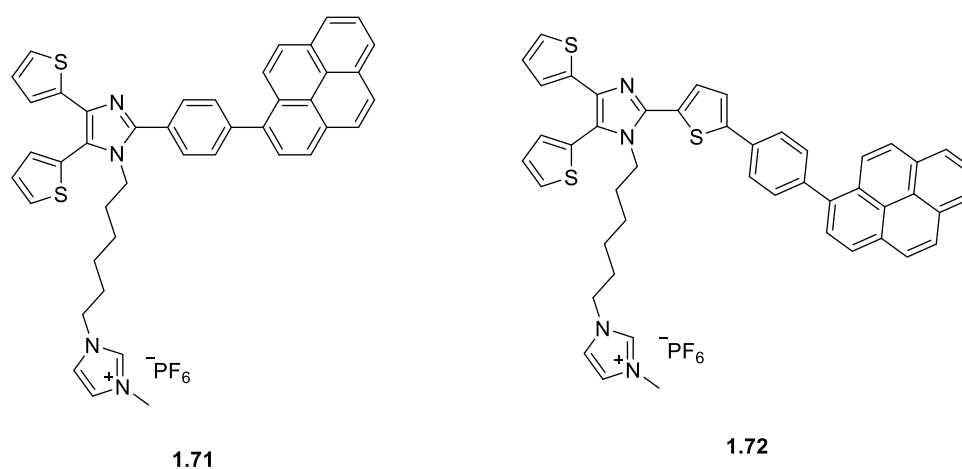


Figure 35: Thenil based emitters examined by Choe and co-workers’.

To be the first group to introduce non-doped red-emitting LECs, Choe and co-workers’ looked into the use of two benzothiadiazole emitters **1.73** and **1.74** (Figure 36) completing their publication of red, green and blue emitting LECs.⁹¹ Devices constructed with emitter **1.73** presented ‘hyper red’ emission colour with the electroluminescence peak centered at 663 nm, the devices reached good maximum luminance of 1393 cd m⁻² with EQE 3.20%. When creating devices with emitter **1.74** a clear orange-red emission with electroluminescence peak at 622 nm was detected with maximum luminance 1955 cd m⁻² and EQE of 3.96%. These devices represent the best EQEs reported by the group to date.

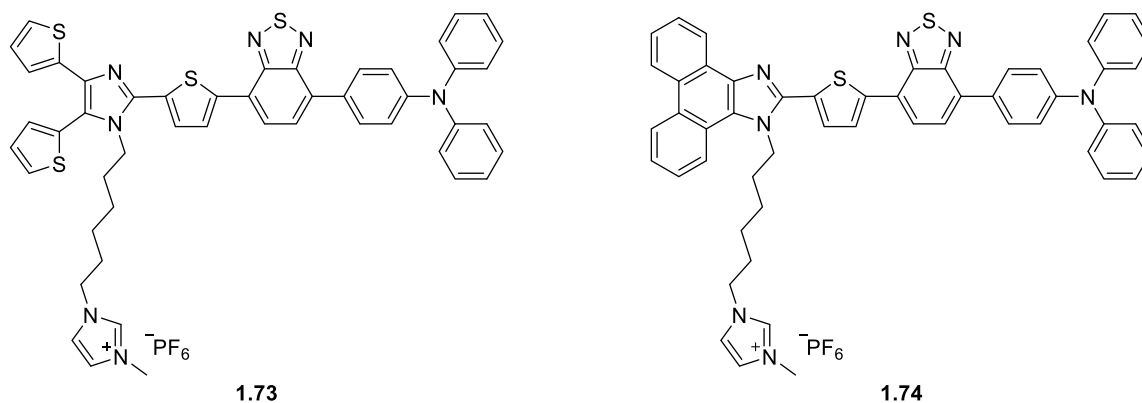


Figure 36: Red emitting benzothiadiazole compounds presented by Choe and co-workers’.

In their most recent work, in 2023, Choe and co-workers’ report the integration of V-shaped acceptor-donor-acceptor emitters **1.79** and **1.80** into LECs.⁹² Inspired by the application of such emitters to OLEDs⁹³⁻⁹⁵ the authors implemented their familiar thenil and phenanthroimidazole acceptors around an acceptor triphenylamine core. Resulting LECs integrating emitters **1.79** and **1.80** revealed electroluminescence at 479 and 458 nm respectively with maximum luminance of 1073 and 899 cd m⁻² and EQE of 1.83 and 1.70%.

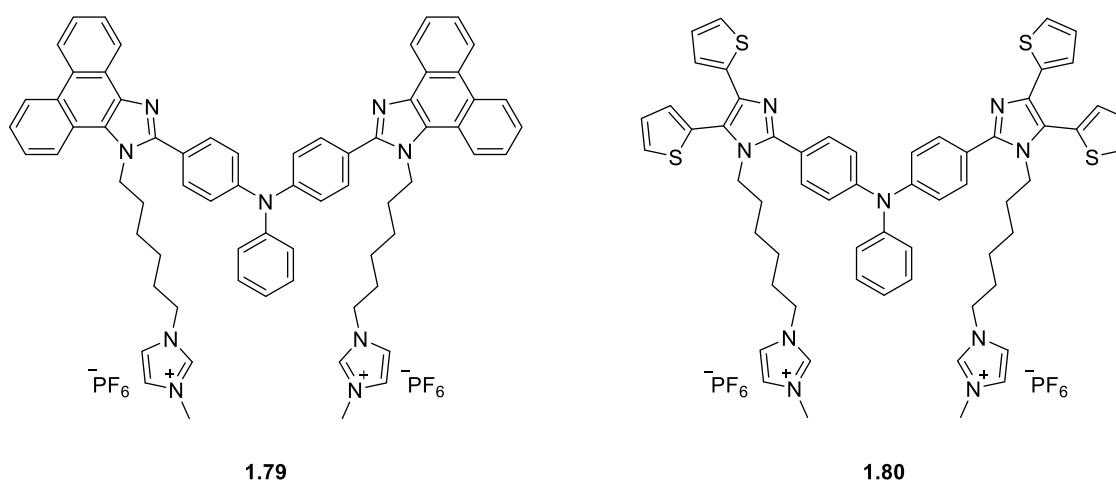


Figure 37: V-shaped acceptor-donor-acceptor emitters investigated by Choe and co-workers’.

1.8.3 Host-Guest Small Molecule LECs

Host-guest type LECs have previously been introduced as devices that incorporate a blend of a semi-conductor host with small concentrations of an emitting guest molecule. To add to this the layer may also contain solid electrolyte, n-doping, and p-doping materials. This can make the fabrication of such layers difficult as ideal concentrations of the constituent materials need to be established however, these efforts have produced the best performing small molecule LECs to date.

An early example of the effectiveness of small molecule host-guest LECs was presented by Su and co-workers' in 2011.⁴⁸ The group use a ionic NIR dye **1.82** as a charge carrying host material and iridium complex **1.81** as the guest emitter. The two materials were selected due to their frontier molecular orbital energies, specifically they possessed similar LUMO energies but emitter with a significant energy offset in the HOMO energy levels. The significantly higher HOMO energy of guest **1.82** impedes hole transport whilst the similar LUMO energies leaves electron transport unaffected. This choice was made to address previously observed imbalances in charge transport.⁹⁶ Four different types of LEC devices were fabricated with various concentrations of host material **1.82**, 0.00, 0.01, 0.10 and 1.00 % by weight. With the concentration of 0.01 % by weight the peak EQE and maximum luminance of the device reached 12.75% and 114 cd m⁻².

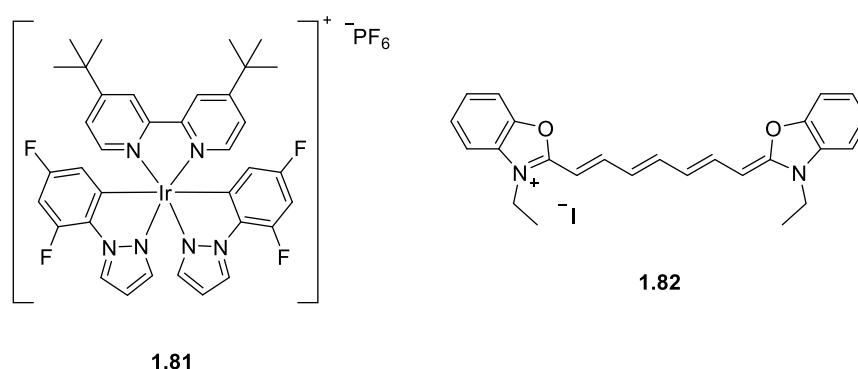


Figure 38: Guest ionic iridium complex (**1.81**) and host ionic NIR dye (**1.82**) introduced by Su and co-workers'.

In the following years a lot of progress was made in the development of host-guest small molecule LECs with an outstanding example being reported by Niu and co-workers' in 2022.⁹⁷ Here, carbazole-based TADF emitter **1.83** along with a host blend of polyvinyl carbazole (**1.07**) and OXD-7 (**1.09**) were used with added electrolyte tetrahexylammonium tetrafluoroborate to formulate an active layer. Concentrations of the guest emitter **1.83** were varied, and performance analysed until an ideal 18% by weight device was produced. This device boasted extremely good performance producing green electroluminescence at 533 nm with an exceptional maximum brightness of 3696 cd m⁻² and impressive EQE of 7.67%. At this point in time this represented the best performing TADF LEC to date.

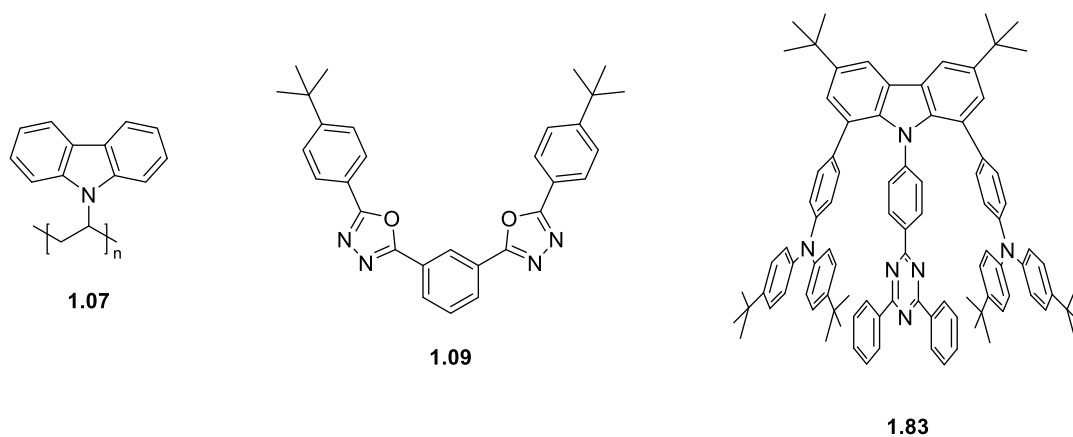


Figure 39: Structures of host materials, poly(9-vinylcarbazole) (**1.07**), OXD-7 (**1.09**), and carbazole-based TADF emitter presented in the work of Niu and co-workers’.

Yao and co-workers’ continued the development of host-guest small molecule LECs following on with the use of TADF emitters.⁹⁸ This work deviated from approaches previously introduced however, as the group looked to exploit the so-called TADF-sensitized fluorescent (TSF) strategy. This strategy integrates a TADF sensitizer with a rapid RISC rate that can more efficiently convert triplet excitons into singlet excitons, these excitons can then be transferred to a TADF emitter with high radiative transition rates for efficient emission.⁹⁹⁻¹⁰² Carbazole based TADF emitter **1.84** was implemented into an LEC device along with TADF sensitizer **1.85**, polyvinyl carbazole, OXD-7 and tetrahexylammonium tetrafluoroborate (ideal ratios were found to be 52.2 wt.% polyvinyl carbazole, 34.8 wt.% OXD-7, 3 wt.% tetrahexylammonium tetrafluoroborate, 8 wt.% **1.85** and, 2 wt.% **1.82**). This afforded a device with an EQE of 9% which was 1.5 times greater than that of LECs fabricated without TADF sensitizer **1.85** and is the highest EQE reported for a TADF LEC thus far.

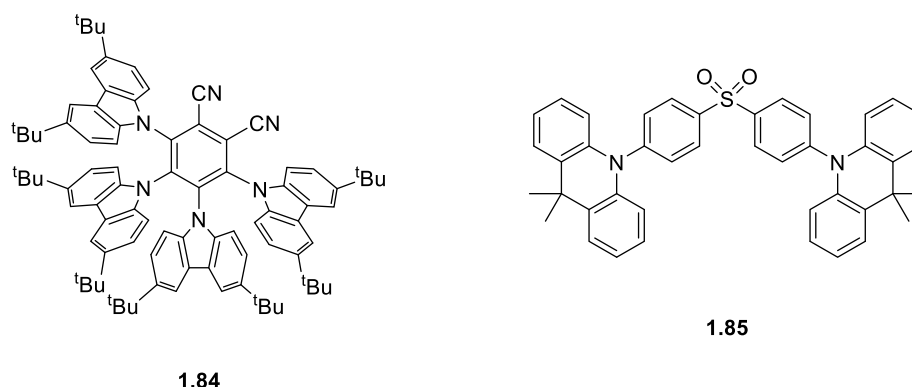


Figure 40: Carbazole-based TADF emitter and diphenylsulfone TADF sensitizer described in the work of Yao and co-workers.

Some of the best performing host-guest small molecule LECs have been introduced to provide context for the performance of the simpler neutral and ionic small molecule LECs. A

comprehensive overview of development of host-guest small molecule LECs can be found in the review of Choe and co-workers.³⁷

1.9 Conclusions and Future Perspectives

The goal of the LEC is to eliminate the need for the sophisticated multilayered structure found in conventional OLEDs.⁵⁶ Small molecule LECs have seen extensive interest and development over the last 25-30 years and are beginning to become an efficient and competitive technology. Recent research has seen a fragmentation of interests between the exceedingly simple ionic and neutral small molecule LECs, which typically limit the number of components in the active layer, and the more complex host-guest type LECs which see the integration of various materials. Host-guest LECs currently enjoy superior results however, considering the added complexity of the fabrication, the results are not necessarily congruent with this effort.

Ionic small molecule LECs seem to present an opportunity as the single-component active layer leads to incredibly simple, easy to fabricate and potentially low-cost devices. To add to this the current best performance levels of ionic small molecule LECs are not drastically outdone by state-of-the-art host-guest LECs. Furthermore, ionic small molecule LECs have not seen extensive application of TADF emitters which currently dominate host-guest LECs, presenting further prospects for improvement.

However, a shortcoming of this field seems to be the lack of molecular design strategies identified by authors in their publications. Various improvements have been noted when derivatising structures of emitters, but often little insight is given as to the reasons behind the improved performance. This presents a further opportunity as being able to outline clear reasons for differences in the performance levels of emitters and, use those reasons to formulate efficient methods for emitter design would bring a much-needed insight into the field.

Chapter 2 Polyoxometalate Anions in LECs

2.1 Background

2.1.1 The Effect of Polyoxometalate Anions on Solid-State Photoluminescence

Ionic small molecule LECs have previously been introduced, and the general trend is the use of hexafluorophosphate anions with an emissive cation. Early work in neutral small molecule LECs evaluated the influence of different doping electrolytes on active layer morphology and device turn-on times.^{103, 104} However, little research has been done to investigate the effect of different anions in ionic small molecule LECs and what has been done has focused around investigating the effects they have on electrochemical doping and device lifetimes.^{105, 106} So far, no group has sought to utilise the counter anion to affect the emissive performance of the cation.

The use of polyoxometalates with organic fluorophores is not without precedent however, the two are usually bound covalently and applied to fields such as bioimaging, catalysis or molecular switches.¹⁰⁷⁻¹⁰⁹ In 2021, Dessapt and co-workers' outlined the potential of polyoxometalate anions to affect the solid state emission intensities of associated emissive cations.¹¹⁰ The group reported that the pairing of BODIPY cation **2.01** with hexatungstate anion **2.02** produced a notable improvement in solid-state emission intensities when compared to pairing with bromide, this effect was reproduced with other polyoxometalate clusters. The effect is expected to be a result of disruption of aggregation in the solid state.

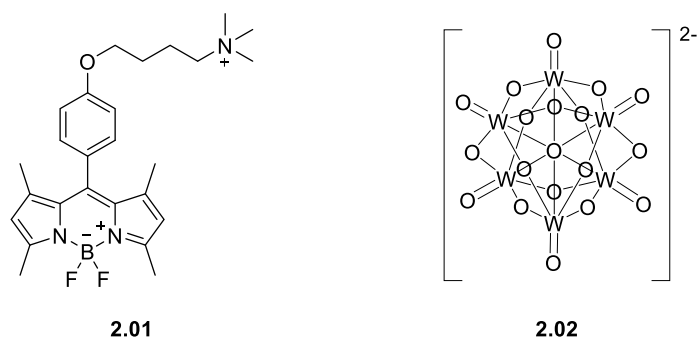


Figure 41: Emissive BODIPY cation and polyoxometalate anion used to enhance solid-state emission performance by Dessapt and co-workers'.

2.1.2 LEC Fabrication and Application to Textiles

The potential types of LEC device have also been summarized and the advantages of ionic small molecule LECs and host-guest small molecule LECs contrasted. However, so far, we have not evaluated the specific nature of the fabrication process. This is because the fabrication process

is different depending on the potential application, the active layer of choice and the processing techniques available to the group.

At the University of Southampton, our collaborators on this project, Beeby and co-workers outlined the fabrication of LEC devices onto woven textiles.¹¹¹ This process began with planarizing of the textile surface to reduce the roughness of the surface which was done by screen-printing a polyurethane layer which the undergoes UV-curing. Next, onto the smooth surface, a silver electrode was spray coated using a silver nanoparticle suspension. This step was performed under inert atmosphere to avoid oxidation of the silver. Next the transparent conductive polymer mixture PEDOT:PSS (**2.03**, Figure 42)¹¹¹ was spray coated onto the silver layer in toluene. This then allowed spray coating of the active layer which was met with initial challenges as the active layer, comprised of the electroluminescent polymer Super Yellow (**2.04**, also known as Livlux®), ion-dissolving polymer PEO and, electrolyte potassium triflate was dissolved in a mixture of cyclohexanone and toluene. The result of this was partial dissolution of the previous PEDOT:PSS layer during spray coating, however the problem was addressed by heating the textile substrate during the spray coating. Finally, the top transparent silver nanowire electrode was deposited which gave the functional LEC device integrated on a textile surface.

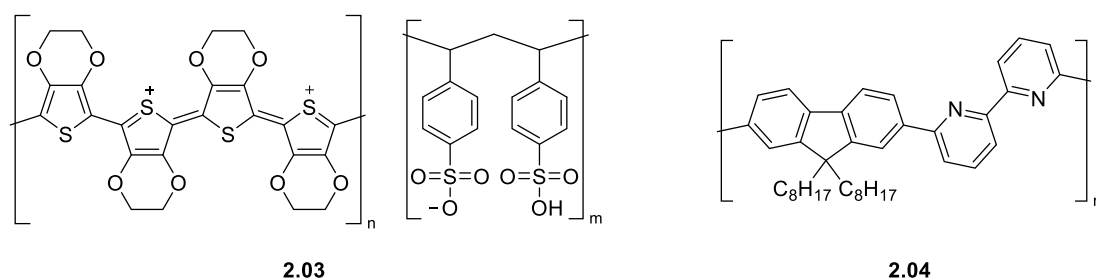


Figure 42: Structures of PEDOT:PSS (**2.03**) and superyellow (**2.04**) implemented in the work of Beeby and co-workers’.

2.1.3 Aims

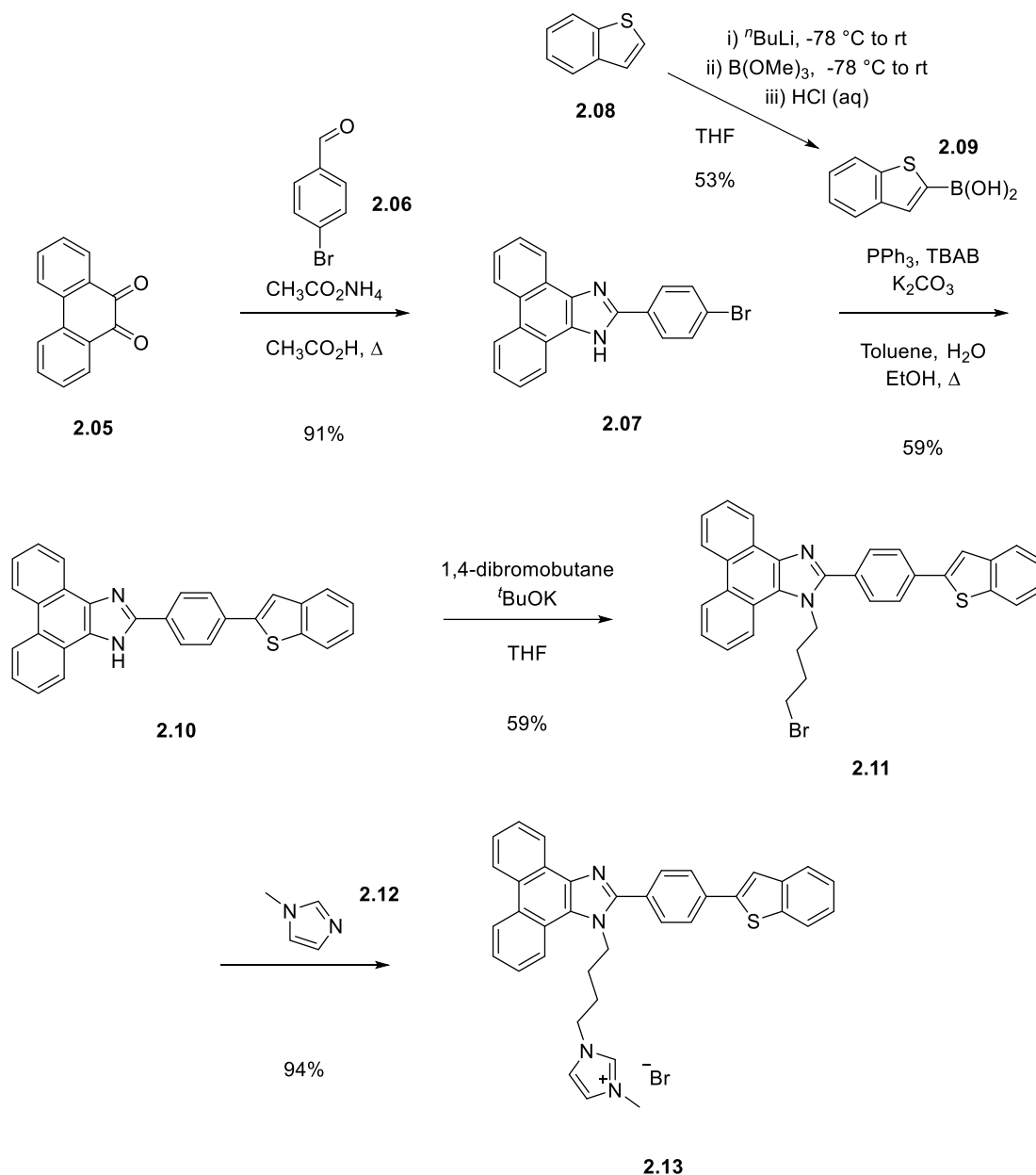
The potential of anions to play an active role in the performance of a cationic emitter has been outlined. We can see that the anion can at least affect the solid-state emission intensities of the cationic emitter but beyond this there has been little investigation of the role it can play. The consideration of the anion as a bystander in the LEC device, only contributing to the mobility of charge needs challenging however, one also must be careful not to disrupt the crucial role the ions play in the active layer. We aim to explore the more active role an anion can take and specifically apply the same improvement in solid-state emission intensities, observed in the work of Dessapt and co-workers’,¹¹⁰ to LEC devices.

The nature of the fabrication process, specifically towards the integration of LEC devices into textiles, has been introduced. We can see that there may be potential challenges with this process such as high temperature deposition of the active layers making thermal stability a factor. Also, the solution processing method itself will require reasonable solubility of the active layer materials in suitable solvents. However, the potential to apply ionic small molecule emitters to this type of device presents opportunities to simplify the fabrication process. Furthermore, the application of TADF type emitters, in-line with current trends in frontier research, presents the chance to improve the performance of these e-textiles.

2.2 Phenanthroimidazole-Polyoxometalate Emitters

2.2.1 Synthesis

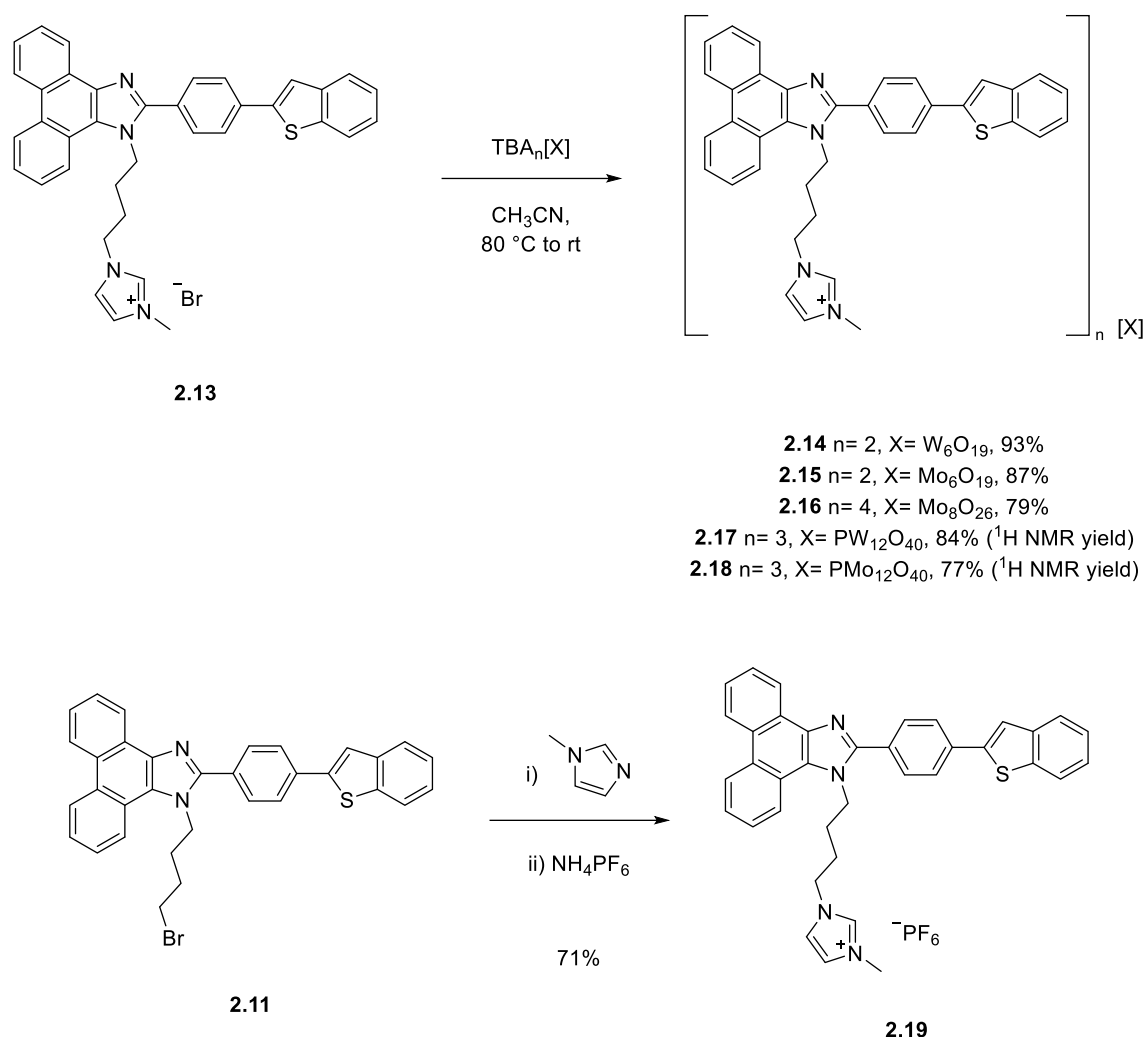
The starting point for our investigation was the synthesis of a suitable small molecule cation to pair with polyoxometalate anions. We selected the phenanthroimidazole system outlined in the work of Choe and co-workers' due to its impressive performance, application in non-doped ionic LECs, its blue emission (a rarer colour from high performance devices) and finally its convergent synthesis that offers the potential of easy derivatisation.¹¹² Synthesis began with the reaction of phenanthrenequinone (**2.05**) with 4-bromo-benzaldehyde (**2.06**) in the presence of excess ammonium acetate which formed phenanthroimidazole **2.07** in high yields (Scheme 3). Then Suzuki coupling with the prepared benzothiophene-2-boronic acid (**2.09**) yielded the conjugated donor-acceptor type backbone **2.10**. Alkylation of the imidazole ring by an S_N2 type reaction followed by reaction with 1-methylimidazole furnished the desired bromide salt **2.13**. This was prepared by adaptation of methods outlined by Choe and co-workers'.¹¹² This preparation worked well on small scale however when trying to scale up the reaction for our next steps problems were encountered during purification of both **2.10** and **2.11**. These materials were simply too insoluble for purification by column chromatography in the described eluent system (hexane/ ethyl acetate). In the end, both recrystallisation and column chromatography in THF-hexane proved a lot more successful.



Scheme 3: Synthesis of ionic phenanthroimidazole emitter **2.12**.

The isolation of the bromide salt **2.13** was followed by the investigation of a series of anion-exchange reactions to produce polyoxometalate salts to be evaluated for solid-state emission. Exchange reactions were performed on bromide salt **2.13** with a series of five tetrabutylammonium (TBA) salts of polyoxometalates (Scheme 4). Due to the likelihood of lower solubility of the newly formed salts, it was expected that the ion exchange reaction would occur readily with precipitation of the phenanthroimidazole-polyoxometalate salts acting as the driving force for the reactions. This was the generally observed case and thus dissolving the bromide salt **2.13** in a minimum amount of hot acetonitrile and adding the desired TBA-polyoxometalate salt in a hot saturated solution produced the phenanthroimidazole-polyoxometalate salts **2.14 - 2.18** in good yields. The confirmation of anion exchange in these reactions could conveniently be observed by ^1H NMR. The absence of TBA as well as a characteristic shift of the three imidazolium protons was observed upon exchange. As a reference structure would be needed to evaluate the

impact of our polyoxometalate anions on emitter performance the hexafluorophosphate salt was also targeted. A one-pot reaction of alkyl bromide **2.11** with 1-methylimidazole (**2.12**) followed by anion exchange by addition ammonium hexafluorophosphate afforded the hexafluorophosphate salt **2.19**.



Scheme 4: Anion exchange reactions.

Problems were encountered however when exchanging the Keggin-type polyoxometalates (heteroatom-containing, $\text{PW}_{12}\text{O}_{40}$ and $\text{PMo}_{12}\text{O}_{40}$). In these cases, the products of the reactions retained relatively large amounts of TBA. This was determined by NMR and is expected to be a result of either incomplete exchange, thus isolation of the polyoxometalate with a mixture of TBA and phenanthroimidazole emitter associated, or simply an inability to remove TBA bromide, the by-product in these exchange reactions. We were informed of inherent difficulties removing TBA bromide from certain polyoxometalate structures by the Errington group at the University of Newcastle, the providers of the TBA-polyoxometalate salts. Attempts to purify these compounds by numerous washes, trituration and precipitation experiments proved unsuccessful therefore yields were calculated by ^1H NMR spectroscopy using an internal standard.

2.2.2 Optical Properties

Absorption and emission data were collected in solutions of DMF using the HORIBA Duetta™ absorption emission spectrometer with Hellma Collect Absorbance/Transmission Cuvette QS/QG Quartz with path length of 10 mm. Samples were prepared at concentrations of approximately 0.025 mg/mL and the varying concentration between samples was accounted for by the plotting of molar absorption coefficient in absorption plots and the normalisation of emission data. The excitation wavelength employed for emission measurements was 350 nm. For compounds **2.14** – **2.19** a characteristic broad absorption was observed between 260 nm and 390 nm (Figure 43b and c). The major observed absorption bands for **2.14** – **2.18** were at 270, 334 and 362 nm, these are expected to be attributed to the π - π^* transitions of the main donor-acceptor backbone. Similar absorption was observed for **2.19**, at 272, 332 and 362 nm. From this absorption data the energy gap for compounds **2.14** – **2.19** was estimated to be 3.24 eV (this is the average value; all band gaps were within ± 0.02 eV of this value). This was calculated using the Tauc plot method.

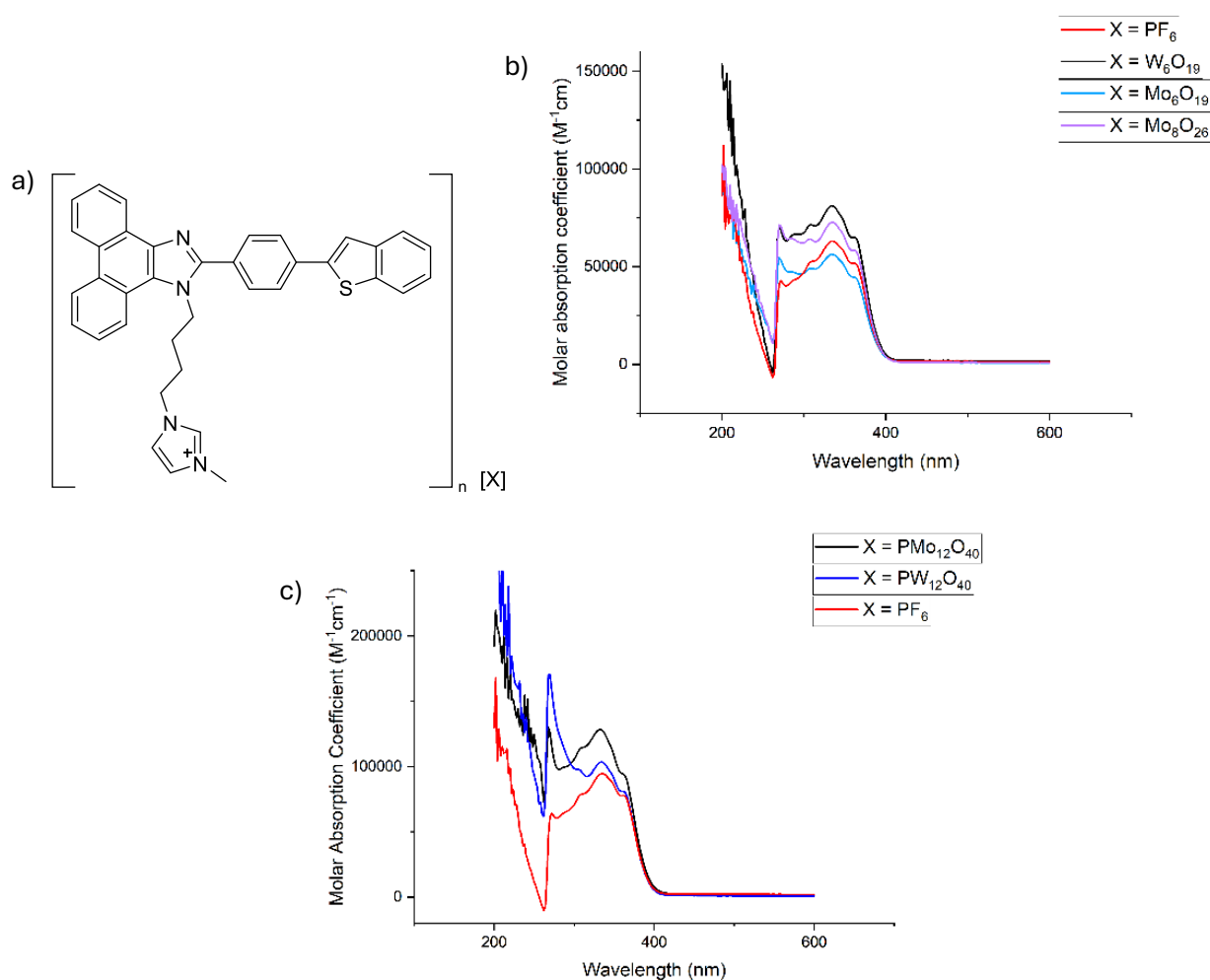


Figure 43: a) Structure of ionic phenanthrimidazole based salts, b) Molar absorbance of **2.14** – **2.16** and **2.19** in DMF, c) Molar absorption of **2.17** – **2.19** in DMF.

Fluorescent emission for compounds **2.14** – **2.19** was measured in DMF and all salts showed a single emission peak at 442 nm (Figure 44). It should be noted that relative fluorescence was plotted however, these intensities were not adjusted for absorbance hence no comparison can be made about the solution emission performance. This is not a problem as we are not investigating emission performance in solution. The observed single emission peak in both polyoxometalate salts and the hexafluorophosphate salt is a positive result as we wanted to confirm that the polyoxometalate anions were not interacting in any way that could lead to quenching of emission. The other notable observation to be made here is the translation of multiple absorption peaks to a single emission peak in all our compounds. Typically, it might be expected that each major absorption be reflected by an independent emission peak. However, here we see a relatively broad single emission peak. One possible reason for this is the aggregation of the emissive molecules in solution. Such aggregation causes restricted molecular motion and reduced non-radiative energy dissipation affecting emission wavelengths. This can result in new emission peaks being observed or can result in broad emission peaks like we see in our plots.¹¹³ In our case it may be that we see multiple broad emission peaks that are overlapping giving the illusion of a single emission peak.

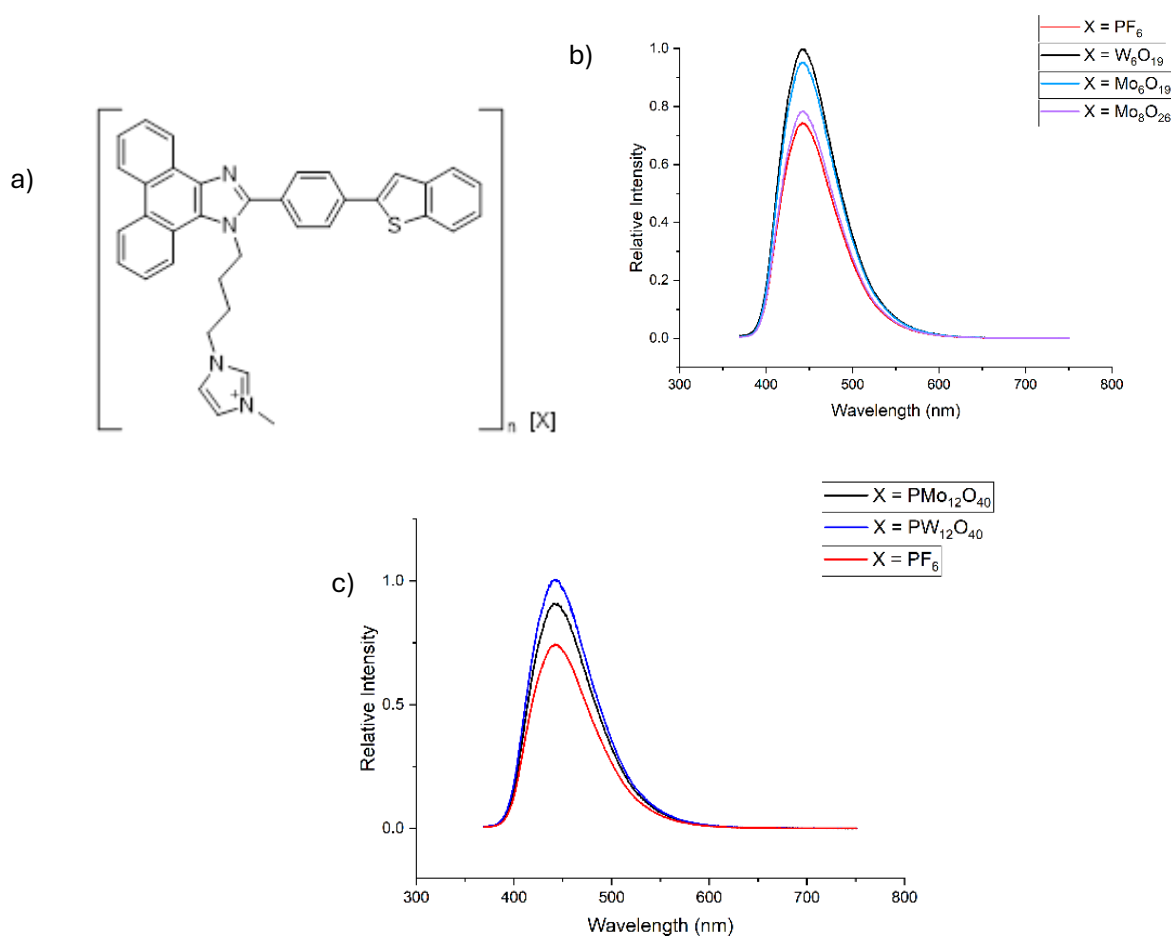


Figure 44: a) Structure of ionic phenanthrimidazole based salts, b) Relative fluorescence intensities of **2.14** – **2.16** and **2.19** in DMF. c) Relative fluorescence intensities of **2.17** – **2.19** in DMF.

2.2.3 Electrochemical Properties

The electrochemical properties of compounds **2.14** – **2.16** and **2.19** have been investigated using cyclic voltammetry (Figures 45 - 48). Cyclic voltammograms were recorded using a 3-electrode configuration with SCE as reference electrode at 100 mV s^{-1} , with a glassy carbon (3 mm \varnothing) working electrode and a Pt counter electrode in degassed unstirred dry DMF with 100 mmol Et_4NBF_4 and 5 mmol of the analysed compound. The optical energy levels of the HOMO and LUMO were examined from the collected data. The HOMO energy level was calculated by equation 6, where E_{ox} is the oxidation onset voltage.

$$6. \text{ HOMO} = -(E_{\text{ox}} + 4.40) \text{ eV}^{112}$$

The oxidation onset voltage was measured to be 1.21 V therefore the HOMO energy calculated to be -5.61 eV. This allows us to calculate an experimental LUMO energy using the HOMO energy as well as the bandgap calculated from the absorption data. In this case, we get an experimental LUMO energy of -2.37 eV. Alternatively, we can calculate the LUMO energy from the reduction onset voltage using equation 7. The onset voltage of reduction was measured to be -1.88 eV which gives a LUMO energy of -2.53 eV and the resulting bandgap would 3.08 eV (this is the average value; all band gaps were within $\pm 0.04 \text{ eV}$ of this value). Both experimentally calculated bandgaps seem to underestimate the bandgap of our compounds however, this is a common problem with the Tauc method known to occur when materials show non-ideal optical behaviour.¹¹⁴ Alternatively the use of CV data is generally seen as a rough approximation due to it actually measuring redox potentials which relate to charge transfer reactions, not the actual orbital energies involved in the band gap.¹¹⁵

$$7. \text{ LUMO} = -(E_{\text{red}} + 4.40) \text{ eV}$$

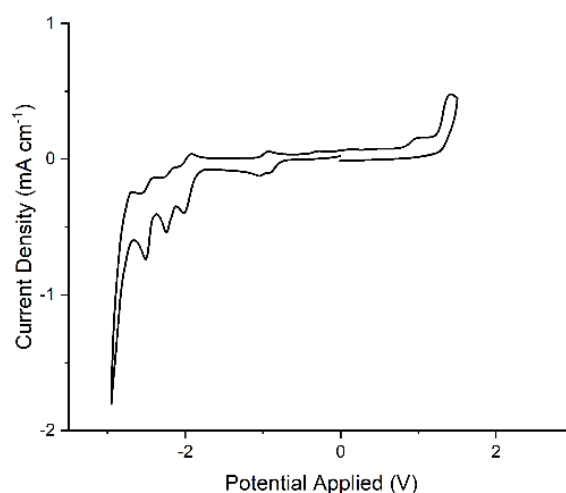


Figure 45: Cyclic voltammogram of **2.14**.

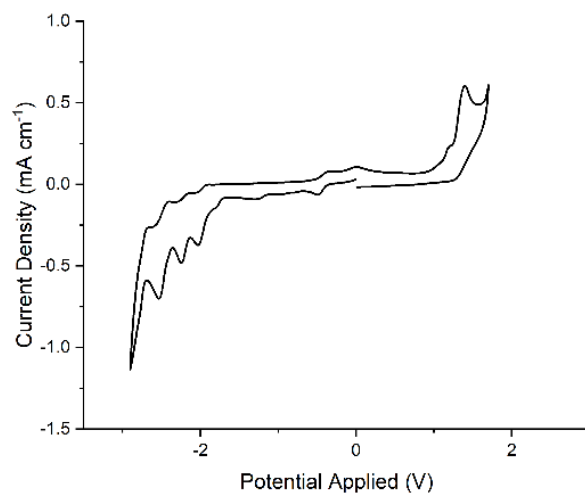


Figure 46: Cyclic voltammogram of **2.15**.

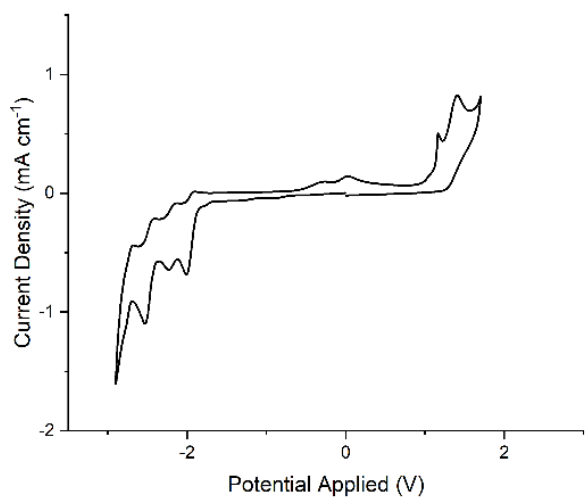


Figure 47: Cyclic voltammogram of **2.16**.

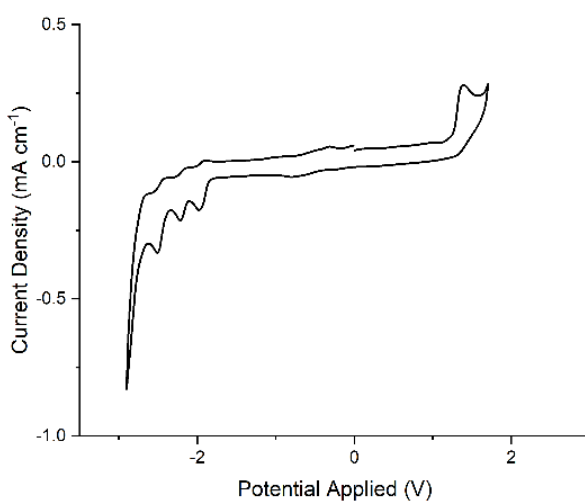


Figure 48: Cyclic voltammogram of **2.19**.

2.2.4 Solid-state Photoluminescent Properties

Solid-state photoluminescent absorption and emission measurements were performed using a Thorlabs-supplied 340 nm laser (M340L4) with a power output of 53 mW (minimum) and 700 mA served as the excitation source for photoluminescence emission which was lowered to 500 mA when analysing polyoxometalate containing compounds. An adjustable Collimation Adapter (SM2F32-A) featuring a Ø2" Lens with AR Coating and a wavelength range of 200 nm–700 nm was used in conjunction with the 340 nm laser source for photoluminescent absorption measurements. Measurements were performed on spray-coated films. The coated film on a glass ITO slide possessed a thickness of 250 nm.

The pivotal part of our work with polyoxometalate anions centred around the potential ability of the polyoxometalates to enhance the performance of our emissive cations in solid-state. To establish whether this was the case, solid-state absorption and emission data was collected (Figure 49). The performance of phenanthroimidazole-polyoxometalate salts **2.14** – **2.16** and phenanthroimidazole-hexafluorophosphate salt **2.19** was investigated. Compounds **2.17** and **2.18**, containing the Keggin-type polyoxometalates were not analysed as the potential contamination with TBA bromide could interfere with any conclusions about their performance. The solid-state absorption of compounds **2.14** – **2.16** and **2.19** was characteristically broad with absorbance between 200 and 400 nm. This presented little to distinguish the compounds which is theoretically a positive as we expect the cationic emitter, that is the same in each salt, to be responsible for absorption. However, it is notable the molybdenum containing compounds show slightly diminished absorbance above 300 nm although the reasoning for this is unclear.

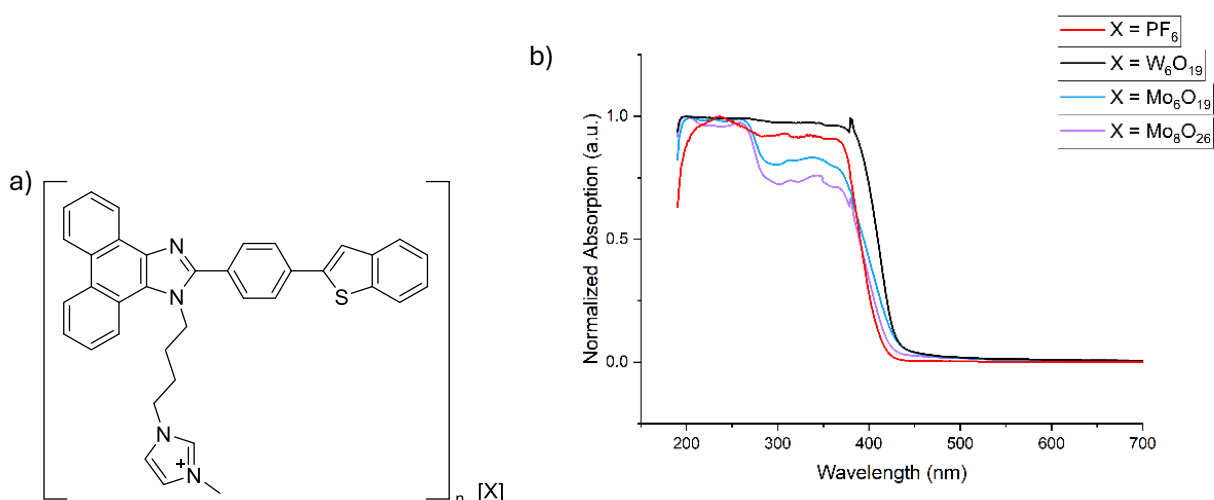


Figure 49: a) Structure of ionic phenanthroimidazole based salts, b) solid-state absorption of **2.14** – **2.16** and **2.19**.

Photoluminescent emission data was then collected to facilitate a comparison of emission intensity with and without an associated polyoxometalate anion. In general, we can see that

polyoxometalate containing compounds **2.14** – **2.16** show more intense emission than the hexafluorophosphate analogue **2.19** (Figure 50). Direct comparison cannot be established from the data presented here as the strength of the excitation source was reduced for measurements of polyoxometalate salts **2.14** – **2.16**. This is due to the polyoxometalate containing compounds **2.14** – **2.16** being less absorbing of the excitation laser than sample **2.19** which can be rationalised by the fact that the thin-films of compounds **2.14** – **2.16** are more than fifty percent, by weight, polyoxometalate. These anions do not absorb at this energy which meant the strength of the excitation source had to be reduced to avoid saturation of the detector. This manifests in large emission peaks observed at 343 nm which belong to the excitation source (Figure 50c). Here we can draw the conclusion of more intense emission observed in the polyoxometalate containing compounds despite lowering in strength of the excitation source. This could represent enhanced solid-state emission due to the presence of polyoxometalate anions however changing the strength of the detector may have an unknown effect.

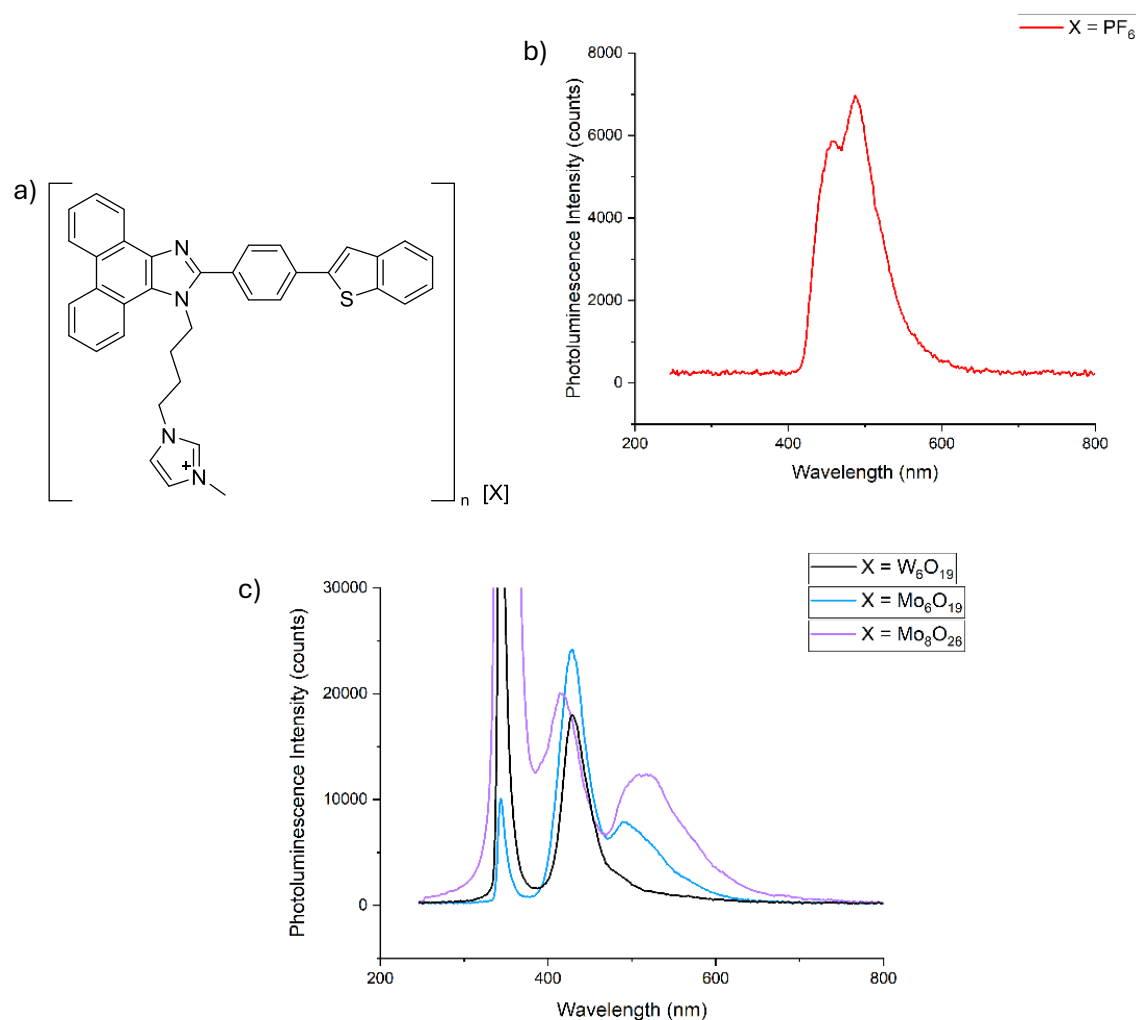


Figure 50: Structure of ionic phenanthrimidazole based salts, b) solid-state photoluminescence of **2.19**, c) solid-state photoluminescence of **2.14** – **2.16**.

The next thing to be noted is the red-shifted emission of the phenanthroimidazole-hexafluorophosphate salt **2.19** when compared to its solution emission. A shift in the emission wavelength from solution to solid-state is not uncommon and is to be expected due to the significant intermolecular forces in closely packed solids that are likely to impact HOMO and LUMO energies. However, in this case we see a significant shift with the photoluminescent emission wavelength of 489 nm. This differs drastically from compounds **2.14** – **2.16** that show major emission at 429 nm which is much closer to what was expected. To add to that literature compound, that only differs from ours by an extra two carbons in the pendant alkyl chain, is reported to have a photoluminescent emission of 435 nm.¹¹²

It can be very difficult to predict and rationalise differences in wavelengths as ideas on the matter are difficult to prove. For example, in this case it may be the four-carbon pendant alkyl chain is the perfect length to allow the imidazole ring to bend back on the structure and have π -stacking or dipole-dipole type interaction with one part of our structure (Figure 51). The electron-rich nature of this ring may be substantial enough to stabilise the HOMO or destabilise the LUMO which would reduce the bandgap in the molecule resulting in a redshift. The significant difference in photoluminescent emission wavelength with the hexafluorophosphate anion compared to when the polyoxometalates are used could be a result of the large polyoxometalate anions disrupting this effect in those structures. We do see a still very prevalent secondary emission peak in **2.19** at 430 nm where the described conformational effect may not be present.

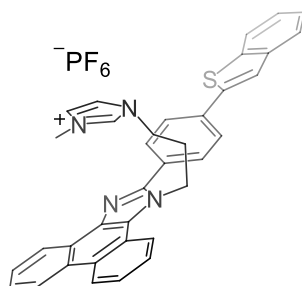


Figure 51: Potential conformer of compound **2.19** in solid-state.

Another point about the photoluminescent emission data acquired is that the molybdenum-containing polyoxometalate salts **2.15** and **2.16** show a dual-emission character which is somewhat unexpected. From the solution emission data (Figure 44b) we thought we had established a lack of quenching of our emission by the polyoxometalate anions. This was expected to be the case due to the large bandgaps generally observed in polyoxometalates.¹¹⁶ However, the solid-state photoluminescent data for hexamolybdate salt **2.15** shows major emission at 429 nm but also red-shifted emission at 493 nm. A similar, more pronounced, situation is present in octamolybdate salt **2.16** that shows major emission at 415 nm with a red-shifted emission also at 517 nm. A potential explanation for this would be that we have some of our cationic emitter, associated to the polyoxometalate anion, in a different conformation like

was suggested for compound **2.19**. This idea is unlikely however due to the absence of such a peak in the photoluminescent emission spectrum of hexatungstate salt **2.14**. Interaction of the polyoxometalate species with the emitter could lead to quenching of emission by electron transfer from the excited cationic emitter to the polyoxometalate resulting in non-radiative decay and there is precedent for such an effect outlined in the literature (Figure 52).¹¹⁷ This effect would likely be limited to the molybdenum containing salts due to the smaller HOMO-LUMO energy gap for molybdenum type polyoxometalates compared to that of the tungsten containing structures.¹¹⁸ However, this does not explain the secondary emission peak as emissive relaxation from the polyoxometalate through charge recombination, similar to the exciplex outlined in Figure 26, is without precedent.

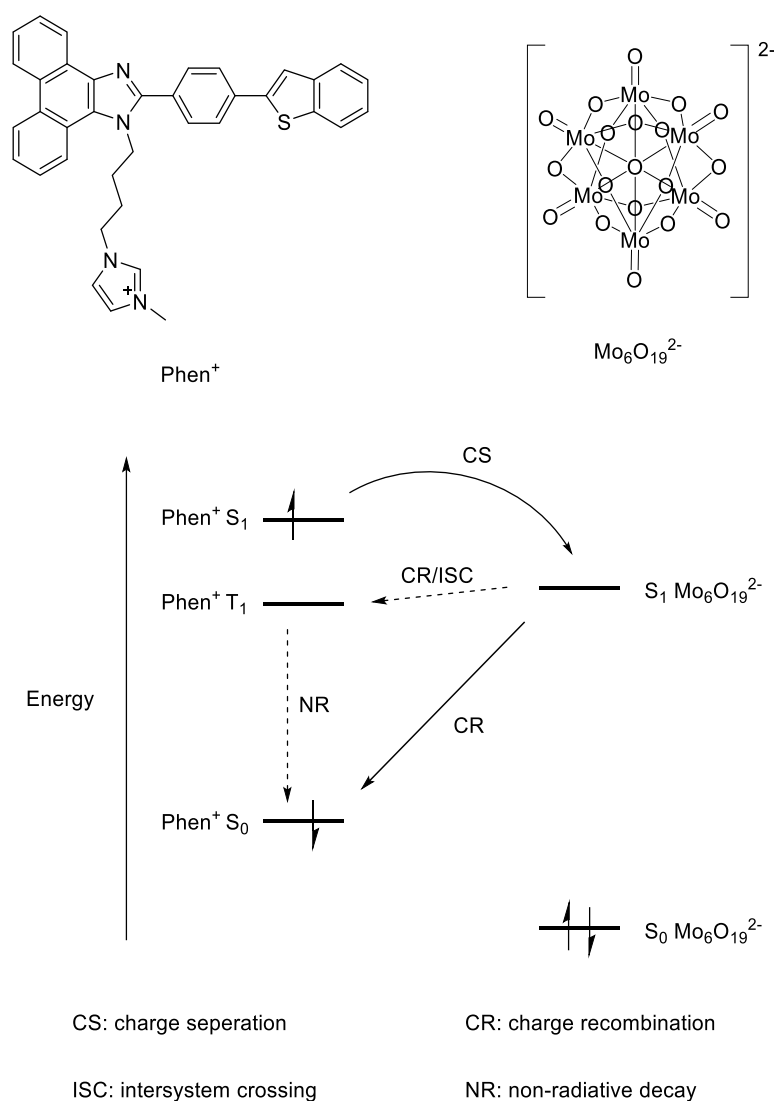


Figure 52: Non-radiative decay pathways that may influence the emissive character of molybdenum containing salts **2.15** and **2.16**.

2.2.5 LEC Fabrication and Testing

With our ionic emitters synthesised and the improvement of solid-state photoluminescence performance observed when pairing with polyoxometalate anions, we could now move on to integration of the emitters into an LEC device. Devices were fabricated by our collaborators at the University of Southampton; Katie Court, Yi Li and Sasikumar Arumugam working under the supervision of Prof. Stephen Beeby.

This process began with the washing of an ITO glass slide with deionised water and acetone followed by UV ozone treatment in sequence to remove any surface contamination. A PEDOT:PSS suspension in water was then spin coated directly on the ITO slide and annealed on a hotplate at 120 °C for 20 min. Spin coating of the active layer followed which used DMF solutions of our ionic emitters with varying concentrations due to the relative solubility of each emitter (desirable solubility was 0.2 g/mL). We had to use DMF as opposed to the favoured acetonitrile for this process due to the low solubility of our emitters in acetonitrile. Annealing of the spin coated active layer was undertaken at 70 °C for 5 h in a nitrogen filled box oven. The silver top electrode was then sputter coated through a pre-defined shadow mask and finally the device encapsulated with an epoxy-resin.

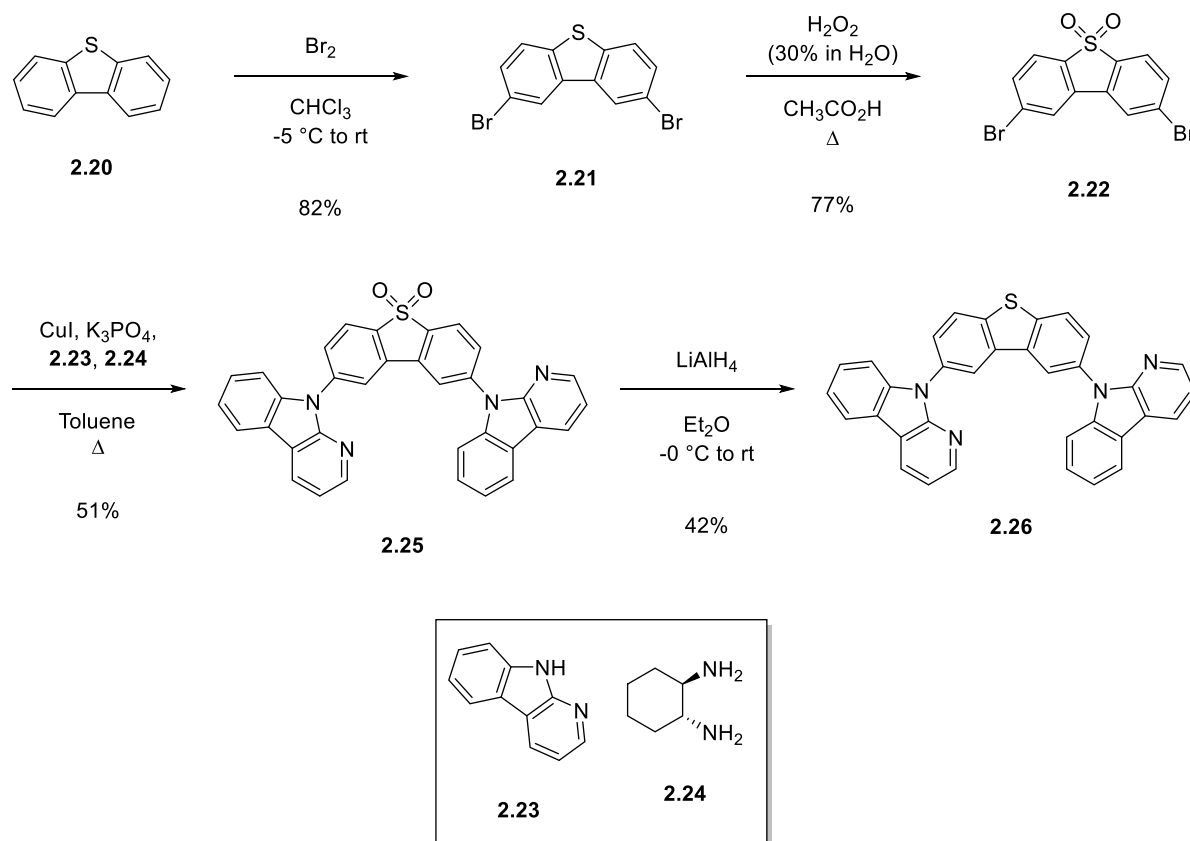
Testing of the formulated devices disappointingly resulted in only one working device for phenanthroimidazole-hexatungstate salt **2.14** out of nine fabricated. This device showed very weak emission at approximately 500 nm. Use of the molybdenum containing salts **2.15** and **2.16** resulted in no working devices, however it was noted that the compounds were readily precipitating from the solutions before spin coating resulting in patchy layers. We did, as expected, see working devices with phenanthroimidazole-hexafluorophosphate salt **2.19** producing emission at 500 nm.

With these results we had various potential issues to address. Firstly, the poor solubility of our compounds was resulting in difficulties producing suitable film formations. Secondly, there was a prevalent reporting of devices short circuiting which may indicate the presence of moisture in the active layer, this issue may have been compounded by using the hygroscopic DMF solutions. Finally, the general poor performance from our polyoxometalate containing salts in LEC devices suggests a potential shortcoming of these anions. This may be related to the charge mobility in the device as, although our salts as a whole show redox activity, the polyoxometalate is unlikely to undergo oxidation as the metal is already in its highest oxidation state. Therefore, the spatial separation that is enhancing our solid-state emission may be hindering the movement of holes.

2.2.6 Doped Layer Formulation

Due to the likely need to change the cationic emitter in our salts to achieve improved solubility we first investigated the potential charge mobility issues in our layer. To do this we decided to fabricate LEC devices with a doped or host-guest active layer. If we found that devices were successful when hole-transport, electron transport or solid electrolyte were added to the active layer then we may be able to make deductions about the shortcomings of our ionic emitters.

To investigate this, we first needed to decide suitable host materials to pair our ionic emitters with. A commonly encountered host material is the blend of PVK and OXD-7. For our compounds PVK, which plays the role of hole transport material, is a suitable choice due to its low HOMO energy (-5.8 eV)⁴⁹ however, the use of OXD-7 as an electron transport material would be inappropriate as our emitters LUMO (-2.37 eV) is significantly higher in energy than that of OXD-7. Therefore we needed to identify a suitable replacement and this came in the form of dibenzothiophene **2.26** (Scheme 5) with a LUMO level of -2.39 eV.¹¹⁹ The electron-transport material boasted a similar LUMO energy to our cationic emitter which should result in unaffected electron transport. Synthesis of the electron-transport material started with bromination of dibenzothiophene which was followed by oxidation to the corresponding sulfone **2.22**. This step was to activate the material for the subsequent Ullmann coupling reaction with α -carboline (**2.23**). Finally, reduction of the sulfone furnished our desired electron-transport material **2.26**.



Scheme 5: Synthesis of electron transport material for host-guest active layer formulation.

A series of different doped active layer solutions were prepared to attempt to establish whether charge mobility was the main problem inhibiting our device performance (Table 1). We decided to study molybdenum containing polyoxometalate salt **2.15** due to it producing no working LECs in the first round of testing. In host-guest devices an emitter concentration of 17.8% by weight was used as that would result in a 5% by weight presence of the cationic emitter. A host blend of hole and electron transport materials as well as solid electrolyte was used in entry 1, these ratios were established from successful literature setups.⁹⁸ Apart from this formulations using only hole or electron transport material were tested as well as just doping with solid electrolyte.

Table 1: Doped active layer formulations.

Entry	Wt. % 2.15	Wt. % PVK	Wt. % 2.26	Wt. % TBABF ₄	Number of functional devices
1	17.8	48.0	32.0	2.2	1/12
2	17.8	0.0	80.0	2.2	0/12
3	17.8	80.0	0.0	2.2	4/12
4	80.0	0.0	0.0	20.0	3/12

Entries 1, 3 and 4 produced some working LECs however, the devices showed no emission and were very prone to short circuiting. The fabrication of functional LECs with these doped formulations does suggest that our polyoxometalate anions may not be suitable in the charge carrying process. The lack of emission observed with these devices indicates that the host-guest combinations maybe not be effective at trapping excited states on the guest emitter although, our goal in this work was not the production of host-guest type LECs therefore additional investigation around this idea was not conducted.

Though this progress in understanding our active layer was encouraging, issues were reported again in thin film formation. The use of DMF in the spin coating process was resulting in inconsistent formation of active layers. It was suggested that the variance in our results, such as a working device with phenanthroimidazole-hexatungstate salt **2.14** in the first round of testing and the relatively unreliable success of devices fabricated this time, may be a result of the use of DMF. We were strongly advised to switch to acetonitrile due to the uneven thin-film formation observed with our compounds (Figure 53).

The Phenom G6 ProX Scanning Electron Microscope (SEM) system was employed to capture cross-sectional SEM images of the LEC devices to assess the thickness of the functional layers.

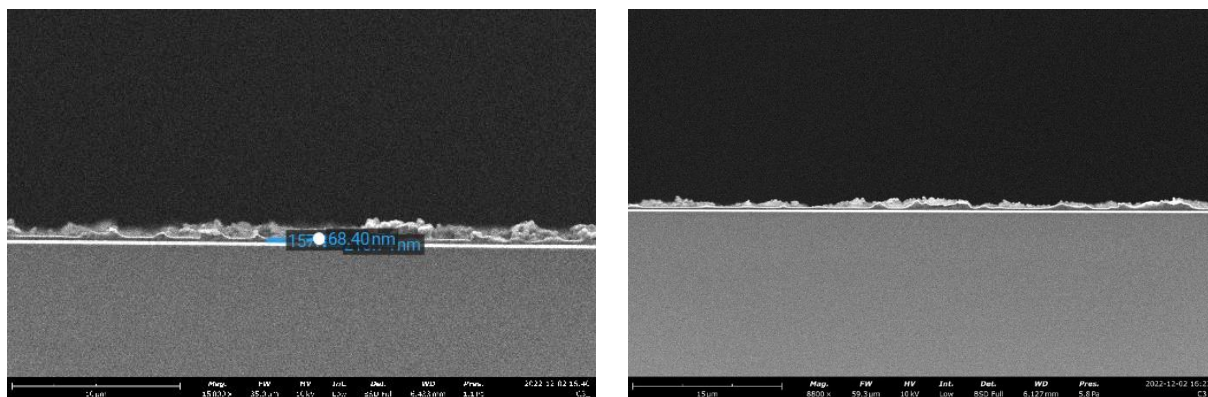


Figure 53: SEM imaging of uneven doped active layers. Left - entry 1. Right - entry 2

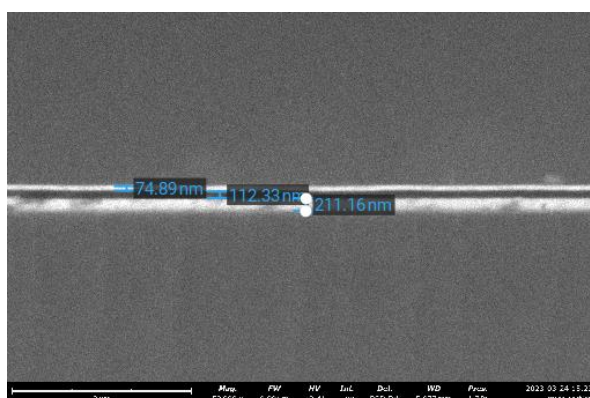


Figure 54: SEM imaging of a uniform active layer.

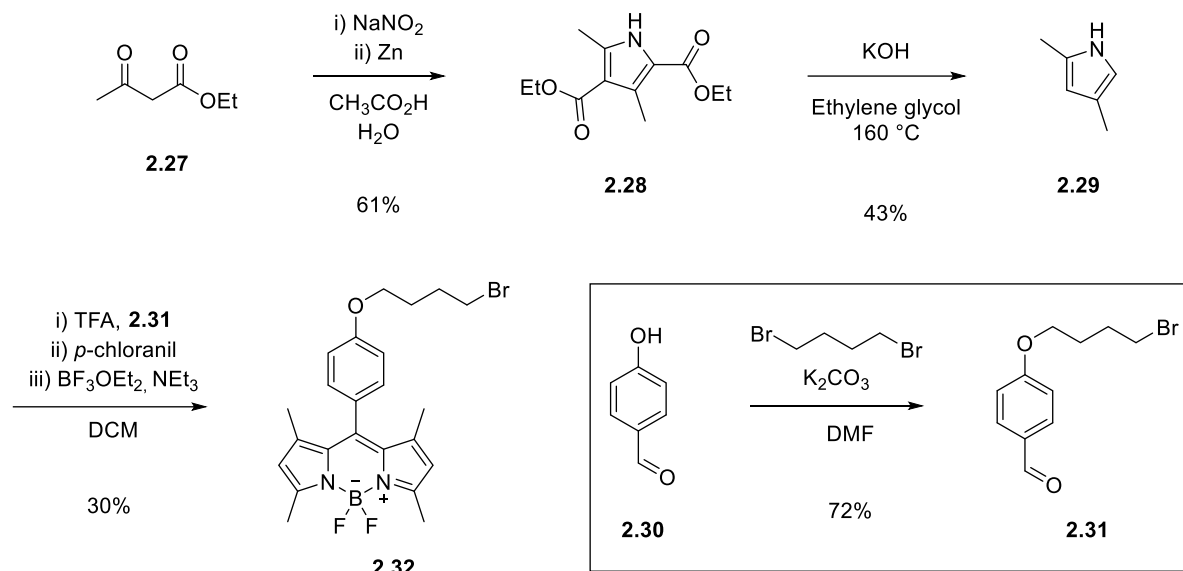
2.3 BODIPY-Polyoxometalate Emitters

2.3.1 Synthesis

To achieve higher solubility when incorporating polyoxometalate anions into emissive salts we needed to target a readily soluble cationic emitter. Along with this consideration we also wanted to target a smaller bandgap emitter with a lower LUMO energy. This was to see if this would affect the observation of a secondary emission peak when incorporating molybdenum containing polyoxometalates. In principle, if electron transfer is happening between the LUMO of our cationic emitter and the LUMO of associated anion then a lower LUMO energy in the cationic emitter would disrupt this process. We decided to target a BODIPY emitter as BODIPY's show high solubility, with some structures even exhibiting solubility in water.¹²⁰ Furthermore, BODIPY structures with emission colours ranging from blue to red have been reported making targeting a structure with a low lying LUMO trivial.^{121, 122}

Our synthesis began with the Knorr pyrrole synthesis in which we took ethyl acetoacetate (**2.27**) and reacted it with half an equivalent sodium nitrite followed by reduction with zinc (Scheme 6). The formed mixture of primary amine and remaining ethyl acetoacetate can then cyclise to form pyrrole **2.28**. Hydrolysis and decarboxylation then afforded dimethylpyrrole **2.29**. We could then

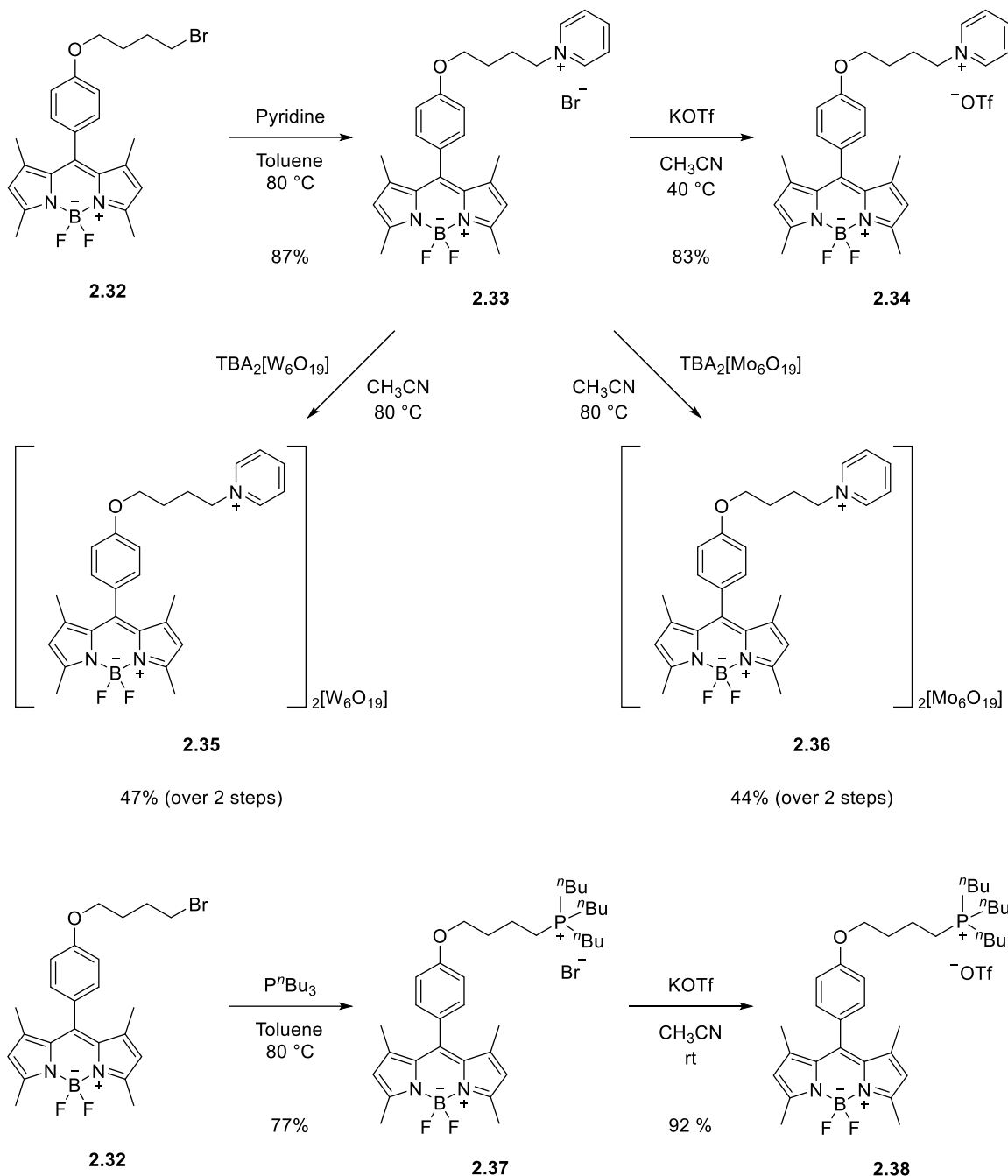
form our BODIPY moiety in a 3-step one-pot reaction, the first of these steps being the condensation of two equivalents of **2.29** with prepared the aldehyde **2.31**. This produced the corresponding dipyrromethene which was then oxidised with *p*-chloranil to convert it to the dipyrromethene, and finally complexation of boron afforded the desired alkylated BODIPY scaffold ready to be converted to a salt.



Scheme 6: Synthesis of BODIPY **2.32**.

To isolate our emissive salt we next looked to continue with the synthesis outlined by Dessapt and co-workers',¹¹⁰ this was to substitute the alkyl bromide of **2.32** with trimethylamine. However, to our surprise attempts to substitute with this nitrogen nucleophile led to the isolation of complex mixtures seemingly a result of degradation. There is evidence of instability of BODIPYs in alkaline solution, where hydrolysis of the nitrogen-boron bonds is the first step of degradation that can ultimately lead to the recovery of mono-pyrrole products.¹²³ Our attempted approach did employ aqueous solutions of trimethylamine so we assumed this could be our problem. We initially tried to switch to organically soluble nitrogen nucleophiles like triethylamine and *N*-methyl morpholine, but again complex mixtures were obtained. Believing the base strength of the nucleophile may be our issue we then tried pyridine and tri-butyl phosphine and pleasingly we found success with this method.

Substitution reactions on alkylated BODIPY **2.32** with pyridine and tributyl phosphine proceeded smoothly to afford bromides salts **2.33** and **2.37** (Scheme 7). Anion exchange was performed with potassium triflate to provide our reference ionic BODIPY emitters **2.34** and **2.38**. Reaction of bromide salt **2.33** with TBA salts of our polyoxometalates resulted in incomplete exchange in the first attempts however, putting the reaction back on a second time afforded our desired BODIPY-polyoxometalate salts **2.35** and **2.36**, albeit with diminished yield due to the initial isolation.



Scheme 7: Synthesis of BODIPY-triflate emitters (**2.34** and **2.38**) and BODIPY-polyoxometalate emitters (**2.35** and **2.36**).

2.3.2 Optical Properties

Absorption and emission data were collected in solutions of acetonitrile using the HORIBA Duetta™ absorption emission spectrometer with Hellma Collect Absorbance/Transmission Cuvette QS/QG Quartz with path length of 10 mm. Samples were prepared at concentrations of approximately 0.025 mg/mL and the varying concentration between samples was accounted for by the plotting of molar absorption coefficient in absorption plots and the normalisation of emission data. The excitation wavelength employed for emission measurements was 350 nm

Analysis of our salts optical properties revealed consistent results with no variation between triflate and polyoxometalate anions or between terminal pyridine or phosphine cations. All salts displayed a sharp absorbance at 502 nm in DMSO with emission being found at 517 nm (Figure 55b and d). This represented a prominent green emission in solution.

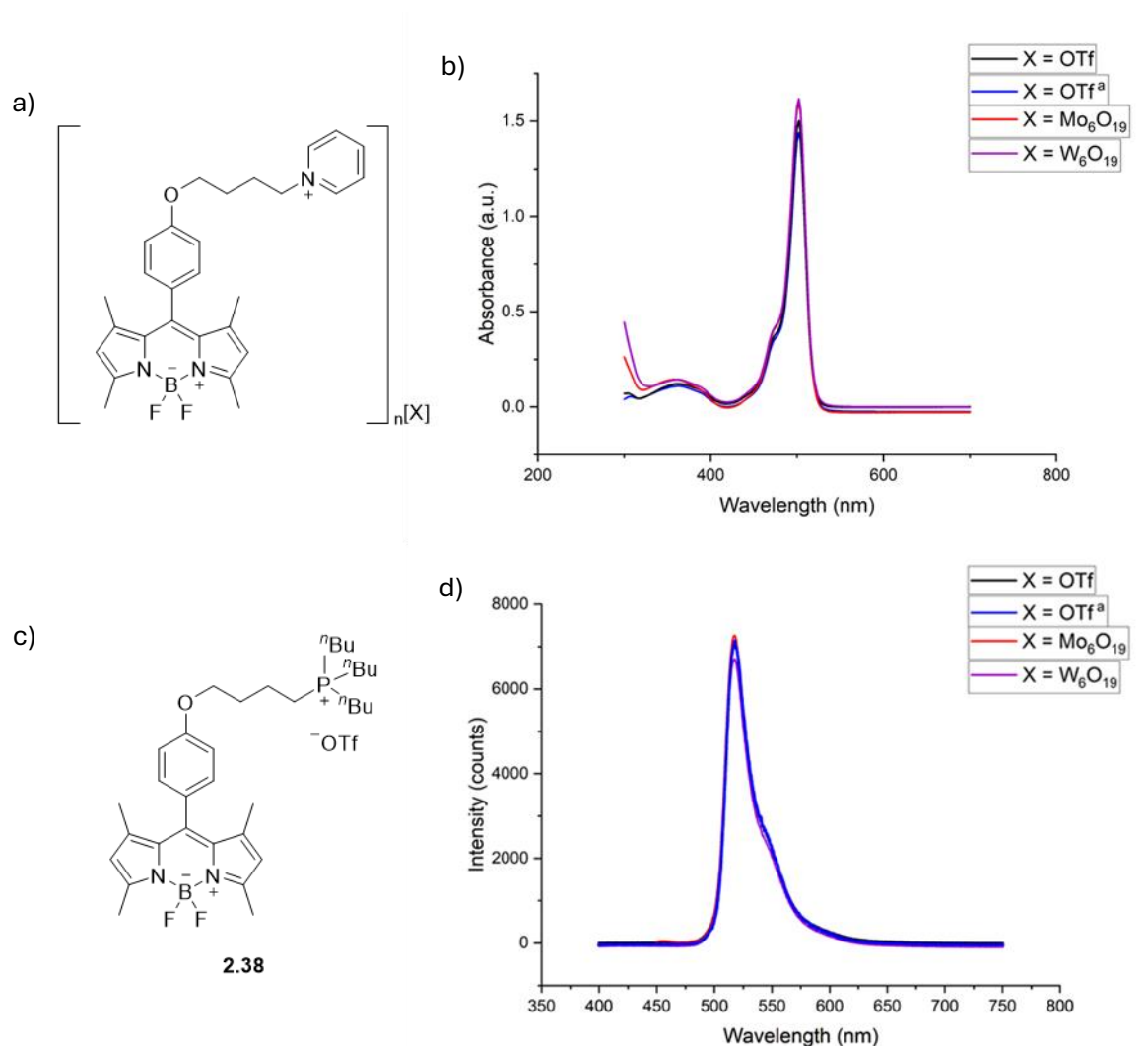


Figure 55: a) Structure of emissive pyridine containing BODIPY salts, b) absorbance of salts **2.34** - **2.36** and **2.38** in DMSO, c) structure of emissive phosphine containing BODIPY salts, d) emission of salts **2.34** - **2.36** and **2.38** in DMSO. ^a Phosphine-BODIPY cation.

2.3.3 Photoluminescent Properties

Solid-state photoluminescent absorption and emission measurements were performed using a Thorlabs-supplied 340 nm laser (M340L4) with a power output of 53 mW (minimum) and 700 mA served as the excitation source for photoluminescence emission which was lowered to 500 mA when analysing polyoxometalate containing compounds. An adjustable Collimation Adapter (SM2F32-A) featuring a Ø2" Lens with AR Coating and a wavelength range of 200 nm–700 nm was used in conjunction with the 340 nm laser source for photoluminescent absorption

measurements. Measurements were performed on spray-coated films. The coated film on a glass ITO slide possessed a thickness of 250 nm.

We next looked to examine the photoluminescent properties of our ionic emitters to establish if the improvement of emissive performance, when pairing with a polyoxometalate anion, was maintained. This trend indeed continued with our polyoxometalate salts routinely outperforming our reference triflate salts (Figure 56b and d). All compounds showed similar emission wavelengths between 570 nm (**2.35**) and 585 nm (**2.38**) which represents yellow emission. The only compound with a prevalent secondary emission peak was our pyridinium-triflate salt **2.34**. This is expected to be due to conformational variance in which the pendant pyridinium can affect the bandgap of the emissive BODIPY as was previously suggested for **2.19** (Figure 51). We fabricated phosphonium emitter **2.38** to attempt to test this theory as a non-aromatic pendant group will not have π -stacking interactions that facilitate the proximity of the pendant group to the emissive core. We can see that phosphonium emitter **2.38** does not possess such a broad emissive profile which supports our idea.

Also of note is the absence of a secondary, red-shifted, emission peak in our molybdenum containing salt **2.36**. We hypothesised that using a cationic emitter with a lower LUMO energy would inhibit any electron transfer between cation and anion. As we see no red-shifted emission it represents a small amount of evidence supporting emissive charge recombination in molybdenum containing salts **2.15** and **2.16**.

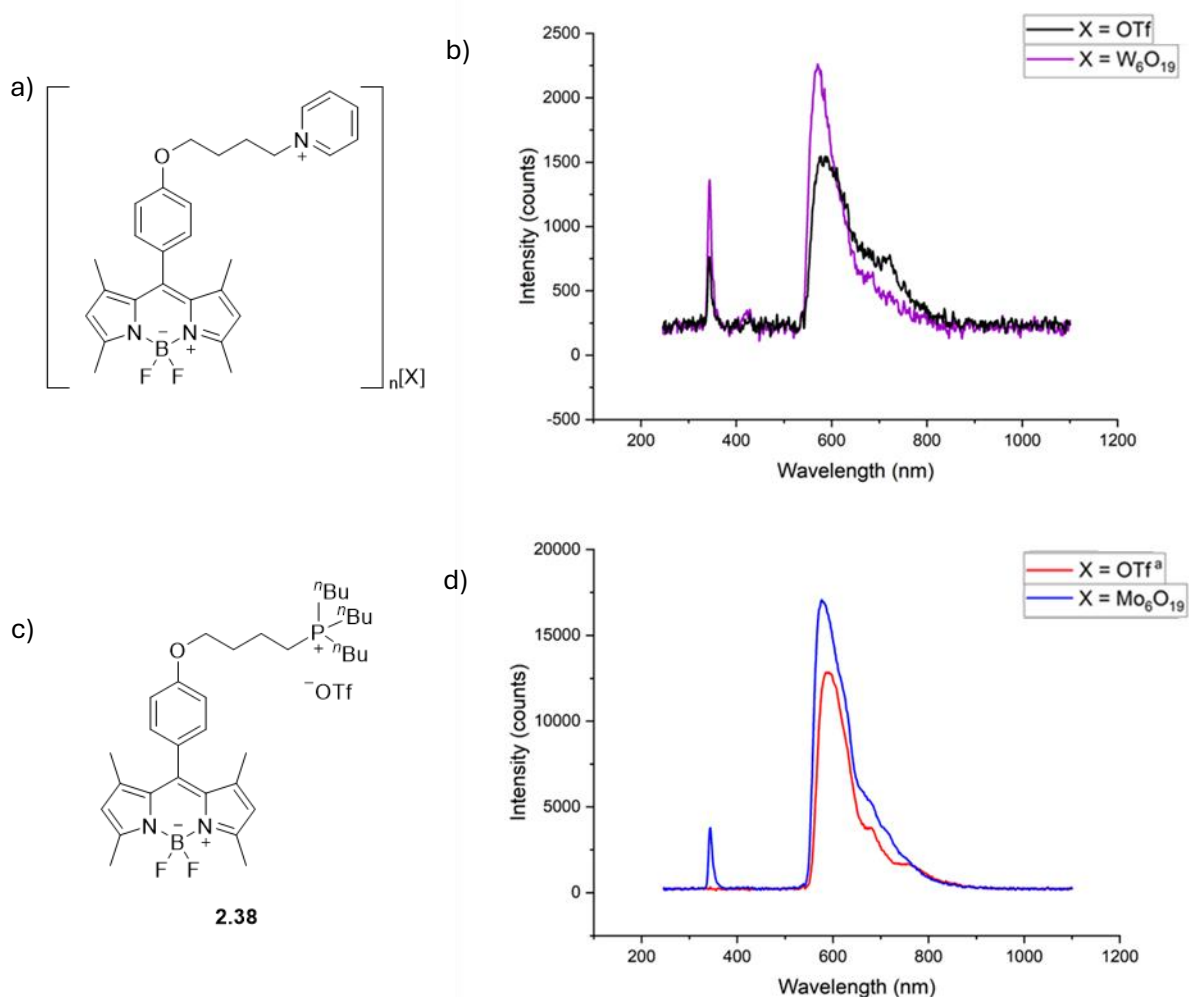


Figure 56: a) Structure of emissive pyridine containing BODIPY salts, b) solid-state photoluminescence of salts **2.34** and **2.35**, c) structure of emissive phosphine containing BODIPY salts, d) solid-state photoluminescence of salts **2.36** and **2.38**.^a

Phosphine-BODIPY cation

2.3.4 LEC Fabrication and Testing

LEC devices were fabricated by the same method outlined in section 2.2.5. This time, as was our aim, we managed to spray coat our active layers in acetonitrile due to the much-improved solubility of the BODIPY cation. This resulted in significantly better thin-film formation, enhancing both uniformity and thickness of the layers (Figure 57).

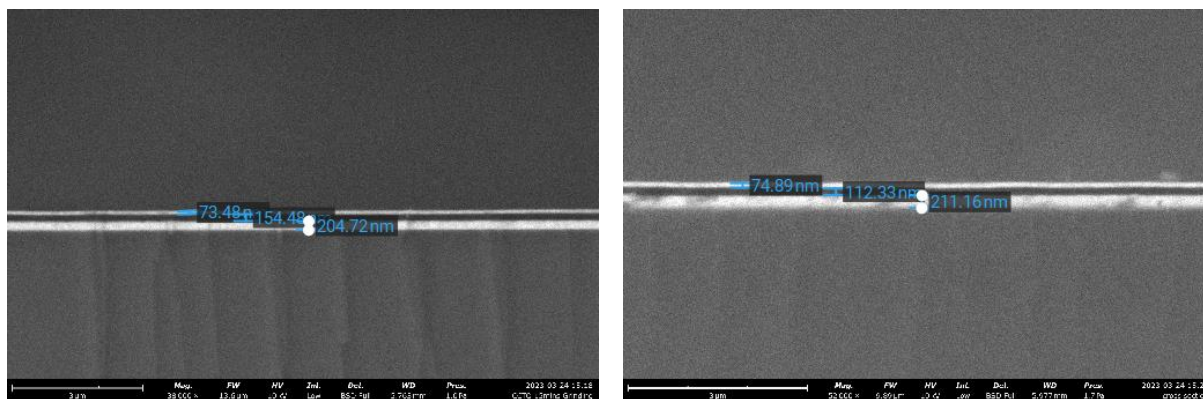


Figure 57: SEM cross-section analysis of active layers. Left – BODIPY-triflate salt **2.34**. Right – BODIPY-hexatungstate **2.35**.

Sadly, the resulting performance of the fabricated devices was like that of our first tested devices. The devices employing BODIPY-triflate **2.34** in its active layer were consistently functional with 7 out of 9 of the fabricated devices producing emission. Electroluminescence was observed at 603 nm revealing orange emission (Figure 58). Devices fabricated using BODIPY polyoxometalate salts **2.35** and **2.36** produced no working cells conclusively proving that the issue was not the use of DMF in fabrication but more likely the charge carrying potential of our counter anions. Finally, devices employing our BODIPY-phosphonium cation also produced functional cells (4 out of 12) however the emission from these devices was too weak to capture.

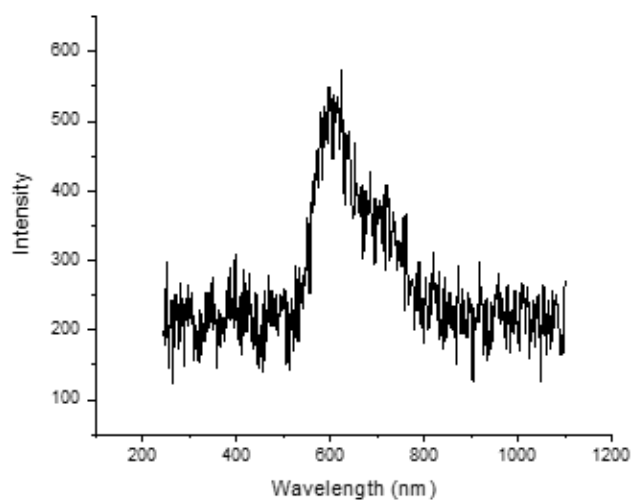
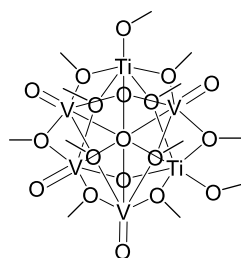


Figure 58: Electroluminescence of BODIPY triflate **2.34**.

2.4 Conclusions and Future Perspectives

We have successfully synthesised various novel, polyoxometalate containing emissive salts. These ionic emitters have demonstrated enhance solid-state emission that is expected to be a result of disruption of aggregation in the solid-state. The large polyoxometalate anions effectively space the cationic emitters away from each other reducing the concentration quenching effect commonly observed in solid-state emission. We have investigated the optical, photoluminescent and electrochemical properties of our emitters and studied physical properties such as solubility and thermal stability. Finally, our study led us to the implementation of our novel materials into LECs. In this research we have realised the shortcomings of our polyoxometalate anions in this technology with their inability to effectively support the movement of holes in the active layer being the principle suspected reason behind the failure of our devices.

The theory that our polyoxometalates cannot facilitate hole injection suggests the need for a redox active polyoxometalate that could potentially perform the way we desire. Such systems are rare however recently, the development of redox active vanadium clusters for application to redox flow batteries may have provided a solution to our problem.¹²⁴⁻¹²⁶ These clusters show reversible oxidation and reduction with electrochemical stability making them suitable candidates for our work. Unfortunately, such materials are usually only prepared by a handful of people worldwide therefore we could not investigate the application of these clusters to our work.



2.39

Figure 59: Structure of redox active vanadium polyoxometalate cluster.

Chapter 3 Carbazole-Based TADF Emitters

3.1 Background

3.1.1 4CzIPN

We have previously outlined the effectiveness of TADF type emitters when applied to host-guest small molecule LECs. However, the application of such emitters to ionic light emitting electrochemical cells remains seldom. At the point of undertaking this work, TADF emitters had been thrust into the spotlight due to their continuing improved performance in both OLEDs and LECs. One of the most prominent TADF emitter to see application to these devices during this time was the carbazole-based emitter 4CzIPN (**1.10**, Figure 59). Edman and co-workers published twice with this emitter, first in 2017, with the fabrication of a device employing guest emitter 4CzIPN with host material *p*-CBP (**3.01**).¹²⁷ The LEC demonstrated a maximum brightness of 760 cd m⁻². Then, in 2019, the group published a host-guest LEC device utilising emitter 4CzIPN, host blend of PVK and OXD-7, and solid electrolyte tetrahexylammonium hexafluorophosphate. This device achieved a peak luminance of 430 cd m⁻² with an EQE of 1.8%.⁴⁹

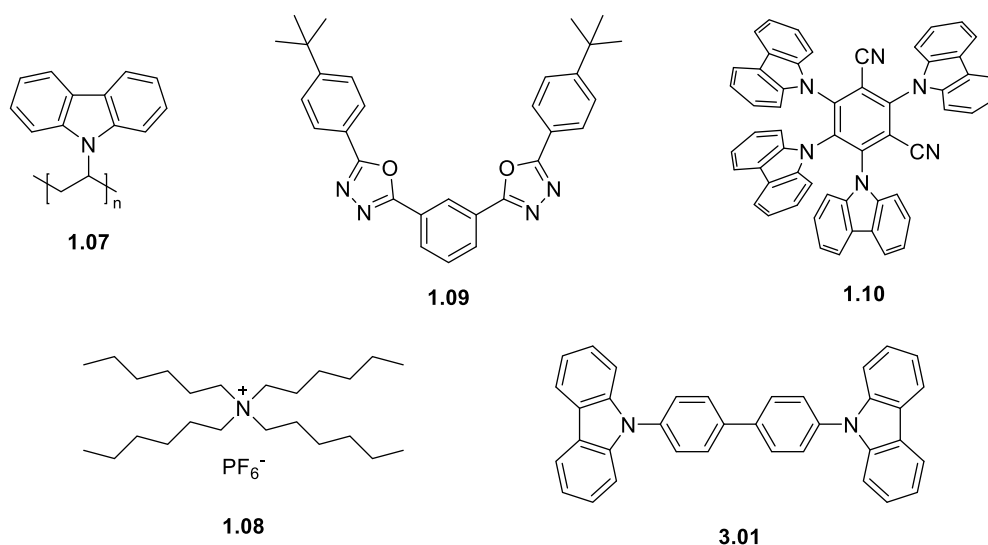
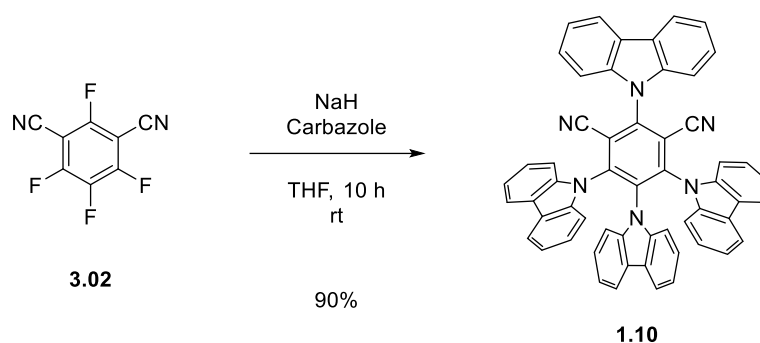


Figure 59: Structure of 4CzIPN (**1.10**), PVK (**1.07**), tetrahexylammonium hexafluorophosphate (**1.08**), OXD-7 (**1.09**), *p*-CBP (**3.01**).

Furthermore, in the field of OLEDs 4CzIPN has seen extensive application. Kido and co-workers reported OLEDs with 13.0% EQE at a luminance of 1000 cd m⁻² when using this emitter.¹²⁸ Then later continued their work achieving an EQE of 25.7% at a luminance of 1000 cd m⁻², again using 4CzIPN as their emitter.¹²⁹ Various other investigation has been done in the application of this emitter to OLEDs.¹³⁰⁻¹³²

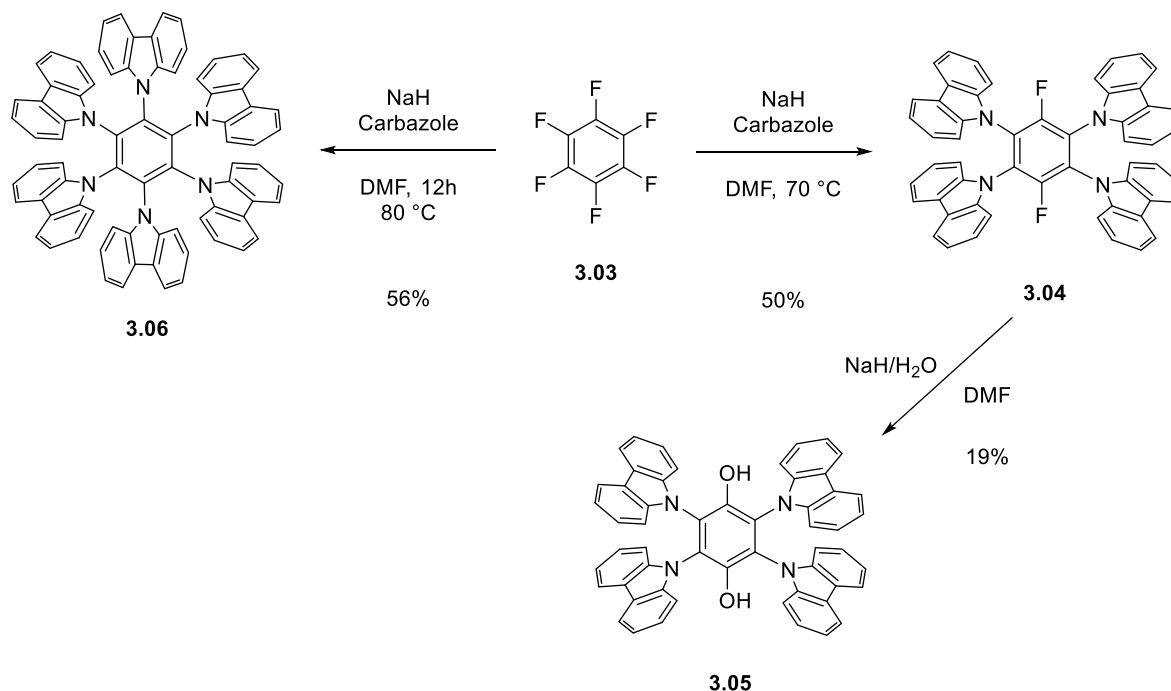
3.1.2 S_NAr Reactions on Polyfluorinated Aromatics

Such TADF emitters as 4CzIPN are often synthesised by nucleophilic aromatic substitution (S_NAr) reactions on polyfluorinated aromatics. These reactions are somewhat well explored however, substituting four positions in one step has meant that the exploration of partial substitution or the selectivity of which positions substitution may favour has received less investigation. Although, this is to be somewhat to be expected due to the rare need for sequential S_NAr reactions. 4CzIPN was first synthesised by Adachi and co-workers', in 2012, by substituting the four fluorine positions of tetrafluoroisophthalonitrile (**3.02**) with carbazole in a single step (Scheme 8).¹³²



Scheme 8: Adachi and co-workers' synthesis of 4CzIPN.

A similar approach was seen in the work of Feng and co-workers when they targeted carbazole containing compounds **3.04** and **3.05** in their study of room temperature phosphorescence. These compounds were formed again by substituting four fluorine positions in a single step, this time on hexafluorobenzene (**3.03**), which gave **3.04** and further treatment with hydroxide resulted in the substitution of the two remaining fluorine's (Scheme 9).¹³³ Alternatively, in the research of Yang and co-workers' this substitution reaction was taken further with prolonged heating in an excess of carbazole and sodium hydride resulting in substitution at all six positions in a single step.¹³⁴ These investigations highlight the potential to control or limit substitution giving the ability to substitute different nucleophiles in sequential reactions.



Scheme 9: S_NAr reactions with carbazole and hexafluorobenzene (**3.03**).

Underpinning these type of substitution is the fundamental kinetic studies of Rodionov and Furin who, in 1990, studied the favoured position of substitution in these kind of sequential S_NAr reactions of polyfluorinated aromatics.¹³⁵ This study was covered well in the book chapter of Steel and indicates that substitution is observed at the position with the most ortho and meta fluorine atoms (Figure 60).¹³⁶

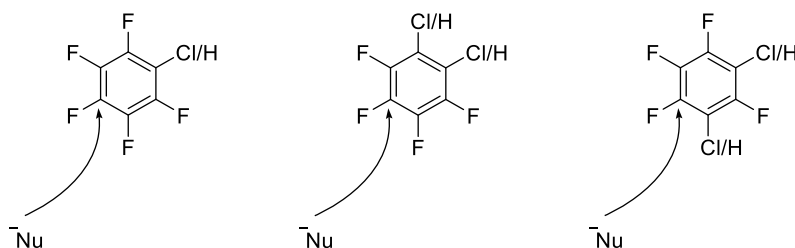
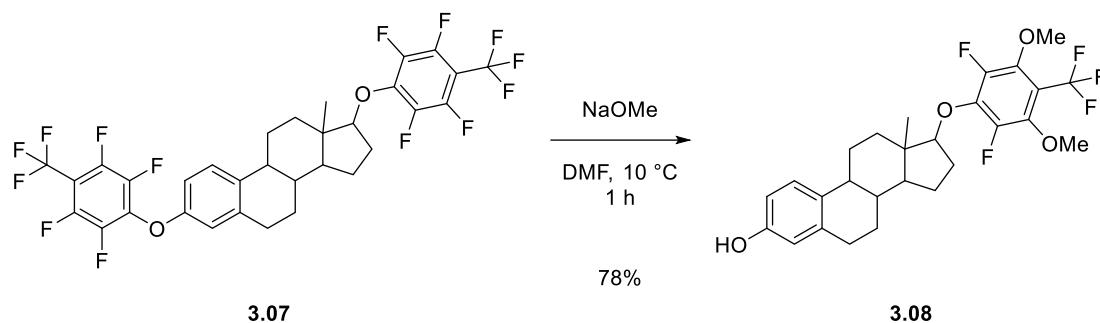


Figure 60: Preferred position of S_NAr .

A practical example of this effect was observed in the selective phenol deprotection reaction of Jarman and McCague (Scheme 10).¹³⁷ In this reaction, treatment of diol **3.07** with sodium methoxide resulted in selective cleaving of the phenolic heptafluoro-*p*-tolyl protecting group and also methoxide substitution on the reaming protecting group. The positions of substitution were ortho to one fluorine, meta to another and finally ortho to the more electron withdrawing trifluoromethyl group.



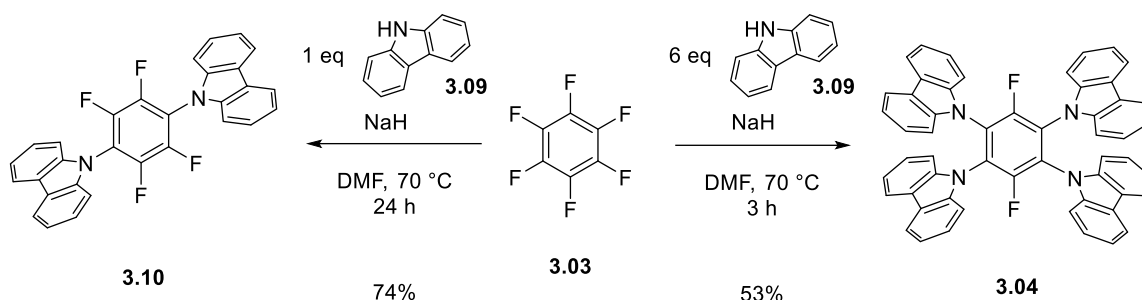
Scheme 10: Selective deprotection of phenol by Jarman and McCague.

3.1.3 Aims

The potential of TADF emitters in LECs is undeniable with some of the devices leading the way in terms of performance employing such emitters. Specifically, carbazole-based TADF emitters have seen extensive application, and their conveniently simple preparation makes them even more appealing. The ability to introduce a huge amount of complexity to a simple substrate by S_NAr reactions and the potential to control such reactions presents an opportunity to be able to create and derivatise complex emitters in minimal synthetic steps. We would like to explore the ability to control these reactions as limiting the reaction of a polyfluorinated aromatic to a single or double substitution would allow for the introduction of various nucleophiles to the same system. This creates a huge chance to tune emission wavelength and a simple way to introduce charge in the formation of the desired emissive salts.

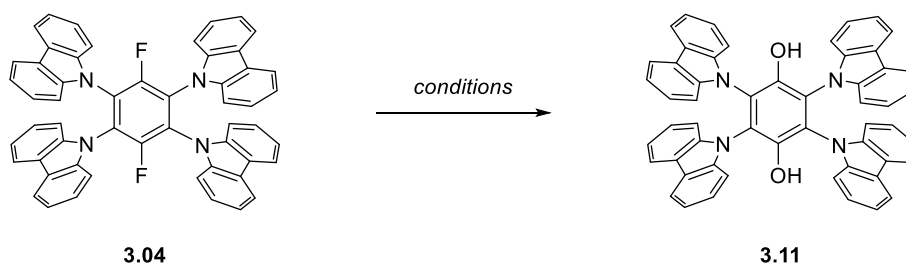
3.2 S_NAr of Hexafluorobenzene Towards Ionic Carbazole-Based Emitters

Our investigation began with the study of the hexafluorobenzene substitutions outline by Feng and co-workers.¹³³ We looked to replicate their work and establish the ability to limit the extent of substitution further. Reaction of hexafluorobenzene (**3.03**) with 6 equivalents of carbazole reliably produced the tetra substituted product **3.04** although complex mixtures, presumed to contain products with varying degrees of substitution, were observed by TLC (Scheme 11). The mixtures proved difficult to separate as poor solubility made effective separation of these closely related structures problematic by column chromatography. However, recrystallisation successfully afforded pure material that seemed to represent the major product of the reaction. We looked to limit the extent of substitution next and found that using one equivalent of carbazole was the most effective way to isolate of the di substituted product **3.10**. Attempts to limit substitution further were unsuccessful however as even using less than one equivalent of carbazole in cooled conditions saw the mixture of mono and di substituted products form within 5 minutes.



Scheme 11: SNAr reactions of hexafluorobenzene with carbazole.

With the ability to limit the degree of substitution clear, we looked to investigate the substitution of the final two fluorine atoms of **3.04**. This would allow us to functionalise hexafluorobenzene three different nucleophiles in sequential S_NAr reactions. This would be convenient as the introduction of charge through this final two positions would allow easy access to ionic emitters. Disappointingly, our attempts to replicate the hydroxide substitution outlined by Feng and co-workers¹³³ was unsuccessful. The group reported substitution even upon aqueous work up of tetra substituted product **3.04**. However, our probing (Table 2) revealed a quite unreactive nature of to these two final positions, potentially a result of steric hinderance from the bulky carbazole group or maybe due to the absence of ortho and meta-activating groups.

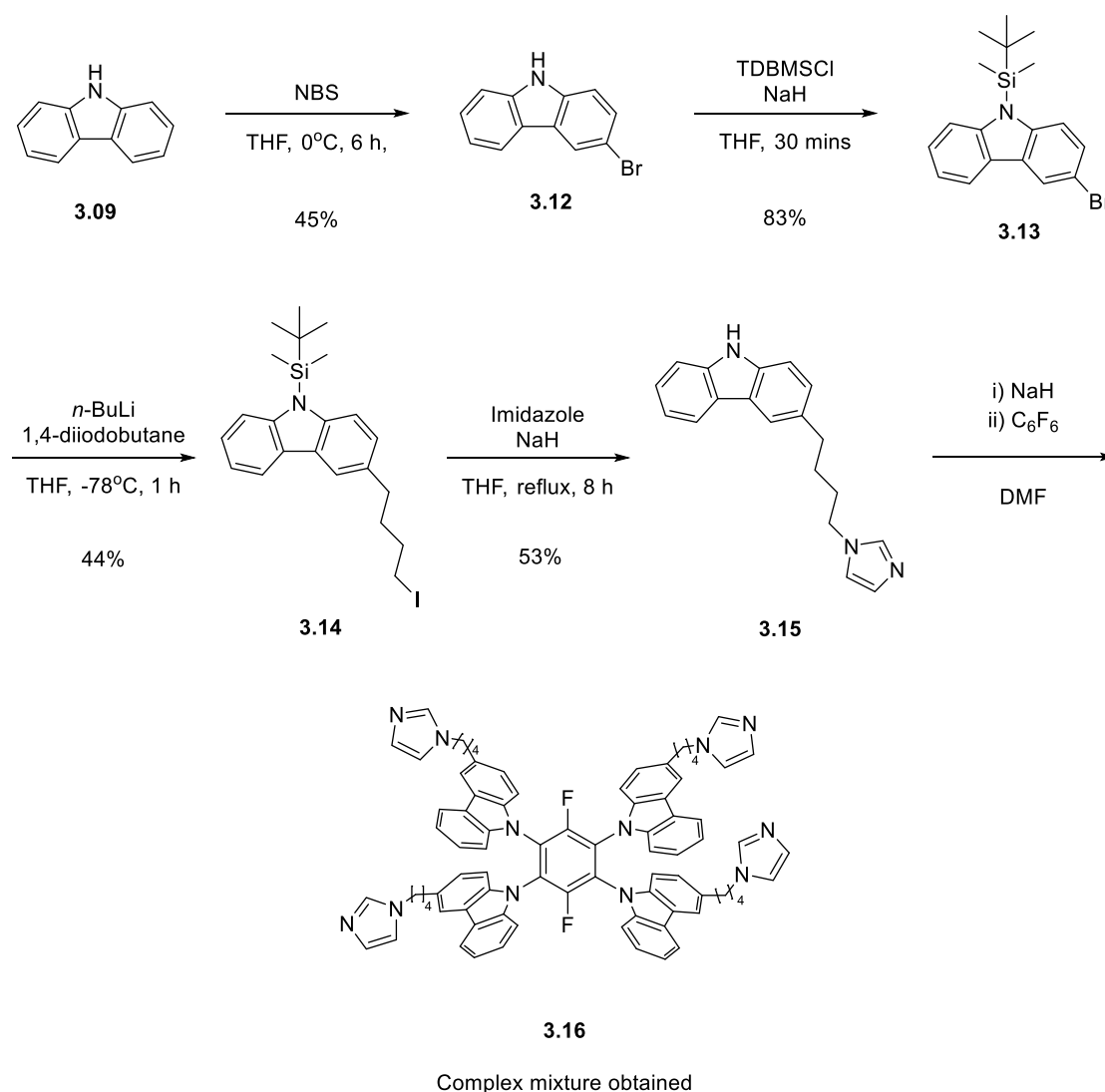


Scheme 12: Attempted SNAr reactions of tetra-carbazolyl **3.04**.

Table 2: Conditions for attempted SNAr reactions of tetra-carbazolyl **3.04**.

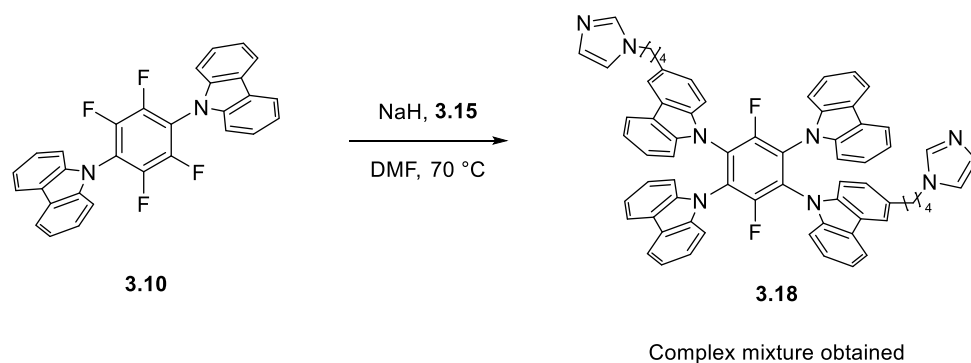
Entry	Conditions	Result (yield %)
1	NaOH, DMF, 100 °C, 7 h	tetra-carbazolyl 3.04 recovered (91%)
2	NaOH, DMF, Δ , 3 h	tetra-carbazolyl 3.04 recovered (88%)
3	NaOH, CH ₃ CN, Δ , 16 h	tetra-carbazolyl 3.04 recovered (94%)
4	NaH, MeOH, Δ , 7 h	tetra-carbazolyl 3.04 recovered (85%)
5	NaOMe (25% in MeOH), Δ , 72 h	tetra-carbazolyl 3.04 recovered (77%)

After encountering this small setback, we had to change our approach and look to introduce charge through the derivatisation of some or all our carbazole units. To do this we looked to introduce a pendant alkyl chain as was seen in the ionic TADF emitters **1.52** and **1.53** (Figure 28) explored by Wong and co-workers'.⁷⁵ This effort began with the mono bromination of carbazole (**3.09**) with NBS to afford bromocarbazole **3.12** which was then followed by nitrogen protection with the tert-butyldimethylsilyl group (Scheme 13). Subsequent lithium halogen exchange and reaction with 1,4-diiodobutane furnished alkylated carbazole **3.14**. Finally, substitution of the pendant alkyl iodide with imidazole in the presence of sodium hydride and somewhat surprising deprotection under the same conditions produced our desired imidazole bearing carbazole **3.15**. We then tried to incorporate this derivatised carbazole nucleophile by the previously explored nucleophilic aromatic substitution reaction. This however was not successful as the obtained complex mixtures were not purifiable by recrystallisation and this was expected to be the result of the conformational freedom the alkyl chains offer being counterproductive to the formation of crystals.



Scheme 13: Attempted introduction of charge via pendant alkyl chains.

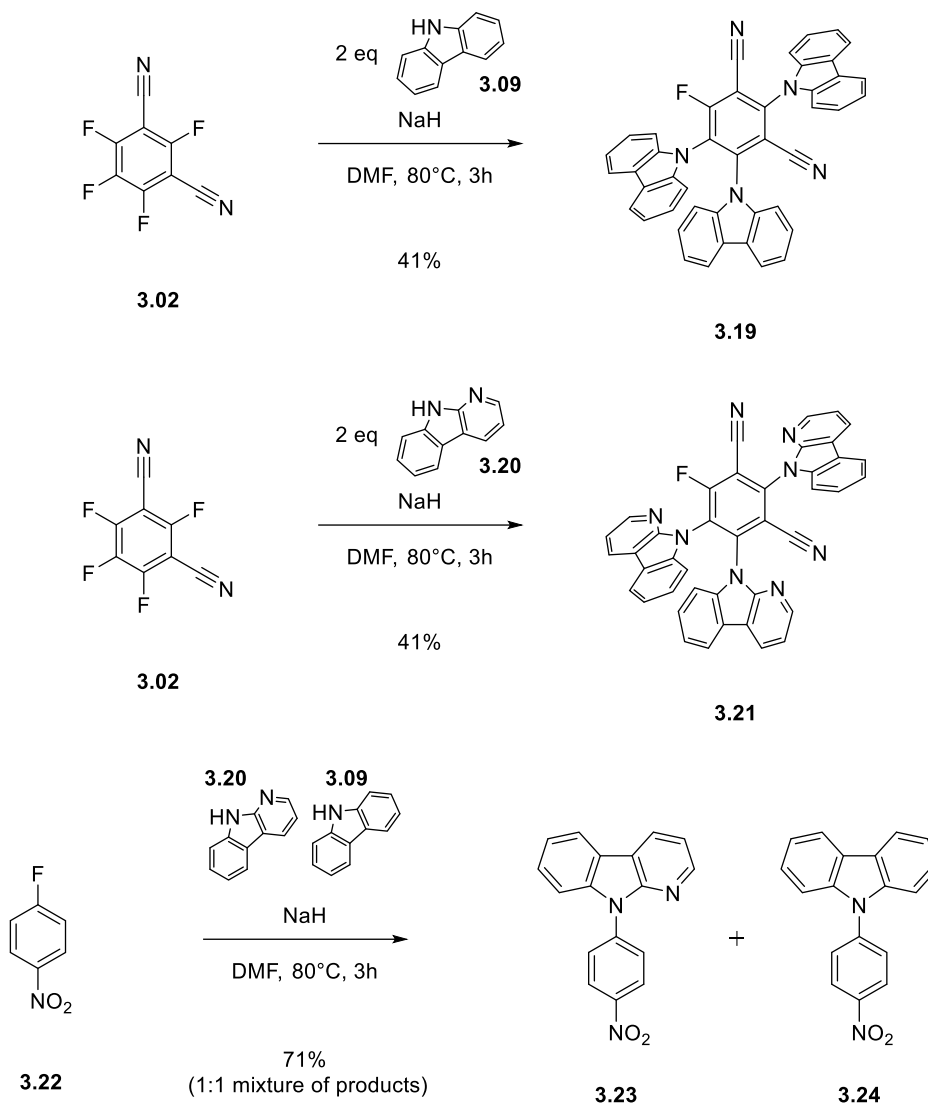
Due to the complex mixture obtained previously we assumed the use of our di-carbazolyl substituted product **3.10** would limit the number of products formed (Scheme 14). However, once again we appeared to obtain a complex mixture leading us to reconsider whether we were seeing further substitution of last two fluorine atoms. Mass spectrometry of our mixture did not suggest this was the case leading to the conclusion that the restricted rotation of our carbazole groups was resulting in regioisomeric mixtures due to the asymmetric nature of our derivatised alkylated carbazole (**3.16**). Separation of this mixture proved to be incredibly difficult leading us to reconsider our approach.



Scheme 14: Attempted $\text{S}_{\text{N}}\text{Ar}$ of our di-carbazolyl product **3.09**.

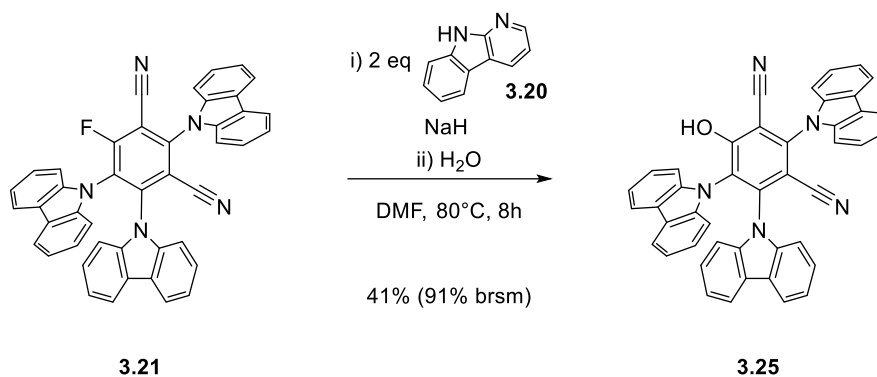
3.3 $\text{S}_{\text{N}}\text{Ar}$ of Tetrafluoroisophthalonitrile Towards Ionic Carbazole-Based Emitters

Whilst exploring the ability to control the $\text{S}_{\text{N}}\text{Ar}$ reactions of hexafluorobenzene we also wanted to do the same with the tetrafluoroisophthalonitrile scaffold due to its use in the synthesis of 4CzIPN. Tetrafluoroisophthalonitrile (**3.02**) is limited to four substitution reactions therefore we started by probing the substitution of only one or two positions. Interestingly, we found it very difficult to limit the extent of substitution, observing the formation of the tri-substituted compound **3.19** predominantly when using both one and two equivalents of carbazole. Even when we ran these reactions at room temperature the tri-substituted carbazole **3.19** was our major product. Unable to affect the reactivity of our fluorinated aromatic scaffold easily we attempted the substitution reaction with α -carboline as a slightly less reactive nucleophile. However, we observed the same results in this case with the tri-substituted product **3.21** being formed preferentially. Further investigation of whether there was an exploitable difference in the reactivity of carbazole (**3.09**) and α -carboline (**3.20**) revealed no real difference when using a mixture of the two nucleophiles in the $\text{S}_{\text{N}}\text{Ar}$ reaction of 4-fluoronitrobenzene (**3.22**).



Scheme 15: S_NAr reactions of tetrafluoroisophthalonitrile (**3.02**) with carbazole (**3.09**) and α -carboline (**3.20**) and the examination of their reactivity.

Though unable to achieve mono or di-substitution of tetrafluoroisophthalonitrile the tri-substituted product **3.19** still present the opportunity for introduction of charge and completion of the synthesis of an ionic emitter through substitution of the final remaining fluorine. We attempted to do this simply by the reaction with α -carboline (**3.20**) as the extra nitrogen in the ring system can be alkylated to introduce charge.¹³⁸ Frustratingly, attempts to substitute the final position with α -carboline were unsuccessful and to add this setback obtained diminished recovery of our starting material due to significant hydroxide substitution upon aqueous work up. This result shows that the final position is still reactive to S_NAr and the synthesis of 4CzIPN (Scheme 8) suggests that there should be no steric issue with substitution of the final position but despite trying to force the reaction, no α -carboline substitution was observed.

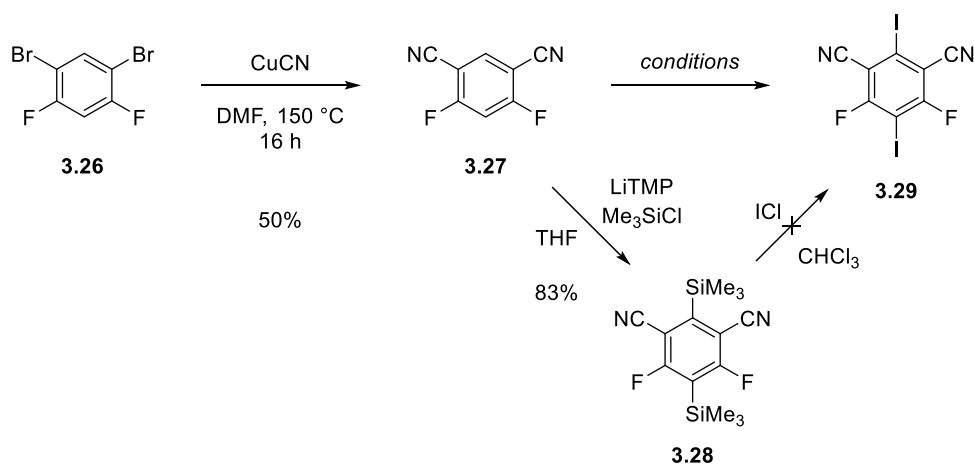


Scheme 16: S_NAr reaction of tri-carbazolyl compound **3.21**.

3.4 A New Approach

As a result of our unsuccessful attempts to really exploit the controlled S_NAr reactions of polyfluorinated aromatics we looked for a different approach. This being the introduction of orthogonal functional groups that can be substituted by different reactions. Our idea was to exploit the differing reactivity of fluorine and iodine towards S_NAr and cross coupling reactions, this should eliminate any issue with trying to control the extent of substitution. Also, it could allow us to bolster the somewhat lacking yields we have seen from recrystallisation of the complex mixtures obtained previously.

We started this inquiry with the reaction of 2,4-dibromo-1,5-difluorobenzene (**3.26**) with copper (I) cyanide to yield difluoroisophthalonitrile (**3.27**) which we be the focus of our work (Scheme 17). We looked now to introduce two iodine groups via ortho lithiation then trapping the lithiated species with iodine (Scheme 17). The most standard literature conditions of LDA and iodine saw no reaction however, these conditions have not been reported for successful iodination with two ortho nitrile groups (Table 3, entry 1). Uchiyama published direct ortho cupration between two nitrile groups with a tetramethylpiperidino-cuprate which could then be treated with iodine to afford the iodinated product.¹³⁹ However, our attempts yielded a mixture of the mono-iodinated products (Table 3, entry 2). Further investigation revealed the work of Daugulis and co-workers who reported base-mediated halogenation of acidic sp² C-H bonds but application of this method to our substrate again saw no return (Table 3, entry 3). Finally, we came to conditions outlined by Martin and co-workers' where they employed LiTMP as a more basic substitute for LDA citing its necessity to deprotonate more stubborn substrates.¹⁴⁰ We tried their in-situ trapping method which added our substrate (**3.27**) to a low temperature mixture (-78 °C) of LiTMP and the desired electrophile yielding silylated product **3.28** with trimethylsilyl chloride and diiodinated product **3.29** with iodine (Table 3, entry 4). Attempts to convert the silylated product with iodine monochloride were unsuccessful.

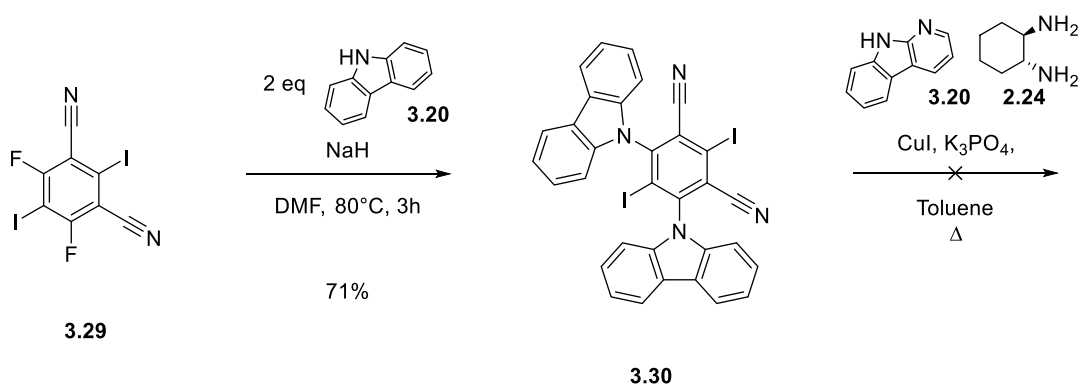


Scheme 17: Synthesis of diiodo-difluoro target **3.29**.

Table 3: Conditions tried for diiodination of **3.27**.

Entry	Conditions	Result (yield %)
1	LDA, I ₂ , THF, -78 °C to rt, 16 h	No reaction
2	MeCu(TMP)(CN)Li ₂ , THF, -78 °C to rt, 16 h	Mixture of mono-iodinated products
3	^t BuOLi, I ₂ , DMF, 80 °C, 3 h	No reaction
5	LiTMP, I ₂ , THF, -78 °C to rt, 16 h	3.29 isolated (44%)

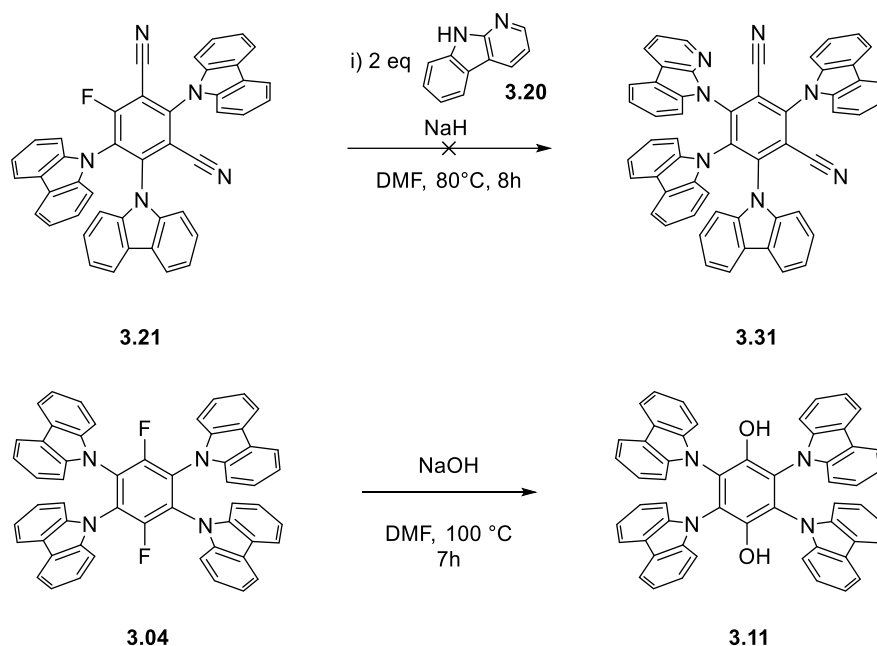
With our orthogonally functionalised aromatic system **3.29** in hand our next step was to evaluate the substitution and cross-coupling reactions. The S_NAr reaction with carbazole proceeded well to give di-carbazolyl **3.30** (Scheme 18). We then attempted an Ullmann coupling with α-carboline but did not observe the formation of our desired product. Palladium-catalysed cross coupling conditions were also attempted but the same result encountered. We wondered if the issue may be steric hindrance and if reversing the order of our steps may be the better approach. Sadly, at this point we ran out of time to continue our investigation.



Scheme 18: Attempted S_NAr cross-coupling approach.

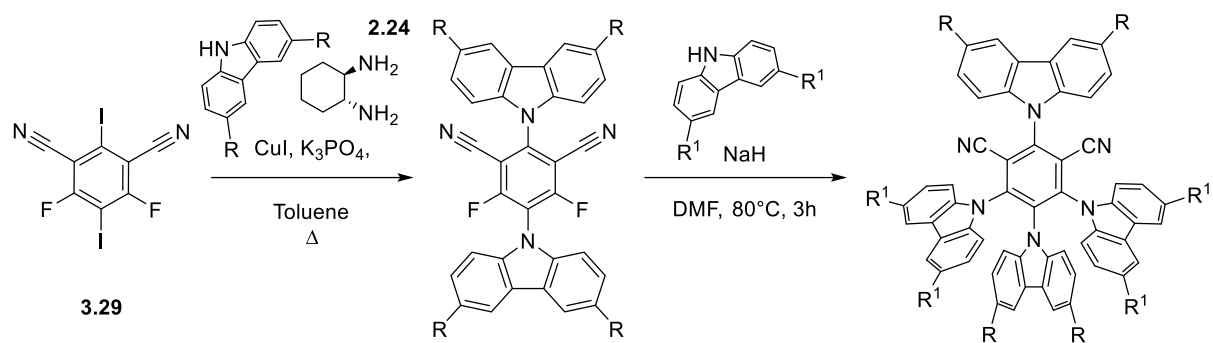
3.5 Conclusions and Future Perspectives

Our investigation of an efficient approach to tetra-substituted carbazole-based emitters has yielded various insight into the reactivity of polyfluorinated aromatic systems. We have demonstrated the ability to limit and control the extent of substitution to some degree, however, have failed to capitalise on this achievement. Specifically, we note the strange apparent reduced reactivity of isolated tetra and tri-substituted compounds **3.04** and **3.21** with further substitution of these compounds proving difficult (Scheme 19).



Scheme 19: Unsuccessful S_NAr attempts.

We explored and achieved an effective synthesis of the diiodo-difluoro compound **3.29** with the utility of this compound sadly not yet fully investigated. Its reactivity towards S_NAr has been established however the cross-coupling step still requires further probing. With this method in hand, we could hope for it to be applied to a convenient preparation of derivitised TADF systems and allow an effective investigation to how the introduction of charge affects the TADF properties of the system. Libraries of such systems have not been explored as introducing small derivatisations is challenging with the standard S_NAr approach to the synthesis of these compounds. We hope our approach could offer a solution to this and help push forward our understanding of how structural changes affect the TADF phenomena (Scheme 20).



Scheme 20: Proposed method to access derivatised carbazole-based TADF emitters.

Chapter 4 Introduction to the Indolocarbazole Alkaloids and their Synthesis

In Chapter 4 we move away from the investigation of fluorescent materials for application to LEC devices and introduce and contextualize the second body of work which is described in Chapter 5.

4.1 Indolocarbazole Alkaloids

4.1.1 Discovery and Interest

While screening for microbial alkaloids at the Kitasato Institute in 1977, Omura and co-workers isolated an alkaloid in a culture of actinomycete (*Streptomyces* strain AM-2282).¹⁴¹ Initial testing of AM-2282 showed promising hypotensive activity along with antimicrobial activity against fungi and yeast.^{141, 142} The alkaloid, later renamed staurosporine (**4.01**, Figure 60), was comprised of an indolocarbazole core bearing a sugar connected by glycosyl linkages at both indolic nitrogens. This structure was determined by X-ray crystallography later in 1994.¹⁴³

A galvanising moment for the interest in staurosporine related compounds was Tamaoki and co-workers' report, in 1986, of staurosporine's potent inhibitory activity for protein kinase C (PKC).^{144, 145} This contributed to a drastic increase in the number of staurosporine related papers, in particular in 1992 when over 450 papers were published including staurosporine in their titles.¹⁴⁶ Thus, in the 30 years after the initial discovery staurosporine, various indolocarbazole compounds (Figure 2) have been isolated from actinomycetes, myxomycetes (slime molds) and cyanobacteria.^{147, 148}

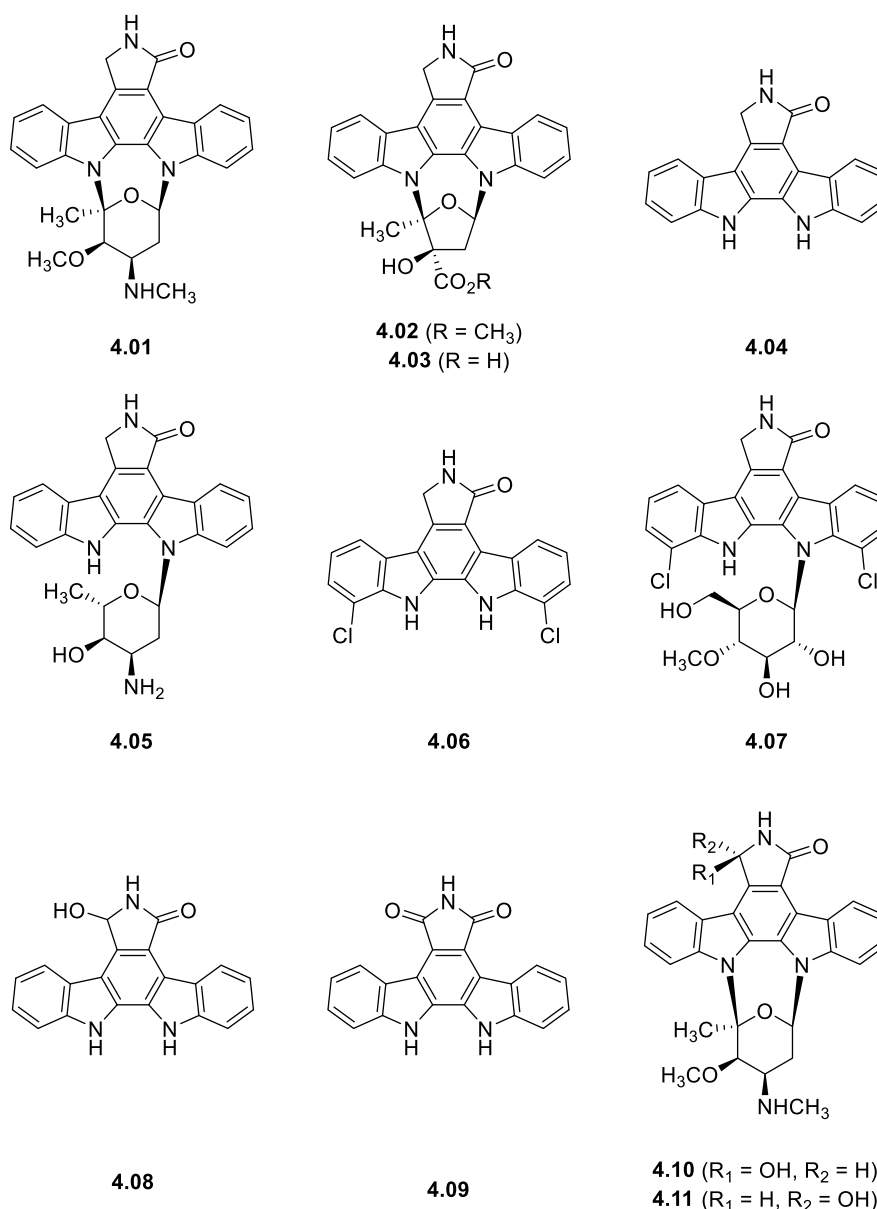


Figure 60: Structures of staurosporine (**4.01**), K252a (**4.02**), K252b (**4.03**), staurosporine aglycone (**4.04**), holyrine (**4.05**), rebeccamycin Aglycone (**4.06**), rebeccamycin (**4.07**), 7-hydroxy-K252c (**4.08**), acryiaflavin A (**4.09**), UCN-01 (**4.10**) and UCN-02 (**4.11**).

4.1.2 PKC Inhibition

Protein kinases are generally classified into serine/threonine kinases and tyrosine kinases. PKC belongs to the former, catalysing phosphorylation at serine and threonine and is thought to play a part in the regulation of many cellular processes crucial for growth, differentiation, and tumour promotion.¹⁴⁵

The activity of PKC has been explored in detail.¹⁴⁹ Extracellular agonists bind specifically to a cell surface receptor. These then activate phospholipase C, either by direct phosphorylation if the receptor is a tyrosine-specific protein kinase or via a G-protein. Phospholipase C then cleaves

phosphatidylinositol-4-5-bisphosphate (PIP₂, **4.13**, Figure 61) to release inositol triphosphate (IP₃, **4.12**, Figure 61) and diacylglycerol (DAG, **4.15**, Figure 61). IP₃ then mobilizes Ca²⁺ ions stored in the endoplasmic reticulum which, along with DAG, activates PKC. PKC catalyses the ATP-dependent phosphorylation of substrate proteins, ultimately resulting in a cellular response (Figure 62).^{149, 150}

PKC inhibitors can be categorised into two groups depending on whether their activity targets the regulatory or catalytic domain. Staurosporine targets the catalytic domain, by blocking the ATP binding sight in the protein kinase^{151, 152} and shows high levels of PKC inhibition (IC₅₀ = 2.7 nm).^{145, 153} This made it and related compounds interesting targets as potent and selective inhibitors are required to deduce the physiological role of protein kinases.¹⁴⁵

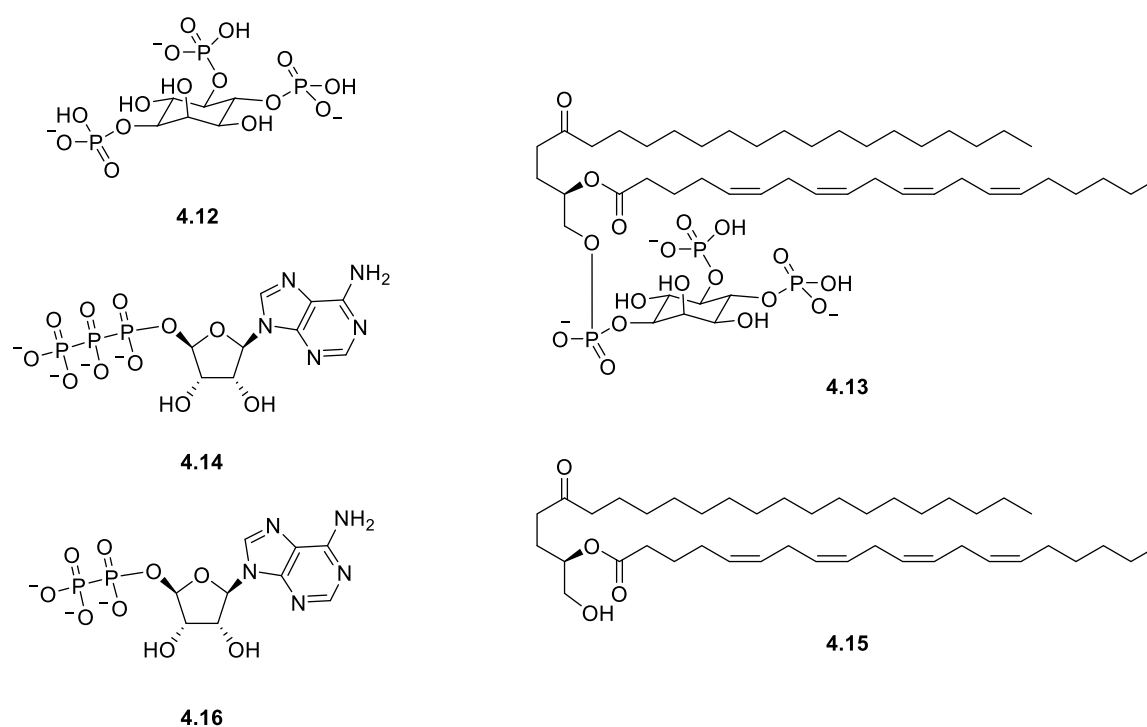


Figure 61: Structures of IP₃ (**4.12**), PIP₂ (**4.13**), ATP (**4.14**), DAG (**4.15**) and ADP (**4.16**).

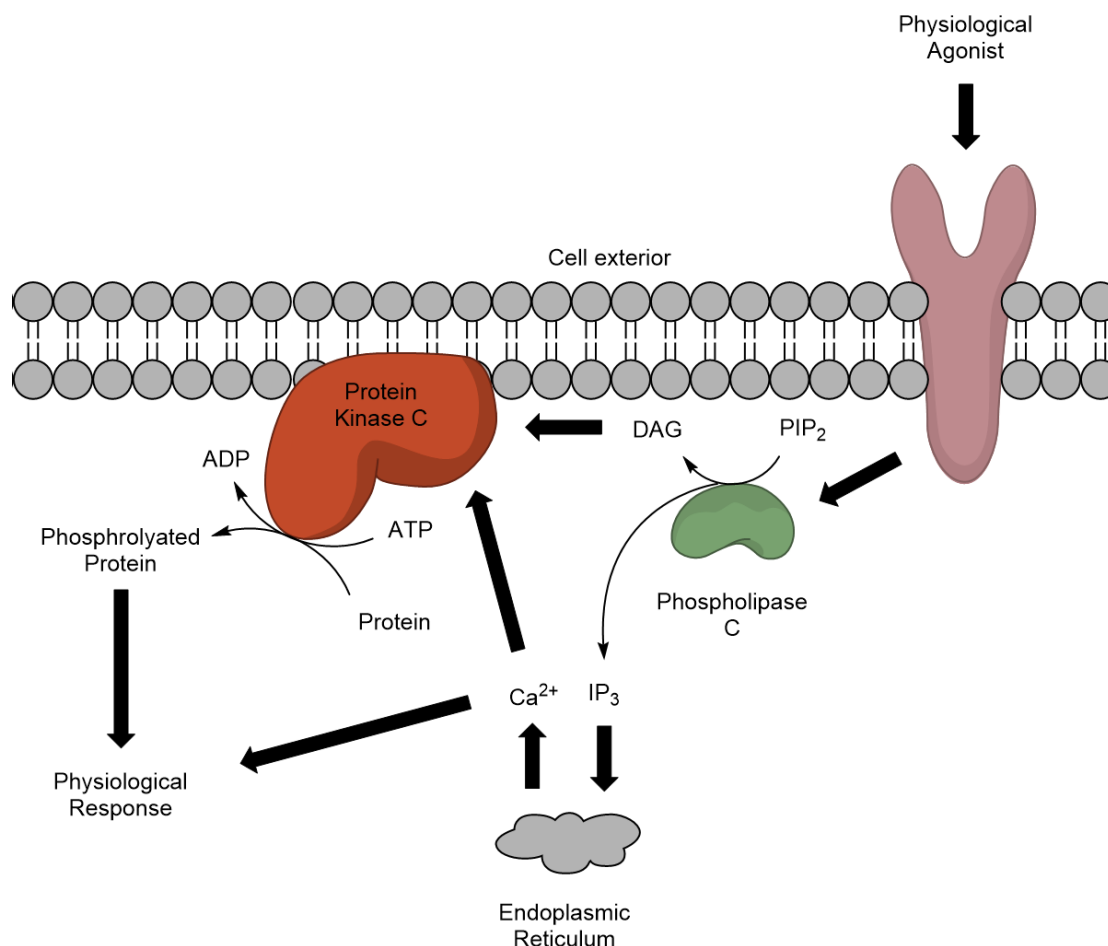
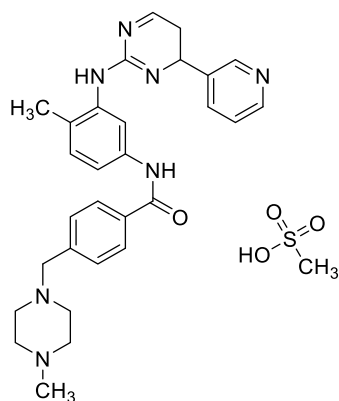


Figure 62: Protein kinase C-mediated signal transduction.

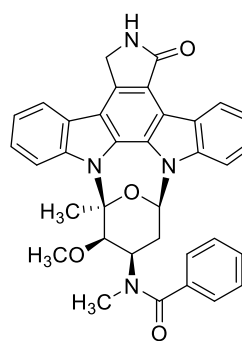
4.2 Indolocarbazole Alkaloids and Their Anti-cancer and Antifungal Properties

4.2.1 Anti-cancer Activity

Since the 1980s, protein kinases have been the primary cellular targets when it comes to anti-cancer agents, becoming the second most important group of drug targets after G-protein-coupled receptors.¹⁵⁴ This culminated in various commercialised treatments utilising derivatives of staurosporine or other indolocarbazole alkaloids. The first of these kinase inhibitors to gain FDA approval and reach the market was Gleevec/Glivec® (**4.16**, Figure 63) also known as Imatinib which was approved in 2001.¹⁵⁰ This kinase inhibitor, was introduced as a treatment chronic myeloid leukaemia (CML) and revolutionised the treatment of the disease. The introduction of this treatment was so prolific that CML's status was changed to chronic disease from potentially fatal cancer and the treatment was known to be highly selective with limited side effects.¹⁵⁵⁻¹⁵⁷



4.16



4.17

Figure 63: Structures of Imatinib/Glivec® (4.16) and Midostaurin/Rydapt® (4.17).

UCN-01 (4.10, Figure 60) is another indolocarbazole alkaloid that has shown anti-cancer activity. It is known to inhibit various protein kinases and has been a part of phase I and II trials for treatment of leukaemias, lymphomas, advanced solid tumours, melanomas, and small-cell lung cancer.¹⁵⁸⁻¹⁶⁰

Finally, Midostaurin (trade name of Rydapt®) was approved for clinical use in 2017. This is a derivative of staurosporine, made via a semi-synthetic derivatisation. This is a non-specific kinase inhibitor and was approved for its activity on the FLT3 kinase but also shows inhibitory activity against PKC and VEGF.¹⁵⁰ Midostaurin has been shown to prevent tumour angiogenesis and cell proliferation, and it has also been tested against acute myeloid leukaemia.¹⁶¹

4.2.2 Antifungal Activity

Staurosporine's antifungal activity was reported along with its initial discovery in 1977, discussing its *in vitro* activity against various fungi. Against human pathogenic fungi, staurosporine was found to be most active against *Candida pseudotropicalis* and *Aspergillus breuipus* (MIC = 3.13 µg/mL for both). The alkaloid also showed activity against *Candida albicans* and *Aspergillus niger* (MIC = 6.25 and 25 µg/mL respectively) and for hytopathogenic fungi *Piricularia oryzae* and *Sclerotiniu cinereci* outstanding effectiveness was reported (MIC = 0.78 µg/mL).^{141, 162} The antifungal activity of staurosporine and related alkaloids was overshadowed subsequently due to the discovery of their PKC inhibition properties and thus their application to anti-cancer therapeutics.

However recently changes in the challenges in the field of antifungal medicine have led to increased pursuit of a broad spectrum of antifungal agents. This is mainly to combat the increased prevalence of multi-drug resistant fungal infections.^{163, 164} Specifically members of the genus *Candida* have recently been added to the list of priority pathogens, one being *Candida auris*, a multidrug-resistant yeast that in 2016 became associated with invasive healthcare

associated infections throughout the world.¹⁶⁵ Staurosporine has been demonstrated to have potent anti-*Candida* activity^{164, 166-168} which is renewing the continued interest around the indolocarbazole alkaloids and their therapeutic potential. Demonstrating this, in 2023, another novel staurosporine derivative (**4.18**, Figure 64) was reported and this compound demonstrated anti-fungal activity against *Candida albicans* (MIC = 12.5 $\mu\text{g/mL}$).¹⁶⁹

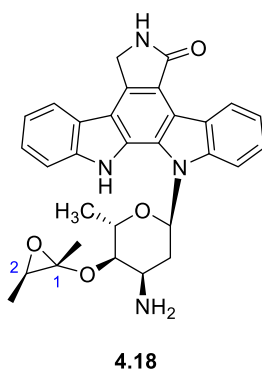
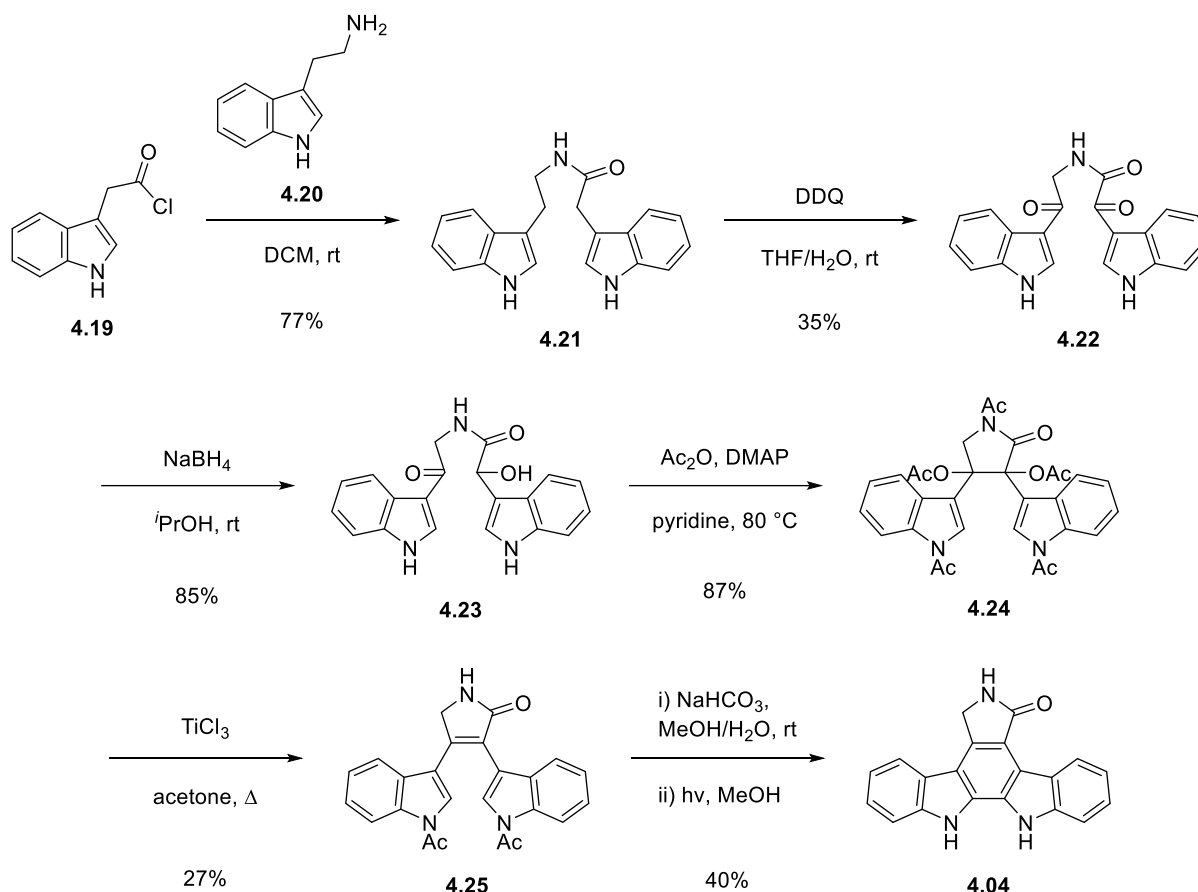


Figure 64: Structure of recently published staurosporine derivative (**4.18**).

4.3 Synthesis of the Staurosporine Aglycone

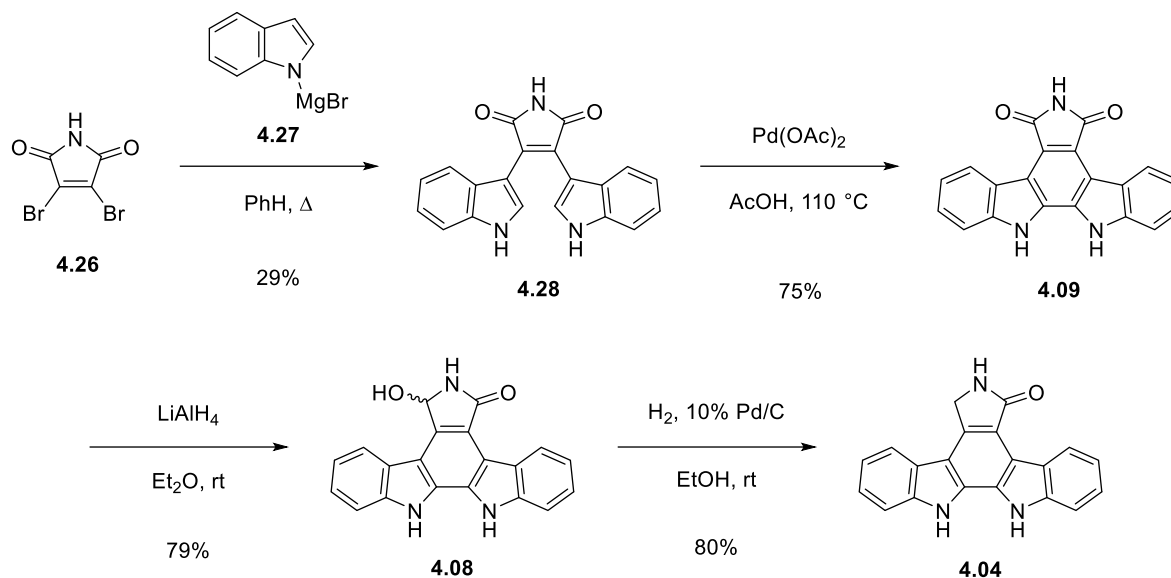
The extensive therapeutic application of the indolocarbazole alkaloids has made the effective synthesis and derivatisation of this family of compounds a priority. To outline the efforts made we begin with the journey to achieve an efficient synthesis of the staurosporine aglycone (**4.04**), the most popular natural product in the family.

The first synthesis of the staurosporine aglycone was reported in 1983 by Winterfeldt and collaborators (Scheme 21).¹⁷⁰ In this preparation tryptamine (**4.20**) was coupled with acid chloride **4.19** to give an amide (**4.21**) which was subsequently oxidised at the benzylic positions to create oxoacetamide **4.22**. The oxoacetamide was then reduced selectively due to its electron deficiency to give the corresponding hydroxyacetamide **4.23**. Treating the hydroxyacetamide with acetic anhydride (and DMAP) resulted in acylation and cyclisation to the lactam **4.24**. However, further treatment with TiCl_3 was required form the conjugated lactam **4.25**. Finally, deprotection of the acylated indoles followed by a photochemical cyclisation gave the staurosporine aglycone (**4.04**) in a reasonable yield.



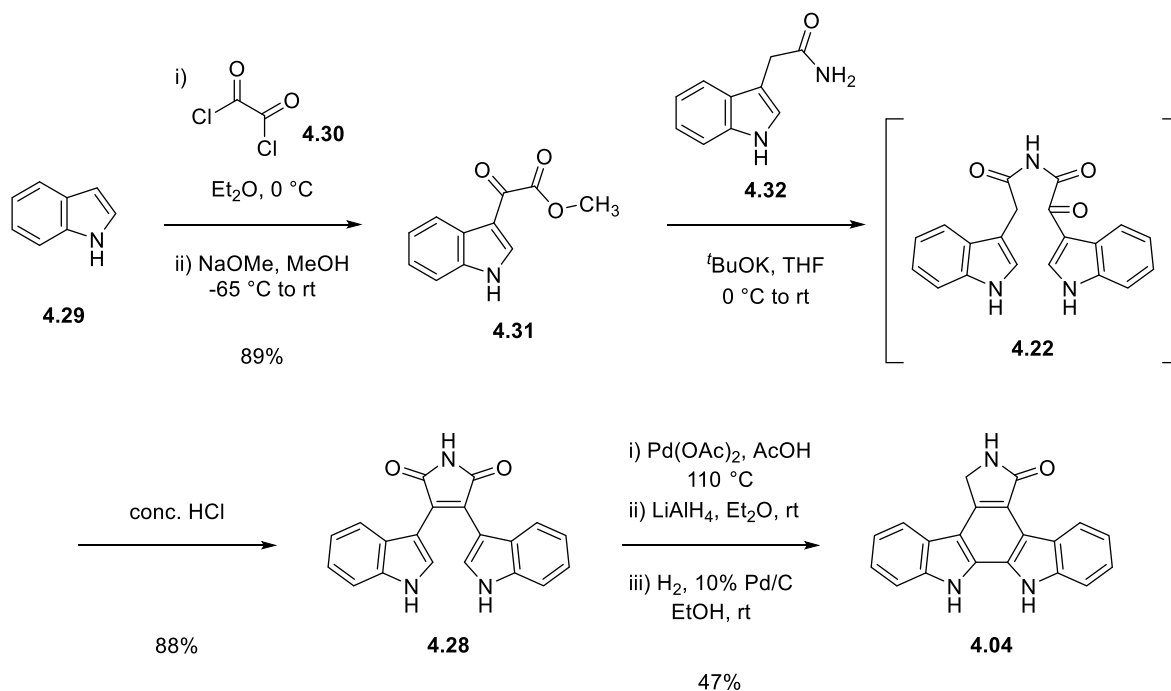
Scheme 21: Synthesis of the staurosporine aglycone by Winterfeldt and co-workers’.

After this initial synthesis there still appeared to be room to improve on the approach, both in terms of the length of the route and the overall yield. In 1993, Hill and collaborators developed a short approach (Scheme 22)¹⁷¹, building on the earlier work of Steglich^{172, 173} and later Weinreb¹⁷⁴. This approach reacted dibromomaleimide (**4.26**) with magnesiated indole **4.27** to give bisindolylmaleimide (**4.28**) which then underwent an oxidative cyclisation in acetic acid to give acryiaflavin A (**4.09**). Acryiaflavin A was then treated with lithium aluminium hydride to give 7-hydroxy-K252c and further reduction with hydrogen and palladium on carbon gave the staurosporine aglycone (**4.04**). This method was the shortest approach at the time and benefited from being a protecting group free approach.



Scheme 22: Synthesis of the staurosporine aglycone by Hill and co-workers’.

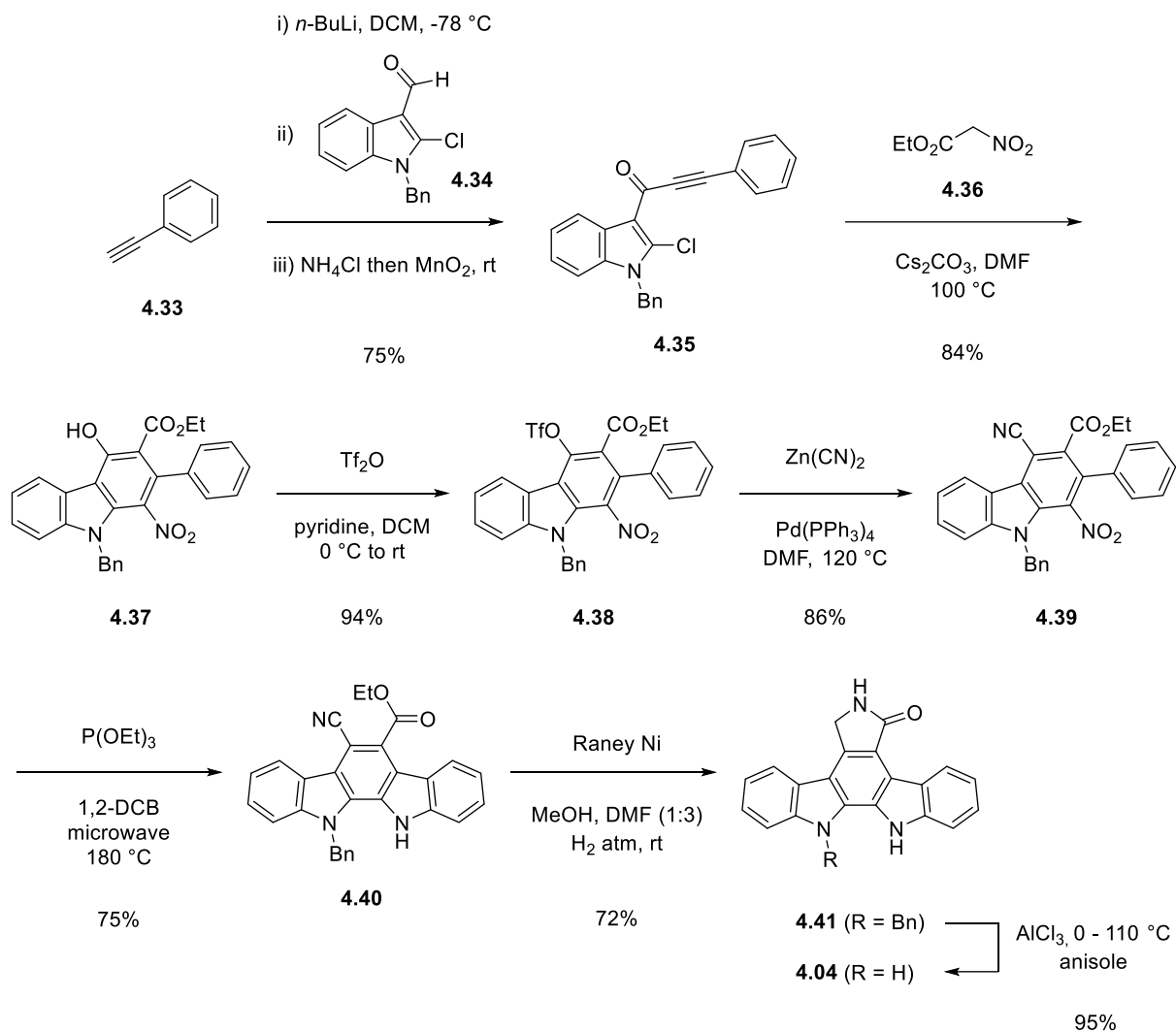
Another hallmark approach in the journey to achieve an efficient high yielding synthesis was the work of Faul and collaborators. Faul and co-workers’ initially worked on a modification of Hill and co-workers’ approach using dichloromaleimide which resulted in a highly effective synthesis yielding 34% over the short 4-step approach.¹⁷⁵ The group then came back with a second, more novel, approach in 1998 (Scheme 23).¹⁷⁶ In this approach they took indole (**4.29**) and performed an electrophilic aromatic substitution with oxalyl chloride (**4.30**) followed by an esterification with sodium methoxide to give the ester **4.31**. This ester then underwent a Perkin-type condensation reaction to give intermediate **4.22** which was treated with acid and cyclised to give bisindolylmaleimide (**4.28**). This then underwent the same oxidative cyclisation followed by the same two-step reduction approach that was outlined by Hill and co-workers’ and resulted in the highest yielding approach giving the staurosporine aglycone in a total 36% yield (over 5 steps).



Scheme 23: Synthesis of the staurosporine aglycone by Faul and co-workers’.

The most recent synthesis, published in 2019, is that of Pabbaraja and co-workers’ (Scheme 24).¹⁷⁷ This method takes phenyl acetylene in the presence of *n*-butyllithium and adds the aldehyde **4.34** where addition to the carbonyl followed by workup results in the alkynol which is oxidised, to ynone **4.35** by manganese dioxide without isolation. The ynone was then treated with ethyl nitroacetate (**4.36**) in basic conditions which is expected to first trigger a Michael addition of the nitromethane-derived anion to the alkyne, this is followed by an aldol-type addition to access a cyclobutene intermediate. The strained system is expected to open in a retro-nitroaldol process which is then followed by generation of an iminium ion which facilitates the final C-C bond formation, aromatisation of the intermediate yields carbazole **4.37**. The alcohol of this carbazole is then activated by formation of the corresponding triflate **4.38** which then allows for a Negishi-coupling forming the cyanated carbazole **4.39**. Cadogan’s reductive cyclisation is the next step and affords the indolocarbazole **4.40**, subsequent reduction with Raney nickel sees formation of the desired lactam **4.41**. Finally, deprotection of the indolic nitrogen with aluminium trichloride and anisole yields the staurosporine aglycone. Although this method is not as high yielding, the final benzyl protected aglycone (**4.41**) is an attractive intermediate for accessing those alkaloids containing only a single indolic glycosyl linkage.

This has highlighted a few of the key approaches to the synthesis of the staurosporine aglycone however, the review by Chambers and co-workers gives a very complete overview of the efforts conducted towards the synthesis of the staurosporine aglycone.¹⁷⁸

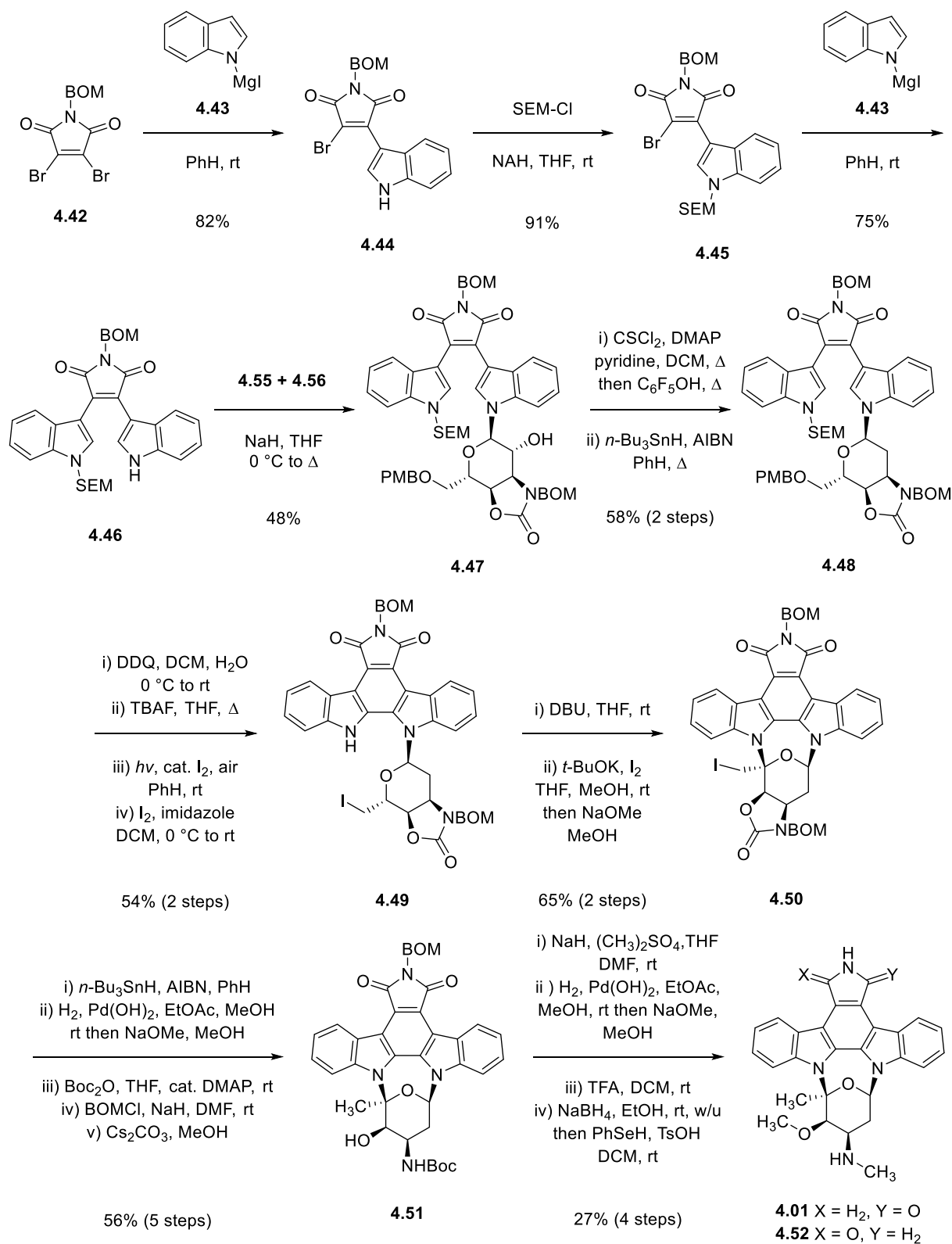


Scheme 24: Synthesis of the staurosporine aglycone by Pabbaraja and co-workers'.

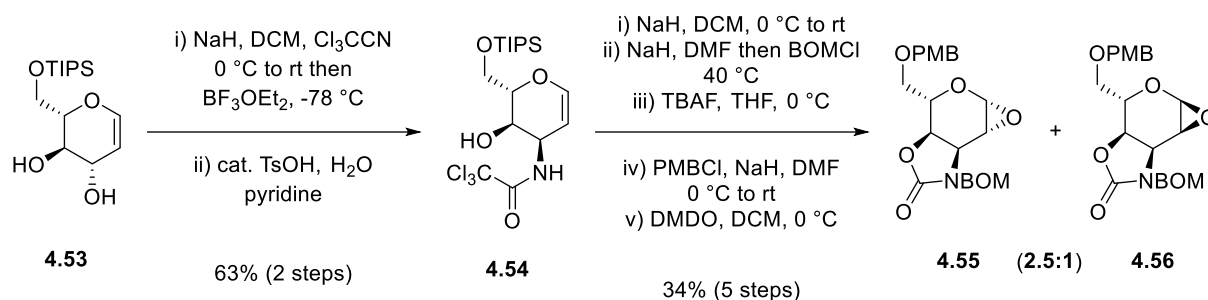
4.4 Synthesis of Staurosporine

As has been outlined in sections 4.1.1 and 4.1.2, staurosporine is a highly effective therapeutic agent with broad applications due to its non-specific nature and has thus been used extensively in the field of medicinal chemistry. This nature has made an efficient and high yielding approach to staurosporine's synthesis a matter of importance. To date there has only been two methods published for the total synthesis of staurosporine, however recently a new formal synthesis was also published.

The first of these approaches, in 1995, was the work of Danishefsky and collaborators (Scheme 25).^{179, 180} This approach began with the protected dibromomaleimide **4.42** which was subjected to sequential additions of magnesiated indole **4.43** that allowed for protection of a single indole group yielding bisindolylmaleimide **4.46**. The single available indolic nitrogen had been positioned for the ensuing glycosylation. The sugar to be used for this step was prepared from the protected L-glucal derivative **4.53** (Scheme 26) by formation of the bis-(trichloroacetimidate), which then formed an oxazoline that was next hydrolysed to give the trichloroacetimidate **4.54**. The trichloroacetimidate was treated with sodium hydride to form the desired oxazoline and this was followed by protecting group manipulations before the final oxidation with 2,2-dimethyldioxirane afforded a 2.5 to 1 mixture of epoxides **4.55** and **4.56**. Glycosylation of the unprotected indole followed yielding alcohol **4.47** which was then subjected to deoxygenation conditions giving the glycosylated bisindolylmaleimide **4.48**. Subsequent deprotection of SEM and PMB groups followed by oxidative photocyclization and finally iodination gave rise to acryiaflavin A derivative **4.49**. The stage was set for the formation of the second glycosyl linkage, this was performed through elimination of iodide to give an exocyclic double bond that, upon treatment with potassium *tert*-butoxide and iodine, provided the desired cyclic structure **4.50**. Dehalogenation preceded deprotection of the BOM groups, this was followed by selective Boc protection of the oxazoline ring then reprotection of the maleimide with BOM-Cl and finally reaction with caesium carbonate and methanol to provide alcohol **4.51**. Methylation of the alcohol and amine groups was up next and ensuing BOM deprotection allowed for the final 2-step maleimide reduction to yield a 1 to 1 mixture of staurosporine (**4.01**) and *iso*-staurosporine (**4.52**).

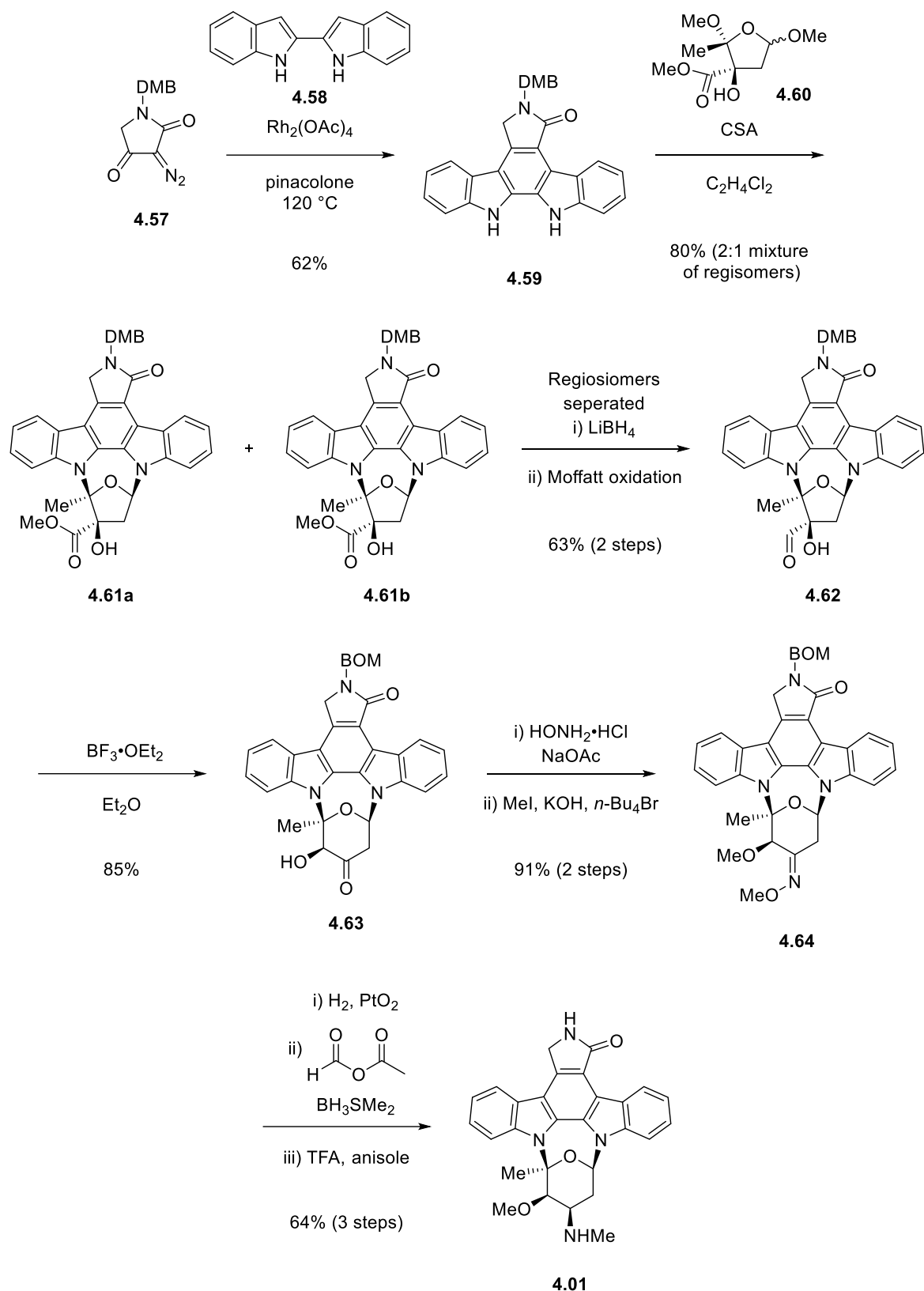


Scheme 25: Total synthesis of staurosporine (**4.01**) by Danishefsky and co-workers.

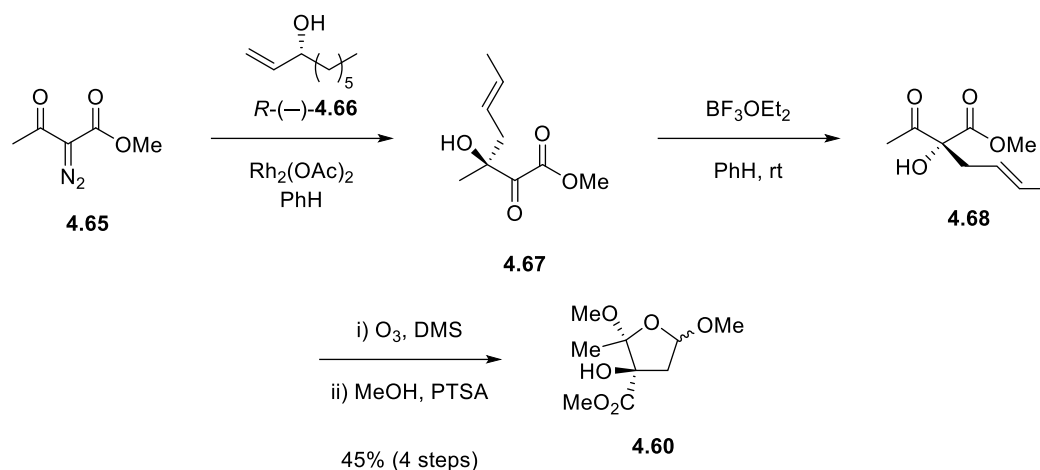


Scheme 26: Preparation of the requisite sugar in Danishefsky and co-workers' approach to the synthesis of staurosporine (4.01).

The second methodology was outlined by Wood and co-workers' in 1996 (Scheme 27 and 28).¹⁸¹⁻¹⁸³ This approach begins with a coupling of diazolactam **4.57** with 2,2'-biindole (**4.58**) in a cycloaromatisation producing staurosporine aglycone derivative **4.59**. This can then undergo the key double glycosidation step with the readied furanose **4.60**, prepared by a novel tandem rearrangement protocol that combines methyl 2-diazo-3-oxobutyrates (**4.65**) and *R*-(-)-**4.66** to furnish alcohol **4.68** in a single pot and allows subsequent ozonolysis then acid-mediated cyclisation to give furanose **4.60**. Glycosidation proceeded by the formation of two regioisomers in a 2:1 ratio, fortunately the distribution of products favoured the desired regioisomer **4.61a** corresponding to K252a. Reduction of **4.61** to the corresponding alcohol then oxidation to the aldehyde **4.62** followed, setting up for the $\text{BF}_3 \cdot \text{OEt}_2$ mediated ring expansion to afford ketone **4.63**. Amination with hydroxylamine hydrochloride with ensuing methylation gave ketoxime **4.64** which was the subject of a stereoselective reduction, mono-methylation and DMB deprotection to give staurosporine (**4.01**).

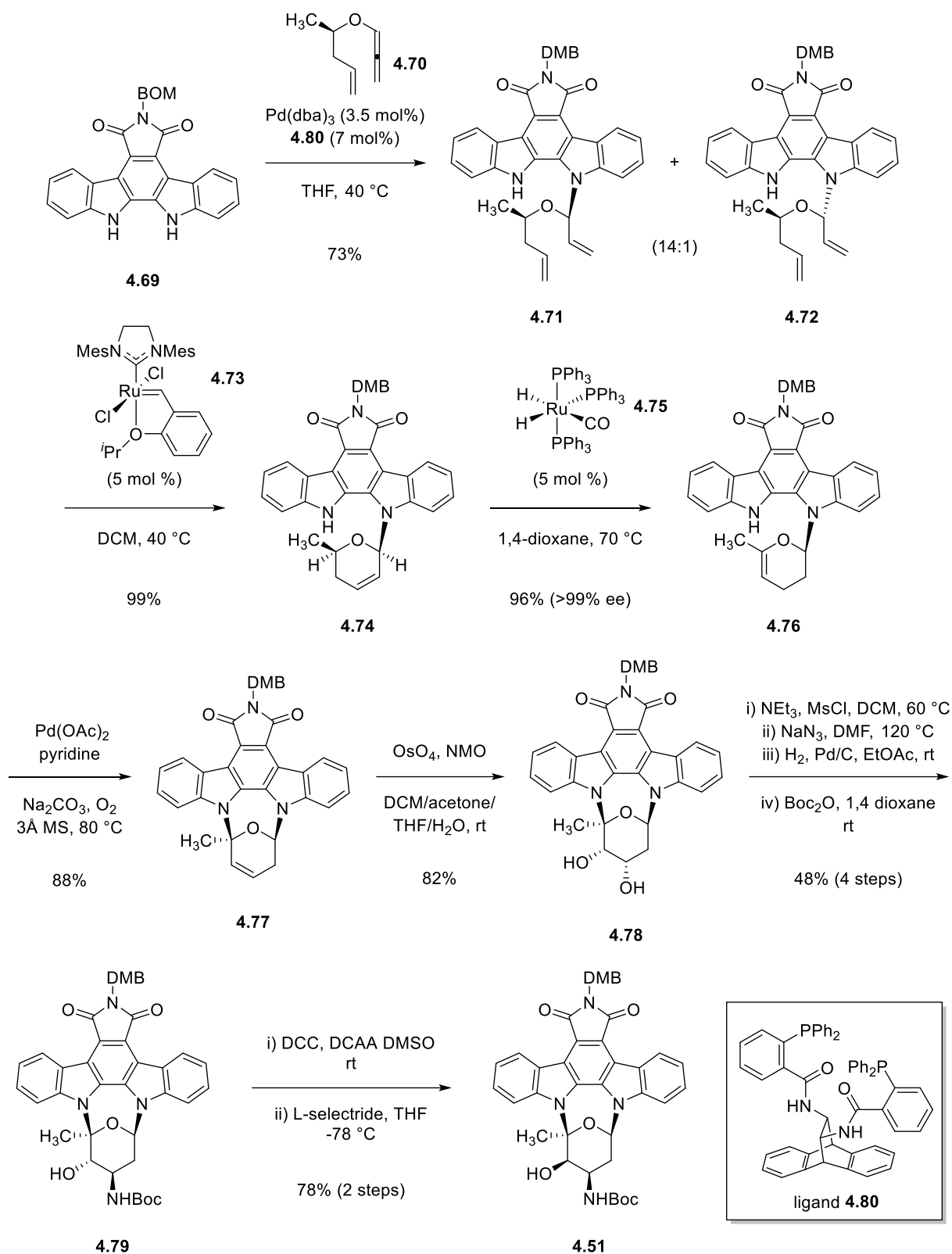


Scheme 27: Total synthesis of the staurosporine (**4.01**) by Wood and co-workers’.



Scheme 28: Wood and co-workers' preparation of furanose **4.60**.

The final, and most recent, approach was made in 2021 by Seo and co-workers' (Scheme 29).¹⁸⁴ This actually represented a formal synthesis of staurosporine whereby the group synthesised a protected derivative of 7-oxostaurosporine (**4.51**), intersecting with Danishefsky and co-workers' method. The synthesis begins with the protected form of acryiaflavin A **4.69** which can form the first glycosidic bond by asymmetric addition of alkoxyallene **4.70** under palladium catalysis. This reaction was earlier published by the group¹⁸⁵ and in this case, after tuning of the ligand, a 14:1 diastereoselectivity could be achieved with ligand **4.80**. The diene **4.71** was then poised for RCM with the 2nd generation Hoveyda–Grubbs catalyst (**4.73**) resulting in a near quantitative yield of cyclic allylic acetal **4.74**. Next, once again based on the groups earlier work,^{186, 187} a chemoselective olefin migration was performed to afford enol acetal **4.76** with incredibly high retainment of chirality. The second glycosidic link was then installed using palladium (II) acetate under oxygen atmosphere to give the cyclised product **4.77**. *Syn*-dihydroxylation followed to yield diol **4.78** which was then activated by selective mono-mesylation, reacted with sodium azide, subsequently reduced, and finally protected to produce the protected amine **4.79**. Inversion of C₂-OH stereochemistry could now be achieved by oxidation then diastereoselective reduction delivering alcohol **4.51** and intersecting with Danishefsky's and co-workers' route.



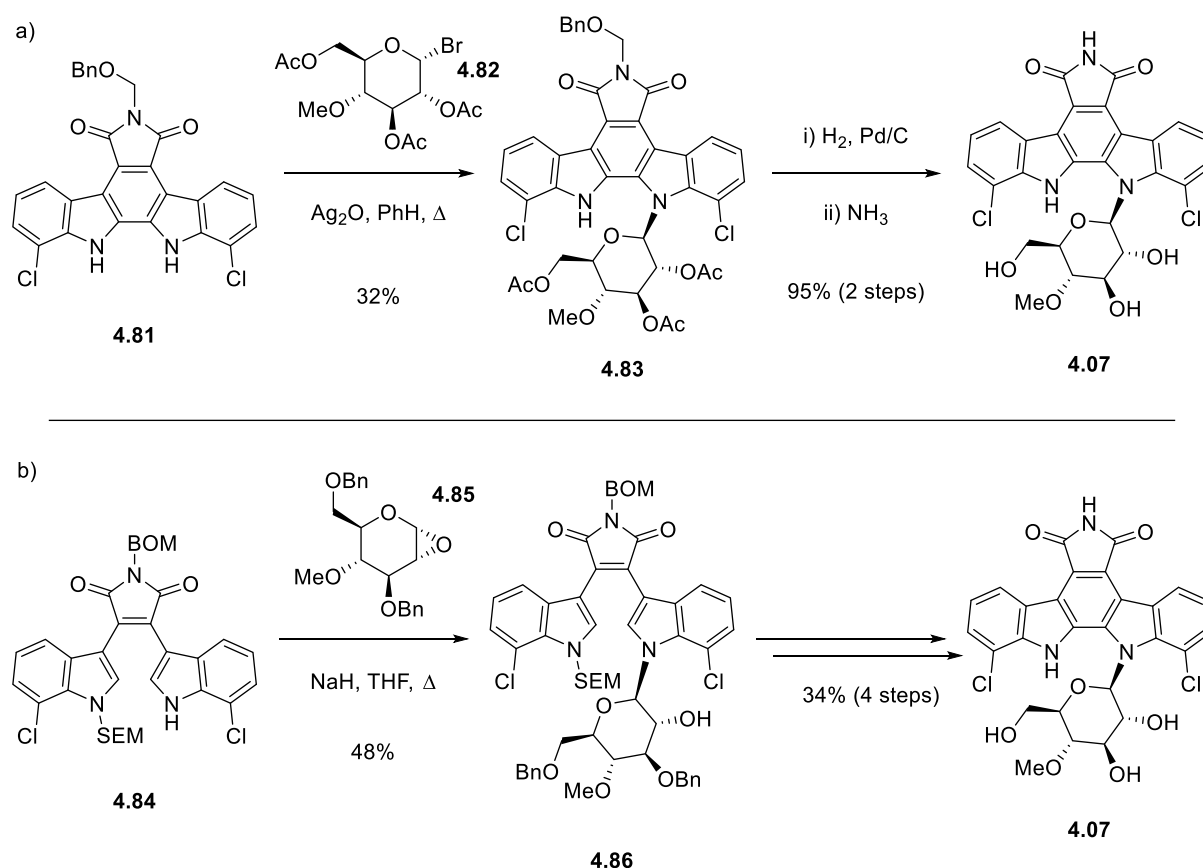
Scheme 29: Formal synthesis of the staurosporine (**4.01**) by Seo and co-workers’.

4.5 Glycosylation of Indolocarbazole Alkaloids

As has already been introduced, the indolocarbazole alkaloids have shown extensive promise for their medicinal and biological applications.¹⁸⁸ A common theme among some of the most useful alkaloids in this family is the presence of a sugar bound to either one or both indolic nitrogens.

This feature has added complexity to the task of synthesising these natural products and derivatising them. Previously, in the efforts to synthesise staurosporine (**4.01**), we have seen 3 different attempts to introduce these sugar moieties, similar works have been attempted in the pursuit of the total synthesis of related alkaloids.

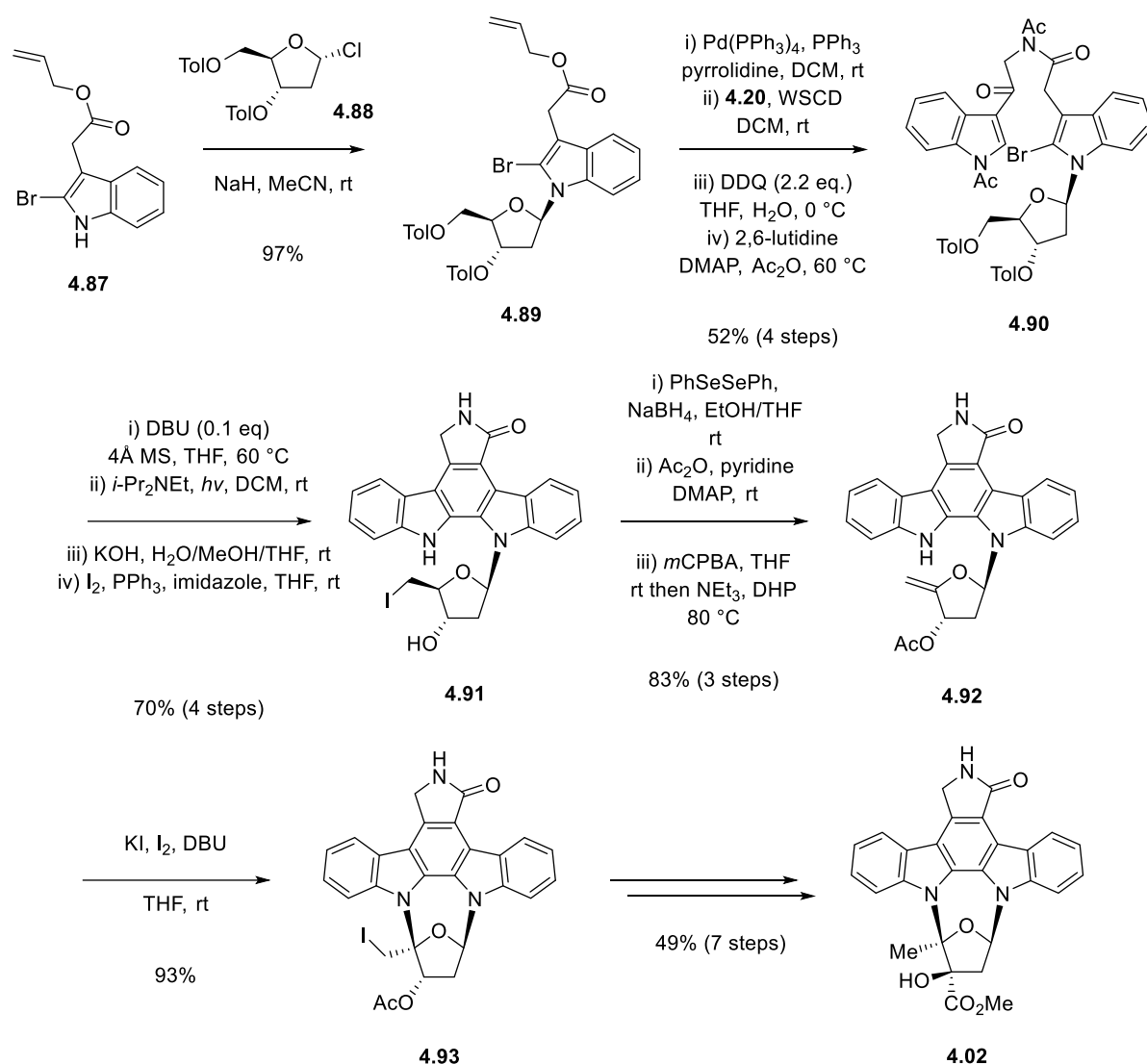
Rebeccamycin (**4.07**), as the most potent indolocarbazole antitumor agent,¹⁸⁹⁻¹⁹¹ has been the subject of synthetic investigations that have yielded good routes to the natural product. First isolated by Clardy and co-workers' in 1985 (Scheme 30a),¹⁹² their method built protected rebeccamycin aglycone **4.81** and subjected it to a silver promoted Koenigs-Knorr glycosylation with halogenated sugar **4.82**. This allowed for subsequent deprotection to produce rebeccamycin (**4.07**) in a total of 6 steps with 8% yield. Later, in 1993, Danishefsky and co-workers' tried their hand at the synthesis using a similar approach to the one they later applied to staurosporine (Scheme 30b).¹⁹³ The protected bisindolylmaleimide **4.84** was glycosylated using the epoxidised carbohydrate **4.85**. This was followed by oxidative cyclisation and deprotection steps to afford rebeccamycin (**4.07**) with a total yield of 10% over 8 steps.



Scheme 30: a) Synthesis of the rebeccamycin (**4.07**) by Clardy and co-workers', b) Synthesis of the rebeccamycin (**4.07**) by Danishefsky and co-workers'

K252a (**4.02**) is another indolocarbazole alkaloid bearing 2 glycosidic links, like staurosporine. This nature introduces a regioselectivity issue in the pursuit of an effective synthesis. So far, none of the syntheses discussed have successfully addressed this issue in the glycosidation steps,

and instead groups have simply obtained mixtures in the formation of their glycosidic links or produced mixtures in late stage maleimide reduction. The work of Fukuyama and co-workers with their synthesis of K252a, in 1999 (Scheme 31),¹⁹⁴ represents the first regioselective approach. To achieve this, they prepared brominated indole **4.87** and treated it with sodium hydride then reacted it with furanose **4.88** to furnish *N*-glycosylated indole **4.89**. Deprotection of the allyl ester allowed for the amide coupling with tryptamine (**4.20**) in the presence of WSCD (1-Ethyl-3-(3-dimethylaminopropyl)carbodiimide) to precede benzylic oxidation with DDQ and acetylation of the indole and amide nitrogens to give bisindole **4.90**. Cyclisation to the corresponding lactam was followed by photocyclisation then deprotection of the acyl and toluoyl groups to allow for substitution of the primary alcohol and produce iodide **4.91**. Here we can see the completion of regioselective glycosylation of the staurosporine aglycone moiety.



Scheme 31: Regioselective glycosylation in the total synthesis of K252a (**4.02**) by Fukuyama and co-workers’.

4.6 Conclusions and Future Perspectives

The indolocarbazole alkaloids are undeniably an important class of natural products and some of them and their derivatives show incredible evidence of being potent therapeutic agents. Demonstrating this has been their application to the treatment of chronic myeloid leukaemia, lymphomas, advanced solid tumours, melanomas, and small-cell lung cancer.¹⁵⁵⁻¹⁶⁰ However, beyond this the PKC inhibition property that is characteristic of staurosporine and some of its derivatives proves to be an invaluable tool in deducing the physiological role of protein kinases.^{145,}

153

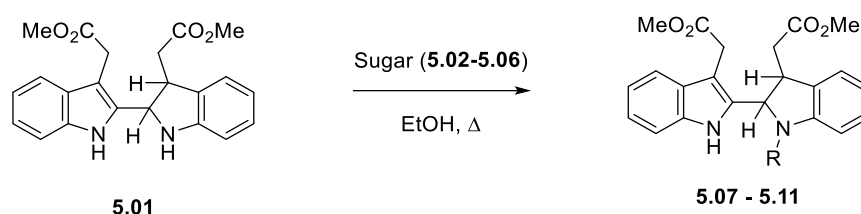
Due to these medicinal applications the indolocarbazole natural products have long been the subject of synthetic investigations to try and produce these useful compounds in an efficient and economical manner. These investigations have yielded promising results; however some major challenges remain unaddressed. Chiefly, the application of regioselective approaches in efforts towards the derivatisation of the staurosporine aglycone remain elusive or inefficient. Fukuyama and co-workers have worked to resolve the regioselectivity in a creative and successful manner. However, the 21-step approach towards the synthesis of K252a does not represent a useful, widely applicable approach to the indolocarbazole alkaloids due to its length.¹⁹⁴ The asymmetric nature of the staurosporine aglycone provides a level of complexity to the total synthesis of it and its derived natural products leaving an opportunity for new and inventive approaches to address this.

Chapter 5 Regioselective Functionalisation of the Staurosporine Aglycone

5.1 Background

5.1.1 Indoline Glycosylation

In chapter 4, the formation of glycoside linkages between various carbohydrates and indolocarbazoles were evaluated. However, the use of indolyindoline systems provides a unique way to differentiate the reactivity of two nitrogens. Chisolm and co-workers reported investigations along these lines in 1995.¹⁹⁵ They explored the glycosylation of 2,2'-indolyindoline **5.01** (Scheme 32) with the thought that such reaction could find extensive application to the total synthesis of the indolocarbazole alkaloids.

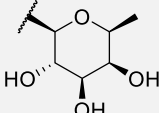
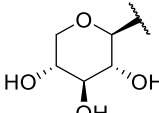
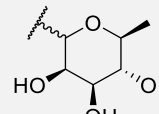


Scheme 32: Investigation of the glycosylation of 2,2'-indolyindolines by Chisolm and co-workers'.

Investigation showed selectivity for the indoline nitrogen with good yields when refluxing in ethanol and mostly in the presence of the weak acid catalyst ammonium sulfate (Table 4). The group subsequently showed the smooth oxidation of product **5.07** with DDQ to give the corresponding glycosylated bisindole in an 88% yield.

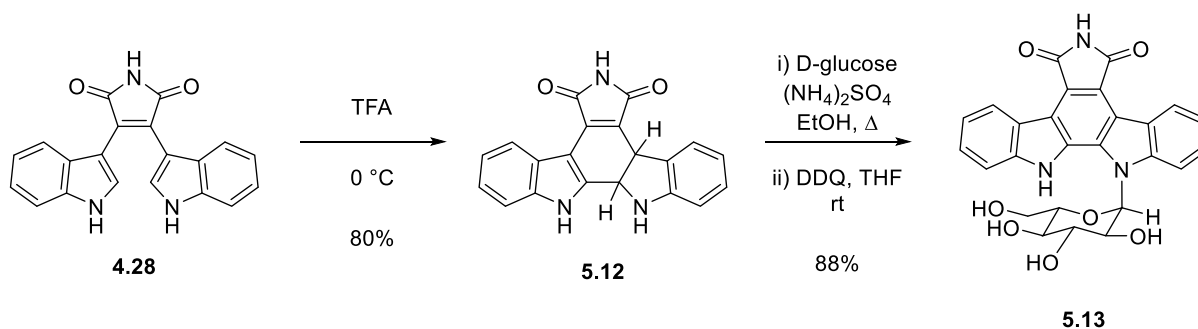
Table 4: Glycosylation 2,2'-Indolyindoline **5.01** by Chisolm and co-workers.

Sugar	Additive	Yield (%)	Product (R =)
D-Glucose	b	93	<p>5.07</p>
D-Galactose	b	68	<p>5.08</p>

L-Fucose	a	95	 5.09
D-Xylose	a	85	 5.10
L-Rhamnose	b	72	 5.11^c

^a No additive. ^b 3 eq. of ammonium sulfate added. ^c 1:1 Mixture of anomers obtained.

Faul and co-workers then took the next step in this path with their exploration of the glycosylation of what could be seen as the indolyndoline precursor to acryiaflavin A **5.12**. In 2004, the group showed the ability to cyclise bisindolylmaleimide (**4.28**) under acid conditions to form indolyndoline **5.12** which could be selectively substituted and the indoline nitrogen with a desired sugar (Scheme 33).¹⁹⁶ To add to that, the glycosylated indoline could be oxidised efficiently without isolation to provide the sugar bearing indolocarbazole **5.13** in high yield. Similarly to Chisolm and co-workers, the success of the reaction was demonstrated with a selection of common sugars where yields ranged from 49–97%.



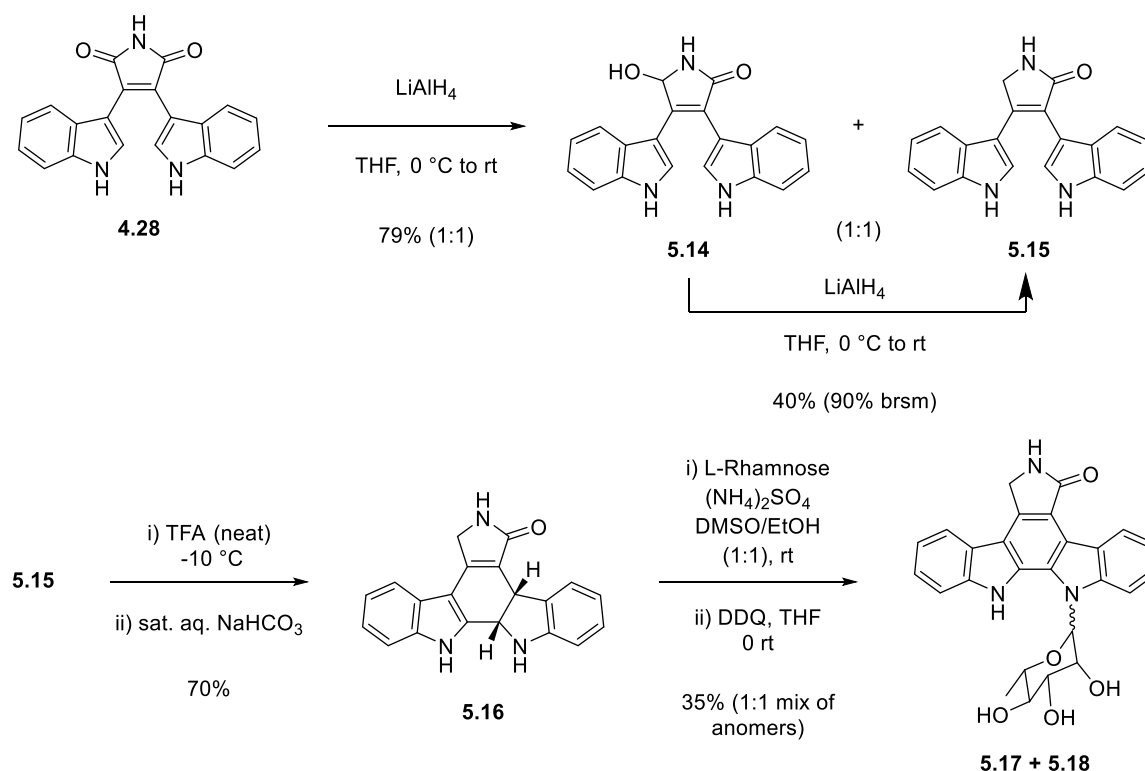
Scheme 33: Faul and co-workers' efforts to prepare indolocarbazole glycoside analogues of acryiaflavin A.

5.1.2 Previous Work in the Brown Group

The promising potential of indolyndoline systems looked ready to be capitalised upon in the wake of Faul and co-worker's publication, however to this date, this approach has not been applied to the regioselective derivatisation of the staurosporine aglycone. This set the stage for the Brown group to pick up this work and attempt to resolve this synthetic challenge. Much of this work was performed by George Chambers, and is outlined thoroughly in his thesis.¹⁹⁷ In this work

there were expansive attempts made to tackle the regioselectivity problem currently discussed and also make improvements toward a practical and scalable synthesis of the staurosporine aglycone. Where we will focus is the culmination of this work which led to a breakthrough in the use of an indolyldoline in the regioselective functionalisation of the staurosporine aglycone.

Bisindolylmaleimide (**4.28**) was reduced with LiAlH_4 yielding a 1 to 1 mixture of hydroxy lactam **5.14** and lactam **5.15**. Efforts to push this to completion were made however treating the hydroxy lactam with LiAlH_4 again only saw a similar conversion as the first attempt. Nevertheless, the good yield and starting material recovery meant the process was not wasteful. This was followed by an acid cyclisation, similar to that of Faul and co-workers,¹⁹⁶ which yield indolyldoline **5.16**. This system was the subject of extensive unsuccessful attempts towards glycosylation. Some of the results are outlined in Table 5. To add to these, silver promoted Koenigs-Knorr type glycosylations with halogenated sugars were also attempted with no success. The breakthrough came upon addition of DMSO to the ethanol solvent system to fully solubilise the entire mixture. Although seemingly obvious, previously successful glycosylations performed in the group had occurred with stirred suspensions so complete dissolution of starting materials had not been considered vital to success. Successful glycosylation of indoline **5.16** was performed with L-rhamnose yielding a 1:1 mixture of anomers after oxidation with DDQ, of which the alpha anomer (**5.17**) is the natural product K252d, which could be separated by column chromatography.



Scheme 34: Chambers' route towards successful glycosylation indolyldoline **5.16** and ultimately total synthesis of K252d (**5.17**).

Table 5: Some of the attempted glycosylation conditions by Chambers.

Entry	Conditions	Crude result (yield %)
1	(NH ₄) ₂ SO ₄ , EtOH, Δ, 14 h	Aglycone 4.04 (65%)
2	(NH ₄) ₂ SO ₄ , EtOH, Δ, 30 h	Aglycone 4.04 (70%)
3	EtOH/H ₂ O, Δ, 5 days	Clean indoline 5.16 ^a
4	(NH ₄) ₂ SO ₄ , CF ₃ CH ₂ OH, rt	Recovered indoline 5.16 ^a
5	(NH ₄) ₂ SO ₄ , HFIP, rt	Aglycone 4.04 and several glycosylated products ^a
6	AcOH, EtOH, 80 °C, 48 h	No observable glycosylated products ^b
7	(NH ₄) ₂ SO ₄ , DMF, Δ 21 h	Aglycone 4.04 isolated ^c

^a Mixture not subjected to oxidation step. ^b Glycosylated material unable to be isolated. Material did not react in presence of DDQ. ^c Lots of degradation.

5.1.3 Aims and Conclusions

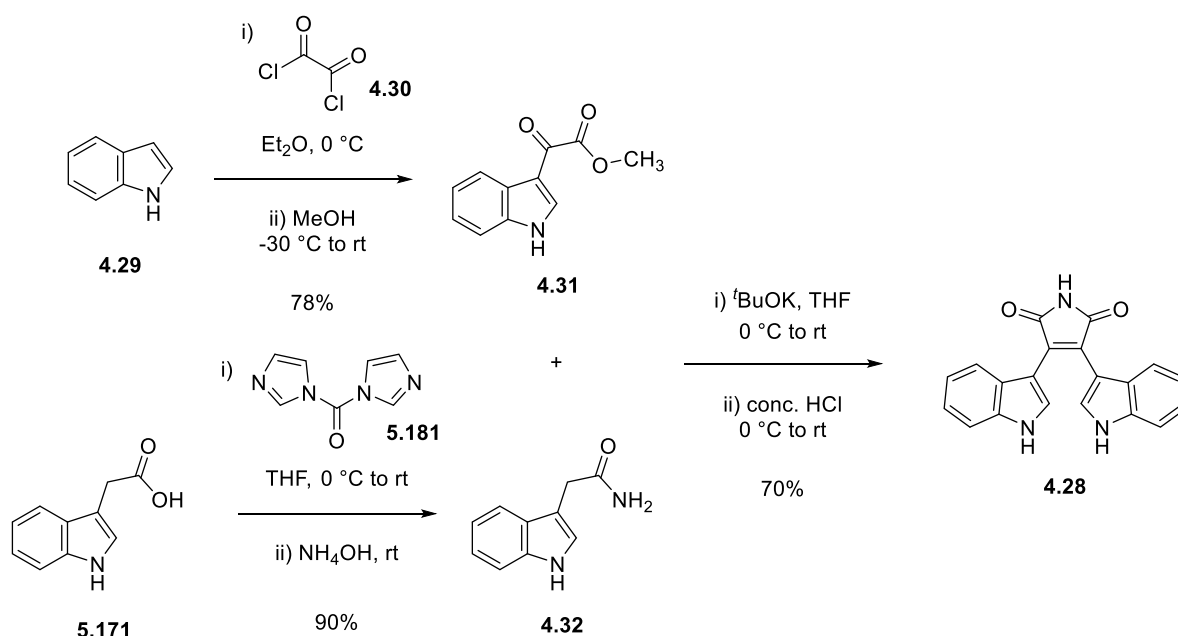
The potential of indole-indoline systems has successfully been applied to a regioselective synthesis of indolocarbazole natural product K252d.¹⁹⁷ This success was through the realisation of the requirement of complete solubilisation in the formation of this particular glycosidic linkage. Sadly, the formation of K252d is as far as the investigation into glycosylation of the asymmetric indole-indoline system **5.16** has progressed which leaves room for further examination of the potential of this approach.

The first aim would be to confirm the reproducibility of this approach and look to enhance the glycosylation step. The reported yield of 35% was the result of complete solubilisation which suggests that other potential methods may have failed due to the same factor, this outlines the need for the re-examination of the optimisation of this reaction. Furthermore, expanding the range of sugars used is a necessity as L-rhamnose was one of the lower yielding sugars in both Faul and Chisholm's work (60 and 72% respectively).^{195, 196}

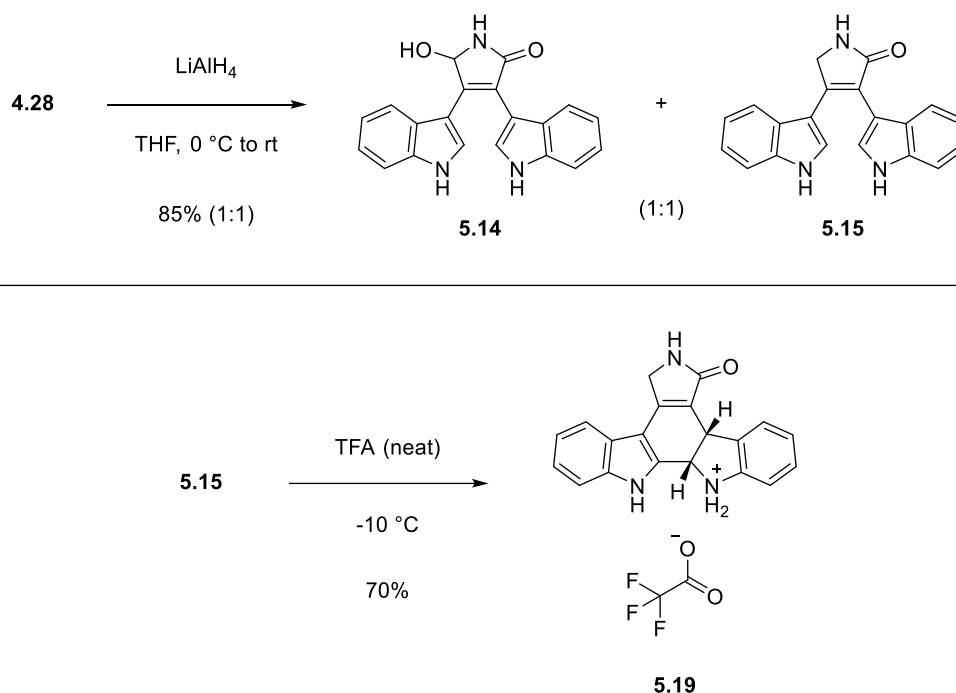
Finally, improvements of the route towards the relevant indole-indoline compound **5.16** may be warranted. The LiAlH₄ reduction step leaves half the isolated material as hydroxy lactam **5.14**, therefore a productive deoxygenation step to convert this to lactam **5.15** would be incredibly beneficial to the overall efficacy of the route. Also, the acid cyclisation in neat TFA is somewhat undesirable due to the large volumes needed for gram scale reactions (30 mL of TFA per gram of lactam **5.15**).¹⁹⁷

5.2 Consolidation of the Brown Group's Approach to a Useful Indole-Indoline System

To begin our inquiry, we first needed the indoline **5.16** in hand which meant repeating the groups previous synthesis.¹⁹⁷ This began with the approach of Faul and co-workers¹⁷⁶ where indole (**4.29**) was subjected to a substitution reaction with oxalyl chloride (**4.30**) with subsequent esterification with methanol affording ester **4.31** (Scheme 35). Amide **4.32** was prepared from commercially available indole-3-acetic acid (**5.171**) using coupling agent CDI (**5.181**) and ammonium hydroxide. Our prepared ester and amide could now be coupled under basic conditions which then yielded bisindolylmaleimide (**4.28**) after treatment with concentrated HCl. Reduction with LiAlH_4 was our next step and, as had been previously reported, creation of a 1:1 mixture of hydroxy lactam **5.14** and lactam of **5.15** was the result (Scheme 36). At this point reflection of our progress reports that we have reproduced all steps with analogous yields and an important development is the successful scaling of all these reactions to >10-gram scale without any notable problems. After separation of hydroxy lactam **5.14** and lactam **5.15** we progressed with a gram scale acid cyclisation furnishing TFA salt **5.19** with a good yield and in a regiocontrolled manner (Scheme 16). Concerned of the potential oxidative instability of the free base of salt **5.19**, we thought storing the compound as the salt and releasing the free base prior to use may be the best approach.



Scheme 35: Preparation of bisindolylmaleimide **4.28**.



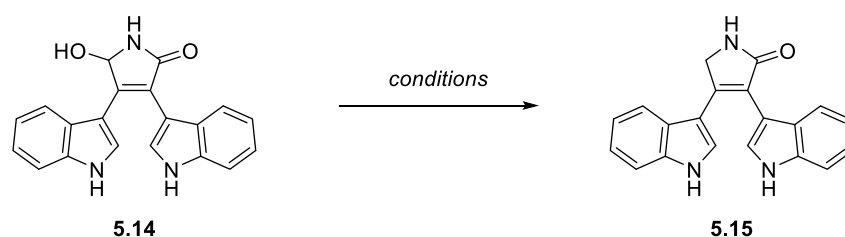
Scheme 36: Preparation of TFA salt **5.19**.

Our route now tested; we decided stockpiling of as much of TFA salt **5.19** as possible would be incredibly helpful in our later pursuit of efficient glycosylation. With this in mind our focus turned to hydroxy lactam **5.14** as efficient deoxygenation could potentially double the amount of lactam **5.15** produced. Evaluation of the literature highlighted our first potential problem, that being that many deoxygenation reactions are performed in non-polar solvents which lactam **5.15** showed little solubility in.¹⁹⁸ Deoxygenation reactions that can be performed in moderately polar solvents (THF) are usually hydride reductions and previous work in the group showed the limitations of this approach. However, there was some precedent for successful reductions of hydroxy lactams using organosilanes in moderately polar or polar solvents. For example, Butenschön and co-workers described the deoxygenation of a phthalimide system with triethylsilane and $\text{BF}_3 \cdot \text{OEt}_2$ in THF.¹⁹⁹ Furman and co-workers described the use of mixed solvent systems of DCM and acetonitrile in the deoxygenation of lactams with triethylsilane and $\text{BF}_3 \cdot \text{OEt}_2$.^{200, 201} Furthermore Xie and co-workers presented the deoxygenation of phthalimide systems with various silanes and KOH in DMF.²⁰²

Acetonitrile was the solvent of choice for our investigation of the silane mediated deoxygenation of hydroxy lactam **5.14** due to it showing acceptable solubility (100 mg dissolved in ≈ 10 mL) at the low temperatures instructed by literature (-25 $^\circ\text{C}$).^{200, 201} Pleasingly our first attempt, based on the procedure of Szcześniak and co-workers' gave us a 38% yield of lactam **5.15** (Table 6, entry 1) that was pure by ^1H NMR without purification. However, the material was noticeably discoloured when compared with material from the original LiAlH_4 reduction, being an orange/brown solid as opposed to the previously isolated off-white solid. A prominent darkening of the reaction mixture

was also observed during warming. Nonetheless, the material appeared pure so was subjected to acid cyclisation conditions but here we encountered a drastic reduction in yield, producing only 15% of the TFA salt **5.19** after purification.

Further analysis of our discoloured material showed a residual peak in the ^{19}F NMR suggesting that BF_3 or BF_2 may be bound to our product. This issue was resolved by washing the material with aqueous acid but no improvement to the following cyclisation was observed. Recrystallisation was unsuccessful and purification by column chromatography again had little effect. Our final line of thinking is that the inhibition of our TFA cyclisation and the discolouration may have the same cause. Therefore, substitution to propionitrile as our solvent allowed for lower temperatures to be achieved and gradual warming as well as a cold quench afforded lactam **5.15** in an improved 60% yield (Table 6, entry 5) as a pale yellow solid. Sadly, the ensuing cyclisation gave a 20% yield, like previous attempts. Thus, due to our main ambition to tackle the regioselective glycosylation being a priority, we had to progress without a convincing answer to this problem.



Scheme 37: Deoxygenation of hydroxy lactam **5.14**.

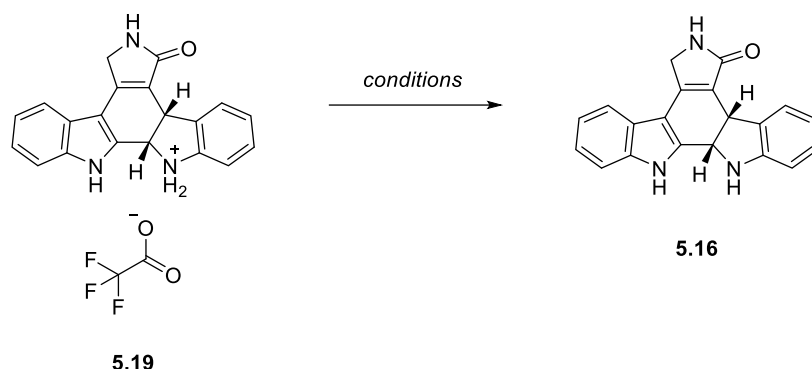
Table 6: Attempted conditions for the deoxygenation of hydroxy lactam **5.14**.

Entry	Conditions	Result (yield %)
1	Et_3SiH (10 eq.), $\text{BF}_3 \cdot \text{OEt}_2$ (3 eq.), CH_3CN , $-20\text{ }^\circ\text{C}$, 4 hours (warm to rt for quench)	Lactam 5.15 isolated (38%) ^b
2	Et_3SiH (10 eq.), $\text{BF}_3 \cdot \text{OEt}_2$ (3 eq.), CH_3CN , $-40\text{ }^\circ\text{C}$, 6 hours (warm to rt for quench)	Lactam 5.15 isolated (51%) ^{ab}
3	TFA (neat), Et_3SiH , $-10\text{ }^\circ\text{C}$	Degradation observed
4	PhSiH_3 (0.33 eq.), K_3PO_4 (0.05 eq.), DMF, rt, 3 days	No reaction observed

5	Et ₃ SiH (10 eq.), BF ₃ •OEt ₂ (3 eq.), CH ₃ CH ₂ CN, -60 to -20 °C, 5 hours	Lactam 5.15 isolated (60%) ^b
6	Et ₃ SiH (10 eq.), BF ₃ •OEt ₂ (6 eq.), CH ₃ CH ₂ CN, -60 to -20 °C, 5 hours	Lactam 5.15 isolated (53%) ^{b c}

^a Material isolated after column chromatography. ^b Isolated material could not be cyclised in TFA with reasonable yield. ^c Gram scale reaction.

Progression of our work now required the conversion of TFA salt **5.19** to the free base **5.16** (Scheme 38). This simple reaction was reportedly previously achieved in the group by sonicating the salt **5.19** in a saturated aqueous solution of sodium bicarbonate. However, to our surprise treatment with these conditions resulted in near quantitative recovery of our starting salt. The only plausible explanation was that the extreme insolubility of the salt made it essentially hydrophobic and thus was not interacting with the basic solution at all. Yet, exposure to more solubilising conditions still resulted in no deprotonation. To overcome this exceedingly odd situation sodium hydride was added to a solution of the salt in DMSO which allowed indoline **5.16** to be recovered in near quantitative yield.



Scheme 38: Deprotonation of TFA salt **5.19**.

Table 7: Attempted conditions for the deprotonation of TFA salt **5.19**.

Entry	Conditions	Result (yield %)
1	Sat. aq. NaHCO ₃ sol. sonication, rt 5 min	Salt 5.19 recovered (94%)
2	Sat. aq. K ₂ CO ₃ sol. sonication, rt, 10 min	Salt 5.19 recovered (97%)

3	Cs ₂ CO ₃ (30 eq.), H ₂ O/EtOH (1:1), rt, 1 h	Salt 5.19 recovered (94%)
4	CsCO ₃ (30 eq.), H ₂ O/DMSO (1:2), rt, 1h	Salt 5.19 recovered (51%) ^a
5	NaHCO ₃ (30 eq.), H ₂ O/DMSO (2:5), 40 °C, 1h	Salt 5.19 recovered (60%) ^a
6	NaH, DMSO, rt, 5 min	Indoline 5.16 isolated (98%)

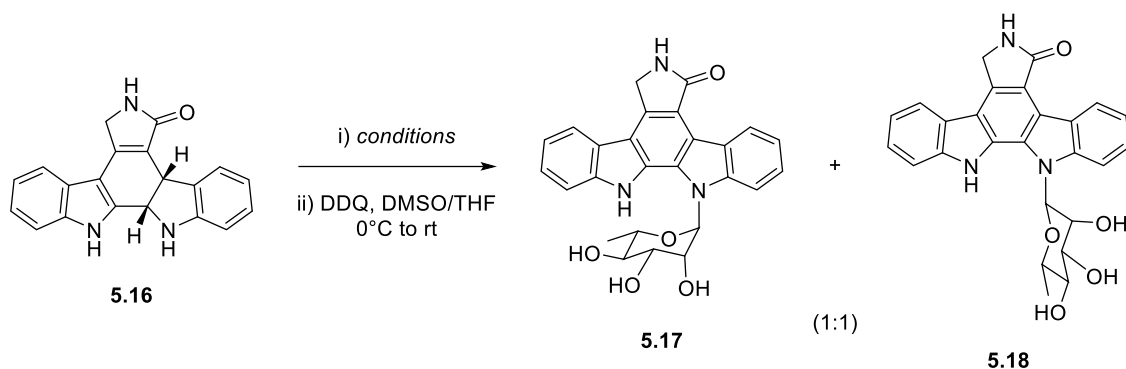
^a Salt **5.19** was recovered by extraction in EtOAc which is not expected to be efficient due to the salt's low solubility in EtOAc.

5.3 Synthesis of K252d and Related Staurosporine Aglycone Glycosidic Analogues

With the previously successful efforts in the group in mind, *N*-glycosylation of indoline **5.16** with L-rhamnose was a good place to begin. This would allow us to test the previously elucidated conditions and complete the synthesis of K252d, allowing us to fully characterise for potential publication.

Previously indicated conditions suggested full dissolution in a 1:1 mixture of DMSO and ethanol. However, straight away we were met with the problem that indoline **5.16** was insoluble at the concentrations suggested. Proceeding with the reaction anyway led to no conversion (Table 8, entry 1) so efforts were made to ensure full dissolution was achieved but still no reaction was observed (Table 8, entry 2). Fearing the low concentration of indoline **5.16** may be leading to a very slow reaction, we biased the solvent system towards DMSO alleviating this somewhat only to see the same result again (Table 8, entry 3). This led to us taking a more aggressive approach, trying Faul and co-workers' conditions¹⁹⁶ with our solvent system and gratifyingly we achieved successful glycosylation (Table 8, entry 4). We attained a 31% yield of the expected mixture of anomers (**5.16** and **5.17**). However, we noted a significantly reduced recovery of aglycone **4.04** (35% compared to 64%). Adjusting the reaction time saw that shorter reactions produce less glycosylated product and give higher aglycone recovery and longer reaction times saw similar yields of glycosylation but lower aglycone recovery (Table 8, entry 5 and 6). This fuelled the conclusion that we were reaching an equilibrium between indoline **5.16** and glycosylated

products **5.17** and **5.18** at the 6–8-hour mark. We could also deduce that degradation of either starting material or product was occurring however, no significant by-products were observed.



Scheme 39: N-glycosylation of indoline **5.16** with L-rhamnose.

To try to influence the equilibrium of *N*-glycosylation drying agents such as silica, alumina, magnesium sulfate and molecular sieves were added. Nevertheless, the yield of glycosylated product remained steadfast. The role of ethanol in the reaction was also scrutinised but removal of this component of our solvent seemingly saw the reaction progress much slower, resulting in diminished yield after 16 hours. Separately we also noted that our sugar was seemingly falling off during in work-up (column chromatography) resulting in difficulty obtaining pure samples. With little success in the optimisation of this reaction, our attention turned to the sugar. Previously, we have mentioned that L-rhamnose was one of the less effective sugars in both Faul and Chisholm's work (60 and 72% respectively)^{195, 196} which led us to wonder if alternate sugars may perform significantly better in our approach.

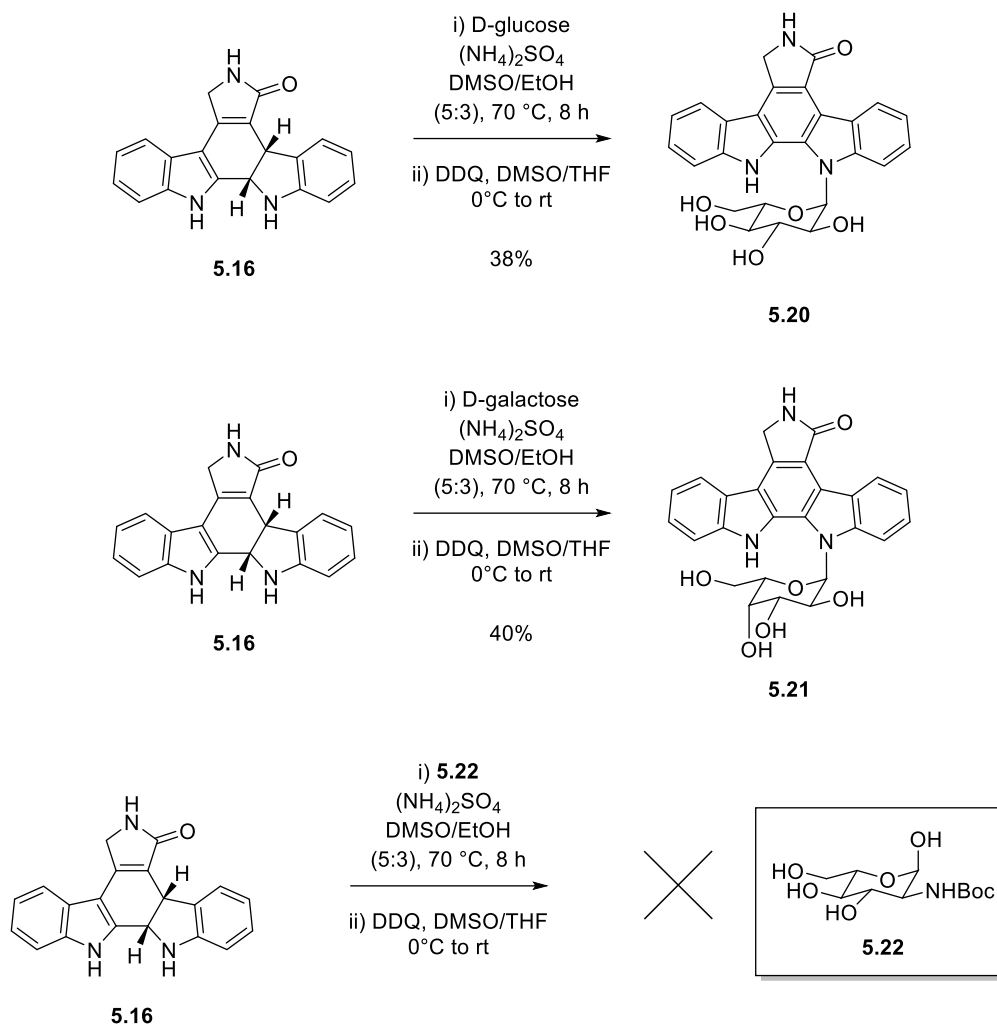
Table 8: Conditions for N-glycosylation of indoline **5.16**.

Entry	Conditions	Result (yield %)
1	L-rhamnose (5 eq.), (NH ₄) ₂ SO ₄ (0.5 eq), DMSO/EtOH (1:1, 23 mg/mL), rt, 2 days	Indoline 5.16 recovered ^a
2	L-rhamnose (5 eq.), (NH ₄) ₂ SO ₄ (0.5 eq), DMSO/EtOH (1:1, 6 mg/mL), rt, 2 days	Indoline 5.16 recovered ^a
3	L-rhamnose (5 eq.), (NH ₄) ₂ SO ₄ (0.5 eq), DMSO/EtOH (5:3, 13 mg/mL), rt, 2 days	Indoline 5.16 recovered ^a
4	L-rhamnose (10 eq.), (NH ₄) ₂ SO ₄ (3 eq), DMSO/EtOH (5:3, 13 mg/mL), 70 °C, 8 h	1:1 mixture of K252d 5.17 and β-K252d 5.18 (31%), aglycone 4.04 (35%)

5	L-rhamnose (10 eq.), (NH ₄) ₂ SO ₄ (3 eq), DMSO/EtOH (5:3, 13 mg/mL), 70 °C, 4 h	1:1 mixture of K252d 5.17 and β-K252d 5.18 (22%), aglycone 4.04 (51%)
6	L-rhamnose (10 eq.), (NH ₄) ₂ SO ₄ (3 eq), DMSO/EtOH (5:3, 13 mg/mL), 70 °C, 12 h	1:1 mixture of K252d 5.17 and β-K252d 5.18 (30%), aglycone 4.04 (21%)
7	L-rhamnose (10 eq.), (NH ₄) ₂ SO ₄ (3 eq), DMSO, 70 °C, 16 h	1:1 mixture of K252d 5.17 and β-K252d 5.18 (24%), aglycone 4.04 (16%)
8	L-rhamnose (10 eq.), (NH ₄) ₂ SO ₄ (3 eq), DMSO/EtOH (5:3, 13 mg/mL), 70 °C, 8 h, 3 Å MS	1:1 mixture of K252d 5.17 and β-K252d 5.18 (28%), aglycone 4.04 (33%)

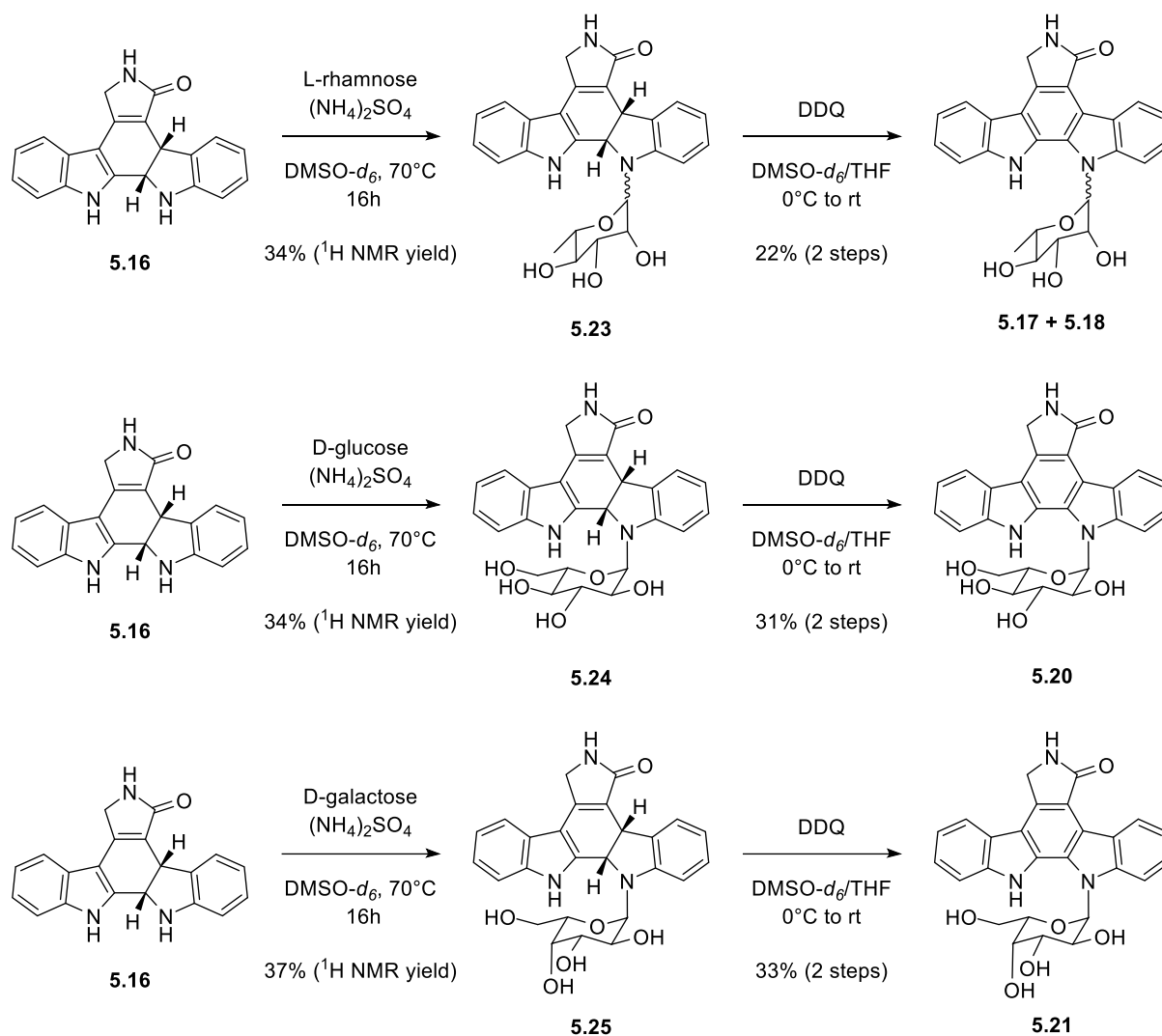
^a Reaction mixture was not treated with DDQ.

The three sugars we had to hand were D-glucose, D-galactose, and D-glucosamine (Boc-protected). Glucose and galactose performed significantly better in Faul and co-workers' studies with yields of glycosylated products of 88% and 96% respectively,¹⁹⁶ glucosamine has not previously been investigated but the presence of the amine group provides opportunity to investigate the tolerance of the reaction. Using our established conditions afforded successful glycosylation producing staurosporine aglycone glycosides **5.20** and **5.21** as single anomers (Scheme 40). We saw reproducibly higher yields (~10%) with glucose and galactose compared to mannose. Although improved, the result still felt somewhat lacking, but investigation seemed to reveal a similar equilibrium being achieved in these reactions. The reaction with Boc-protected glucosamine was sadly unsuccessful with study of the reaction revealing deprotection of the amine being prevalent.



Scheme 40: Glycosylation of indoline **5.16** with different sugars.

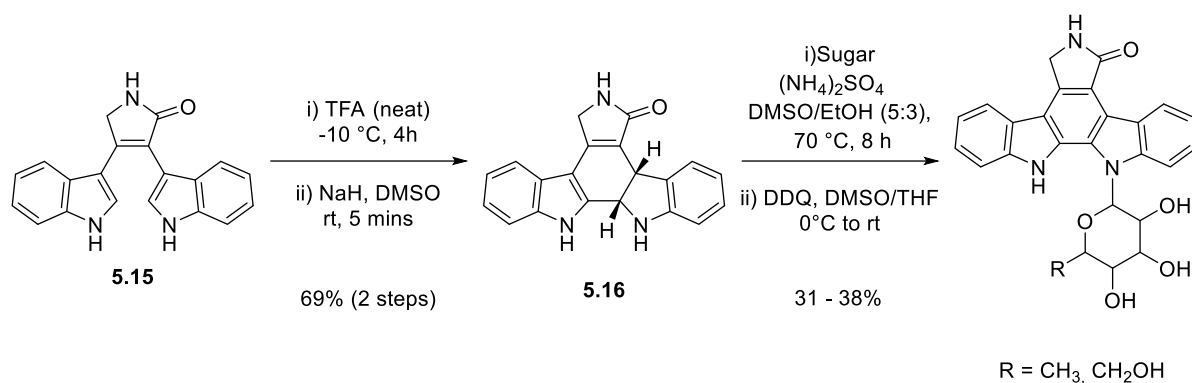
Our investigation of the glycosylation approach revealed what seemed to be a ceiling to the conversion. However, to confirm this conclusion we still needed to verify the efficacy of our DDQ oxidation. Previous work in the group had suggested that the oxidation step could be near quantitative with L-fucose glycosylation of indoline **5.12** furnishing a 97% yield after DDQ oxidation. To test this, we carried out a series of glycosylation reactions in DMSO- d^6 and recorded the NMR yield of the glycosylated indoline before oxidation and compared this with the isolated yield after oxidation (Scheme 41). This revealed that DDQ oxidation of indoline glycosides **5.24** and **5.25**, formed by glycosylation of indoline **5.16** with D-glucose and D-galactose respectively, were near quantitative. However, the DDQ oxidation of indoline glycoside **5.23**, formed by glycosylation with L-rhamnose, resulted in a diminished isolated yield. This inferred that the initial glycosylation step of all reactions was similar in terms of productivity, but the lower yield observed with L-rhamnose was a result of instability during the oxidation step. This is a thought echoed by Faul and co-workers in their analyses.¹⁹⁶



Scheme 41: Evaluation of DDQ oxidation of indoline glycoside intermediates **5.23-5.25**.

5.4 Conclusions and Future Perspectives

Extensive probing of the glycosylation of indole-indoline system **5.16** has been the focus of this short investigation. We can celebrate successfully expanding the range of staurosporine aglycone glycosides isolated with effective glycosylation's with D-glucose and D-galactose being achieved (Scheme 42). Beyond this we have also managed to tackle challenges in reproducing previous work in the group. Much to our surprise some of the steps, expected to be trivial, needed re-evaluation and this also included developing modified conditions for glycosylation reactions. Our exhaustive examination of glycosylation appears to have revealed its limitations, these being an apparent equilibrium in our glycosylation step that is difficult to affect and oxidative instability of some of our glycosylated indolines. To add to that, instability of oxidised glycosylated products during work-up also seems to contribute to reduced returns.



Scheme 42: Cyclisation, glycosylation, and oxidation to regioselectively functionalise the staurosporine aglycone.

With the shortfalls of our method, future work likely needs to reconsider other approaches. In this consideration the main factor is likely the requirement of DMSO to dissolve our indole-indoline system. A comprehensive solvent screen should precede any decisions, but our own experiences suggest that options will be limited. Palladium couplings are routinely performed in polar aprotic solvents such as DMF, therefore an approach similar Seo and co-workers¹⁸⁴ may be the most appealing. However, the selectivity of such techniques for the indoline functionality over that of the indole would need investigating. Apart from this there has also been efforts to achieve glycosylation of indoles (towards glycosylated indolocarbazoles) utilising the Mitsunobu reaction and such attempts often exploit polar aprotic solvent systems.²⁰³

Finally, the original and continued aim of this project is the total synthesis of Staurosporine and derivatives of the natural product towards collaborative investigation of the anti-fungal properties of such compounds. Therefore, application of our successful regioselective methodology to this task would be incredibly satisfying however, to achieve this work still needs to be done to elucidate the most effective regioselective reaction to employ.

Chapter 6 Experimental

6.1 General Procedures

Chemicals were purchased from Sigma–Aldrich, Fisher Scientific, Fluorochem Ltd or Alfa Aesar. NaH was used as a 60% dispersion in oil. All air/moisture sensitive reactions were carried out under an inert atmosphere, in oven–dried or flame–dried glassware. CH₂Cl₂ (from CaH₂) was distilled before use, and where appropriate, other reagents and solvents were purified by standard techniques. Molecular sieves, 3 Å or 4 Å were activated by heating to 130 °C under high vacuum (>0.1 mbar) for 16 hours. TLC was performed on aluminium–precoated plates coated with silica gel 60 with an F254 indicator; visualised under UV light (254 nm) and/or by staining with potassium permanganate. Flash column chromatography was performed using high purity silica gel, pore size 60 Å, 230–400 mesh particle size, purchased from Merck. Automated flash chromatography was performed using the Biotage® Selekt System with Biotage® Sfär Silica D Duo columns with 100 Å pore size and 60 µm particle size. ¹H NMR, ¹⁹F NMR and ¹³C NMR spectra were recorded in CDCl₃ or DMSO-*d*₆ (purchased from Cambridge Isotope Laboratories) at 298 K using Bruker DPX400 (400, 376 and 101 MHz respectively) spectrometers. Chemical shifts are reported on the δ scale in ppm and were referenced to residual solvent (CDCl₃: 7.27 ppm for ¹H NMR spectra and 77.0 ppm for ¹³C NMR spectra. DMSO-*d*₆: 2.50 ppm for ¹H NMR spectra and 39.52 ppm for ¹³C NMR spectra). All spectra were reprocessed using ACD/Labs software version 2015 or ACD/Spectrus. Coupling constants (J) were recorded in Hz. The following abbreviations for the multiplicity of the peaks are s (singlet), d (doublet), t (triplet), q (quartet), quin (quintet), br (broad), and m (multiplet). Electrospray (ES) low resolution mass spectra were recorded on a Waters TQD quadrupole spectrometer coupled to a waters UPLC. Electronimpact (EI) low resolution mass spectra were recorded on a Trace 2000 Series GC–MS coupled to a HP5890 GC. High resolution mass spectra were recorded on a Bruker APEX III FT–ICR mass spectrometer. Fourier–transform infrared (FT IR) spectra are reported in wavenumbers (cm^{–1}) and were collected as solids or neat liquids on a Nicolet 380 using OMNIC software package. Melting points were obtained using a Gallenkamp Electrothermal apparatus.

Solution absorbance and emission data were collected with the HORIBA Duetta™ using Hellma Collect Absorbance/Transmission Cuvette QS/QG Quartz path length 10 mm. Samples were prepared at concentrations of approximately 0.025 mg/mL and the excitation wavelength employed for emission measurements was 350 nm.

Solid-state photoluminescent absorption and emission measurements were performed using a Thorlabs-supplied 340 nm laser (M340L4) with a power output of 53 mW (minimum) and 700 mA served as the excitation source for photoluminescence emission which was lowered to 500 mA

when analysing polyoxometalate containing compounds. An adjustable Collimation Adapter (SM2F32-A) featuring a Ø2" Lens with AR Coating and a wavelength range of 200 nm–700 nm was used in conjunction with the 340 nm laser source for photoluminescent absorption measurements. Measurements were performed on spray-coated films. The coated film on a glass ITO slide possessed a thickness of 250 nm.

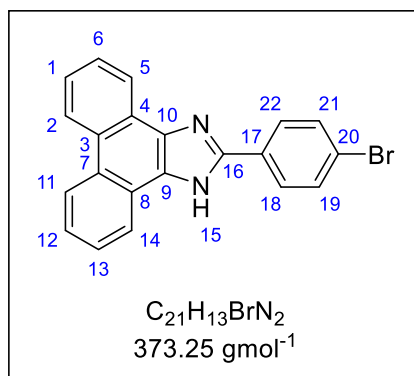
Cyclic voltammograms were recorded using a 3-electrode configuration with SCE as reference electrode at 100 mV s⁻¹, with a glassy carbon (3 mm Ø) working electrode and a Pt counter electrode in degassed unstirred dry DMF with 100 mmol Et₄NBF₄ and 5 mmol of the analysed compound.

LEC device fabrication started with a PEDOT: PSS suspension in water which was first spin coated directly on the ITO patterned substrate and annealed on a hotplate at 120 °C for 20 min in a The UV emitting active layer 5a was spin coated in an ambient environment. The utilised emissive molecule was dissolved in acetonitrile or DMF at a concentration of 0.2 g/mL. Annealing of the spin coated emissive layer was undertaken at 70 °C for 5 h in a nitrogen filled box oven. To complete LEC fabrication, a silver top electrode was sputter coated through a pre-defined shadow mask, by a coating current of 70 mA to achieve a thickness of 100 nm. The top electrode mask was pre-defined to achieve three light emitting pixels (active area of the electrode, 2 mm²). Silver conductive paint was subsequently applied to establish contact points for testing. Finally, the devices were encapsulated by drop casting an epoxy formulation onto the surface and covering with a coverslip. The fully encapsulated system was then UV cured with a 365 nm wavelength mercury lamp. The encapsulation process was performed in an argon filled glove box to avoid oxygen being trapped in the devices.

Phenom G6 ProX Scanning Electron Microscope (SEM) system was employed to capture cross-sectional SEM images of the UV OLEC devices to assess the thickness of the functional layers.

6.2 Procedures and Characterisation Data

2-(4-Bromophenyl)-1H-phenanthro[9,10-d]imidazole (**2.07**)



2-(4-Bromophenyl)-1H-phenanthro[9,10-d]imidazole (**2.07**) was prepared according to the procedure described by J. C. John and co-workers'.¹¹²

Under argon atmosphere phenanthrenequinone (4.00 g, 19.2 mmol), 4-bromobenzaldehyde (3.55 g, 19.2 mmol) and ammonium acetate (14.8 g, 192 mmol) were added to a round-bottomed flask and glacial acetic acid (75 mL) added. The mixture was stirred under reflux and large amounts of precipitate formed. At this point a further 20 mL of glacial acetic acid was added to help the mixture stir more effectively. This mixture was refluxed for 16 hours then allowed to cool to rt. Deionised water (70 mL) was added then the mixture filtered. The isolated solid was washed thoroughly with deionised water then with hexane followed by a small amount of diethyl ether. The material was dried in the vacuum oven at 75 °C to remove residual acetic acid, this afforded the title compound as an off-white solid. (7.48 g, 91%).

M.P. 245 – 248 °C (lit. 244 – 247 °C)²⁰⁴

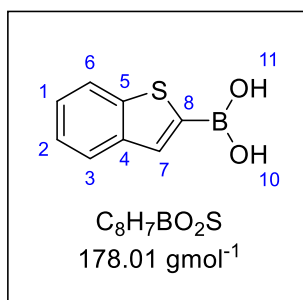
¹H NMR (400 MHz, DMSO-*d*₆, 298 K) δ (ppm) = 13.53 (s, 1H, **15**), 8.84 (dd, J = 13.6, 8.4 Hz, 2H, **2 + 11**), 8.59 (d, J = 7.7 Hz, 1H, **5/14**), 8.53 (d, J = 7.8 Hz, 1H, **5/14**), 8.27 (dt, J = 8.8, 2.1 Hz, 2H, **18 + 22**), 7.81 (dt, J = 8.8, 2.1 Hz, 2H, **19 + 21**), 7.70 – 7.79 (m, 2H, **6 + 13**), 7.64 (dd, J = 13.3, 6.6 Hz, 2H, **1 + 12**)

¹³C NMR (101 MHz, DMSO-*d*₆, 298 K) δ (ppm) = 148.0 (C, **C16**), 137.0 (C, **C10**), 131.9 (CH, **19 + 21**), 129.6 (C, **C17**), 128.0 (CH, **C18 + C22**), 127.9 (C, **C9**), 127.8 (C, **C4/C8**), 127.6 (C, **C4/C8**), 127.2 (CH, **C6/C13**), 127.1 (CH, **C6/C13**), 126.9 (C, **C20**), 125.5 (CH, **C1/C12**), 125.3 (CH, **C1/C12**), 124.1 (CH, **C5/C14**), 123.8 (CH, **C5/C14**), 122.5 (C, **C3/C7**), 122.3 (C, **C3/C7**), 122.0 (CH, **C2/C11**), 121.9 (CH, **C2/C11**)

LRMS ES⁺ m/z = 373.2 [$M^{79}Br+H$]⁺, 375.2 [$M^{81}Br+H$]⁺

FT-IR (neat) ν_{max} 3193, 1683, 1477, 1010, 827, 751, 722 cm^{-1}

Benzo[b]thiophen-2-ylboronic acid (**2.09**)



Benzo[b]thiophen-2-ylboronic acid (**2.09**) was prepared according to the procedure described by K. Górski and co-workers'.²⁰⁵

Benzothiophene (4.34 g, 32.3 mmol) was dissolved in dry THF (40 mL) under argon atmosphere and the solution cooled to -78 °C. Then *n*-BuLi (2.5 M in hexanes, 12.9 mL, 32.3 mmol) was added dropwise. The mixture was stirred for 1 hour and a white precipitate formed. The mixture was allowed to warm to rt before being cooled back down to -78 °C. At -78 °C trimethyl borate (4.06 mL, 36.4 mmol) was added dropwise and once addition was complete the mixture allowed to warm to rt. Aqueous HCl (2 mL of conc HCl in 10 mL of deionised water) was added and the mixture extracted with DCM (3 x 40 mL). The combined organic extracts were dried ($MgSO_4$) and then solvent removed under reduced pressure. To this solid hexane (35 mL) was added and the mixture cooled to 0 °C before filtering. This gave the titled compound as a white solid. (3.04 g, 53%).

M.P. 250 – 253 °C (lit. 260– 262 °C)²⁰⁶

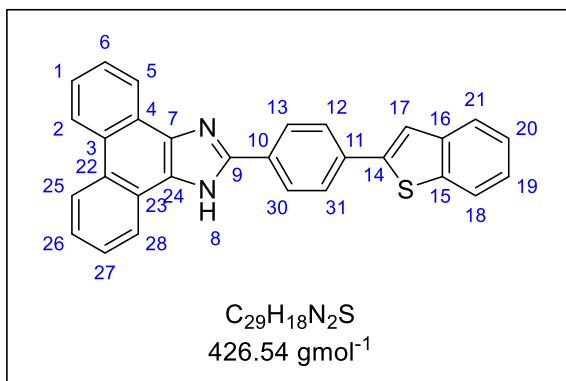
¹H NMR (400 MHz, acetone- d_6 , 298 K) δ (ppm) = 7.93 – 7.98 (m, 2H, **6 + 7**), 7.89 (m, 1H, **3**), 7.56 (s, 1H, **OH**), 7.32 – 7.42 (m, 2H, **1 + 2**)

¹³C NMR (101 MHz, acetone- d_6 , 298 K) δ (ppm) = 143.9 (C, **C5**), 141.3 (C, **C4**), 133.1 (CH, **C7**), 125.3 (C, **C8**), 124.5 (CH, **C1 + C2**), 124.3 (CH, **C3**), 122.7 (CH, **C6**)

LRMS EI m/z = 134.0 (100% $[M-B(OH)_2]^+$)

FT-IR (neat) ν_{max} 3241, 1515, 1343, 1153, 1054, 762, 636 cm^{-1}

2-(4-(Benzo[b]thiophen-2-yl)phenyl)-1H-phenanthro[9,10-d]imidazole (2.10)



2-(4-(Benzo[b]thiophen-2-yl)phenyl)-1H-phenanthro[9,10-d]imidazole (**2.10**) was prepared according to the procedure described by J. C. John and co-workers'.¹¹²

2.07 (6.80 g, 18.2 mmol), benzo[b]thiophen-2-ylboronic acid (4.99 g, 25.2 mmol) and potassium carbonate (12.58 g, 91.0 mmol) were added to a round-bottomed flask under argon atmosphere. Toluene (160 mL) ethanol (80 mL) and deionised water (80 mL) were added, and the mixture degassed for 30 minutes. $Pd(PPh_3)_4$ (1.05 g, 0.91 mmol) and tetrabutylammonium bromide (0.590 g, 1.82 mmol) were added, the mixture heated to 80 °C and stirred for 16 hours. The mixture was then allowed to cool to rt and deionised water (80 mL). The solid precipitate was filtered, and the filtrate extracted with ethyl acetate (3 x 60 mL). The combined organic extracts were washed with brine, dried ($MgSO_4$) and solvent removed under reduced pressure. The extracted material as well as the filtered solid were combined and further purified by silica plug (100% ethyl acetate). This gave the title compound as a yellow solid. (5.27 g, 68%).

M.P. 245 – 248 °C

¹H NMR (400 MHz, $DMSO-d_6$, 298 K) δ (ppm) = 13.56 (s, 1H, **8**), 8.86 (t, J = 8.4 Hz, 2H, **2** + **25**), 8.61 (dd, J = 17.5, 7.3 Hz, 2H, **5** + **28**), 8.43 (d, J = 8.3 Hz, 2H, **13** + **30**), 7.97 – 8.05 (m, 4H, **12** + **17** + **18** + **31**), 7.88 (dd, J = 7.5, 1.2 Hz, 1H, **21**), 7.76 (d, J = 6.7 Hz, 2H, **6** + **27**), 7.65 (t, J = 7.5 Hz, 2H, **1** + **26**), 7.40 (quind, J = 7.4, 1.2 Hz, 2H, **19** + **20**)

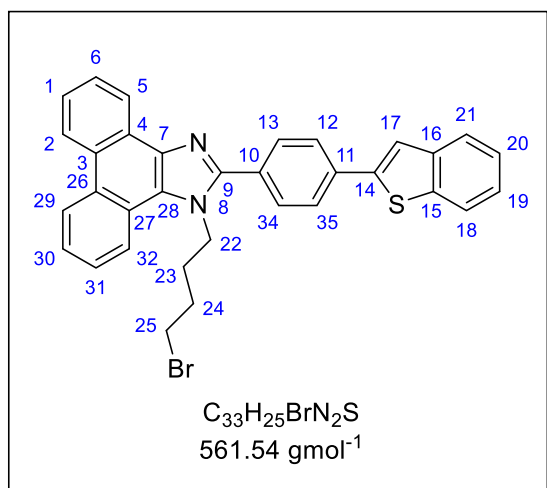
¹³C NMR (101 MHz, $DMSO-d_6$, 298 K) δ (ppm) = 148.5, (C, **C9**), 142.6 (C, **C7/C24**), 140.5 (C, **C15**), 138.7 (C, **C16**), 137.2 (C, **C7/C24**), 134.0 (C, **C10**), 130.2 (C, **C3/C22**), 127.7 (C, **C3/C22**), 127.1 (C, **C6** + **C27**), 126.8 (CH, **C12** + **C31**), 126.5 (CH, **C13** + **C30**), 125.4 (CH, **C1/C26**), 125.3 (CH, **C1/C26**), 124.9 (CH, **C19/C20**), 124.9 (CH, **C19/C20**), 124.1 (CH, **C2/C21/C25**), 123.9 (CH, **C2/C21/C25**), 123.8 (CH, **C2/C21/C25**), 122.5 (CH, **C17/C18**), 122.3 (C, **C4/C22**), 122.0 (CH, **C5** + **C28**), 120.6 (CH, **C17/C18**)

LRMS ES^+ m/z = 427.2 $[M+H]^+$

FT-IR (neat) ν_{max} 3460, 3053, 1616, 1453, 1323, 814, 740, 718 cm^{-1}

2-(4-(Benzo[*b*]thiophen-2-yl)phenyl)-1-(4-bromobutyl)-1H-phenanthro[9,10-*d*]imidazole

(2.11)



2.10 (0.100 g, 0.230 mmol) was dissolved in dry THF (5 mL) under argon atmosphere. The solution was cooled to 0 °C and potassium tert-butoxide (1 M in THF, 1.17 mL, 1.17 mmol) added. This mixture was stirred for 30 minutes as it was allowed to return to rt. 1,4-dibromobutane (0.251 g, 1.17 mmol) was added, the mixture heated to 60 °C and stirred for 16 hours. The mixture was allowed to cool to room temperature then deionised water (2 mL) added. The solid precipitate was filtered, and

the filtrate extracted with ethyl acetate (3 x 5 mL). The combined organic extracts were washed with brine, dried ($MgSO_4$) and solvent removed under reduced pressure. This extracted solid was combined with the filtered solid and the crude material further purified by silica gel column chromatography (hexane:ethyl acetate = 5:1 → 7:3). This gave the title compound as an off-white solid. (76 mg, 59%).

M.P. 168 – 170 °C

1H NMR (400 MHz, $DMSO-d_6$, 298 K) δ (ppm) = 8.99 (dd, J = 8.6, 1.0 Hz, 1H, **29**), 8.87 (d, J = 8.3 Hz, 1H, **2**), 8.62 (dd, J = 7.9, 1.2 Hz, 1H, **5**), 8.46 (d, J = 7.7 Hz, 1H, **32**), 8.00 – 8.06 (m, 4H, **12 + 17 + 18 + 35**), 7.88 – 7.95 (m, 3H, **13 + 21 + 34**), 7.79 (td, J = 7.6, 1.1 Hz, 1H, **31**), 7.63 – 7.76 (m, 3H, **1 + 6 + 30**), 7.42 (quind, J = 7.1, 2.1 Hz, 2H, **19 + 20**), 4.78 (t, J = 7.3 Hz, 1H, **22**), 3.39 (t, J = 6.4 Hz, 2H, **25**), 1.99 (quin, J = 7.3 Hz, 2H, **23**), 1.69 (quin, J = 7.0 Hz, 1H, **24**)

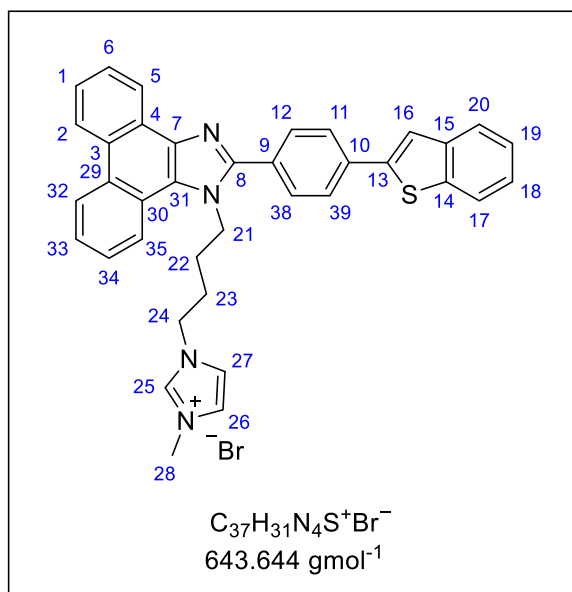
^{13}C NMR (101 MHz, $DMOS-d_6$, 298 K) δ (ppm) = 151.8 (C, **C9**), 142.3 (C, **C14**), 140.4 (C, **C15**), 138.8 (C, **C16**), 137.4 (C, **C7/C28**), 134.3 (C, **C11**), 130.6 (CH, **C13 + C34**), 130.4 (C, **C10**), 128.3 (C, **C27**), 127.7 (C, **C4**), 127.5 (CH, **C31**), 127.3 (CH, **C1/C6**), 126.8 (C, **C3**), 126.2 (CH, **C12 + C35**), 126.0 (C, **C7/C28**), 125.7 (CH, **C1/C6**), 125.2 (CH, **C30**), 125.0 (CH, **C19/C20**), 125.0 (CH, **C19/C20**), 124.5 (CH, **C29**), 123.6 (CH, **C2**), 124.0 (CH, **C21**), 122.8 (C, **C26**), 122.6 (CH, **C17/C18**), 121.9 (CH, **C5**), 121.3 (CH, **C32**), 121.1 (CH, **C17/C18**), 45.8 (CH_2 , **C22**), 34.1 (CH_2 , **C25**), 29.0 (CH_2 , **C24**), 28.3 (CH_2 , **C23**)

LRMS ES⁺ m/z = 561.3 [M⁷⁹Br+H]⁺, 563.3 [M⁸¹Br+H]⁺

HRMS ES⁺ m/z calcd for C₃₃H₂₆BrN₂S / [M⁷⁹Br+H]⁺ requires 561.1000 found 561.0998.
[M⁸¹Br+H]⁺ requires 563.1000 found 563.0981

FT-IR (neat) ν_{max} 3384, 3051, 1571, 1448, 1357, 1162, 748, 722 cm⁻¹

1-(4-(2-(4-(Benzo[*b*]thiophen-2-yl)phenyl)-1H-phenanthro[9,10-*d*]imidazol-1-yl)butyl)-3-methyl-1H-imidazol-3-ium bromide (2.13)



To **2.11** (1.22 g, 2.17 mmol) was added excess 1-methylimidazole (20 mL) and the solution heated to 100 °C under argon atmosphere. The solution was stirred at 100 °C for 2 hours then allowed to cool to rt and deionised water (20 mL) added. IPA (10 mL) was added then HBr (48% aqueous) added slowly to bring the pH of the mixture from approximately 9 to 7 (as indicated by universal indicator paper). These induced large amounts of precipitation, this precipitate was filtered and washed thoroughly with water

followed by washing with small amounts of ethyl acetate and diethyl ether. This gave the title compound as a light-yellow solid. (1.31 g, 94%).

M.P. 177 – 181 °C

¹H NMR (400 MHz, DMSO-*d*₆, 298 K) δ (ppm) = 9.02 (s, 1H, **25**), 8.99 (d, *J* = 8.2 Hz, 1H, **32**), 8.87 (d, *J* = 8.3 Hz, 1H, **2**), 8.61 (d, *J* = 8.2 Hz, 1H, **5**), 8.37 (d, *J* = 8.1 Hz, 1H, **35**), 7.98 – 8.10 (m, 4H, **11 + 16 + 17 + 39**), 7.87 – 7.95 (m, 3H, **12 + 20 + 38**), 7.58 – 7.82 (m, 6H, **1 + 6 + 26 + 27 + 33 + 34**), 7.43 (quind, *J* = 7.1, 1.2 Hz, 2H, **18 + 19**), 4.78 (t, *J* = 6.4 Hz, 2H, **21**), 4.08 (t, *J* = 6.5 Hz, 2H, **24**), 3.74 (s, 3H, **26**), 1.77 – 1.85 (m, 2H, **22**), 1.67 – 1.77 (m, 2H, **23**)

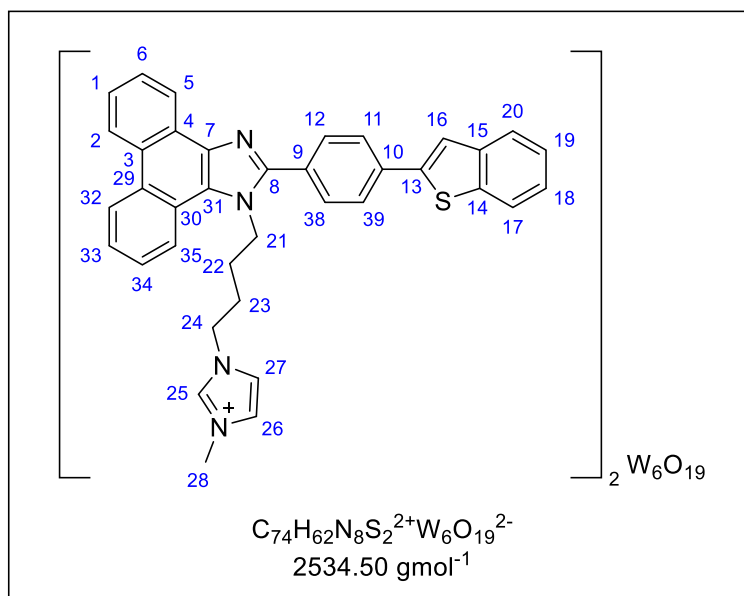
¹³C NMR (101 MHz, DMSO-*d*₆, 298 K) δ (ppm) = 151.8 (C, **C8**), 142.3, (C, **C13**), 140.4 (C, **C14**), 138.8 (C, **C15**), 137.4 (C, **C7/C31**), 136.5 (CH, **C25**), 134.4 (C, **C10**), 130.6 (CH, **C12 + C38**), 130.4 (C, **C9**), 128.3 (C, **C30**), 127.7 (C, **C4**), 127.5 (CH, **C33/C34**), 127.4 (CH, **C1/C6**), 126.8 (C, **C3**), 126.3 (CH, **C11 + C39**), 125.9 (C, **C7/C31**), 125.7 (CH, **C1/C6**), 125.2 (CH, **C33/C34**), 125.1 (CH, **C18/C19**), 125.0 (CH, **C18/C19**), 124.6 (CH, **C32**), 124.1 (CH, **C20**), 123.6 (CH, **C2**), 123.5 (CH, **C26**), 122.8 (C, **C29**), 122.6 (CH, **C16/C17**), 122.0 (CH, **C5**), 121.9 (CH, **C27**), 121.2 (CH, **35**), 121.1 (CH, **C16/17**), 48.1 (CH₂, **C24**), 46.1 (CH₂, **C21**), 35.7 (CH₃, **C28**), 26.5 (CH₂, **C22**), 26.2 (CH₂, **C23**)

LRMS ES⁺ m/z = 563.4 [M-Br]⁺

HRMS ES⁺ m/z calcd for C₃₇H₃₂N₄SBr / [M-Br]⁺ requires 563.2269 found 563.2269

FT-IR (neat) ν_{max} 3049, 1466, 1207, 818, 744, 721 cm⁻¹

1-(4-(2-(4-(Benzo[*b*]thiophen-2-yl)phenyl)-1H-phenanthro[9,10-*d*]imidazol-1-yl)butyl)-3-methyl-1H-imidazol-3-ium hexatungstate (2.14)



2.13 (0.300 g, 0.466 mmol) was dissolved in the minimum required amount of hot acetonitrile (approximately 40 mL at 80 °C) under argon atmosphere. To this was added $(TBA)_2[W_6O_{19}]$ (0.443 g, 0.232 mmol) in warm acetonitrile (10 mL at 50 °C). A yellow precipitate was observed. The mixture was heated at 80 °C under argon atmosphere for 14 hours then the mixture allowed to

cool to rt and the solid filtered. The solid was washed thoroughly with ethyl acetate and diethyl ether. This afforded the title compound as a yellow solid. (445 mg, 93%).

M.P. > 296 °C

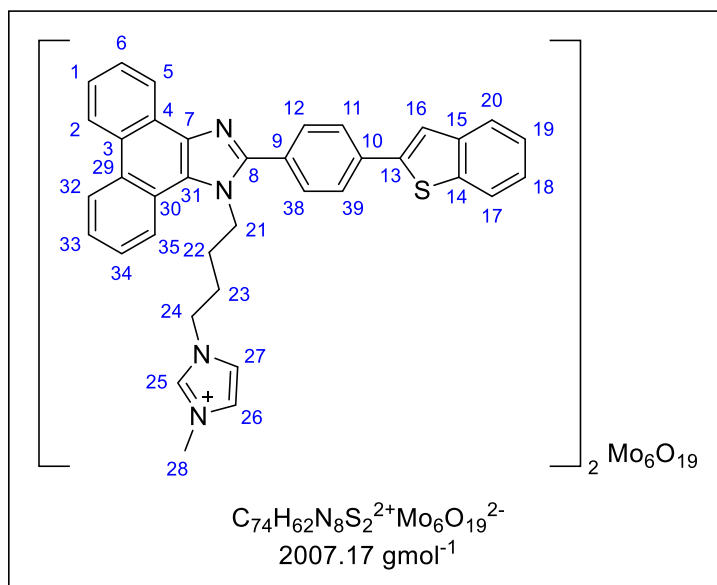
¹H NMR (400 MHz, DMSO-*d*₆, 298 K) δ (ppm) = 9.00 (d, J = 7.7 Hz, 1H, **32**), 8.92 (s, 1H, **25**), 8.88 (d, J = 8.2 Hz, 1H, **2**), 8.61 (dd, J = 7.9, 1.3 Hz, 1H, **5**), 8.37 (d, J = 8.1 Hz, 1H, **35**), 7.99 – 8.10 (m, 4H, **11 + 16 + 17 + 39**), 7.87 – 7.96 (m, 3H, **12 + 20 + 38**), 7.63 – 7.80 (m, 4H, **1 + 6 + 33 + 34**), 7.61 (t, J = 1.7 Hz, 1H, **27**), 7.57 (t, J = 1.7 Hz, 1H, **26**), 7.43 (quind, J = 7.1, 1.5 Hz, 2H, **18 + 19**), 4.79 (t, J = 6.8 Hz, 2H, **21**), 4.06 (t, J = 6.6 Hz, 2H, **24**), 3.73 (s, 3H, **28**), 1.76 – 1.86 (m, 2H, **22**), 1.64 – 1.76 (m, 2H, **23**)

¹³C NMR (101 MHz, DMSO-*d*₆, 298 K) δ (ppm) = 151.8 (C, **C8**), 142.3, (C, **C13**), 140.4 (C, **C14**), 138.8 (C, **C15**), 137.4 (C, **C7/C31**), 136.5 (CH, **C25**), 134.4 (C, **C10**), 130.6 (CH, **C12 + C38**), 130.4 (C, **C9**), 128.3 (C, **C30**), 127.7 (C, **C4**), 127.4 (CH, **C1/C6**), 126.8 (C, **C3**), 126.3 (CH, **C11 + C39**), 125.9 (C, **C7/C31**), 125.7 (CH, **C1/C6**), 125.2 (CH, **C33/34**), 125.1 (CH, **C18/C19**), 125.0 (CH, **C18/C19**), 124.6 (CH, **C32**), 124.0 (CH, **C20**), 123.6 (CH, **C2**), 123.5 (CH, **C26**), 122.8 (C, **C29**), 122.6 (CH, **C16/C17**), 122.0 (CH, **C5**), 121.9 (CH, **C27**), 121.2 (CH, **35**), 121.1 (CH, **C16/17**), 48.1 (CH₂, **C24**), 46.1 (CH₂, **C21**), 35.7 (CH₃, **C28**), 26.5 (CH₂, **C22**), 26.2 (CH₂, **C23**)

HRMS ES⁺ m/z calcd for C₇₄H₆₂N₈S₂W₆O₁₉ / [M-W₆O₁₉]²⁺ requires 563.2269 found 563.2268, ES⁻ m/z = 1407.6 [M-C₇₄H₆₂N₈S₂]⁻

FT-IR (neat) ν_{max} 3127, 1573, 1164, 975, 801, 747, 722 cm⁻¹

1-(4-(2-(4-(Benzo[*b*]thiophen-2-yl)phenyl)-1H-phenanthro[9,10-*d*]imidazol-1-yl)butyl)-3-methyl-1H-imidazol-3-ium hexamolybdate (2.15)



2.13 (0.350 g, 0.542 mmol) was dissolved in the minimum required amount of hot acetonitrile (approximately 40 mL at 80 °C) under argon atmosphere. To this was added $(TBA)_2[Mo_6O_{19}]$ (0.372 g, 0.270 mmol) in warm acetonitrile (10 mL at 50 °C). An orange precipitate was observed. The mixture was heated at 80 °C under argon atmosphere for 14 hours then the mixture allowed to

cool to rt and the solid filtered. The solid was washed thoroughly with ethyl acetate and diethyl ether. This afforded the title compound as an orange solid. (465 mg, 87%).

M.P. 293 °C decomposed

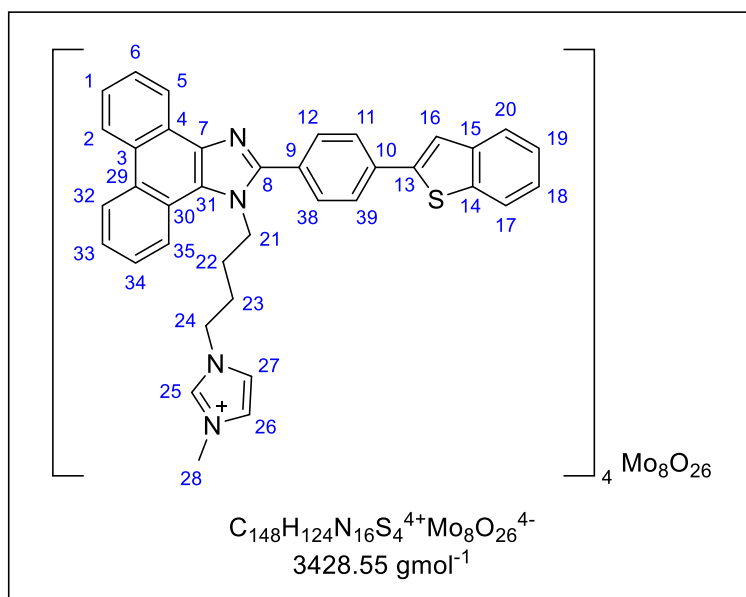
¹H NMR (400 MHz, DMSO-*d*₆, 298 K) δ (ppm) = 8.97 (d, *J* = 8.3 Hz, 1H, **32**), 8.93 (s, 1H, **25**), 8.87 (d, *J* = 8.3 Hz, 1H, **2**), 8.61 (dd, *J* = 7.9, 1.3 Hz, 1H, **5**), 8.36 (d, *J* = 8.2 Hz, 1H, **35**), 7.98 – 8.08 (m, 4H, **11 + 16 + 17 + 39**), 7.87 – 7.95 (m, 3H **12 + 20 + 38**), 7.64 – 7.81 (m, 4H, **1 + 6 + 33 + 34**), 7.60 (t, *J* = 1.7 Hz, 1H, **27**), 7.56 (t, *J* = 1.7 Hz, 1H, **26**), 7.42 (quind, *J* = 7.0, 1.4 Hz, 2H, **18 + 19**), 4.78 (t, *J* = 6.8 Hz, 2H, **21**), 4.06 (t, *J* = 6.7 Hz, 2H, **24**), 3.73 (s, 3H, **28**), 1.76 – 1.85 (m, 2H, **22**), 1.65 – 1.76 (m, 2H, **23**)

¹³C NMR (101 MHz, DMSO-*d*₆, 298 K) δ (ppm) = 151.7 (C, **C8**), 142.3, (C, **C13**), 140.4 (C, **C14**), 138.8 (C, **C15**), 137.4 (C, **C7/C31**), 136.4 (CH, **C25**), 134.4 (C, **C10**), 130.6 (CH, **C12 + C38**), 130.3 (C, **C9**), 128.3 (C, **C30**), 127.7 (C, **C4**), 127.4, (CH, **C33/C34**) 127.4 (CH, **C1/C6**), 126.7 (C, **C3**), 126.3 (CH, **C11 + C39**), 125.9 (C, **C7/C31**), 125.7 (CH, **C1/C6**), 125.2 (CH, **C33/34**), 125.0 (CH, **C18/C19**), 125.0 (CH, **C18/C19**), 124.6 (CH, **C32**), 124.0 (CH, **C20**), 123.6 (CH, **C2**), 123.5 (CH, **C26**), 122.8 (C, **C29**), 122.6 (CH, **C16/C17**), 122.0 (CH, **C5**), 121.9 (CH, **C27**), 121.1 (CH, **35**), 121.1 (CH, **C16/17**), 48.2 (CH₂, **C24**), 46.1 (CH₂, **C21**), 35.7 (CH₃, **C28**), 26.5 (CH₂, **C22**), 26.2 (CH₂, **C23**)

HRMS ES⁺ *m/z* calcd for C₇₄H₆₂N₈S₂Mo₆O₁₉ / [M-Mo₆O₁₉]⁺ requires 563.2269 found 563.2268, ES⁻ *m/z* = 891.3 [M-C₇₄H₆₂N₈S₂]⁻

FT-IR (neat) ν_{max} 3116, 1574, 1165, 953, 788, 746, 721 cm⁻¹

1-(4-(2-(4-(Benzo[*b*]thiophen-2-yl)phenyl)-1H-phenanthro[9,10-*d*]imidazol-1-yl)butyl)-3-methyl-1H-imidazol-3-ium octamolybdate (2.16)



2.13 (1.07 g, 1.09 mmol) was dissolved in the minimum required amount of hot acetonitrile (approximately 60 mL at 80 °C) under argon atmosphere. To this was added $(\text{TBA})_4[\text{Mo}_8\text{O}_{26}]$ (0.594 g, 0.273 mmol) in warm acetonitrile (10 mL at 50 °C). A white precipitate was observed. The mixture was heated at 80 °C under argon atmosphere for 14 hours then the mixture allowed to

cool to rt and the solid filtered. The solid was washed thoroughly with ethyl acetate and diethyl ether. This afforded the title compound as an orange solid. (740 mg, 79%).

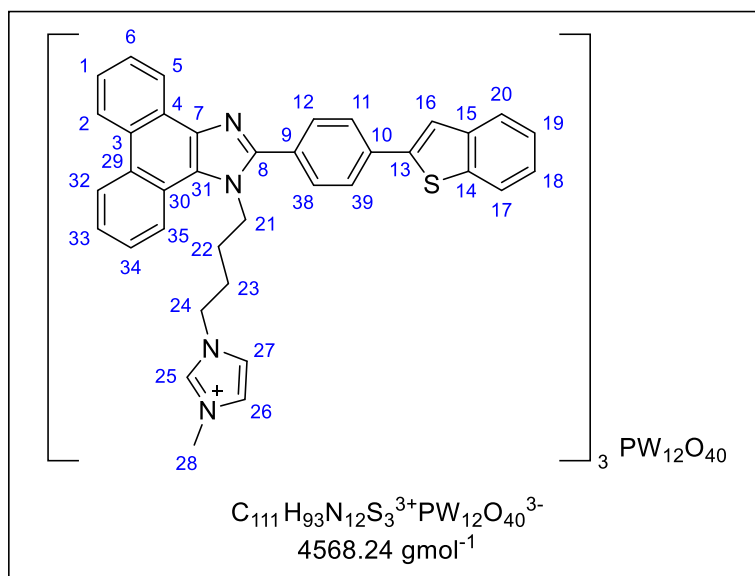
M.P. 260 - 263 °C

$^1\text{H NMR}$ (400 MHz, $\text{DMSO-}d_6$, 298 K) δ (ppm) = 8.99 (s, 1H, **25**), 8.94 (d, J = 8.3 Hz, 1H, **32**), 8.83 (d, J = 8.4 Hz, 1H, **2**), 8.59 (dd, J = 7.9, 1.3 Hz, 1H, **5**), 8.34 (br d, J = 8.2 Hz, 1H, **35**), 7.96 – 8.09 (m, 4H, **11 + 16 + 17 + 39**), 7.87 – 7.94 (m, 3H, **12 + 20 + 38**), 7.79 (t, J = 7.6 Hz, 1H, **34**), 7.61 – 7.73 (m, 3H, **1 + 6 + 33**), 7.56 (t, J = 1.5 Hz, 1H, **27**), 7.51 (t, J = 1.5 Hz, 1H, **26**), 7.39 (sxt d, J = 7.1, 1.5 Hz, 2H, **18 + 19**), 4.68 – 4.85 (m, 2H, **21**), 4.07 (t, J = 6.5 Hz, 2H, **24**), 3.68 – 3.79 (m, 3H, **28**), 1.76 – 1.84 (m, J = 6.0 Hz, 2H, **22**), 1.69 – 1.76 (m, 2H, **23**)

$^{13}\text{C NMR}$ (101 MHz, $\text{DMSO-}d_6$, 298 K) δ (ppm) = 151.7 (C, **C8**), 142.3, (C, **C13**), 140.5 (C, **C14**), 138.8 (C, **C15**), 137.4 (C, **C7/C31**), 136.5 (CH, **C25**), 134.3 (C, **C10**), 130.6 (CH, **C12 + C38**), 130.3 (C, **C9**), 128.2 (C, **C30**), 127.7 (C, **C4**), 127.5, (CH, **C33/C34**) 127.3 (CH, **C1/C6**), 126.8 (C, **C3**), 126.3 (CH, **C11 + C39**), 126.0 (C, **C7/C31**), 125.6 (CH, **C1/C6**), 125.2 (CH, **C33/34**), 124.9 (CH, **C18/C19**), 124.9 (CH, **C18/C19**), 124.4 (CH, **C32**), 124.1 (CH, **C20**), 123.5 (CH, **C2**), 123.5 (CH, **C26**), 122.7 (C, **C29**), 122.5 (CH, **C16/C17**), 122.0 (CH, **C5**), 121.9 (CH, **C27**), 121.1 (CH, **35**), 121.1 (CH, **C16/17**), 48.2 (CH_2 , **C24**), 46.1 (CH_2 , **C21**), 35.6 (CH_3 , **C28**), 26.6 (CH_2 , **C22**), 26.4 (CH_2 , **C23**)

FT-IR (neat) ν_{max} 3054, 1473, 1358, 1167, 949, 913, 749, 724 cm^{-1}

1-(4-(2-(4-(Benzo[*b*]thiophen-2-yl)phenyl)-1H-phenanthro[9,10-*d*]imidazol-1-yl)butyl)-3-methyl-1H-imidazol-3-ium phosphotungstate (2.17)



2.13 (0.224 g, 0.333 mmol) was dissolved in the minimum required amount of hot acetonitrile (approximately 25 mL at 80 °C) under argon atmosphere. To this was added (TBA)₃[PW₁₂O₄₀] (0.400 g, 0.111 mmol) in warm acetonitrile (5 mL at 50 °C). A light brown precipitate was observed. Straight after addition the

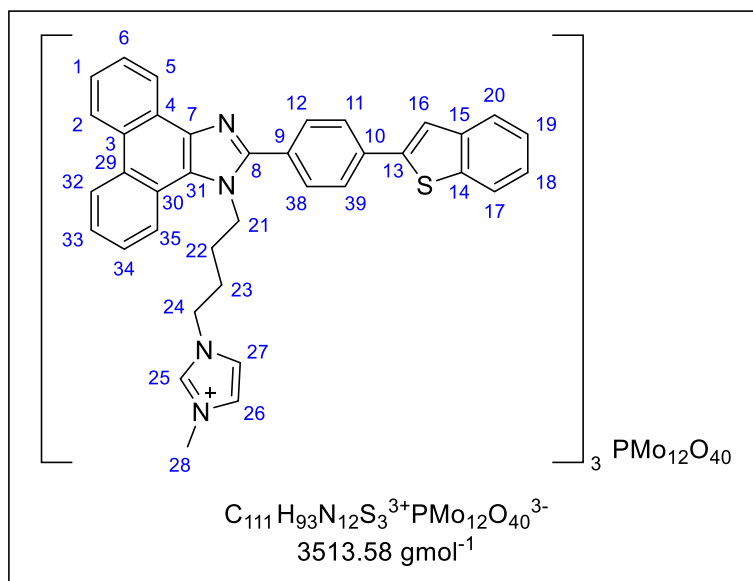
mixture was allowed to cool from 80 °C to rt and stirred under argon atmosphere at rt for a further 14 hours then the brown precipitate filtered. The solid was washed thoroughly with warm acetonitrile, ethyl acetate and diethyl ether. This gave the title compound, **NOT** pure, characterised containing TBA. (422 mg, 84%). Yield is the mass of material – TBA, calculated by ¹H NMR.

¹H NMR (400 MHz, DMSO-*d*₆, 298 K) δ (ppm) = 9.00 (d, *J* = 8.5 Hz, 1H, **32**), 8.92 (s, 1H, **25**), 8.88 (d, *J* = 8.2 Hz, 1H, **2**), 8.61 (dd, *J* = 7.9, 1.3 Hz, 1H, **5**), 8.37 (d, *J* = 8.1 Hz, 1H, **35**), 8.00 – 8.09 (m, 4H, **11 + 16 + 17 + 39**), 7.88 – 7.96 (m, 3H, **12 + 20 + 38**), 7.65 – 7.80 (m, 4H, **1 + 6 + 33 + 34**), 7.61 (t, *J* = 1.7 Hz, 1H, **27**), 7.57 (t, *J* = 1.6 Hz, 1H, **26**), 7.43 (quind, *J* = 7.1, 1.4 Hz, 2H, **18 + 19**), 4.79 (t, *J* = 6.7 Hz, 2H, **21**), 3.99 – 4.11 (m, 2H, **24**), 3.73 (s, 3H, **28**), 1.76 – 1.87 (m, 2H, **22**), 1.64 – 1.76 (m, 2H, **23**)

¹³C NMR (101 MHz, DMSO-*d*₆, 298 K) δ (ppm) = 151.7 (C, **C8**), 142.2, (C, **C13**), 140.4 (C, **C14**), 138.8 (C, **C15**), 136.5 (CH, **C25**), 134.8 (C, **C7/C31**), 134.4 (C, **C10**), 130.6 (CH, **C12 + C38**), 130.2 (C, **C9**), 128.3 (C, **C30**), 127.7 (C, **C4**), 127.4, (CH, **C33/C34**) 127.4 (CH, **C1/C6**), 126.6 (C, **C3**), 126.3 (CH, **C11 + C39**), 125.9 (C, **C7/C31**), 125.8 (CH, **C1/C6**), 125.3 (CH, **C33/34**), 125.1 (CH, **C18/C19**), 125.0 (CH, **C18/C19**), 124.6 (CH, **C32**), 124.0 (CH, **C20**), 123.6 (CH, **C2**), 123.5 (CH, **C26**), 122.7 (C, **C29**), 122.6 (CH, **C16/C17**), 122.0 (CH, **C5**), 121.9 (CH, **C27**), 121.1 (CH, **35**), 121.1 (CH, **C16/17**), 48.2 (CH₂, **C24**), 46.1 (CH₂, **C21**), 35.6 (CH₃, **C28**), 26.6 (CH₂, **C22**), 26.4 (CH₂, **C23**)

FT-IR (neat) ν_{max} 3085, 1469, 1358, 1076, 973, 893, 747, 722 cm^{-1}

1-(4-(2-(4-(Benzo[*b*]thiophen-2-yl)phenyl)-1H-phenanthro[9,10-*d*]imidazol-1-yl)butyl)-3-methyl-1H-imidazol-3-ium phosphomolybdate (2.18)



2.13 (0.350 g, 0.542 mmol) was dissolved in the minimum required amount of hot acetonitrile (approximately 40 mL at 80 °C) under argon atmosphere. To this was added (TBA)₃[PMo₁₂O₄₀] (0.463 g, 0.182 mmol) in warm acetonitrile (10 mL at 50 °C). A green precipitate was observed. The mixture was heated at 80 °C under argon

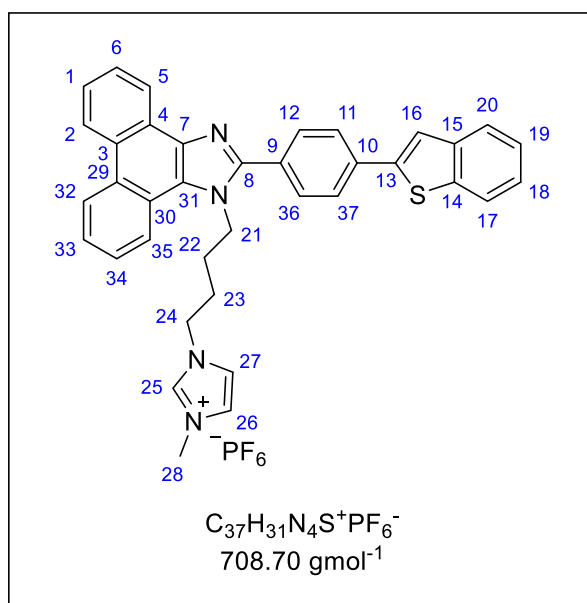
atmosphere for 14 hours then the mixture allowed to cool to rt and the solid filtered. The solid was washed thoroughly with warm acetonitrile, ethyl acetate and diethyl ether. This gave the title compound, **NOT** pure, as a green solid containing TBA. (487 mg, 77%). Yield is the mass of material – TBA, calculated by ¹H NMR.

¹H NMR (400 MHz, DMSO-*d*₆, 298 K) δ (ppm) = 8.99 (d, *J* = 8.3 Hz, 1H, **32**), 8.84 – 8.94 (m, 2H, **2 + 25**), 8.61 (d, *J* = 7.7 Hz, 1H, **5**), 8.37 (d, *J* = 7.9 Hz, 1H, **35**), 7.99 – 8.11 (m, 4H, **11 + 16 + 17 + 39**), 7.88 – 7.96 (m, 3H, **12 + 20 + 38**), 7.81 (t, *J* = 6.6 Hz, 1H, **34**), 7.66 – 7.78 (m, 3H, **1 + 6 + 33**), 7.61 (s, 1H, **27**), 7.57 (s, 1H, **26**), 7.43 (quin, *J* = 6.8 Hz, 2H, **18 + 19**), 4.80 (br s, 2H, **21**), 4.08 (br t, *J* = 5.7 Hz, 2H, **24**), 3.67 – 3.80 (m, 3H, **28**), 1.77 – 1.88 (m, 2H, **22**), 1.73 (br s, 2H, **23**)

¹³C NMR (101 MHz, DMSO-*d*₆, 298 K) δ (ppm) = 151.3 (C, **C8**), 142.2, (C, **C13**), 140.4 (C, **C14**), 138.8 (C, **C15**), 137.2 (C, **C25**), 134.7 (C, **C7/C31**), 130.7 (CH, **C12 + C38**), 128.4 (C, **C30**), 127.8 (C, **C4**), 127.6, (CH, **C34**) 127.4 (CH, **C1/C6**), 126.3 (CH, **C11 + C39**), 126.1 (C, **C7/C31**), 126.1 (CH, **C1/C6**), 125.8 (CH, **C33**), 125.5 (CH, **C1/C6**), 125.1 (CH, **C18/C19**), 125.0 (CH, **C18/C19**), 124.6 (CH, **C32**), 124.1 (CH, **C20**), 123.7 (CH, **C2**), 123.6 (CH, **C26**), 122.5 (C, **C29**), 122.3 (CH, **C27 + C16/C17**), 121.9 (CH, **C5**), 121.2 (CH, **35 + C16/C17**), 48.3 (CH₂, **C24**), 46.2 (CH₂, **C21**), 35.7 (CH₃, **C28**), 26.4 (CH₂, **C22**), 26.2 (CH₂, **C23**)

FT-IR (neat) ν_{max} 3079, 1472, 1060, 952, 877, 796, 749, 722 cm⁻¹

1-(4-(2-(4-(Benzo[*b*]thiophen-2-yl)phenyl)-1*H*-phenanthro[9,10-*d*]imidazol-1-yl)butyl)-3-methyl-1*H*-imidazol-3-ium hexafluorophosphate (2.19)



To **2.11** (0.500 g, 0.893 mmol) was added excess 1-methylimidazole (5 mL) and the solution heated to 100 °C under argon atmosphere. The solution was stirred at 100 °C for 2 hours then allowed to cool to rt. Ammonium hexafluorophosphate (0.440 g, 2.67 mmol) in deionised water (10 mL) was then added to the mixture, which produced a white precipitate, and the mixture stirred at rt for a further 14 hours. To the mixture, deionised water 10 mL was added, and the precipitate then filtered and washed with ethyl acetate

and diethyl ether. This gave the title compound as a white solid. (450 mg, 71%).

M.P. 157 - 159 °C

¹H NMR (400 MHz, DMSO-*d*₆, 298 K) δ (ppm) = 9.00 (d, *J* = 7.8 Hz, 1H, **32**), 8.92 (s, 1H, **25**), 8.88 (d, *J* = 8.2 Hz, 1H, **2**), 8.62 (dd, *J* = 7.9, 1.3 Hz, 1H, **5**), 8.37 (d, *J* = 7.8 Hz, 1H, **37**), 7.99 – 8.08 (m, 4H, **11 + 16 + 17 + 39**), 7.87 – 7.96 (m, 3H, **12 + 20 + 38**), 7.65 – 7.81 (m, 4H, **1 + 6 + 33**), 7.61 (t, *J* = 1.8 Hz, 1H, **27**), 7.58 (t, *J* = 1.7 Hz, 1H, **26**), 7.39 – 7.48 (m, 2H, **18 + 19**), 4.79 (br t, *J* = 6.9 Hz, 2H, **21**), 4.06 (t, *J* = 6.7 Hz, 2H, **24**), 3.69 – 3.76 (m, 3H, **28**), 1.77 – 1.86 (m, 2H, **22**), 1.64 – 1.75 (m, 2H, **23**)

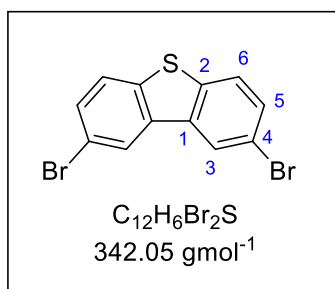
¹³C NMR (101 MHz, DMSO-*d*₆, 298 K) δ (ppm) = 151.8 (C, **C8**), 142.2 (C, **C13**), 140.4 (C, **C14**), 138.8 (C, **C15**), 137.5 (C, **C7/C31**), 136.5 (CH, **C25**), 134.4 (C, **C10**), 130.6 (CH, **C12 + 38**), 130.4 (C, **C9**), 128.3 (C, **C30**), 127.7 (C, **C4**), 127.4 (CH, **C33/C34**), 126.8 (C, **C3**), 126.3 (CH, **C11 + C39**), 125.9 (C, **C7/C31**), 125.7 (CH, **C1/C6**), 125.2 (CH, **C33/C34**), 125.1 (CH, **C18/C19**), 125.0 (CH, **C18/C19**), 124.6 (CH, **C32**), 124.0 (CH, **C20**), 123.6 (CH, **C2**), 123.5 (CH, **C26**), 122.8 (C, **C29**), 122.6 (CH, **C16/C17**), 122.0 (CH, **C5**), 121.9 (CH, **C27**), 121.1 (CH, **C35**), 121.1 (CH, **C16/C17**), 48.2 (CH₂, **C24**), 46.1 (CH₂, **C21**), 35.6 (CH₃, **C28**), 26.5 (CH₂, **C22**), 26.2 (CH₂, **C23**)

LRMS ES⁺ *m/z* = 563.4 [M-PF₆]⁺

HRMS ES⁺ *m/z* calcd for C₃₇H₃₂N₄SPF₆ / [M-PF₆]⁺ requires 563.2269 found 563.2253

FT-IR (neat) ν_{max} 3158, 1671, 1471, 1166, 824, 724, 555 cm⁻¹

2,8-Dibromodibenzo[*b,d*]thiophene (2.21)



2,8-Dibromodibenzo[*b,d*]thiophene was prepared according to the procedure described by Tang and co-workers'.²⁰⁷

Dibenzothiophene (5.00 g, 27.1 mmol) was dissolved in dry chloroform (30 mL) and cooled to -5 °C under nitrogen atmosphere.

To this solution bromine (3.10 mL, 60.5 mmol) was added dropwise maintaining a temperature of between -5 and 0 °C. After addition was completed, the mixture was stirred at 0 °C for 10 minutes then allowed to warm to room temperature. At this point a large amount of precipitate was observed therefore dry chloroform (10 mL) was added to help maintain good stirring. The mixture was stirred at room temperature for 16 hours then the precipitate filtered and washed with methanol (100 mL). This gave the title compound as an off-white powder (7.65 g, 82%).

M.P. 221 - 222 °C (lit 223 - 225 °C)²⁰⁸

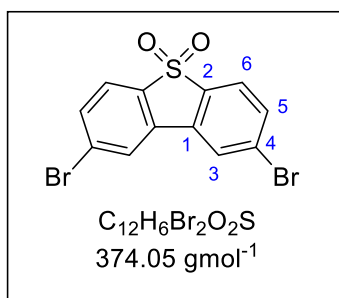
¹H NMR (400 MHz, CDCl₃, 298 K) δ (ppm) = 8.23 (dd, *J* = 2.0, 0.5 Hz, 2H, **3**), 7.71 (dd, *J* = 8.5, 0.4 Hz, 2H, **6**), 7.58 (dd, *J* = 8.4, 2.0 Hz, 2H, **5**)

¹³C NMR (101 MHz, CDCl₃, 298 K) δ (ppm) = 138.6 (C, **C2**), 136.1 (C, **C4**), 130.6 (CH, **C5**), 124.7, (CH, **C3**), 124.2 (CH, **C6**), 118.6 (C, **C1**)

LRMS EI *m/z* = 344.0 (45% [⁸¹Br⁸¹Br]⁺⁺), 342.0 (45% [⁷⁹Br⁸¹Br]⁺⁺), 340 (85% [⁷⁹Br⁷⁹Br]⁺⁺), 182.1 (95% [M-Br₂]⁺)

FT-IR (neat) ν_{max} cm⁻¹ 3370, 3073, 2918, 1874, 1654, 1411, 796

2,8-Dibromodibenzo[*b,d*]thiophene 5,5-dioxide (2.22)



2,8-Dibromodibenzo[*b,d*]thiophene 5,5-dioxide was prepared according to the procedure described by Tang and co-workers'.²⁰⁷

2.21 (7.51 g, 22.0 mmol) was added to glacial acetic acid (150 mL) under nitrogen atmosphere. To this mixture hydrogen peroxide (30% in H_2O , 18.3 mL, 179 mmol) was added then the mixture refluxed for 18 hours. The mixture was then allowed to cool to room temperature and the formed precipitate filtered. The collected precipitate was recrystallised from chloroform to give the title compound as a white solid (6.34 g, 77%).

M.P. > 297 °C (lit 360 - 361 °C)²⁰⁹

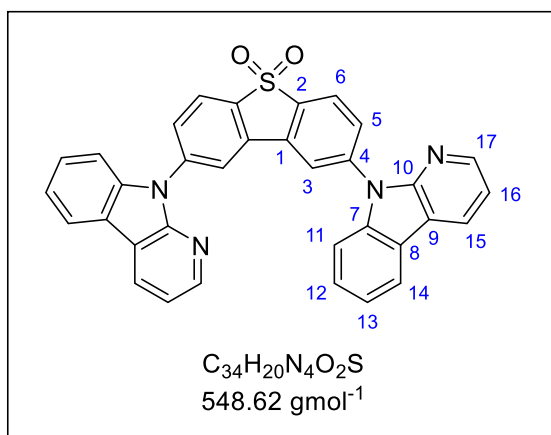
1H NMR (400 MHz, $DMSO-d_6$, 298 K) δ (ppm) = 8.63 (d, J = 1.5 Hz, 1H, **3**), 7.98 (d, J = 8.2 Hz, 1H, **6**), 7.89 (dd, J = 8.2, 1.7 Hz, 1H, **5**)

^{13}C NMR (101 MHz, $DMSO-d_6$, 298 K) δ (ppm) = 136.2 (C, **C4**), 134.2 (CH, **C5**), 131.9 (C, **C2**), 128.5 (C, **C1**), 126.6 (CH, **C3**), 123.9 (CH, **C6**)

LRMS EI m/z = 375.9 (20% [$M^{81}Br^{81}Br$]⁺⁺), 373.9 (40% [$M^{79}Br^{81}Br$]⁺⁺), 371.9 (20% [$M^{79}Br^{79}Br$]⁺⁺)

FT-IR (neat) ν_{max} cm^{-1} 3069, 1557, 1296, 1065, 825, 565

2,8-Bis(9H-pyrido[2,3-*b*]indol-9-yl)dibenzo[*b,d*]thiophene 5,5-dioxide (2.25)



2,8-Bis(9H-pyrido[2,3-*b*]indol-9-yl)dibenzo[*b,d*]thiophene 5,5-dioxide was prepared according to the procedure described by Choi and co-workers'.¹¹⁹

2.22 (200 mg, 0.540 mmol), α -carboline (180 mg, 1.11 mmol), tripotassium phosphate (683 mg, 3.22 mmol), copper (I) iodide (61 mg, 0.320 mmol) and trans-1,2-diaminocyclohexane (40 μ L, 0.320 mmol) were added to a flame dried RBF under nitrogen atmosphere. Dry toluene (20 mL) was then added, and the mixture degassed, by bubbling nitrogen, for 30 minutes. The mixture was then heated to reflux and stirred for 16 hours. The mixture was then allowed to cool to room temperature before the addition of deionised water (20 mL) and DCM (30 mL). The organic layer was separated, and the aqueous layer extracted with DCM (2 x 20 mL). The combined extracts were dried (Na_2SO_4), solvent removed under reduced pressure and the resulting crude material purified by silica gel column chromatography (DCM/ethyl acetate, 1:1) followed by recrystallisation from toluene. This yielded the title compound as a white solid (151 mg, 51%).

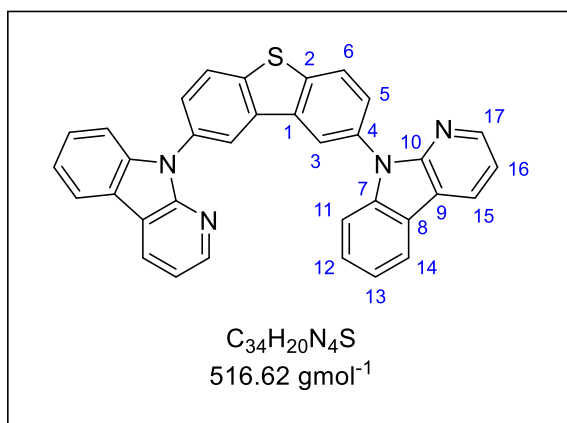
M.P. 361 °C decomposed.

1H NMR (400 MHz, $CDCl_3$, 298 K) δ (ppm) = 8.74 (d, J = 1.2 Hz, 2H, **3**), 8.66 (dd, J = 7.7, 1.3 Hz, 2H, **11**), 8.46 (dd, J = 4.8, 1.3 Hz, 2H, **17**), 8.32 (t, J = 8.5 Hz, 4H, **14** + **15**), 8.04 (dd, J = 8.2, 1.6 Hz, 2H, **6**), 7.66 (d, J = 8.2 Hz, 2H, **5**), 7.52 (t, J = 7.0 Hz, 2H, **12**), 7.44 – 7.33 (m, 4H, **13** + **16**)

^{13}C NMR (101 MHz, $CDCl_3$, 298 K) δ (ppm) = 151.0, 146.4, 141.4, 138.6, 135.6, 132.2, 129.8, 129.2, 127.5, 123.3, 122.0, 121.5, 121.5, 120.7, 117.2, 116.0, 110.6

LRMS ES^+ m/z = 549.4 $[M+H]^+$

2,8-Bis(9H-pyrido[2,3-b]indol-9-yl)dibenzo[b,d]thiophene (2.26)



2,8-Bis(9H-pyrido[2,3-b]indol-9-yl)dibenzo[b,d]thiophene was prepared according to the procedure described by Choi and co-workers'.¹¹⁹

To **2.25** (900 mg, 1.64 mmol) in dry diethyl ether (10 mL) was added $LiAlH_4$ (2 M in THF, 4.10 mL, 8.22 mmol) dropwise at 0 °C under argon atmosphere. The mixture was allowed to warm to room temperature and stirred for 16 hours. Deionised water was then added dropwise at 0 °C until the mixture stopped bubbling upon addition. DCM (20 mL) and deionised water (15 mL) were then added, and the organic layer separated. The organic layer was washed with deionised water (2 x 10 mL), dried (Na_2SO_4) and the solvent removed under reduced pressure. The crude material was purified by silica gel column chromatography (hexane/DCM, 4:1 → 1:1). This gave the title compound as a white solid (361 mg, 42%).

M.P. 318 - 319 °C

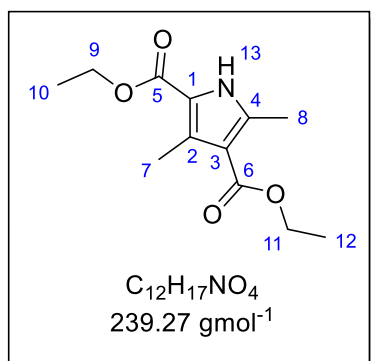
1H NMR (400 MHz, $CDCl_3$, 298 K) δ (ppm) = 8.48 (dd, J = 4.9, 1.7 Hz, 2H, **17**), 8.41 (td, J = 3.8, 1.7 Hz, 4H, **14** + **15**), 8.14 (d, J = 8.2 Hz, 4H, **3** + **11**), 7.79 (dd, J = 8.5, 2.0 Hz, 2H, **6**), 7.53 – 7.45 (m, 4H, **5** + **12**), 7.38 – 7.32 (m, 2H, **13**), 7.25 (dd, J = 7.6, 5.0 Hz, 2H, **16**)

^{13}C NMR (101 MHz, $DMSO-d_6$, 298 K) δ (ppm) = 152.0, 146.3, 140.4, 139.6, 136.5, 133.2, 128.5, 127.1, 126.7, 124.1, 121.1, 121.0, 120.9, 120.8, 116.5, 116.1, 110.3

LRMS ES^+ m/z = 517.4 $[M+H]^+$

FT-IR (neat) ν_{max} cm^{-1} 3050, 1572, 1450, 1405, 766, 631

Diethyl 3,5-dimethyl-1H-pyrrole-2,4-dicarboxylate (2.28)



Diethyl 3,5-dimethyl-1H-pyrrole-2,4-dicarboxylate was prepared according to the procedure described by G. Meng and co-workers.²¹⁰

Ethyl acetoacetate (100 mL, 0.780 mol) and glacial acetic acid (100 mL) were stirred at 0 °C. To this mixture sodium nitrite (27.3 g, 0.320 mol) in deionised water (40 mL) was added dropwise at <10 °C. The mixture was stirred at <10 °C for 2.5 hours. Zinc powder (51.3 g, 0.780 mol) was then added portion wise (11 x 4.60 g) while maintaining a temperature of <25 °C. The mixture was then heated to 45 °C and stirred for 15 minutes, followed by heating at 95 °C for 1 hour. The mixture was then allowed to cool to rt and the precipitate filtered and washed thoroughly with water (\approx 200 mL). The crude solid was then recrystallised from ethanol (repeated 3 times) to give the title compound as a pale yellow solid (56.84 g, 61%).

M.P. 132 - 134 °C (lit 133 - 134 °C)²¹⁰

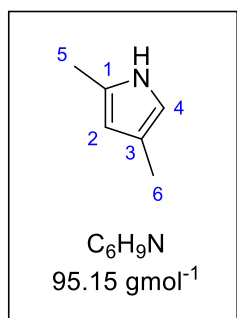
1H NMR (400 MHz, $CDCl_3$, 298 K) δ (ppm) = 9.25 (br s, 1H, **13**), 4.32 (dq, J = 16.3, 7.1 Hz, 4H, **9 + 11**), 2.55 (d, J = 17.9 Hz, 6H, **7 + 8**), 1.37 (td, J = 7.1, 5.1 Hz, 6H, **10 + 12**)

^{13}C NMR (101 MHz, $CDCl_3$, 298 K) δ (ppm) = 165.5 (C, **C6**), 161.8 (C, **C5**), 139.0 (C, **C4**), 130.9 (C, **C2**), 117.9 (C, **C1**), 113.6 (C, **C3**), 60.3 (CH_2 , **C9/C11**), 59.5 (CH_2 , **C9/C11**), 14.4 (CH_3 , **10**), 14.4 (CH_3 , **C12**), 14.3 (CH_3 , **C7/C8**), 12.0 (CH_3 , **C7/C8**)

LRMS ES^+ m/z = 240.3 $[M+H]^+$

FT-IR (neat) ν_{max} cm^{-1} 3261, 2978, 1665, 1435, 1259, 1086, 787

2,4-Dimethyl-1H-pyrrole (2.29)



2,4-Dimethyl-1H-pyrrole was prepared according to the procedure described by H. Yuwei and co-workers.²¹¹

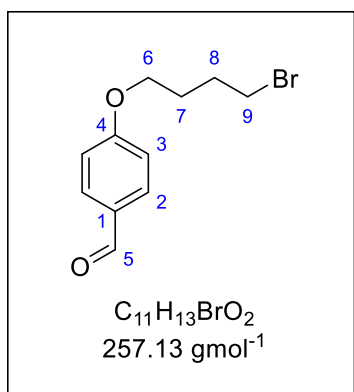
Diethyl 3,5-dimethyl-1H-pyrrole-2,4-dicarboxylate (3.00 g, 14.0 mmol) was added to ethylene glycol (10 mL) under argon atmosphere. Potassium hydroxide (4.00 g, 72.0 mmol) was added, and the mixture heated to 160 °C and stirred for 6 hours. The mixture was then allowed to cool to rt and extracted with chloroform (3 x 20 mL) and the combined extracts dried (Na_2SO_4). The solvent was then removed under reduced pressure and the crude product further purified by vacuum distillation to give the title compound as a colourless liquid. (0.57 g, 43%).

1H NMR (400 MHz, $CDCl_3$, 298 K) δ (ppm) = 6.46 (s, 1H, **4**), 5.82 (s, 1H, **2**), 2.29 (s, 3H, **5**), 2.15 (s, 3H, **6**)

^{13}C NMR (101 MHz, $CDCl_3$, 298 K) δ (ppm) = 127.6 (C, **C1**), 119.0 (C, **C3**), 113.8 (CH, **C4**), 107.6 (C, **C2**), 12.9 (CH_3 , **C5**), 11.8 (CH_3 , **C6**)

FT-IR (neat) ν_{max} cm^{-1} 3264, 1670, 1261, 1195, 1088, 788

4-(4-Bromobutoxy)benzaldehyde (2.31)



4-(4-Bromobutoxy)benzaldehyde was prepared according to the procedure described by Wang, J L and co-workers.²¹²

4-hydroxybenzaldehyde (10.0 g, 0.0821 mol) and potassium carbonate (22.6 g, 0.170 mol) were stirred in dry DMF (200 mL) under argon atmosphere. The mixture was stirred at room temperature for 1 hour. 1,4-dibromobutane (35.4 g, 0.170 mol) in dry DMF (50 mL) was then slowly added by cannula transfer over 30 minutes. This mixture was then stirred at room temperature for 48 hours. The mixture was then filtered and then filtrate extracted with ethyl acetate (3 x 100 mL) after addition of deionised water (200 mL). The combined organic extracts were dried ($MgSO_4$) and concentrated under reduced pressure. The crude material was purified by silica gel column chromatography (hexane:ethyl acetate =6:1). This gave the title compound as a pale-yellow oil which became a white solid upon storage in the fridge. (15.16 g, 72%).

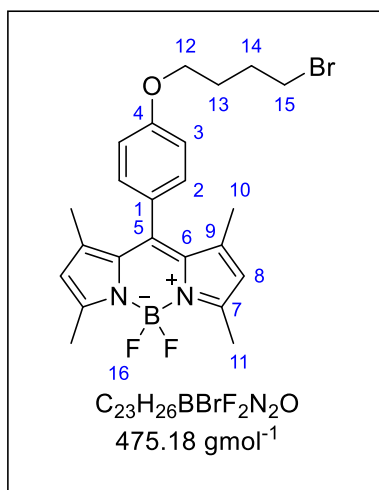
M.P. 42 - 44 °C (lit 42 - 44 °C)²¹³

¹H NMR (400 MHz, $CDCl_3$, 298 K) δ (ppm) = 9.89 (s, 1H, **5**), 7.83 (dt, J = 8.9, 2.1 Hz, 2H, **2**), 6.99 (d, J = 8.7 Hz, 2H, **3**), 4.09 (t, J = 6.0 Hz, 2H, **6**), 3.50 (t, J = 6.5 Hz, 2H, **9**), 2.12 – 2.04 (m, 2H, **7**), 2.04 – 1.96 (m, 2H, **8**)

¹³C NMR (101 MHz, $CDCl_3$, 298 K) δ (ppm) = 190.7 (CH, **C5**), 163.9 (C, **C4**), 132.0 (CH, **C2**), 130.0 (C, **C1**), 114.7 (CH, **C3**), 67.2 (CH_2 , **C6**), 33.2 (CH_2 , **C9**), 29.3 (CH_2 , **C7/C8**), 27.7 (CH_2 , **C7/C8**)

LRMS ES^+ m/z = 257.2 [$M^{79}Br + H$]⁺, 259.2 [$M^{81}Br + H$]⁺

4,4-Difluoro-8-(4-(4-bromobutoxy)phenyl)-1,3,5,7-tetramethyl-4-bora-3a,4a-diaza-s-indacene (2.32)



4,4-difluoro-8-(4-(4-Bromobutoxy)phenyl)-1,3,5,7-tetramethyl-4-bora-3a,4a-diaza-s-indacene was prepared according to the procedure described by Wang. J L and co-workers.²¹²

2,4-dimethylpyrrole (0.380 g, 4.00 mmol) and 4-(4-bromobutoxy)benzaldehyde (0.513 g, 2.00 mmol) were dissolved in DCM (100 mL) and the mixture degassed for 30 minutes by bubbling argon through the solution. TFA (0.1 mL)

was then added and the mixture stirred at rt for 2 hours. The mixture was then washed with aqueous NaOH (1 M, 200 mL) followed by deionised water (200 mL) and then dried (Na_2SO_4). The mixture was then concentrated to approximately 50 mL and *p*-chloranil (0.732 g, 3.00 mmol) added and the mixture stirred for 30 minutes at rt. Triethylamine (5 mL) was then added followed quickly by the addition of boron trifluoride diethyl etherate (8 mL, 60.00 mmol) dropwise (WARNING: significant evolution of dense vapours). The mixture was stirred at rt for 16 hours then washed with saturated $NaHCO_3$ (200 mL) and deionised water (100 mL). The isolated organic phase was dried (Na_2SO_4) and the solvent removed under reduced pressure. The crude solid was purified by silica gel column chromatography (PET ether/ hexane = 20:1 \rightarrow 10:1). This gave the title compound as a bright orange solid (0.29 g, 30%).

M.P. 134 - 136 °C (lit 134 - 136 °C)

1H NMR (400 MHz, $CDCl_3$, 298 K) δ (ppm) = 7.16 (d, J = 7.7 Hz, 2H, **2**), 6.99 (d, J = 7.5 Hz, 2H, **3**), 5.98 (s, 2H, **8**), 4.06 (t, J = 6.1 Hz, 2H, **12**), 3.52 (t, J = 6.6 Hz, 2H, **15**), 2.55 (s, 6H, **11**), 2.15 – 2.08 (m, 2H, **13**), 2.06 – 1.98 (m, 2H, **14**), 1.44 (s, 6H, **10**)

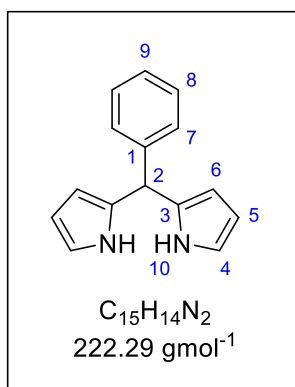
^{13}C NMR (101 MHz, $CDCl_3$, 298 K) δ (ppm) = 159.4 (C, **C4**), 155.2 (C, **C7**), 143.1 (C, **C6**), 141.8 (C, **C5**), 131.2 (C, **C9**), 129.2 (CH, **C2**), 127.0 (C, **C1**), 121.1 (CH, **C8**), 115.0 (CH, **C3**), 66.9 (CH₂, **C12**), 33.3 (CH₂, **C15**), 29.43 (CH₂, **C13/C14**), 27.81 (CH₂, **C13/C14**), 14.5 (CH₃, **C10**), 14.5 (CH₃, **C11**)

^{19}F NMR (376 MHz, $CDCl_3$, 298 K) δ (ppm) = -113.2 (s, **F16**), -115.0 (s, **F17**)

LRMS ES⁺ m/z = 427.3 [M⁷⁹Br + H]⁺, 429.3 [M⁸¹Br + H]⁺

FT-IR (neat) ν_{max} cm⁻¹ 3368, 2913, 1407, 1077, 968, 703

2,2'-(Phenylmethylene)bis(1H-pyrrole)



2,2'-(Phenylmethylene)bis(1H-pyrrole) was prepared according to the procedure described by E. N. Durantini and co-workers'.²¹⁴

Benzaldehyde (0.82 mL, 8.00 mmol) was added to pyrrole (12.4 mL, 0.180 mol) under argon atmosphere. To this mixture TFA (0.1 mL) was added and the mixture allowed to stir at room temperature for 30 minutes. DCM (100 mL) and NaOH (0.1 M, 100 mL) were added, and the organic phase separated and subsequently washed with deionised water (100 mL) and dried (Na_2SO_4). The solvent was removed under reduced pressure and the crude product purified by silica gel column chromatography (hexane/ethyl acetate/triethylamine = 14:5:1) This gave the title compound as an off-white solid (1.26 g, 71%).

M.P. 99 - 101 °C (lit 102 - 103 °C)²¹⁵

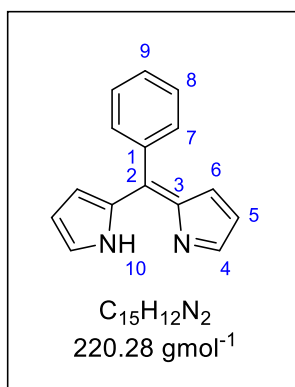
¹H NMR (400 MHz, $CDCl_3$, 298 K) δ (ppm) = 7.91 (br s, 2H, **10**), 7.36 – 7.22 (m, 5H, **7 + 8 + 9**), 6.71 (td, J = 2.7, 1.6 Hz, 2H, **4**), 6.18 (q, J = 2.7 Hz, 2H, **5**), 5.96 – 5.92 (m, 2H, **6**), 5.49 (s, 1H, **2**)

¹³C NMR (101 MHz, $CDCl_3$, 298 K) δ (ppm) = 142.1 (C, **C1**), 132.5 (C, **C3**), 128.6 (CH, **C7**), 128.4 (CH, **C8**), 127.0 (CH, **C9**), 117.2 (CH, **C4**), 108.4 (CH, **C5**), 107.2 (CH, **C6**), 44.0 (CH, **C2**)

LRMS ES^+ m/z = 223.3 $[M+H]^+$

FT-IR (neat) ν_{max} cm^{-1} 3339, 3139, 1455, 1113, 1024, 713

2-(Phenyl(2H-pyrrol-2-ylidene)methyl)-1H-pyrrole



2-(Phenyl(2H-pyrrol-2-ylidene)methyl)-1H-pyrrole was prepared according to the procedure described by K. Siwawannapong and co-workers'.²¹⁶

2,2'-(Phenylmethylene)bis(1H-pyrrole) (657 mg, 2.96 mmol) was dissolved in dry toluene (36 mL) under argon atmosphere and DDQ (680 mg, 2.96 mmol) added. The mixture was stirred at room temperature for 1 hour and then the mixture poured into deionised water (200 mL). The resulting mixture was stirred vigorously and treated with 2 M HCl until pH \approx 3 and the acidified mixture washed with ethyl acetate (3 x 100 mL). The aqueous layer was then treated with 5 M NaOH until pH \approx 12 and then extracted with ethyl acetate (3 x 100 mL), the combined organic extracts were dried ($MgSO_4$) then concentrated under reduced pressure. This gave the title compound as a pale brown oil (333 mg, 51%).

M.P. 168 - 171 $^{\circ}C$

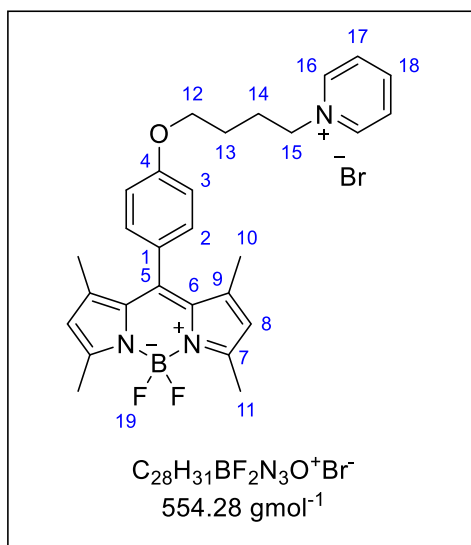
1H NMR (400 MHz, $CDCl_3$, 298 K) δ (ppm) = 7.67 (t, J = 1.3 Hz, 2H, **4**), 7.53 – 7.43 (m, 5H, **7** + **8** + **9**), 6.62 (dd, J = 4.2, 1.0 Hz, 2H, **6**), 6.41 (dd, J = 4.2, 1.5 Hz, 2H, **5**)

^{13}C NMR (101 MHz, $CDCl_3$, 298 K) δ (ppm) = 143.6 (CH, **C4**), 141.9 (C, **C3**), 140.8 (C, **C1**), 137.2 (C, **C2**), 130.7 (CH, **C6**), 128.8 (CH, **C7**), 128.8 (CH, **C8**), 127.5 (CH, **C9**), 117.6 (CH, **C5**)

LRMS ES^+ m/z = 221.2 $[M+H]^+$

FT-IR (neat) ν_{max} cm^{-1} 3504, 1563, 1381, 1073, 938, 714

4,4-Difluoro-8-(4-(4-pyridin-1-iumbutoxy)phenyl)-1,3,5,7-tetramethyl-4-bora-3a,4a-diaza-s-indacene bromide (2.33)



2.32 (0.100 g, 0.201 mmol) was dissolved in dry toluene (1 mL) under argon atmosphere. Pyridine (0.02 mL, 0.242 mmol) was added, and the mixture heated to 80 °C and stirred for 48 hours. An orange precipitate was observed. The mixture was allowed to cool to rt and the precipitate filtered then washed with toluene (3 mL). Drying gave the title compound as a dark orange solid (0.098 g, 88%).

M.P. 244 - 247 °C

$^1\text{H NMR}$ (400 MHz, $\text{DMSO}-d_6$, 298 K) δ (ppm) = 9.17 (d, J = 5.6 Hz, 2H, **16**), 8.63 (t, J = 7.6 Hz, 1H, **18**), 8.19 (dd, J = 7.7, 6.7 Hz, 2H, **17**), 7.26 (d, J = 8.6 Hz, 2H, **2**), 7.10 (d, J = 8.8 Hz, 2H, **3**), 6.17 (s, 2H, **8**), 4.73 (t, J = 7.3 Hz, 2H, **15**), 4.08 (t, J = 6.2 Hz, 2H, **12**), 2.44 (s, 6H, **11**), 2.13 (quin, J = 7.5 Hz, 2H, **14**), 1.78 (qd, J = 7.3, 6.1 Hz, 2H, **13**), 1.39 (s, 6H, **10**)

$^{13}\text{C NMR}$ (101 MHz, $\text{DMSO}-d_6$, 298 K) δ (ppm) = 159.0 (C, **C4**), 154.6 (C, **C7**), 145.5 (CH, **C18**), 144.8 (CH, **C16**), 142.6 (C, **C9**), 142.1 (C, **C5**), 131.0 (C, **C6**), 129.1 (CH, **C2**), 128.1 (CH, **C17**), 126.0 (C, **C1**), 121.2 (CH, **C8**), 115.1 (CH, **C3**), 66.9 (CH_2 , **C12**), 60.4 (CH_2 , **C15**), 27.7 (CH_2 , (**C13/C14**), 25.2 (CH_2 , **C13/C14**), 14.2 (CH_3 , **C11**), 14.2 (CH_3 , **C10**)

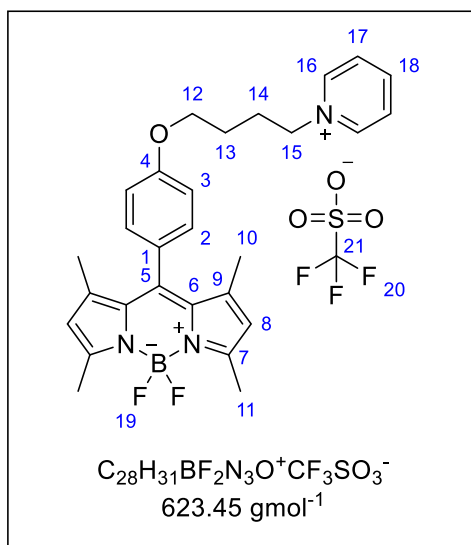
$^{19}\text{F NMR}$ (376 MHz, $\text{DMSO}-d_6$, 298 K) δ (ppm) = -143.5 (s, **F19**)

LRMS $\text{ES}^+ m/z$ = 474.3 $[\text{M}-\text{Br}]^+$

HRMS $\text{ES}^+ m/z$ calcd for $\text{C}_{28}\text{H}_{31}\text{BF}_2\text{N}_3\text{OBr}^+ / [\text{M}-\text{Br}]^+$ requires 474.2528 found 474.2538

FT-IR (neat) ν_{max} cm^{-1} 2497, 2871, 1545, 1153, 969, 699, 688

4,4-Difluoro-8-(4-(4-pyridin-1-iumbutoxy)phenyl)-1,3,5,7-tetramethyl-4-bora-3a,4a-diaza-s-indacene trifluoromethanesulfonate (2.34)



2.33 (70 mg, 0.126 mmol) was added to dry acetonitrile (10 mL) under argon atmosphere. Potassium triflate (0.232 g, 1.26 mmol) in deionised water (5 mL) was then added and the mixture heated to 40 °C and stirred for 6 hours. The mixture was then allowed to cool and filtered. The solvent was removed from the filtrate and the crude solid was triturated with deionised water (2 x 10 mL) then with toluene (10 mL). The resulting solid was collected by filtration and washed thoroughly with water (50 mL) then toluene (50 mL) and finally diethyl ether (30 mL).

Drying gave the title compound as an orange-red solid. (67 mg, 83%).

M.P. 263 °C decomposed.

¹H NMR (400 MHz, DMSO-*d*₆, 298 K) δ (ppm) = 9.13 (dd, *J* = 6.6, 1.2 Hz, 2H, **16**), 8.62 (t, *J* = 7.5 Hz, 1H, **18**), 8.18 (t, *J* = 6.7 Hz, 2H, **17**), 7.26 (d, *J* = 8.6 Hz, 2H, **2**), 7.10 (d, *J* = 8.6 Hz, 2H, **3**), 6.17 (s, 2H, **8**), 4.70 (t, *J* = 7.3 Hz, 2H, **15**), 4.08 (t, *J* = 6.2 Hz, 2H, **12**), 2.44 (s, 6H, **11**), 2.17 – 2.07 (m, 2H, **14**), 1.85 – 1.71 (m, 2H, **13**), 1.39 (s, 6H, **10**)

¹³C NMR (101 MHz, DMSO-*d*₆, 298 K) δ (ppm) = 159.1 (C, **C4**), 154.7 (C, **C7**), 145.6 (CH, **C18**), 144.8 (CH, **C16**), 142.7 (C, **C9**), 142.1 (C, **C5**), 131.1 (C, **C6**), 129.2 (CH, **C2**), 128.2 (CH, **C17**), 126.0 (C, **C1**), 121.3 (CH, **C8**), 115.1 (CH, **C3**), 67.0 (CH₂, **C12**), 60.5 (CH₂, **C15**), 27.7 (CH₂, (**C13/C14**), 25.3 (CH₂, **C13/C14**), 14.2 (CH₃, **C11**), 14.2 (CH₃, **C10**)

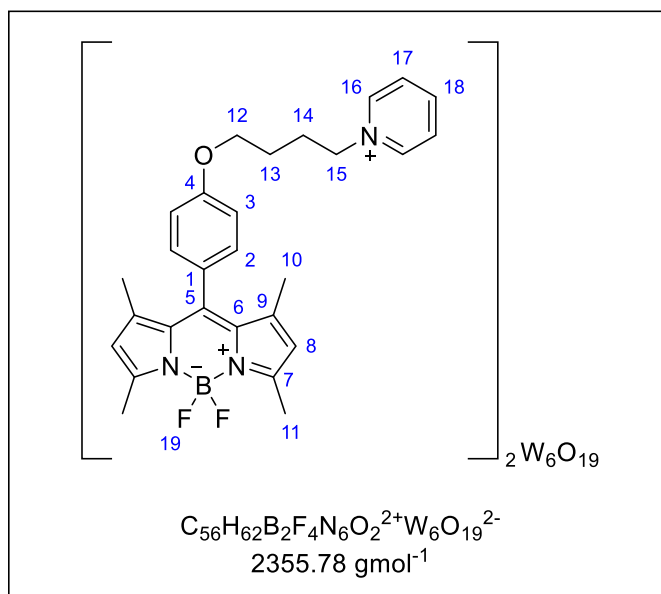
¹⁹F NMR (376 MHz, DMSO-*d*₆, 298 K) δ (ppm) = -77.8 (s, **F20**), -143.5 (s, **F19**)

LRMS ES⁺ *m/z* = 474.4 [M-CF₃SO₃]⁺

HRMS ES⁺ *m/z* calcd for C₂₈H₃₁BF₂N₃OCF₃SO₃ / [M-CF₃SO₃]⁺ requires 474.2528 found 474.2542

FT-IR (neat) ν_{max} cm⁻¹ 2927, 1542, 1250, 1152, 970, 763, 636

4,4-Difluoro-8-(4-(4-pyridin-1-iumbutoxy)phenyl)-1,3,5,7-tetramethyl-4-bora-3a,4a-diaza-s-indacene hexatungstate (2.35)



2.33 (70 mg, 0.126 mmol) was added to dry acetonitrile under argon atmosphere and the mixture heated to 80 °C. (TBA)₂[W₆O₁₉] (0.131 g, 0.0690 mmol) was dissolved in dry acetonitrile (5 mL at 50 °C) and the warm solution added to the mixture. The mixture was stirred at 80 °C for 16 hours then allowed to cool to rt. The mixture was concentrated under reduced pressure (to approximately 5 mL) and a small amount of orange

precipitate was observed. Toluene (10 mL) was added, and the mixture sonicated for 1 minute which gave a large amount of orange precipitate. This crude material was filtered, dried, and analysed however the presence of TBA showed the reaction was incomplete. The crude material (0.130 g) was dissolved in dry acetonitrile (15 mL) and heated to 80 °C. **2.33** (40 mg, 0.722 mmol) was added and the mixture stirred at 80 °C for 16 hours. The mixture was allowed to cool and concentrated under reduced pressure (to around 5 mL). Toluene (10 mL) was added, and the mixture sonicated for 1 minute, the resulting solid was filtered and washed with ice cold acetonitrile (3 mL) followed by diethyl ether (10 mL). Drying gave the title compound as a red solid (69 mg, 42%).

M.P. 240 °C decomposed.

¹H NMR (400 MHz, DMSO-*d*₆, 298 K) δ (ppm) = 9.13 (d, *J* = 5.6 Hz, 2H, **16**), 8.62 (t, *J* = 7.8 Hz, 1H, **18**), 8.18 (t, *J* = 7.1 Hz, 2H, **17**), 7.26 (d, *J* = 8.6 Hz, 2H, **2**), 7.10 (d, *J* = 8.7 Hz, 2H, **3**), 6.17 (s, 2H, **8**), 4.71 (t, *J* = 7.3 Hz, 2H, **15**), 4.08 (t, *J* = 6.2 Hz, 2H, **12**), 2.44 (s, 6H, **11**), 2.13 (quin, *J* = 7.5 Hz, 2H, **14**), 1.86 – 1.71 (m, 2H, **13**), 1.39 (s, 6H, **10**)

¹³C NMR (101 MHz, DMSO-*d*₆, 298 K) δ (ppm) = 159.1 (C, **C4**), 154.7 (C, **C7**), 145.5 (CH, **C18**), 144.8 (CH, **C16**), 142.7 (C, **C9**), 142.1 (C, **C5**), 131.1 (C, **C6**), 129.1 (CH, **C2**), 128.1 (CH, **C17**), 126.0 (C, **C1**), 121.3 (CH, **C8**), 115.1 (CH, **C3**), 66.9 (CH₂, **C12**), 60.5 (CH₂, **C15**), 27.7 (CH₂, (**C13/C14**), 25.2 (CH₂, **C13/C14**), 14.2 (CH₃, **C11**), 14.2 (CH₃, **C10**)

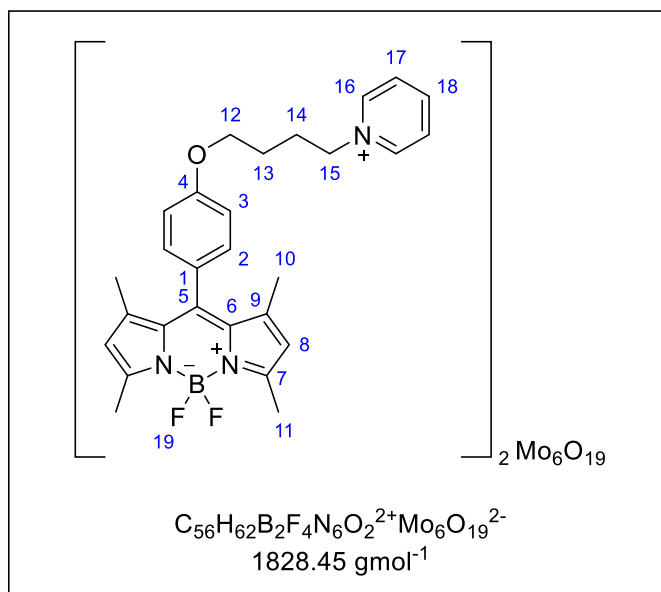
^{19}F NMR (376 MHz, DMSO- d_6 , 298 K) δ (ppm) = -143.2 (s, **F19**)

LRMS $\text{ES}^+ m/z = \text{ES}^+ m/z = 474.4$ $[\text{M}-\text{W}_6\text{O}_{19}]^+$

HRMS $\text{ES}^+ m/z$ calcd for $\text{C}_{56}\text{H}_{62}\text{B}_2\text{F}_4\text{N}_6\text{O}_2\text{W}_6\text{O}_{19} / [\text{M}-\text{W}_6\text{O}_{19}]^{2+}$ requires 474.2528 found 474.2516

FT-IR (neat) ν_{max} cm^{-1} 3068, 2941, 1541, 1194, 976, 799

4,4-Difluoro-8-(4-(4-pyridin-1-iumbutoxy)phenyl)-1,3,5,7-tetramethyl-4-bora-3a,4a-diaza-s-indacene hexamolybdate (2.36)



2.33 (0.112 g, 0.198 mmol) was added to dry acetonitrile under argon atmosphere and the mixture heated to 80 °C. (TBA)₂[Mo₆O₁₉] (0.131 g, 0.0690 mmol) was dissolved in dry acetonitrile (5 mL at 50 °C) and the warm solution added to the mixture. The mixture was stirred at 80 °C for 16 hours then allowed to cool to rt. The mixture was concentrated under reduced pressure (to approximately 5 mL) and a small amount of orange

precipitate was observed. Toluene (10 mL) was added, and the mixture sonicated for 1 minute which gave a large amount of orange precipitate. This precipitate was filtered and washed with ice cold acetonitrile (5 mL) and diethyl ether (10 mL). Drying afforded the title compound as an orange solid (85 mg, 67%).

M.P. 280 °C decomposed.

¹H NMR (400 MHz, DMSO-*d*₆, 298 K) δ (ppm) = 9.13 (d, *J* = 5.5 Hz, 2H, **16**), 8.62 (t, *J* = 7.8 Hz, 1H, **18**), 8.18 (dd, *J* = 7.6, 6.7 Hz, 2H, **17**), 7.26 (d, *J* = 8.7 Hz, 2H, **2**), 7.10 (d, *J* = 8.7 Hz, 2H, **3**), 6.17 (s, 2H, **8**), 4.71 (t, *J* = 7.3 Hz, 2H, **15**), 4.08 (t, *J* = 6.2 Hz, 2H, **12**), 2.44 (s, 6H, **11**), 2.13 (quin, *J* = 7.5 Hz, 2H, **14**), 1.85 – 1.72 (m, 2H, **13**), 1.39 (s, 6H, **10**)

¹³C NMR (101 MHz, DMSO-*d*₆, 298 K) δ (ppm) = 159.1 (C, **C4**), 154.6 (C, **C7**), 145.5 (CH, **C18**), 144.8 (CH, **C16**), 142.7 (C, **C9**), 142.1 (C, **C5**), 131.1 (C, **C6**), 129.1 (CH, **C2**), 128.1 (CH, **C17**), 126.0 (C, **C1**), 121.3 (CH, **C8**), 115.1 (CH, **C3**), 66.9 (CH₂, **C12**), 60.5 (CH₂, **C15**), 27.7 (CH₂, (**C13/C14**), 25.3 (CH₂, **C13/C14**), 14.2 (CH₃, **C11**), 14.2 (CH₃, **C10**)

¹⁹F NMR (376 MHz, DMSO-*d*₆, 298 K) δ (ppm) = -143.2 (s, **F19**)

LRMS ES⁺ *m/z* = 474.4 [M-Mo₆O₁₉]⁺

HRMS ES⁺ *m/z* calcd for C₅₆H₆₂B₂F₄N₆O₂Mo₆O₁₉ / [M-Mo₆O₁₉]²⁺ requires 474.2528 found 474.2517

FT-IR (neat) ν_{max} cm^{-1} 3066, 2940, 1541, 954, 784, 582

Chemical structure of the cationic part of a phosphonium salt, with atoms numbered 1 through 20. The structure features a central boron atom (B⁺) bonded to two fluorine atoms (F) and two nitrogen atoms (N⁻). The nitrogens are part of a fused ring system. A phenyl group is attached to the boron, and a long alkyl chain is attached to the phosphorus atom (P⁺). The counterion is a bromide ion (Br⁻).

$C_{35}H_{53}BF_2N_2OP^+Br^-$
 671.50 g mol⁻¹

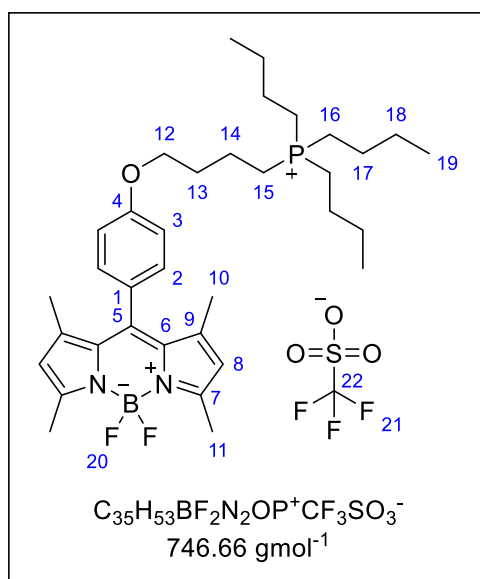
gave the title compound as an orange oil (104 mg, 77%).

¹³C NMR (101 MHz, DMSO-*d*₆, 298 K) δ (ppm) = 159.1 (C, **C4**), 154.7 (C, **C7**), 142.7 (C, **C9**), 142.1 (C, **C5**), 131.1 (C, **C6**), 129.2 (CH, **C2**), 126.0 (C, **C1**), 121.3 (CH, **C8**), 115.1 (CH, **C3**), 66.5 (CH₂, **C12**), 23.4 (CH₂, **C13**), 23.3 (CH₂, **C16**), 22.6 (CH₂, **C15**), 22.6 (CH₂, **C14**), 17.6 (CH₂, **C17**), 17.1 (CH₂, **C18**), 14.2 (CH₃, **C10**), 14.2 (CH₃, **C11**), 13.3 (CH₃, **C19**)

LRMS ES⁺ *m/z* = 597.5 [M-Br]⁺

FT-IR (neat) ν_{max} cm^{-1} 3385, 2917, 2849, 1508, 1155, 972, 705

4,4-Difluoro-8-(4-(4-tributylphosphoniumbutoxy)phenyl)-1,3,5,7-tetramethyl-4-bora-3a,4a-diaza-s-indacene trifluoromethanesulfonate (2.38)



2.37 (70 mg, 0.131 mmol) was added to dry acetonitrile (10 mL) under argon atmosphere. Potassium triflate (0.232 g, 1.26 mmol) in deionised water (5 mL) was then added and the mixture heated to 40 °C and stirred for 6 hours. The mixture was then allowed to cool and filtered. The solvent was removed from the filtrate and the crude solid was triturated with deionised water (2 x 10 mL) then with toluene (10 mL). The resulting solid was collected by filtration and washed thoroughly with water (50 mL) then toluene (50 mL) and finally diethyl ether (30 mL). Drying gave the title compound as an orange oil. (55 mg, 56%).

M.P. 150 - 154 °C

¹H NMR (400 MHz, DMSO-*d*₆, 298 K) δ (ppm) = 7.28 (d, *J* = 8.8 Hz, 2H, **2**), 7.11 (d, *J* = 8.7 Hz, 2H, **3**), 6.18 (s, 2H, **8**), 4.10 (t, *J* = 6.1 Hz, 2H, **12**), 2.44 (s, 6H, **11**), 2.36 – 2.26 (m, 2H, **15**), 2.25 – 2.16 (m, 6H, **16**), 1.89 (quin, *J* = 6.6 Hz, 2H, **13**), 1.70 (sxt, *J* = 7.7 Hz, 2H, **14**), 1.52 – 1.33 (m, 18H, **10 + 17 + 18**), 0.92 (t, *J* = 7.1 Hz, 9H, **19**)

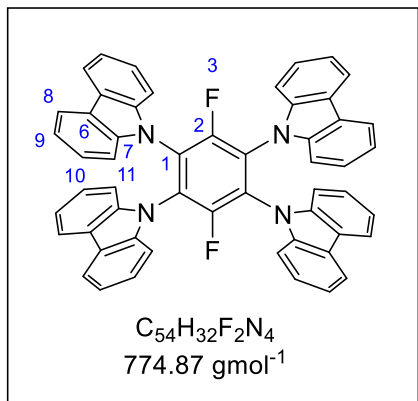
¹³C NMR (101 MHz, DMSO-*d*₆, 298 K) δ (ppm) = 159.1 (C, **C4**), 154.7 (C, **C7**), 142.7 (C, **C9**), 142.1 (C, **C5**), 131.1 (C, **C6**), 129.2 (CH, **C2**), 126.0 (C, **C1**), 121.3 (CH, **C8**), 115.1 (CH, **C3**), 66.5 (CH₂, **C12**), 23.4 (CH₂, **C13**), 23.3 (CH₂, **C16**), 22.6 (CH₂, **C15**), 22.6 (CH₂, **C14**), 17.5 (CH₂, **C17**), 17.1 (CH₂, **C18**), 14.2 (CH₃, **C10**), 14.1 (CH₃, **C11**), 13.2 (CH₃, **C19**)

¹⁹F NMR (376 MHz, DMSO-*d*₆, 298 K) δ (ppm) = -77.5 (s, **F21**), -143.2 (s, **F20**)

HRMS ES⁺ *m/z* calcd for C₃₅H₅₃BF₂N₂OPCF₃SO₃ / [M-CF₃SO₃]⁺ requires 597.3956 found 597.3944

FT-IR (neat) ν_{max} cm⁻¹ 2931, 2874, 1542, 1257, 1153, 1029, 972, 636

9,9',9'',9'''-((1*r*,2*s*,4*s*,5*s*)-3,6-difluorobenzene-1,2,4,5-tetrayl)tetrakis(9H-carbazole) (3.04)



9,9',9'',9'''-((1*r*,2*s*,4*s*,5*s*)-3,6-difluorobenzene-1,2,4,5-tetrayl)tetrakis(9H-carbazole) (**3.04**) was prepared according to the procedure described by H. Feng and co-workers'.¹³³

To a stirred suspension of NaH (60% in mineral oil, 1.45 g, 36.0 mmol) in dry DMF (12 mL) was added a solution of carbazole (3.00 g, 18.0 mmol) in dry DMF (12 mL) dropwise, at 10 °C, under argon atmosphere. The resulting mixture was shielded from light and stirred for 30 minutes at rt before addition of a solution of hexafluorobenzene (0.591 g, 3.00 mmol) in dry DMF (6 mL). The mixture was heated to 70 °C and stirred for 3 hours. The reaction was then allowed to cool and quenched slowly with water until H₂ evolution ceased. The precipitate formed was filtered and washed with water to give an off-white solid. This solid was recrystallised from toluene to yield the title compound as white, needle-like, crystals. (1.23 g, 1.59 mmol, 53%).

M.P. 250 °C decomposed.

¹H NMR (400 MHz, CDCl₃, 298K) δ (ppm) = 7.77-7.82 (m, 8H, **8**), 7.24-7.28 (m, 8H, **10**), 7.09-7.16 (m, 16H, **9 + 11**)

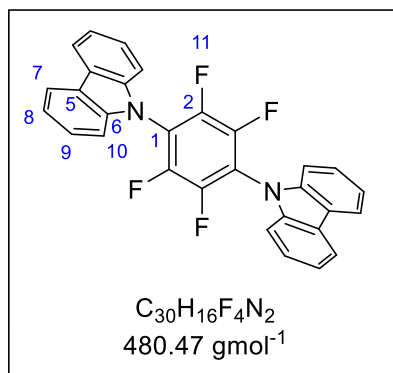
¹³C NMR (101 MHz, CDCl₃, 298 K) δ (ppm)= 139.0 (C, **C7**), 125.7 (CH, **C10**), 124.0 (C, **C6**), 120.9 (CH, **C9**), 120.1 (CH, **C8**), 109.9 (CH, **C11**)

¹⁹F NMR (376 MHz, CDCl₃, 298 K) δ (ppm) = -119.4 (s, **F15**)

HRMS ES⁺ m/z calcd for C₅₄H₃₃F₂N₄ / [M+H]⁺ requires 775.2673 found 775.2653

FT-IR (neat) ν_{max} 2981, 1621, 1439, 1222, 837, 741 cm⁻¹

9,9'-(perfluoro-1,4-phenylene)bis(9H-carbazole) (3.10)



To a stirred suspension of NaH (60% in mineral oil, 0.320 g, 4.00 mmol) in dry DMF (5 mL) was added a solution of carbazole (0.666 g, 2.00 mmol) in dry DMF (5 mL) dropwise, at 10 °C, under argon atmosphere. The resulting mixture was shielded from light and stirred for 30 minutes at rt before addition of a solution of hexafluorobenzene (0.372 g, 2.00 mmol) in dry DMF (3 mL). The mixture was heated to 70 °C and stirred for 30 minutes then stirred for a further 24 hours at rt.

The reaction was then quenched slowly with water until H_2 evolution ceased. The precipitate formed was filtered and washed with water to give an off-white solid. This solid was recrystallised from toluene to yield the title compound as white, needle-like, crystals. (0.24 g, 7.31 mmol, 73%).

M.P. 235 °C decomposed.

1H NMR (400 MHz, $CDCl_3$, 298K) δ (ppm) = 8.20 (d, J = 8.2 Hz, 4H, **7**), 7.55 (ddd, J = 8.3, 7.2, 1.2 Hz, 4H, **9**), 7.42 (t, J = 7.4 Hz, 4H, **8**), 7.33 (d, J = 8.2 Hz, 4H, **10**)

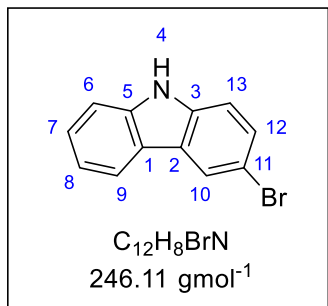
^{13}C NMR (101 MHz, $CDCl_3$, 298K) δ (ppm) = 139.8 (C, **C6**), 126.6 (CH, **C9**), 124.3 (C, **C5**), 121.5 (CH, **C8**), 120.7 (CH, **C7**), 109.9 (CH, **C10**)

^{19}F NMR (376 MHz, $CDCl_3$, 298 K) δ (ppm) = -141.3 (s, **F11**)

HRMS ES^+ m/z calcd for $C_{30}H_{17}F_4N_2$ / $[M+H]^+$ requires 481.1328 found 481.1327

FT-IR (neat) ν_{max} 3049, 1603, 1520, 1230, 1029 cm^{-1}

3-bromo-9H-carbazole (**3.12**)



3-bromo-9H-carbazole (**3.12**) was prepared according to the procedure described by M. Y. Wong and co-workers'.⁷⁵

Carbazole (6.58 g, 39.3 mmol) was dissolved in THF (100 mL). To this a solution of NBS (7.00 g, 39.3 mmol), that had been recrystallised from water, in THF (100 mL) was added dropwise at 0 °C. The reaction mixture was stirred at 0 °C for 6 hours then allowed to stir at rt for a further 12 hours. After this THF was removed under reduced pressure then ethyl acetate (100 mL) and deionised water (100 mL) were added. The separated aqueous layer was extracted with ethyl acetate (2 x 50 mL) and the combined organic extracts washed with brine and dried ($MgSO_4$). Solvent was removed under reduced pressure and the isolated white solid recrystallised from chloroform:IPA (1:1) to yield the title compound as white flakes. (4.36 g, 17.72 mmol, 45%).

M.P. 197 - 198 °C (lit 195 - 196 °C)²¹⁷

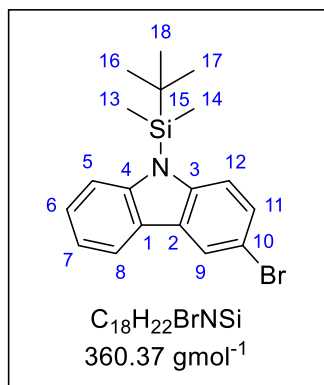
¹H NMR (400 MHz, $CDCl_3$, 298K) δ (ppm) = 8.20 (d, J = 2.0 Hz, 1H, **10**), 8.04 (dd, J = 7.8, 0.9 Hz, 1H, **9**), 7.51 (dd, J = 8.6, 2.0 Hz, 1H, **6**), 7.42-7.47 (m, 2H, **7 + 12**), 7.32 (d, J = 8.6 Hz, 1H, **13**), 7.23-7.33 (m, 2H, **7 + 8**)

¹³C NMR (101 MHz, $CDCl_3$, 298K) δ (ppm) = 139.8 (C, **C5**), 138.0 (C, **C3**), 128.5 (C, **C12**), 126.6 (CH, **C7**), 125.2 (C, **C1**), 123.1 (C, **C2**), 122.4 (CH, **C9**), 120.5 (CH, **C10**), 119.9 (CH, **C8**), 112.2 (CH, **C13**), 112.0 (C, **C11**), 110.8 (CH, **C6**)

LRMS EI m/z = 247.0 (96% [$M^{81}Br$]⁺⁺), 245.0 (100% [$M^{79}Br$]⁺⁺), 166.1 (95% [$M-Br$]⁺)

FT-IR (neat) ν_{max} 3401, 3048, 1723, 1598, 1438, 809, 723 cm^{-1}

3-bromo-9-(tert-butyldimethylsilyl)-carbazole (**3.13**)



3-bromo-9-(tert-butyldimethylsilyl)-carbazole (**3.13**) was prepared according to the procedure described by M. Y. Wong and co-workers'.⁷⁵

To a stirred suspension of NaH (60% in mineral oil, 0.65 g, 16.1 mmol) in dry THF (20 mL) was added a solution of 3-bromo-9H-carbazole (2.64 g, 10.7 mmol) in dry THF (20 mL) dropwise under argon atmosphere. The mixture was stirred for 30 minutes, at rt, then *t*-butyldimethylsilyl chloride (1.77 g, 11.8 mmol) was added. The reaction mixture was stirred for 30 minutes then poured onto ice cold deionised water (80 mL). This was then extracted with DCM (2 x 80 mL) and the combined organic extracts dried (Na_2SO_4). Solvent was removed under reduced pressure and the remaining residue purified by silica gel column chromatography (hexane 100%). This yielded the product as a white solid. (3.11 g, 8.63 mmol, 83%).

M.P. 98 - 99 °C (lit 98 - 99 °C)⁷⁵

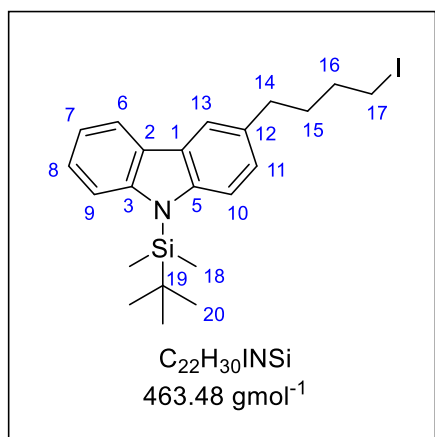
¹H NMR (400 MHz, $CDCl_3$, 298K) δ (ppm) = 8.18 (dd, J = 2.1, 0.6 Hz, 1H, **9**), 8.02 (d, J = 7.6 Hz, 1H, **8**), 7.61 (d, J = 7.6 Hz, 1H, **5**), 7.39-7.50 (m, 3H, **8 + 12 + 13**), 7.23-7.28 (m, 1H, **6**), 1.05 (s, 9H, **16 + 17 + 18**), 0.76 (s, 6H, **13 + 14**)

¹³C NMR (101 MHz, $CDCl_3$, 298K) δ (ppm) = 145.4 (C, **C3**), 143.7 (C, **C4**), 123.2 (C, **C2**), 127.8 (CH, **C11**), 126.0 (CH, **C6**), 125.2 (C, **C1**), 122.5 (CH, **C9**), 120.0 (CH, **C7**), 119.9 (CH, **C8**), 115.4 (C, **C10**), 114.2 (CH, **C12**), 112.5 (CH, **C5**), 26.5 (CH_3 , **C16 + C17 + C18**), 20.5 (C, **C15**)

LRMS EI m/z = 361.1 (50% [$M^{81}Br$]⁺⁺), 359.1 (48% [$M^{79}Br$]⁺⁺), 304.0 (100% [$M^{81}Br-C_4H_9$]⁺), 302.0 (89% [$M^{79}Br-C_4H_9$]⁺)

FT-IR (neat) ν_{max} 2949, 2856, 1438, 1268, 1209, 1012, 804 cm^{-1}

9-(tert-butyldimethylsilyl)-3-(4-iodobutyl)-carbazole (**3.14**)



9-(tert-butyldimethylsilyl)-3-(4-iodobutyl)-carbazole (**3.14**) was prepared according to the procedure described by M. Y. Wong and co-workers'.⁷⁵

To a solution of **3.13** (2.00 g, 5.55 mmol) in dry THF (30 mL) was added *n*-BuLi (2.5 M in hexanes, 2.67 mL, 6.65 mmol) at -78 °C under argon atmosphere. The mixture was stirred for 30 minutes then added, via cannula, to a solution of 1,4-diiodobutane (2.58 g, 8.35 mmol) in dry THF (20 mL) at -78 °C. The mixture was stirred for a further 30 minutes, warmed to rt, then poured slowly onto ice cold deionised water (75 mL). This mixture was extracted with DCM (3 x 50 mL) and the combined organic layers dried (Na₂SO₄). Solvent was then removed under reduced pressure to leave a colourless oil which was purified by silica gel column chromatography (hexane:DCM = 1:0 → 5:1) affording the title compound as a colourless oil. (1.17 g, 2.53 mmol, 44%).

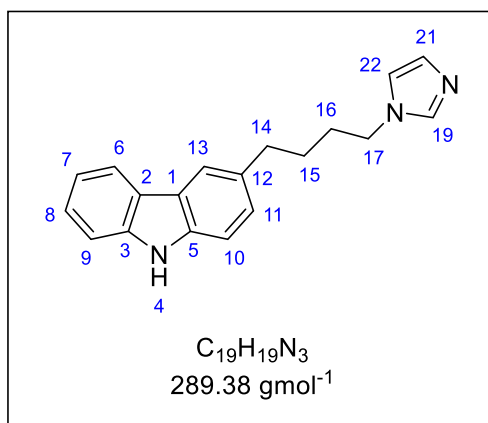
¹H NMR (400 MHz, CDCl₃, 298K) δ (ppm) = 8.05 (d, *J* = 7.6 Hz, 1H, **6**), 7.86 (d, *J* = 2.5 Hz, 1H, **13**), 7.59 (dt, *J* = 8.5, 0.9 Hz, 1H, **9**), 7.52 (d, *J* = 8.3 Hz, 1H, **10**), 7.35 (ddd, *J* = 8.4, 7.1, 1.5 Hz, 1H, **7**), 7.16-7.25 (m, 2H, **8 + 11**), 3.24 (t, *J* = 6.9 Hz, 2H, **17**), 2.81 (t, *J* = 7.4 Hz, 2H, **14**), 1.89-1.97 (m, 2H, **16**), 1.81-1.88 (m, 2H, **15**), 1.05 (br s, 9H, **20**), 0.75 (s, 6H, **18**)

¹³C NMR (101 MHz CDCl₃, 298K) δ (ppm) = 145.3 (C, **C3**), 143.5 (C, **C5**), 132.9 (C, **C12**), 126.4 (CH, **C11**), 126.1 (C, **C1**), 125.9 (CH, **C8**), 125.1 (C, **C2**), 119.7 (CH, **C6**), 119.4 (CH, **C7**), 119.1 (CH, **C13**), 114.0 (CH, **C9**), 113.9 (CH, **C10**), 34.6 (CH₂, **C14**), 33.0 (CH₂, **C15/C16**), 32.8 (CH₂, **C15/C16**), 26.6 (CH₃, **C20**), 20.6 (C, **C19**), 7.0 (CH₃, **C18**)

LRMS EI *m/z* = 463.0 [M]⁺⁺

FT-IR (neat) *v*_{max} 2926, 2855, 1601, 1448, 1256, 1210, 966, 805 cm⁻¹

3-(4-(1H-imidazol-1-yl)butyl)-9H-carbazole (**3.15**)



3-(4-(1H-imidazol-1-yl)butyl)-9H-carbazole (**3.15**) was prepared according to the procedure described by M. Y. Wong and co-workers'.⁷⁵

Imidazole (0.443 g, 6.24 mmol) was dissolved in dry THF (20 mL) under argon atmosphere. To this solution, NaH (60% in mineral oil, 0.251 g, 6.24 mmol) was added portion wise at rt. The mixture was stirred for 30 minutes then a solution of **3.14** (1.45 g, 3.21 mmol) in dry THF (10 mL) was added and the mixture refluxed for 4 hours. The mixture was then cooled to rt before a second, portion wise, addition of NaH (60% in mineral oil, 0.25 g, 6.24 mmol). The resulting mixture was refluxed for a further 4 hours, cooled to rt then slowly poured onto ice cold deionised water (25 mL). This was then extracted with DCM (3 x 50 mL) and the combined organic layers dried (Na_2SO_4). Solvent was removed under reduced pressure to give an orange solid which was purified by silica gel column chromatography (hexane:DCM:triethylamine = 4:1:5%). The isolated product was washed with water to yield the title compound as an off-white solid. (491 mg, 1.70 mmol, 53%).

M.P. 169 - 172 °C (lit 166 - 167 °C)⁷⁵

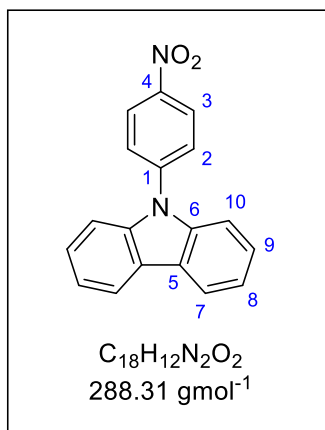
¹H NMR (400 MHz, $CDCl_3$, 298 K) δ (ppm) = 8.26 (br s, 1H, **4**), 8.06 (dq, J = 7.7, 0.8 Hz, 1H, **6**), 7.85 (t, J = 0.8 Hz, 1H, **13**), 7.47 (s, 1H, **19**), 7.40-7.42 (m, 2H, **8 + 9**), 7.35 (d, J = 8.3 Hz, 1H, **10**), 7.18-7.25 (m, 2H, **7 + 11**), 7.07 (s, 1H, **21**), 6.89 (s, 1H, **22**), 3.95 (t, J = 7.0 Hz, 2H, **17**), 2.82 (t, J = 7.4 Hz, 2H, **14**), 1.81-1.91 (m, 2H, **16**), 1.69-1.79 (m, 2H, **15**)

¹³C NMR (101 MHz, $CDCl_3$, 298 K) δ (ppm) = 139.9 (C, **C3**), 138.1 (C, **C5**), 137.1 (CH, **C19**), 132.5 (C, **C12**), 129.4 (CH, **C21**), 126.4 (CH, **C8**), 125.8 (CH, **C11**), 123.5 (C, **C1**), 123.1 (C, **C2**), 120.2 (CH, **C6**), 119.6 (CH, **C7**), 119.3 (CH, **C13**), 118.8 (CH, **C22**), 110.6 (CH, **C9/C10**), 110.5 (CH, **C9/C10**), 47.0 (CH_2 , **C17**), 35.3 (CH_2 , **C14**), 30.6 (CH_2 , **C16**), 29.0 (CH_2 , **C15**)

LRMS ES^+ m/z = 290.2 $[M+H]^+$

FT-IR (neat) ν_{max} 3023, 2934, 2856, 1610, 1481, 1327, 1240, 810, 735 cm^{-1}

9-(4-Nitrophenyl)-9H-carbazole (**3.24**)



9-(4-Nitrophenyl)-9H-carbazole (**3.24**) was prepared according to the procedure described by L. Shi and co-workers'.²¹⁸

4-fluoronitrobenzene (150 mg, 1.06 mmol) and carbazole (194 mg, 1.16 mmol) were dissolved in dry DMF (10 mL) under nitrogen atmosphere. Potassium carbonate (162 mg, 1.16 mmol) was then added, and the mixture heated to 150 °C and stirred for 16 hours. The

mixture was allowed to cool to room temperature and then poured into deionised water (100 mL) and a yellow precipitate observed. The precipitate was filtered and washed with deionised water (100 mL) and then the isolated solid recrystallized from ethanol to yield the title compound as yellow crystals (263 mg, 86%).

M.P. 208 - 209 °C (lit 208 - 210 °C)²¹⁹

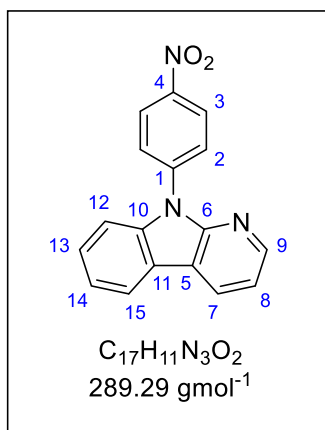
¹H NMR (400 MHz, DMSO-*d*₆, 298 K) δ (ppm) = 8.50 (d, J = 9.0 Hz, 2H, **3**), 8.28 (dq, J = 7.8, 0.7 Hz, 2H, **7**), 7.98 (d, J = 9.0 Hz, 2H, **2**), 7.56 (dt, J = 8.2, 0.9 Hz, 2H, **10**), 7.48 (ddd, J = 8.3, 7.1, 1.2 Hz, 2H, **9**), 7.35 (ddd, J = 7.8, 7.0, 1.1 Hz, 2H, **8**)

¹³C NMR (101 MHz, DMSO-*d*₆, 298 K) δ (ppm) = 145.4 (C, **C1**), 142.9 (C, **C4**), 139.2 (C, **C6**), 127.0 (CH, **C2**), 126.6 (CH, **C9**), 125.6 (CH, **C3**), 123.4 (C, **C5**), 121.1 (CH, **C8**), 120.7 (CH, **C7**), 109.9 (CH, **C10**)

LRMS ES⁺ m/z = 289.3 [M+H]⁺

FT-IR (neat) ν_{max} cm⁻¹ 3051, 2918, 1594, 1478, 1312, 741, 718

9-(4-Nitrophenyl)-9H-pyrido[2,3-b]indole (**3.23**)



9-(4-Nitrophenyl)-9H-pyrido[2,3-b]indole (**3.23**) was prepared by adapting the procedure described by L. Shi and co-workers'.²¹⁸

4-fluoronitrobenzene (150 mg, 1.06 mmol) and α -carboline (196 mg, 1.16 mmol) were dissolved in dry DMF (10 mL) under nitrogen atmosphere. Potassium carbonate (162 mg, 1.16 mmol) was then added, and the mixture heated to 150 °C and stirred for 16 hours. The

mixture was allowed to cool to room temperature and then poured into deionised water (100 mL) and a yellow precipitate observed. The precipitate was filtered and washed with deionised water (100 mL) and then the isolated solid recrystallized from ethanol to yield the title compound as yellow/brown solid (236 mg, 77%).

M.P. 186 - 188 °C

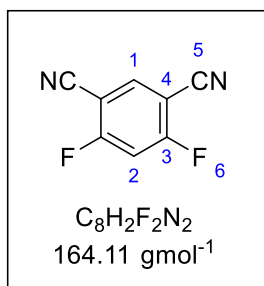
¹H NMR (400 MHz, DMSO-*d*₆, 298 K) δ (ppm) = 8.68 (dd, J = 7.7, 1.6 Hz, 1H, **7**), 8.50 – 8.46 (m, 3H, **3 + 9**), 8.33 (dt, J = 7.5, 1.0 Hz, 1H, **15**), 8.07 (d, J = 9.3 Hz, 2H, **2**), 7.67 (d, J = 8.3 Hz, 1H, **12**), 7.56 (ddd, J = 8.3, 7.1, 1.2 Hz, 1H, **13**), 7.45 – 7.39 (m, 2H, **8 + 14**)

¹³C NMR (101 MHz, DMSO-*d*₆, 298 K) δ (ppm) = 150.7 (C, **C6**), 146.4 (CH, **C9**), 145.3 (C, **C1**), 141.7 (C, **C4**), 138.2 (C, **C10**), 129.3 (CH, **C7**), 127.6 (CH, **C13**), 127.3 (CH, **C2**), 124.8 (CH, **C3**), 121.8 (CH, **C14**), 121.7 (CH, **C15**), 121.0 (C, **C5**), 117.5 (CH, **C8**), 116.2 (C, **C11**), 110.5 (CH, **C12**)

LRMS ES⁺ m/z = 290.2 [M+H]⁺

FT-IR (neat) ν_{max} cm⁻¹ 3057, 1592, 1514, 1410, 1346, 854, 731

4,6-Difluoroisophthalonitrile (**3.27**)



4,6-Difluoroisophthalonitrile (**3.27**) was prepared by according to the procedure described by N. Nazarpack-Kandlousy and co-workers'.²²⁰

2,4-Dibromo-1,5-difluorobenzene (4.75 g, 17.5 mmol) was dissolved in dry DMF (70 mL) under argon atmosphere. Copper (I) cyanide (6.92 g, 77.2 mmol) was then added, and the mixture heated to 150 °C for 16 hours. The mixture was then allowed to cool to room temperature and filtered. The filtrate was concentrated under reduced pressure then DCM (150 mL) and ice-cold deionised water (50 mL) added. The aqueous layer was separated and extracted with DCM (2 x 30 mL) then the combined organic extracts washed with deionised water (3 x 50 mL). The organic extracts were dried (Na_2SO_4) and the solvent removed under reduced pressure. The resulting crude material was purified (Biotage Selekt, hexane/DCM, 9:1 → 1:1) to yield the title compound as a white solid (1.44 g, 50%).

M.P. 121 - 123 °C

$^1\text{H NMR}$ (400 MHz, CDCl_3 , 298 K) δ (ppm) = 8.02 (t, J = 6.7 Hz, 1H, **1**), 7.22 (t, J = 8.4 Hz, 1H, **2**)

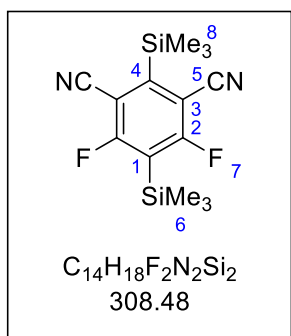
$^{13}\text{C NMR}$ (101 MHz, CDCl_3 , 298 K) δ (ppm) = 166.1 (dd, J = 272.5, 13.6 Hz, C, **C3**), 138.1 (t, J = 2.6 Hz, CH, **C1**), 110.9 (C, **C5**), 107.1 (t, J = 24.2 Hz, C, **C4**), 100.2 (dd, J = 13.2, 8.8 Hz, CH, **C2**)

$^{19}\text{F NMR}$ (376 MHz, CDCl_3 , 298 K) Shift (ppm) = -90.5 (**F6**)

LRMS EI m/z = 164.0 (100% $[\text{M}]^{++}$)

FT-IR (neat) ν_{max} cm^{-1} 3137, 3061, 2245, 1591, 1499, 1308, 1094, 873

4,6-difluoro-2,5-bis(trimethylsilyl)isophthalonitrile (**3.28**)



2,2,6,6-Tetramethylpiperidine (0.685 mL, 4.02 mmol) was dissolved in dry THF (7 mL) under argon atmosphere. The solution was cooled to -78 °C and n-BuLi (2.5 M in hexanes, 1.46 mL, 3.66 mmol) added slowly. The mixture was stirred at -78 °C for 40 minutes then Me₃SiCl (0.930 mL, 7.32 mmol) was added dropwise followed by the dropwise addition of **3.27** (200 mg, 1.22 mmol) in dry THF (8 mL). The temperature was maintained at -78 °C for 30 minutes then the reaction mixture was allowed to naturally warm to room temperature as it was stirred overnight. To quench the reaction sat. aq. NH₄Cl solution (10 mL) was added. The mixture was then extracted with ethyl acetate (3 x 15 mL) and the combined organic extracts washed with deionised water (15 mL) and brine (15 mL) then dried (MgSO₄). The solvent was removed under reduced pressure and the resulting crude product was purified (Biotage Selekt, hexanes/ethyl acetate, 99:1 → 9:1) to yield the title compound as a white solid (254 mg, 83%).

M.P. 115 - 118 °C

¹H NMR (400 MHz, CDCl₃, 298 K) δ (ppm) = 0.62 (s, 3H, **6**), 0.44 (s, 3H, **8**)

¹³C NMR (101 MHz, CDCl₃, 298 K) δ (ppm) = 170.3 (dd, *J* = 266.3, 17.6 Hz, C, **C2**), 155.2 (C, **C4**), 117.4 (t, *J* = 35.9 Hz, 1C, C, **C4**), 113.3 (C, **C5**), 104.1 (dd, *J* = 14.7, 8.1 Hz, C, **C1**), 0.0 (CH₃, **C8**) -0.4 (t, *J* = 2.6 Hz, CH₃, **C6**)

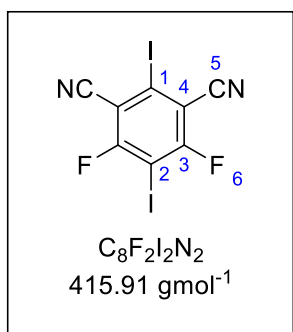
¹⁹F NMR (376 MHz, CDCl₃, 298 K) Shift (ppm) = -79.2 (**F6**)

LRMS EI *m/z* = 308.1 (0.5% [M]⁺⁺), 293.1 (100% [M-CH₃]⁺)

HRMS EI *m/z* calcd for C₁₄H₁₈F₂N₂Si₂ / [M]⁺⁺ requires 308.0976 found 308.0971

FT-IR (neat) ν_{max} cm⁻¹ 2961, 2234, 1523, 1370, 1232, 1078, 837

4,6-Difluoro-2,5-diiodoisophthalonitrile (**3.29**)



2,2,6,6-Tetramethylpiperidine (0.685 mL, 4.02 mmol) was dissolved in dry THF (7 mL) under argon atmosphere. The solution was cooled to -78 °C and n-BuLi (2.5 M in hexanes, 1.46 mL, 3.66 mmol) added slowly. The mixture was stirred at -78 °C for 40 minutes then **3.27** (200 mg, 1.22 mmol) in dry THF (8 mL) was added dropwise. The mixture was stirred at -78 °C for 1 hour then iodine (1.86 g, 7.32 mmol) added portion wise.

The temperature was maintained at -78 °C for 30 minutes then the reaction mixture was allowed to naturally warm to room temperature as it was stirred overnight. To quench the reaction sat. aq. $Na_2S_2O_3$ solution (20 mL) was added. The mixture was then extracted with ethyl acetate (3 x 15 mL) and the combined organic extracts washed with deionised water (15 mL) and brine (15 mL) then dried ($MgSO_4$). The solvent was removed under reduced pressure and the resulting crude product was purified (Biotage Selekt, hexanes/ethyl acetate, 20:1 → 5:1) to yield the title compound as a yellow solid (225 mg, 44%).

M.P. 105 - 107 °C

^{13}C NMR (101 MHz, $CDCl_3$, 298 K) δ (ppm) = 166.3 (dd, J = 263.4, 10.3 Hz, C, **C3**), 113.5 (C, **C5**), 109.2 (C, **C1**), 107.8 (dd, J = 14.7, 8.1 Hz, C, **C2**), 76.2 (t, J = 31.9 Hz, C, **C4**)

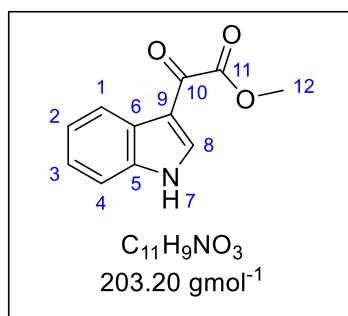
^{19}F NMR (376 MHz, $CDCl_3$, 298 K) Shift (ppm) = -70.1 (**F6**)

LRMS EI m/z = 415.7 (100% $[M]^{++}$)

HRMS EI m/z calcd for $C_8F_2I_2N_2$ / $[M]^{++}$ requires 415.8119 found 415.8117

FT-IR (neat) ν_{max} cm^{-1} 2961, 2238, 1559, 1407, 1107, 725

Methyl 2-(1H-indol-3-yl)-2-oxoacetate (4.31)



Methyl 2-(1H-indol-3-yl)-2-oxoacetate (**4.31**) was prepared by adapting the procedure described by Faul and co-workers'.¹⁷⁶

To a solution of indole (20.0 g, 171 mmol) in dry diethyl ether (200 mL) at 0 °C under nitrogen atmosphere was added oxalyl chloride (17.0 mL, 188 mmol) dropwise over 10 minutes. The resulting mixture was stirred at 0 °C for 2 hours before cooling to -30 °C and adding dry methanol (20 mL) dropwise over 10 minutes. The mixture was then allowed to warm to room temperature and stirred for 30 minutes. The resulting precipitate was filtered and washed with deionised water (200 mL) and diethyl ether (250 mL). The solid was then taken in methanol (400 mL) and the mixture refluxed for 30 minutes before allowing the mixture to cool to room temperature and stirring for 16 hours. The mixture was then filtered and the solid washed with ice-cold methanol (100 mL) followed by ice-cold diethyl ether (200 mL). This gave the title compound as an orange solid (27.2 g, 78%).

M.P. 212 - 214 °C (lit 208 - 210 °C)²²¹

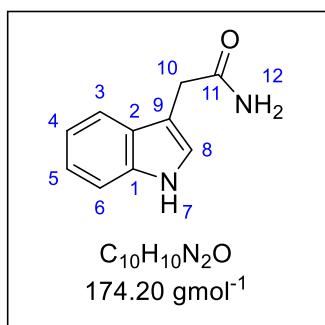
¹H NMR (400 MHz, DMSO-*d*₆, 298 K) δ (ppm) = 12.41 (br s, 1H, **7**), 8.45 (d, *J* = 3.4 Hz, 1H, **8**), 8.19-8.14 (m, 1H, **1**), 7.58 – 7.53 (m, 1H, **4**), 7.32 – 7.25 (m, 2H, **2 + 3**), 3.89 (s, 3H, **12**)

¹³C NMR (101 MHz, DMSO-*d*₆, 298 K) δ (ppm) = 178.7 (C, **C10**), 164.0 (C, **C11**), 138.4 (CH, **C8**), 136.7 (C, **C5**), 125.5 (C, **C6**), 123.8 (CH, **C3**), 122.8 (CH, **C2**), 121.1 (CH, **C1**), 112.7 (CH, **C4**), 112.4 (C, **C9**), 52.5 (CH₃, **C12**)

LRMS ES⁺ *m/z* = 204.2 [M+H]⁺

FT-IR (neat) ν_{max} cm⁻¹ 3192, 2952, 1731, 1612, 1416, 1113, 752

2-(1H-Indol-3-yl)acetamide (4.32)



2-(1H-Indol-3-yl)acetamide (**4.32**) was prepared according to the procedure described by Li and co-workers'.²²²

Indole-3-acetic acid (12.5 g, 71.4 mmol) was dissolved in dry THF (250 mL) under nitrogen atmosphere and CDI (15.7 g, 97.0 mmol) was added at 0 °C. After stirring for 30 minutes the solution was allowed to warm to room temperature and stirred for a further 2 hours. The reaction was quenched by the dropwise addition of ammonium hydroxide (35%, 50 mL). Once the addition was complete the mixture was stirred at room temperature for a further 30 minutes before concentrating the mixture under reduced pressure to yield an off-white solid. This solid was taken in ethyl acetate (400 mL) and deionised water (400 mL) added. The phases were then separated, and the organic phase washed with deionised water (200 mL) and brine (200 mL). The organic layer was then dried (MgSO₄) and the solvent removed under reduced pressure to yield the title compound as a white solid (11.2 g, 90%).

M.P. 148 - 149 °C (lit 148 - 150 °C)²²³

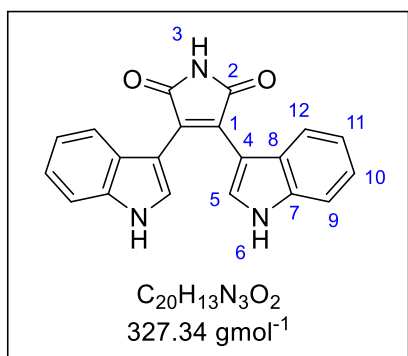
¹H NMR (400 MHz, DMSO-*d*₆, 298 K) δ (ppm) = 10.87 (br s, 1H, **7**), 7.59 (d, *J* = 7.3 Hz, 1H, **3**), 7.37 (dt, *J* = 7.8, 1.0 Hz, 1H, **6**), 7.33 (br s, 1H, **12a**), 7.22 (d, *J* = 2.2 Hz, 1H, **8**), 7.09 (ddd, *J* = 8.1, 7.0, 1.1 Hz, 1H, **5**), 7.00 (ddd, *J* = 7.9, 7.0, 1.0 Hz, 1H, **4**), 6.88 (br s, 1H, **12b**), 3.46 (s, 2H, **10**)

¹³C NMR (101 MHz, DMSO-*d*₆, 298 K) δ (ppm) = 173.1 (C, **C11**), 136.2 (C, **C1**), 127.3 (C, **C2**), 123.8 (CH, **C8**), 121.0 (CH, **C5**), 118.7 (CH, **C3**), 118.3 (CH, **C4**), 111.4 (CH, **C6**), 109.1 (C, **C9**), 32.6 (CH₂, **C10**)

LRMS ES⁺ *m/z* = 175.2 [M+H]⁺

FT-IR (neat) *v*_{max} cm⁻¹ 3381, 3193, 1614, 1407, 1096, 736

3,4-Di(1H-indol-3-yl)-1H-pyrrole-2,5-dione (**4.28**)



3,4-Di(1H-indol-3-yl)-1H-pyrrole-2,5-dione (**4.28**) was prepared according to the procedure described by Faul and co-workers'.¹⁷⁶

To a solution of **4.32** (11.0 g, 63.2 mmol) and **4.31** (15.5 g, 76.3 mmol) in dry THF (200 mL) at 0 °C under argon atmosphere was added potassium tert-butoxide (21.3 g, 189 mmol) portion wise (10 x 2.13 g portions) over a 20-minute period. The resulting slurry was allowed to warm to room temperature and stirred for 16 hours. The mixture was then cooled to 0 °C and concentrated HCl (30 mL) was added dropwise over 15 minutes. The resulting mixture was allowed to warm to room temperature and stirred for 6 hours before the addition of deionised water (150 mL) and ethyl acetate (200 mL). The phases were separated, and the aqueous phase extracted with ethyl acetate (3 x 150 mL) then the combined organic extracts were washed with brine (300 mL) and dried ($MgSO_4$). Solvent was then removed under reduced pressure to afford a red solid which was purified by recrystallisation from ethanol. This afforded the ethanol mono-adduct of the title compound as a red solid (18.54 g, 70%).

M.P. 163 - 164 °C (lit 158 - 160 °C)²²⁴

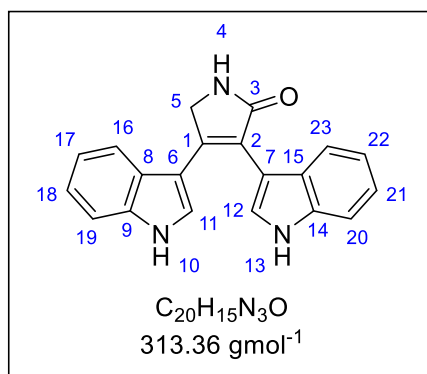
¹H NMR (400 MHz, DMSO- d_6 , 298 K) δ (ppm) = 11.64 (d, J = 2.3 Hz, 2H, **6**), 10.89 (s, 1H, **3**), 7.73 (d, J = 2.8 Hz, 2H, **5**), 7.36 (d, J = 8.1 Hz, 2H, **9**), 6.97 (ddd, J = 8.1, 7.0, 1.1 Hz, 2H, **10**), 6.81 (d, J = 8.1 Hz, 2H, **12**), 6.62 (ddd, J = 8.1, 7.1, 1.0 Hz, 2H, **11**), 4.35 (t, J = 5.1 Hz, 1H, CH_3CH_2OH), 3.44 (qd, J = 7.0, 5.0 Hz, 2H, CH_3CH_2OH), 1.06 (t, J = 7.0 Hz, 3H, CH_3CH_2OH)

¹³C NMR (101 MHz, DMSO- d_6 , 298 K) δ (ppm) = 173.0 (C, **C2**), 135.9 (C, **C7**), 129.1 (CH, **C5**), 127.7 (C, **C1**), 125.4 (C, **C8**), 121.5 (CH, **C10**), 120.9 (CH, **C12**), 119.3 (CH, **C11**), 111.7 (CH, **C9**), 105.6 (C, **C4**), 56.0 (CH_3CH_2OH), 18.55 (CH_3CH_2OH)

LRMS ES^- m/z = 326.7 [$M-H$]⁻

FT-IR (neat) ν_{max} cm^{-1} 3351, 2972, 1698, 1339, 995, 745

3,4-Di(1H-indol-3-yl)-1,5-dihydro-2H-pyrrol-2-one (5.15)



3,4-Di(1H-indol-3-yl)-1,5-dihydro-2H-pyrrol-2-one (5.15) was prepared according to the procedure outlined by P. D. Davis and co-workers'.²²⁵

4.28 (15.3 g, 41.1 mmol) was dissolved under argon atmosphere in dry THF (350 mL). $LiAlH_4$ (61.6 mL, 123 mmol) was then added dropwise at 0 °C over 30 minutes. The mixture was then allowed to warm to room temperature and stirred for 72 hours. The mixture was then cooled to 0 °C and quenched by the dropwise addition of deionised water until the mixture stopped bubbling upon addition (THIS QUENCH WAS PERFORMED VERY SLOWLY, CAUTION H_2 EVOLUTION). The solution was then acidified to $pH \approx 2$ by the dropwise addition of 2 M HCl. The mixture was then extracted with ethyl acetate (3 x 200 mL) and the combined extracts were washed with sat. aq. $NaHCO_3$ solution (200 mL) followed by brine (200 mL). The extracts were then dried ($MgSO_4$) and the solvent removed under reduced pressure. The residue was purified silica gel column chromatography (DCM/MeOH, 49:1 \rightarrow 9:1) to yield the title compound as an off white solid (5.35 g, 41%).

M.P. 292 - 295 °C (lit 290 - 293 °C)²²⁶

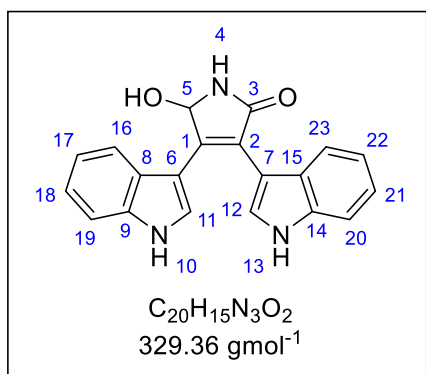
1H NMR (400 MHz, $DMSO-d_6$, 298 K) δ (ppm) = 11.36 (br d, J = 2.0 Hz, 1H, **10**), 11.24 (d, J = 2.1 Hz, 1H, **13**), 8.19 (s, 1H, **4**), 7.47 (d, J = 2.4 Hz, 1H, **12**), 7.41 – 7.34 (m, 1H, **19**), 7.31 – 7.27 (m, 2H, **11 + 16**), 7.03 (overlapping ddd, J = 8.1, 7.0, 1.1 Hz, 2H, **18 + 21**), 6.95 (d, J = 7.9 Hz, 1H, **23**), 6.85 (ddd, J = 8.1, 7.1, 1.1 Hz, 1H, **17**), 6.74 (ddd, J = 8.0, 7.0, 1.0 Hz, 1H, **22**), 4.54 (s, 2H, **5**)

^{13}C NMR (101 MHz, $DMSO-d_6$, 298 K) δ (ppm) = 174.1 (C, **C3**), 144.2 (C, **C1**), 136.1 (C, **C9**), 136.0 (C, **C14**), 126.5 (CH, **C11**), 126.1 (CH, **C12**), 125.4 (C, **C15**), 125.1 (C, **C8**), 121.5 (CH, **C18**), 121.4 (C, **C2**), 120.8 (CH, **C21**), 120.5 (CH, **C23**), 120.4 (CH, **C16**), 119.7 (CH, **C17**), 118.5 (CH, **C22**), 111.9 (CH, **C19**), 111.5 (CH, **C20**), 109.9 (C, **C6**), 107.5 (C, **C7**), 48.2 (CH_2 , **C5**)

LRMS ES^+ m/z = 314.3 $[M+H]^+$

FT-IR (neat) ν_{max} cm^{-1} 3402, 3204, 1657, 1237, 737

5-Hydroxy-3,4-di(1H-indol-3-yl)-1,5-dihydro-2H-pyrrol-2-one (5.14)



5-Hydroxy-3,4-di(1H-indol-3-yl)-1,5-dihydro-2H-pyrrol-2-one (**5.14**) was obtained as a by-product in the synthesis of **5.15**, as a golden brown solid (5.86 g, 44%).

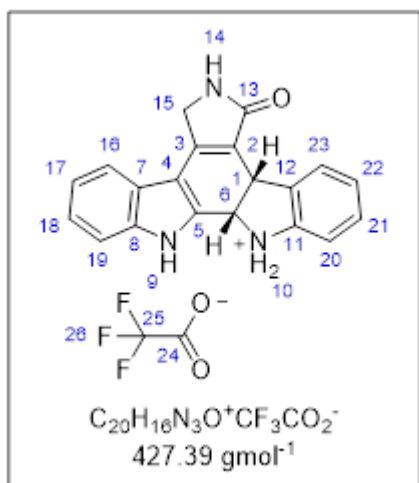
M.P. 250 °C decomposed.

1H NMR (400 MHz, DMSO- d_6 , 298 K) δ (ppm) = 11.38 (d, J = 2.3 Hz, 1H, **10**), 11.25 (d, J = 2.2 Hz, 1H, **13**), 8.49 (d, J = 1.1 Hz, 1H, **4**), 7.49 (d, J = 2.6 Hz, 1H, **12**), 7.45 (d, J = 2.7 Hz, 1H, **11**), 7.37 (d, J = 7.9 Hz, 1H, **20**), 7.34 (d, J = 8.1 Hz, 1H, **19**), 7.17 (d, J = 8.1 Hz, 1H, **16**), 7.04 – 6.93 (m, 3H, **18 + 21 + 23**), 6.71 (dddd, J = 11.6, 7.9, 7.0, 1.0 Hz, 1H, **11**), 6.06 – 5.97 (m, 2H, **5 + OH**)

^{13}C NMR (101 MHz, DMSO- d_6 , 298 K) δ (ppm) = 172.2 (C, **C3**), 146.0 (C, **C1**), 136.1 (C, **C9**), 135.9 (C, **C14**), 127.5 (CH, **C11**), 126.5 (CH, **C12**), 125.7 (C, **C8**), 125.5 (C, **C15**), 121.4 (C, **C2**), 121.2 (CH, **C16**), 121.2 (CH, **C23**), 120.9 (CH, **C18**), 120.8 (CH, **C21**), 119.2 (CH, **C17**), 118.5 (CH, **C22**), 111.5 (CH, **19/20**), 111.4 (CH, **19/20**), 109.4 (C, **C6**), 107.1 (C, **C7**), 79.44 (CH, **C5**)

FT-IR (neat) ν_{max} cm^{-1} 3381, 3251, 1663, 1239, 1045, 738

7-Oxo-6,7,7b,12,12a,13-hexahydro-5H-indolo[2,3-a]pyrrolo[3,4-c]carbazol-12-ium
trifluoroacetate (5.19)



TFA (42 mL) was degassed by bubbling argon and cooled to -10 °C. **5.15** (1.40 g, 4.47 mmol) was then added and the mixture stirred at -10 °C for 5 hours. Deionised water (50 mL) was then added dropwise at -10 °C and a yellow/white precipitate was observed. The mixture was then poured into ice water (100 mL) and the precipitate filtered, washed thoroughly with deionised water (\approx 200 mL) then diethyl ether (50 mL). The solid was triturated with diethyl ether (2 x 100 mL) to yield the title compound as an off white solid (1.00 g, 70%).

M.P. 285 °C decomposed.

¹H NMR (400 MHz, DMSO-*d*₆, 298 K) δ (ppm) = 11.55 (s, 1H, **9**), 7.96 (s, 1H, **14**), 7.50 (d, *J* = 7.7 Hz, 1H, **16**), 7.44 (d, *J* = 8.1 Hz, 1H, **19**), 7.30 (d, *J* = 7.5 Hz, 1H, **23**), 7.12 (td, *J* = 7.1, 1.2 Hz, 1H, **18**), 7.07 (td, *J* = 7.8, 1.2 Hz, 1H, **17**), 6.92 (t, *J* = 7.3 Hz, 1H, **21**), 6.59 (d, *J* = 7.7 Hz, 1H, **20**), 6.55 (td, *J* = 7.4, 0.9 Hz, 1H, **22**), 6.02 (br s, 1H, **10**), 5.48 (d, *J* = 11.5 Hz, 1H, **6**), 4.56 – 4.47 (m, 2H, **1 + 15a**), 4.45 – 4.37 (m, 1H, **15b**)

¹³C NMR (101 MHz, DMSO-*d*₆, 298 K) δ (ppm) = 173.8 (C, **C13**), 149.9 (C, **C11**), 146.4 (C, **C3**), 139.7 (C, **C5**), 136.4 (C, **C8**), 130.4 (C, **C12**), 127.4 (CH, **C21**), 124.9 (CH, **C23**), 123.0 (C, **C2/C7**), 121.8 (C, **C2/C7**), 121.8 (CH, **C18**), 120.5 (CH, **C17**), 118.9 (CH, **C16**), 117.9 (CH, **C22**), 112.1 (CH, **C19**), 108.7 (CH, **C20**), 105.2 (C, **C4**), 56.0 (CH, **C6**), 45.4 (CH₂, **C15**), 39.6 (CH, **C1**)

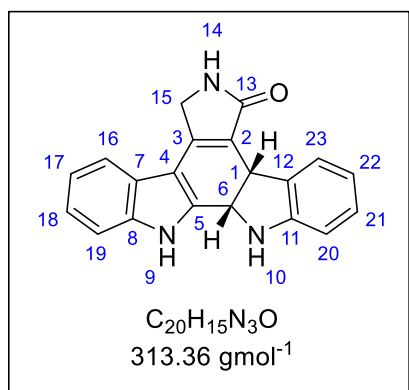
¹⁹F NMR (376 MHz, DMSO-*d*₆, 298 K) δ (ppm) = -73.3 (s, **F26**)

LRMS ES⁺ *m/z* = 314.3 [M-CF₃CO₂]⁺

HRMS ES⁺ *m/z* calcd for C₂₀H₁₆N₃OCF₃CO₂ / [M-CF₃CO₂]⁺ requires 314.1293 found 314.1281

FT-IR (neat) ν_{max} cm⁻¹ 3400, 3273, 1649, 1466, 1228, 729

4b,6,7,12,12b,13-Hexahydro-5H-indolo[2,3-a]pyrrolo[3,4-c]carbazol-5-one (5.16)



5.19 (250 mg, 0.584 mmol) was dissolved in dry DMSO (4 mL). Sodium hydride (60% in mineral oil, 47 mg, 1.17 mmol) was then added and the mixture stirred at room temperature for 5 minutes. Deionised water (50 mL) was then added slowly (first 5 mL added dropwise), and a white precipitate as observed. The precipitate was filtered and washed with diethyl ether (30 mL) to yield the title compound as a white

solid (180 mg, 98%).

M.P. 280 °C decomposed.

1H NMR (400 MHz, DMSO- d_6 , 298 K) δ (ppm) = 11.54 (s, 1H, **9**), 7.95 (s, 1H, **14**), 7.50 (d, J = 7.6 Hz, 1H, **16**), 7.43 (d, J = 7.8 Hz, 1H, **19**), 7.30 (d, J = 7.3 Hz, 1H, **23**), 7.15 – 7.04 (m, 2H, **17 + 18**), 6.91 (tt, J = 7.6, 1.0 Hz, 1H, **21**), 6.58 (d, J = 7.8 Hz, 1H, **20**), 6.55 (td, J = 7.3, 1.0 Hz, 1H, **22**), 6.01 (s, 1H, **10**), 5.47 (dd, J = 11.5, 1.5 Hz, 1H, **6**), 4.56 – 4.46 (m, 2H, **1 + 15a**), 4.45 – 4.34 (m, 1H, **23b**)

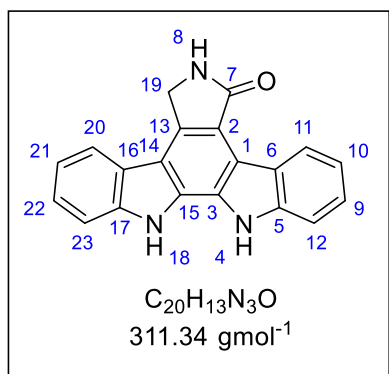
^{13}C NMR (101 MHz, DMSO- d_6 , 298 K) δ (ppm) = 173.7 (C, **C13**), 149.9 (C, **C11**), 146.4 (C, **C3**), 139.6 (C, **C5**), 136.4 (C, **C8**), 130.4 (C, **C12**), 127.4 (CH, **C21**), 124.9 (CH, **C23**), 123.0 (C, **C2/C7**), 121.8 (C, **C2/C7**), 121.8 (CH, **C18**), 120.5 (CH, **C17**), 118.9 (CH, **C16**), 117.8 (CH, **C22**), 112.0 (CH, **C19**), 108.7 (CH, **C20**), 105.2 (C, **C4**), 56.0 (CH, **C6**), 45.3 (CH₂, **C15**), 39.6 (CH, **C1**)

LRMS ES^+ m/z = 314.3 $[M+H]^+$

HRMS ES^+ m/z calcd for $C_{20}H_{15}N_3O$ / $[M+H]^+$ requires 314.1293 found 314.1280

FT-IR (neat) ν_{max} cm^{-1} 3398, 3270, 1648, 1467, 1228, 729

Staurosporine aglycone/K252c (4.04)



5.19 (40.0 mg, 0.0940 mmol) was dissolved in dry DMSO (5 mL) under argon atmosphere. Dry THF (1 mL) and DDQ (42.0 mg, 1.85 mmol) were then added, and the mixture stirred at room temperature for 4 hours. Ethyl acetate (5 mL) was then added to the mixture and the mixture washed with sat. aq. $NaHCO_3$ solution (7 x 5 mL) until the washings were colourless. The organic layer was dried ($MgSO_4$), and the solvent removed under reduced pressure. The resulting solid was purified by

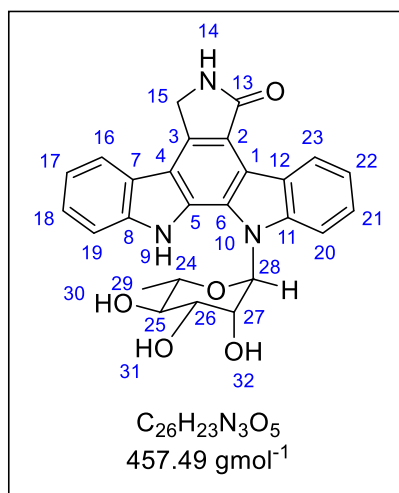
silica gel column chromatography (DCM/MeOH, 99:1 \rightarrow 9:1) affording the title compound as a yellow solid (13.2 mg, 44%).

M.P. 280 °C decomposed (lit 310 °C decomposed)²²⁷

1H NMR (400 MHz, $DMSO-d_6$, 298 K) δ (ppm) = 11.51 (s, 1H, **18**), 11.34 (s, 1H, **4**), 9.26 (d, J = 7.8 Hz, 1H, **11**), 8.51 (s, 1H, **8**), 8.04 (d, J = 7.7 Hz, 1H, **20**), 7.80 (d, J = 8.1 Hz, 1H, **23**), 7.74 (d, J = 8.1 Hz, 1H, **12**), 7.46 (quin, J = 7.3 Hz, 2H, **9** + **22**), 7.30 (t, J = 7.4 Hz, 1H, **21**), 7.25 (t, J = 7.3 Hz, 1H, **10**), 4.98 (s, 2H, **19**)

^{13}C NMR (101 MHz, $DMSO-d_6$, 298 K) δ (ppm) = 172.4 (C, **C7**), 139.2 (C, **C17**), 139.1 (C, **C5**), 132.9 (C, **C13**), 127.9 (C, **C3/C15**), 125.4 (C, **C3/C15**), 125.3 (CH, **C11**), 125.0 (CH, **C9**), 125.0 (CH, **C22**), 122.9 (C, **C6**), 122.6 (C, **C16**), 121.1 (CH, **C20**), 119.9 (CH, **C21**), 119.0 (CH, **C10**), 118.9 (C, **C2**), 115.7 (C, **C1/C6**), 114.2 (C, **C1/C6**), 111.9 (CH, **C23**), 111.4 (CH, **C12**), 45.3 (CH_2 , **C19**)

LRMS ES^+ m/z = 312.3 $[M+H]^+$

K252d (5.17)

5.16 (100 mg, 0.320 mmol) was dissolved in a mixture dry DMSO (5 mL) and dry EtOH (3 mL) under argon atmosphere. The mixture was degassed by bubbling argon for 15 minutes then L-rhamnose (290 mg, 1.60 mmol) and ammonium sulfate (127 mg, 0.960 mmol) added. The mixture was heated to 70 °C and stirred for 8 hours. The mixture was allowed to cool to room temperature and stirred for 16 hours. At this point the mixture was concentrated under reduced pressure to remove EtOH and dry THF (3 mL) added. DDQ (109 mg, 0.480 mmol)

was then added, and the mixture stirred for a further 3 hours at room temperature. Ethyl acetate (10 mL) was then added, and the mixture washed with sat. aq. NaHCO_3 solution (7 x 10 mL) until the washings were colourless then with brine (10 mL) and finally the separated organic layer dried (MgSO_4). Solvent was then removed under reduced pressure and the crude material purified (Biotage Selekt, Ethyl acetate/MeOH/ NEt_3 , 96:0:4 → 80:16:4). This gave the title compound as a 1:1 mixture of anomers (45.4 mg, 31%). The anomers were separated (Biotage Selekt, Hexane/Ethyl acetate/ NEt_3 48:48:4 → Ethyl acetate/MeOH/ NEt_3 , 80:16:4) which afforded K252d as a pale yellow solid.

$$[\alpha]_D^{25} + 41^\circ \text{ (c = 0.11, MeOH) (lit } + 30^\circ, \text{ c = 0.4, MeOH)}^{228}$$

M.P. 240 °C decomposed (lit 240 - 245 °C decomposed)²²⁸

$^1\text{H NMR}$ (500 MHz, $\text{DMSO}-d_6$, 298 K) δ (ppm) = 11.68 (s, 1H, **9**), 9.47 (d, $J = 7.3$ Hz, 1H, **23**), 8.55 (s, 1H, **14**), 8.07 (d, $J = 7.8$ Hz, 1H, **16**), 7.69 (d, $J = 8.6$ Hz, 1H, **20**), 7.60 (d, $J = 8.1$ Hz, 1H, **19**), 7.52 – 7.45 (m, 2H, **18 + 21**), 7.30 (overlapping t, $J = 7.3$ Hz, 2H, **17 + 22**), 6.69 (d, $J = 2.7$ Hz, 1H, **30**), 6.39 (d, $J = 9.4$ Hz, 1H, **28**), 5.40 (d, $J = 3.8$ Hz, 1H, **31**), 5.06 – 4.95 (m, 3H, **15 + 32**), 4.53 – 4.43 (m, 2H, **24 + 27**), 4.17 (d, $J = 3.1$ Hz, 1H, **26**), 4.04 (t, $J = 2.8$ Hz, 1H, **25**), 1.70 (d, $J = 7.2$ Hz, 3H, **29**)

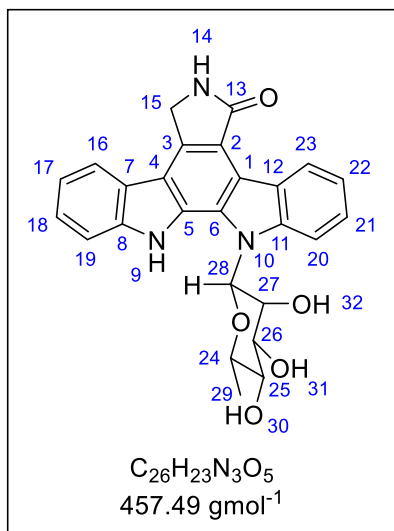
$^{13}\text{C NMR}$ (125 MHz, $\text{DMSO}-d_6$, 298 K) δ (ppm) = 172.3 (C, **C13**), 140.2 (C, **C11**), 139.0 (C, **C8**), 133.9 (C, **C3**), 127.5 (C, **C5**), 125.6 (CH, **C23**), 125.2 (CH, **C21**), 125.1 (CH, **C18**), 124.5 (C, **C6**), 122.3 (C, **C12**), 121.8 (C, **C7**), 121.2 (CH, **C16**), 119.8 (CH, **C17**), 119.3 (CH, **C22**), 118.6 (C, **C2**), 117.5 (C, **C1**), 114.9 (C, **C4**), 111.2 (CH, **C19**), 109.8 (CH, **C20**), 77.2 (CH, **C28**), 76.5 (CH, **C24**), 71.7 (CH, **C26**), 71.5 (CH, **C25**), 66.9 (CH, **C27**), 45.2 (CH_2 , **C15**), 15.35 (CH_3 , **C29**)

LRMS ES⁺ m/z = 458.3 [M+H]⁺

HRMS ES⁺ m/z calcd for C₂₆H₂₃N₃O₅ / [M+H]⁺ requires 458.1716 found 458.1704

FT-IR (neat) ν_{max} cm⁻¹ 3436, 3312, 1647, 1391, 1052, 734

β -K252d (5.18)



β -K252d (**5.18**) was isolated as a white solid.

$[\alpha]_D^{25}$ -50° ($c = 0.08$, MeOH)

M.P. 230 $^\circ C$ decomposed.

1H NMR (500 MHz, DMSO- d_6 , 298 K) δ (ppm) = 11.04 (s, 1H, **9**), 9.50 (d, $J = 7.4$ Hz, 1H, **23**), 8.51 (s, 1H, **14**), 8.05 (d, $J = 7.9$ Hz, 1H, **16**), 7.86 (d, $J = 8.5$ Hz, 1H, **20**), 7.71 (d, $J = 8.1$ Hz, 1H, **19**), 7.52 – 7.44 (m, 2H, **18 + 21**), 7.29 (q, $J = 7.1$ Hz, 2H, **17 + 22**), 6.44 (s, 1H, **28**), 5.63 (d, $J = 4.8$ Hz, 1H, **32**), 5.26 (d, $J = 4.7$ Hz, 1H, **30**), 5.05 (d, $J = 6.0$ Hz, 1H, **31**), 4.97 (s, 2H, **15**), 4.04 (s, 1H, **27**), 3.95 (br s, 1H, **26**), 3.79 (m, 2H, **24 + 25**), 1.46 (d, $J = 5.5$ Hz, 3H, **29**)

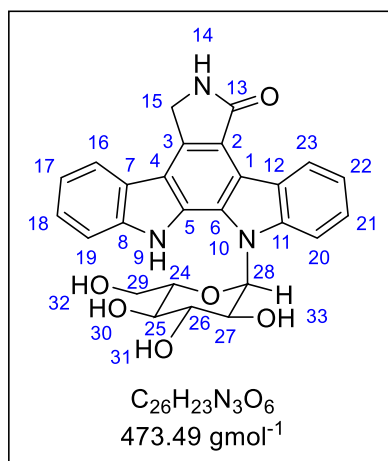
^{13}C NMR (125 MHz, DMSO- d_6 , 298 K) δ (ppm) = 172.3 (C, **C13**), 138.9 (C, **C11**), 138.1 (C, **C8**), 133.8 (C, **C3**), 128.2 (C, **C5**), 126.2 (C, **C6**), 125.7 (CH, **C23**), 125.2 (CH, **C18 + C21**), 122.7 (C, **C12**), 121.9 (C, **C7**), 121.1 (CH, **C16**), 119.6 (CH, **C17**), 119.6 (CH, **C22**), 118.3 (C, **C2**), 117.2 (C, **C1**), 114.7 (C, **C4**), 111.1 (CH, **C19**), 110.4 (CH, **C20**), 84.9 (CH, **C28**), 76.0 (CH, **C25**), 72.8 (CH, **C26**), 72.1 (CH, **C24**), 71.4 (CH, **C27**), 45.1 (CH₂, **C15**), 18.48 (CH₃, **C29**)

LRMS ES^+ $m/z = 458.3$ [$M+H$] $^+$

HRMS ES^+ m/z calcd for $C_{26}H_{23}N_3O_5$ / [$M+H$] $^+$ requires 458.1716 found 458.1701

FT-IR (neat) ν_{max} cm^{-1} 3389, 1654, 1329, 1065, 740

13-((2R,3S,4R,5R,6S)-3,4,5-Trihydroxy-6-(hydroxymethyl)tetrahydro-2H-pyran-2-yl)-6,7,12,13-tetrahydro-5H-indolo[2,3-a]pyrrolo[3,4-c]carbazol-5-one (5.20)



5.16 (100 mg, 0.320 mmol) was dissolved in a mixture dry DMSO (5 mL) and dry EtOH (2 mL) under argon atmosphere. The mixture was degassed by bubbling argon for 15 minutes then D-glucose (288 mg, 1.60 mmol) and ammonium sulfate (127 mg, 0.960 mmol) added. The mixture was heated to 70 °C and stirred for 5 hours. The mixture was allowed to cool to room temperature and stirred for 16 hours then heated to 70 °C for another 3 hours. The mixture was allowed to cool and concentrated under reduced pressure to remove EtOH and dry

THF (2 mL) added. DDQ (109 mg, 0.480 mmol) was then added, and the mixture stirred for a further 3 hours at room temperature. Ethyl acetate (20 mL) was then added, and the mixture washed with sat. aq. NaHCO_3 solution (7 x 15 mL) until the washings were colourless then with brine (10 mL) and finally the separated organic layer dried (MgSO_4). Solvent was then removed under reduced pressure and the crude material purified (Biotage Selekt, Ethyl acetate/MeOH/ NEt_3 , 96:0:4 → 80:16:4). This yielded the title compound as a pale orange solid (58.2 mg, 38%).

$$[\alpha]_D^{25} + 102^\circ \text{ (c = 0.12, MeOH)}$$

M.P. 270 °C decomposed.

$^1\text{H NMR}$ (400 MHz, CD_3OD , 298 K) δ (ppm) = 9.30 (d, J = 7.34 Hz, 1H, **23**), 7.89 (d, J = 7.8 Hz, 1H, **16**), 7.74 (d, J = 8.8 Hz, 1H, **19**), 7.68 (d, J = 8.1 Hz, 1H, **20**), 7.53 – 7.36 (m, 2H, **18** + **21**), 7.31 – 7.20 (m, 2H, **17** + **22**), 6.16 (d, J = 8.8 Hz, 1H, **28**), 4.84 – 4.81 (m, 2H, **15**), 4.36 – 4.21 (m, 2H, **24** + **27**), 4.07 (dd, J = 11.4, 2.6 Hz, 1H, **29a**), 3.99 (dd, J = 9.8, 1.5 Hz, 1H, **29b**), 3.88 (t, J = 9.0 Hz, 1H, **26**), 3.77 (t, J = 9.2 Hz, 1H, **25**)

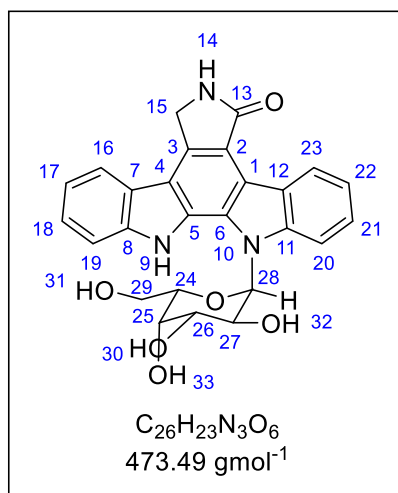
$^{13}\text{C NMR}$ (101 MHz, CD_3OD , 298 K) δ (ppm) = 175.5 (C, **C13**), 142.6 (C, **C11**), 141.6 (C, **C8**), 136.0 (C, **C3**), 129.1 (C, **C5**), 126.8 (CH, **C23**), 126.5 (CH, **C21**), 126.4 (CH, **C18**), 126.2 (C, **C6**), 124.3 (C, **C12**), 124.2 (C, **C12**), 121.7 (C, **C7**), 121.2 (CH, **C16**), 120.8 (CH, **C17**), 120.5 (CH, **C22**), 119.0 (C, **C2**), 117.0 (C, **C1**), 113.0 (C, **C4**), 111.3 (CH, **C19**), 86.5 (CH, **C24**), 78.6 (CH, **C28**), 74.7 (CH, **C25**), 69.3 (CH, **C27**), 60.1 (CH_2 , **C29**), 46.8 (CH_2 , **C15**)

LRMS ES⁺ m/z = 474.4 [M+H]⁺

HRMS ES⁺ m/z calcd for C₂₆H₂₃N₃O₆ / [M+H]⁺ requires 474.1665 found 474.1651

FT-IR (neat) ν_{\max} cm⁻¹ 3311, 1656, 1455, 1246, 1055, 742

13-((2R,3S,4R,5S,6S)-3,4,5-Trihydroxy-6-(hydroxymethyl)tetrahydro-2H-pyran-2-yl)-6,7,12,13-tetrahydro-5H-indolo[2,3-a]pyrrolo[3,4-c]carbazol-5-one (5.21)



5.16 (100 mg, 0.320 mmol) was dissolved in a mixture dry DMSO (5 mL) and dry EtOH (2 mL) under argon atmosphere. The mixture was degassed by bubbling argon for 15 minutes then D-galactose (288 mg, 1.60 mmol) and ammonium sulfate (127 mg, 0.960 mmol) added. The mixture was heated to 70 °C and stirred for 5 hours. The mixture was allowed to cool to room temperature and stirred for 16 hours then heated to 70 °C for another 3 hours. The mixture was allowed to cool and concentrated under reduced pressure to remove EtOH and dry

THF (2 mL) added. DDQ (109 mg, 0.480 mmol) was then added, and the mixture stirred for a further 3 hours at room temperature. Ethyl acetate (20 mL) was then added, and the mixture washed with sat. aq. NaHCO_3 solution (7 x 15 mL) until the washings were colourless then with brine (10 mL) and finally the separated organic layer dried (MgSO_4). Solvent was then removed under reduced pressure and the crude material purified (Biotage Selekt, Ethyl acetate/MeOH/ NEt_3 , 96:0:4 → 80:16:4). This yielded the title compound as a pale yellow solid (60.8 mg, 40%).

$$[\alpha]_D^{25} + 32^\circ \text{ (c = 0.11, MeOH)}$$

M.P. 270 °C decomposed.

$^1\text{H NMR}$ (400 MHz, CD_3OD , 298 K) δ (ppm) = 8.94 (d, J = 8.1 Hz, 1H, **23**), 7.68 – 7.76 (m, 2H), 7.65 (d, J = 8.1 Hz, 1H, **16**), 7.51 – 7.33 (m, 2H, **19** + **20**), 7.29 – 7.17 (m, 2H, **18** + **21**), 7.17 – 7.03 (m, 2H, **17** + **22**), 6.07 (d, J = 9.3 Hz, 1H, **28**), 4.85 (s, 2H, **15**), 4.68 – 4.52 (m, 2H, **24**), 4.38 – 4.23 (m, 2H, **26** + **27**), 4.14 (t, J = 6.1 Hz, 1H, **25**), 4.05 – 3.87 (m, 2H, **29**)

$^{13}\text{C NMR}$ (101 MHz, $\text{DMSO}-d_6$, 298 K) δ (ppm) = 172.3 (C, **C13**), 140.2 (C, **C11**), 139.3 (C, **C8**), 133.9 (C, **C3**), 127.5 (C, **C5**), 125.5 (CH, **C23**), 125.3 (CH, **C21**), 125.0 (CH, **C18**), 124.3 (C, **C6**), 122.2 (C, **C12**), 121.7 (C, **C7**), 121.0 (CH, **C16**), 119.7 (CH, **C17**), 119.3 (CH, **C22**), 118.4 (C, **C2**), 117.4 (C, **C1**), 114.8 (C, **C4**), 111.5 (CH, **C19**), 110.3 (CH, **C20**), 84.8 (CH, **C24**), 78.5 (CH, **C28**), 74.2 (CH, **C25**), 71.3 (CH, **C26**), 69.1 (CH, **C27**), 59.8 (CH_2 , **C29**), 45.6 (CH_2 , **C15**)

LRMS ES⁺ m/z = 474.3 [M+H]⁺

HRMS ES⁺ m/z calcd for C₂₆H₂₃N₃O₆ / [M+H]⁺ requires 474.1665 found 474.1649

FT-IR (neat) ν_{\max} cm⁻¹ 3327, 1654, 1454, 1329, 1078, 744

List of References

1. Ghahremani Honarvar, M.; Latifi, M., Overview of wearable electronics and smart textiles. *J. Textile Inst.* **2017**, *108* (4), 631-652.
2. Mondal, K., Recent Advances in Soft E-Textiles. *Inventions* **2018**, *3* (2), 23.
3. Ruckdashel, R. R.; Khadse, N.; Park, J. H., Smart E-Textiles: Overview of Components and Outlook. *Sensors* **2022**, *22* (16), 6055.
4. Sibinski, M.; Jakubowska, M.; Sloma, M., Flexible Temperature Sensors on Fibers. *Sensors* **2010**, *10* (9), 7934-7946.
5. Vatansever, D.; Siores, E.; Hadimani, R.; Shah, T., Smart woven fabrics in renewable energy generation. In *Advances in modern woven fabrics technology*, 2011; pp 23-38.
6. Bedeloglu, A.; Demir, A.; Bozkurt, Y.; Sariciftci, N. S., A Photovoltaic Fiber Design for Smart Textiles. *Text. Res. J.* **2010**, *80* (11), 1065-1074.
7. Coyle, S.; Lau, K. T.; Moyna, N.; Gorman, D. O.; Diamond, D.; Francesco, F. D.; Costanzo, D.; Salvo, P.; Trivella, M. G.; Rossi, D. E. D.; Taccini, N.; Paradiso, R.; Porchet, J. A.; Ridolfi, A.; Luprano, J.; Chuzel, C.; Lanier, T.; Revol-Cavalier, F.; Schoumacker, S.; Mourier, V.; Chartier, I.; Convert, R.; De-Moncuit, H.; Bini, C., BIOTEX—Biosensing Textiles for Personalised Healthcare Management. *IEEE Trans.* **2010**, *14* (2), 364-370.
8. Brosteaux, D.; Axisa, F.; Gonzalez, M.; Vanfleteren, J., Design and Fabrication of Elastic Interconnections for Stretchable Electronic Circuits. *IEEE Electron Device Lett.* **2007**, *28* (7), 552-554.
9. Dias, T.; Monaragala, R., Development and analysis of novel electroluminescent yarns and fabrics for localized automotive interior illumination. *Text. Res. J.* **2012**, *82* (11), 1164-1176.
10. Janietz, S.; Gruber, B.; Schattauer, S.; Schulze, K., Integration of OLEDs in Textiles. *J. Adv. Sci. Technol. Res* **2013**, *80*, 14-21.
11. Singha, K.; Kumar, J.; Pandit, P., Recent Advancements in Wearable & Smart Textiles: An Overview. *Mater. Today: Proc.* **2019**, *16*, 1518-1523.
12. Hayward, J. *E-Textiles 2019-2029: Technologies, Markets and Players*; IDTechX Research, 2019.
13. Data, P.; Takeda, Y., Recent Advancements in and the Future of Organic Emitters: TADF- and RTP-Active Multifunctional Organic Materials. *Asian J. Chem.* **2019**, *14* (10), 1613-1636.
14. Thejo Kalyani, N.; Dhoble, S. J., Organic light emitting diodes: Energy saving lighting technology—A review. *Renew. Sust. Energ. Rev.* **2012**, *16* (5), 2696-2723.
15. Takahashi, T., Semiconductor Devices. In *Encyclopedia of Condensed Matter Physics*, Bassani, F.; Liedl, G. L.; Wyder, P., Eds. Elsevier: Oxford, 2005; pp 264-273.
16. Townsend, J. S., *A modern approach to quantum mechanics*. McGraw-Hill: New York, 1992.
17. Borden, W. T.; Hoffmann, R.; Stuyver, T.; Chen, B., Dioxygen: What Makes This Triplet Diradical Kinetically Persistent? *Journal of the American Chemical Society* **2017**, *139* (26), 9010-9018.

18. Yersin, H.; Rausch, A. F.; Czerwieniec, R.; Hofbeck, T.; Fischer, T., The triplet state of organo-transition metal compounds. Triplet harvesting and singlet harvesting for efficient OLEDs. *Coord. Chem. Rev.* **2011**, 255 (21), 2622-2652.
19. Baldo, M. A.; O'Brien, D. F.; You, Y.; Shoustikov, A.; Sibley, S.; Thompson, M. E.; Forrest, S. R., Highly efficient phosphorescent emission from organic electroluminescent devices. *Nature* **1998**, 395 (6698), 151-154.
20. Li, T.-Y.; Wu, J.; Wu, Z.-G.; Zheng, Y.-X.; Zuo, J.-L.; Pan, Y., Rational design of phosphorescent iridium(III) complexes for emission color tunability and their applications in OLEDs. *Coord. Chem. Rev.* **2018**, 374, 55-92.
21. Chiang, C.-J.; Kimyonok, A.; Etherington, M. K.; Griffiths, G. C.; Jankus, V.; Turksoy, F.; Monkman, A. P., Ultrahigh Efficiency Fluorescent Single and Bi-Layer Organic Light Emitting Diodes: The Key Role of Triplet Fusion. *Adv. Funct. Mater.* **2013**, 23 (6), 739-746.
22. Parker, C. A.; Bowen, E. J., Sensitized P-type delayed fluorescence. *Proc. R. Soc. A: Math. Phys. Eng. Sci.* **1963**, 276 (1364), 125-135.
23. Dias, F. B.; Penfold, T. J.; Monkman, A. P., Photophysics of thermally activated delayed fluorescence molecules. *Methods Appl. Fluoresc.* **2017**, 5 (1), 012001.
24. Hu, R.; Leung, N. L. C.; Tang, B. Z., AIE macromolecules: syntheses, structures and functionalities. *Chem. Soc. Rev.* **2014**, 43 (13), 4494-4562.
25. Li, Q.; Li, Z., The Strong Light-Emission Materials in the Aggregated State: What Happens from a Single Molecule to the Collective Group. *Adv Sci (Weinh)* **2017**, 4 (7), 1600484.
26. Mei, J.; Leung, N. L. C.; Kwok, R. T. K.; Lam, J. W. Y.; Tang, B. Z., Aggregation-Induced Emission: Together We Shine, United We Soar! *Chem. Rev.* **2015**, 115 (21), 11718-11940.
27. Leung, N. L. C.; Xie, N.; Yuan, W.; Liu, Y.; Wu, Q.; Peng, Q.; Miao, Q.; Lam, J. W. Y.; Tang, B. Z., Restriction of Intramolecular Motions: The General Mechanism behind Aggregation-Induced Emission. *Chem.--Eur. J.* **2014**, 20 (47), 15349-15353.
28. Salehi, A.; Fu, X. Y.; Shin, D. H.; So, F., Recent Advances in OLED Optical Design. *Adv. Funct. Mater.* **2019**, 29 (15).
29. Adachi, C., Third-generation organic electroluminescence materials. *Jpn. J. Appl. Phys.* **2014**, 53 (6).
30. Tang, C. W.; VanSlyke, S. A., Organic electroluminescent diodes. *Appl. Phys. Lett.* **1987**, 51 (12), 913-915.
31. Ma, Y.; Zhang, H.; Shen, J.; Che, C., Electroluminescence from triplet metal—ligand charge-transfer excited state of transition metal complexes. *Synth. Met.* **1998**, 94 (3), 245-248.
32. Endo, A.; Ogasawara, M.; Takahashi, A.; Yokoyama, D.; Kato, Y.; Adachi, C., Thermally Activated Delayed Fluorescence from Sn(4+)–Porphyrin Complexes and Their Application to Organic Light Emitting Diodes — A Novel Mechanism for Electroluminescence. *Adv. Mater.* **2009**, 21 (47), 4802-4806.
33. Fresta, E.; Costa, R. D., Beyond traditional light-emitting electrochemical cells – a review of new device designs and emitters. *J. Mater. Chem. C.* **2017**, 5 (23), 5643-5675.
34. Hu, T.; He, L.; Duan, L.; Qiu, Y., Solid-state light-emitting electrochemical cells based on ionic iridium(III) complexes. *J. Mater. Chem.* **2012**, 22 (10), 4206-4215.

35. Tang, S.; Tan, W.-Y.; Zhu, X.-H.; Edman, L., Small-molecule light-emitting electrochemical cells: evidence for in situ electrochemical doping and functional operation. *Chem. Commun.* **2013**, 49 (43), 4926-4928.
36. Meier, S. B.; Tordera, D.; Pertegás, A.; Roldán-Carmona, C.; Ortí, E.; Bolink, H. J., Light-emitting electrochemical cells: recent progress and future prospects. *Mater. Today* **2014**, 17 (5), 217-223.
37. Kanagaraj, S.; Puthanveedu, A.; Choe, Y., Small Molecules in Light-Emitting Electrochemical Cells: Promising Light-Emitting Materials. *Adv. Funct. Mater.* **2020**, 30 (33), 1907126.
38. Su, H.-C.; Chen, Y.-R.; Wong, K.-T., Recent Progress in White Light-Emitting Electrochemical Cells. *Adv. Funct. Mater.* **2020**, 30 (33), 1906898.
39. Gong, J.-R.; Wan, L.-J.; Lei, S.-B.; Bai, C.-L.; Zhang, X.-H.; Lee, S.-T., Direct Evidence of Molecular Aggregation and Degradation Mechanism of Organic Light-Emitting Diodes under Joule Heating: an STM and Photoluminescence Study. *J. Phys. Chem. B.* **2005**, 109 (5), 1675-1682.
40. Kondakov, D. Y.; Pawlik, T. D.; Nichols, W. F.; Lenhart, W. C., Free-radical pathways in operational degradation of OLEDs. *J. Inf. Disp.* **2008**, 16 (1), 37-46.
41. Kondakov, D. Y., Role of chemical reactions of arylamine hole transport materials in operational degradation of organic light-emitting diodes. *J. Appl. Phys.* **2008**, 104 (8), 084520.
42. Wang, R.; Wang, Y.-L.; Lin, N.; Zhang, R.; Duan, L.; Qiao, J., Effects of ortho-Linkages on the Molecular Stability of Organic Light-Emitting Diode Materials. *Chem. Mater.* **2018**, 30 (24), 8771-8781.
43. Kuhn, H., Classical Aspects of Energy Transfer in Molecular Systems. *J. Chem. Phys.* **1970**, 53 (1), 101-108.
44. Lee, J.; Aizawa, N.; Numata, M.; Adachi, C.; Yasuda, T., Versatile Molecular Functionalization for Inhibiting Concentration Quenching of Thermally Activated Delayed Fluorescence. *Adv. Mater.* **2017**, 29 (4), 1604856.
45. Staroske, W.; Pfeiffer, M.; Leo, K.; Hoffmann, M., Single-Step Triplet-Triplet Annihilation: An Intrinsic Limit for the High Brightness Efficiency of Phosphorescent Organic Light Emitting Diodes. *Phys. Rev. Lett.* **2007**, 98 (19), 197402.
46. Jacquemin, D.; Escudero, D., The short device lifetimes of blue PhOLEDs: insights into the photostability of blue Ir(III) complexes. *Chem. Sci. J.* **2017**, 8 (11), 7844-7850.
47. Kim, H. S.; Park, S.-R.; Suh, M. C., Concentration Quenching Behavior of Thermally Activated Delayed Fluorescence in a Solid Film. *J. Phys. Chem. C.* **2017**, 121 (26), 13986-13997.
48. Liao, C.-T.; Chen, H.-F.; Su, H.-C.; Wong, K.-T., Tailoring balance of carrier mobilities in solid-state light-emitting electrochemical cells by doping a carrier trapper to enhance device efficiencies. *J. Mater. Chem.* **2011**, 21 (44), 17855-17862.
49. Lundberg, P.; Tsuchiya, Y.; Lindh, E. M.; Tang, S.; Adachi, C.; Edman, L., Thermally activated delayed fluorescence with 7% external quantum efficiency from a light-emitting electrochemical cell. *Nat. Commun.* **2019**, 10 (1), 5307.
50. Li, Y.; Liu, J.-Y.; Zhao, Y.-D.; Cao, Y.-C., Recent advancements of high efficient donor-acceptor type blue small molecule applied for OLEDs. *Mater. Today* **2017**, 20 (5), 258-266.

51. Duan, L.; Qiao, J.; Sun, Y.; Qiu, Y., Strategies to Design Bipolar Small Molecules for OLEDs: Donor-Acceptor Structure and Non-Donor-Acceptor Structure. *Adv. Mater.* **2011**, *23* (9), 1137-1144.
52. Skórka, Ł.; Filapek, M.; Zur, L.; Matecki, J. G.; Pisarski, W.; Olejnik, M.; Danikiewicz, W.; Krompiec, S., Highly Phosphorescent Cyclometalated Iridium(III) Complexes for Optoelectronic Applications: Fine Tuning of the Emission Wavelength through Ancillary Ligands. *J. Phys. Chem. C.* **2016**, *120* (13), 7284-7294.
53. Laskar, I. R.; Chen, T.-M., Tuning of Wavelengths: Synthesis and Photophysical Studies of Iridium Complexes and Their Applications in Organic Light Emitting Devices. *Chem. Mater.* **2004**, *16* (1), 111-117.
54. Hundemer, F.; Graf von Reventlow, L.; Leonhardt, C.; Polamo, M.; Nieger, M.; Seifermann, S. M.; Colsmann, A.; Bräse, S., Acceptor Derivatization of the 4CzIPN TADF System: Color Tuning and Introduction of Functional Groups. *ChemistryOpen* **2019**, *8* (12), 1413-1420.
55. Akcelrud, L., Electroluminescent polymers. *Progress in Polymer Science* **2003**, *28* (6), 875-962.
56. Youssef, K.; Li, Y.; O'Keeffe, S.; Li, L.; Pei, Q., Fundamentals of Materials Selection for Light-Emitting Electrochemical Cells. *Adv. Funct. Mater.* **2020**, *30* (33), 1909102.
57. Hill, Z. B.; Rodovsky, D. B.; Leger, J. M.; Bartholomew, G. P., Synthesis and utilization of perylene-based n-type small molecules in light-emitting electrochemical cells. *Chem. Commun.* **2008**, (48), 6594-6596.
58. Lee, S. K.; Zu, Y.; Herrmann, A.; Geerts, Y.; Müllen, K.; Bard, A. J., Electrochemistry, Spectroscopy and Electrogenenerated Chemiluminescence of Perylene, Terrylene, and Quaterylene Diimides in Aprotic Solution. *Journal of the American Chemical Society* **1999**, *121* (14), 3513-3520.
59. Quante, H.; Geerts, Y.; Müllen, K., Synthesis of Soluble Perylenebisamidine Derivatives. Novel Long-Wavelength Absorbing and Fluorescent Dyes. *Chem. Mater.* **1997**, *9* (2), 495-500.
60. Rademacher, A.; Märkle, S.; Langhals, H., Lösliche Perylen-Fluoreszenzfarbstoffe mit hoher Photostabilität. *Chemische Berichte* **1982**, *115* (8), 2927-2934.
61. Kervyn, S.; Fenwick, O.; Di Stasio, F.; Shin, Y. S.; Wouters, J.; Accorsi, G.; Osella, S.; Beljonne, D.; Cacialli, F.; Bonifazi, D., Polymorphism, Fluorescence, and Optoelectronic Properties of a Borazine Derivative. *Chem.--Eur. J.* **2013**, *19* (24), 7771-7779.
62. Sham, I. H. T.; Kwok, C.-C.; Che, C.-M.; Zhu, N., Borazine materials for organic optoelectronic applications. *Chem. Commun.* **2005**, (28), 3547-3549.
63. Subeesh, M. S.; Shanmugasundaram, K.; Sunesh, C. D.; Won, Y. S.; Choe, Y., Utilization of a phenanthroimidazole based fluorophore in light-emitting electrochemical cells. *J. Mater. Chem. C.* **2015**, *3* (18), 4683-4687.
64. Radziszewski, B., Ueber Glyoxalin und seine Homologe. *Berichte der deutschen chemischen Gesellschaft* **1882**, *15* (2), 2706-2708.
65. Weber, M. D.; Adam, M.; Tykwinski, R. R.; Costa, R. D., Controlling the Chromaticity of Small-Molecule Light-Emitting Electrochemical Cells Based on TIPS-Pentacene. *Adv. Funct. Mater.* **2015**, *25* (31), 5066-5074.
66. Weber, M. D.; Wittmann, J. E.; Burger, A.; Malcioğlu, O. B.; Segarra-Martí, J.; Hirsch, A.; Coto, P. B.; Bockstedte, M.; Costa, R. D., From White to Red: Electric-Field Dependent

Chromaticity of Light-Emitting Electrochemical Cells based on Archetypal Porphyrins. *Adv. Funct. Mater.* **2016**, 26 (37), 6737-6750.

67. Weber, K. T.; Karikis, K.; Weber, M. D.; Coto, P. B.; Charisiadis, A.; Charitaki, D.; Charalambidis, G.; Angaridis, P.; Coutsolelos, A. G.; Costa, R. D., Cuning metal core: efficiency/stability dilemma in metallated porphyrin based light-emitting electrochemical cells. *Dalton Transactions* **2016**, 45 (34), 13284-13288.

68. Huo, J.; Zou, W.; Zhang, Y.; Chen, W.; Hu, X.; Deng, Q.; Chen, D., Retracted Article: Facile preparation of bithiazole-based material for inkjet printed light-emitting electrochemical cell. *RSC Adv.* **2019**, 9 (11), 6163-6168.

69. Weber, M. D.; Nikolaou, V.; Wittmann, J. E.; Nikolaou, A.; Angaridis, P. A.; Charalambidis, G.; Stangel, C.; Kahnt, A.; Coutsolelos, A. G.; Costa, R. D., Benefits of using BODIPY-porphyrin dyads for developing deep-red lighting sources. *Chem. Commun.* **2016**, 52 (8), 1602-1605.

70. Fresta, E.; Charisiadis, A.; Cavinato, L. M.; Palandjian, N.; Karikis, K.; Nikolaou, V.; Charalambidis, G.; Coutsolelos, A. G.; Costa, R. D., BODIPY-Pt-Porphyrins Polyads for Efficient Near-Infrared Light-Emitting Electrochemical Cells. *Advanced Photonics Research* **2021**, 2 (7), 2000188.

71. Chen, H.-F.; Liao, C.-T.; Chen, T.-C.; Su, H.-C.; Wong, K.-T.; Guo, T.-F., An ionic terfluorene derivative for saturated deep-blue solid state light-emitting electrochemical cells. *J. Mater. Chem.* **2011**, 21 (12), 4175-4181.

72. Chen, H.-F.; Liao, C.-T.; Su, H.-C.; Yeh, Y.-S.; Wong, K.-T., Highly efficient exciplex emission in solid-state light-emitting electrochemical cells based on mixed ionic hole-transport triarylamine and ionic electron-transport 1,3,5-triazine derivatives. *J. Mater. Chem. C.* **2013**, 1 (31), 4647-4654.

73. Shanmugasundaram, K.; Subeesh, M. S.; Sunesh, C. D.; Chitumalla, R. K.; Jang, J.; Choe, Y., Synthesis and photophysical characterization of an ionic fluorene derivative for blue light-emitting electrochemical cells. *Org. Electron.* **2015**, 24, 297-302.

74. Shanmugasundaram, K.; Subeesh, M. S.; Sunesh, C. D.; Choe, Y., Non-doped deep blue light-emitting electrochemical cells from charged organic small molecules. *RSC Adv.* **2016**, 6 (34), 28912-28918.

75. Wong, M. Y.; Hedley, G. J.; Xie, G.; Kölln, L. S.; Samuel, I. D. W.; Pertegás, A.; Bolink, H. J.; Zysman-Colman, E., Light-Emitting Electrochemical Cells and Solution-Processed Organic Light-Emitting Diodes Using Small Molecule Organic Thermally Activated Delayed Fluorescence Emitters. *Chem. Mater.* **2015**, 27 (19), 6535-6542.

76. Subeesh, M. S.; Shanmugasundaram, K.; Sunesh, C. D.; Nguyen, T. P.; Choe, Y., Phenanthroimidazole Derivative as an Easily Accessible Emitter for Non-Doped Light-Emitting Electrochemical Cells. *J. Phys. Chem. C.* **2015**, 119 (41), 23676-23684.

77. Shanmugasundaram, K.; Subeesh, M. S.; Sunesh, C. D.; Chitumalla, R. K.; Jang, J.; Choe, Y., Green Electroluminescence from Charged Phenothiazine Derivative. *J. Phys. Chem. C.* **2016**, 120 (36), 20247-20253.

78. Shanmugasundaram, K.; Chitumalla, R. K.; Jang, J.; Choe, Y., Phenothiazine based blue emitter for light-emitting electrochemical cells. *New Journal of Chemistry* **2017**, 41 (18), 9668-9673.

79. Wong, M. Y.; La-Placa, M.-G.; Pertegas, A.; Bolink, H. J.; Zysman-Colman, E., Deep-blue thermally activated delayed fluorescence (TADF) emitters for light-emitting electrochemical cells (LEECs). *J. Mater. Chem. C.* **2017**, 5 (7), 1699-1705.

80. Wu, S.; Aonuma, M.; Zhang, Q.; Huang, S.; Nakagawa, T.; Kuwabara, K.; Adachi, C., High-efficiency deep-blue organic light-emitting diodes based on a thermally activated delayed fluorescence emitter. *J. Mater. Chem. C* **2014**, 2 (3), 421-424.
81. Zhang, Q.; Li, J.; Shizu, K.; Huang, S.; Hirata, S.; Miyazaki, H.; Adachi, C., Design of Efficient Thermally Activated Delayed Fluorescence Materials for Pure Blue Organic Light Emitting Diodes. *Journal of the American Chemical Society* **2012**, 134 (36), 14706-14709.
82. Subeesh, M. S.; Nguyen, T. P.; Choe, Y., Blue Light-Emitting Electrochemical Cells Based on Angularly Structured Phenanthroimidazole Derivatives. *J. Phys. Chem. C* **2017**, 121 (27), 14811-14818.
83. Lee, H.; Sunesh, C. D.; Subeesh, M. S.; Choe, Y., Blue-light emitting electrochemical cells comprising pyrene-imidazole derivatives. *Optical Materials* **2018**, 78, 44-51.
84. Jongseong, K.; Shanmugasundaram, K.; Chitumalla, R. K.; Jang, J.; Choe, Y., Phenothiazine derivatives as an easily accessible emitter for green light-emitting electrochemical cells. *Journal of Luminescence* **2018**, 197, 383-388.
85. Shanmugasundaram, K.; John, J. C.; Chitumalla, S.; Jang, J.; Choe, Y., Carbazole based ionic small molecule emitter for non-doped light-emitting electrochemical cells. *Org. Electron.* **2019**, 67, 141-145.
86. Park, J.; Shanmugasundaram, K.; John, J. C.; Choe, Y., Aggregation induced emission small molecules for blue light-emitting electrochemical cells. *Journal of Photochemistry and Photobiology A: Chemistry* **2019**, 374, 10-15.
87. Puthanveedu, A.; Shanmugasundaram, K.; John, J. C.; Choe, Y., Novel Triazine-Based Donor-Acceptor Ionic Green Emitters for Nondoped Light-Emitting Electrochemical Cells. *J. Phys. Chem. C* **2020**, 124 (35), 19273-19281.
88. Bureš, F., Fundamental aspects of property tuning in push-pull molecules. *RSC Adv.* **2014**, 4 (102), 58826-58851.
89. John, J. C.; Shanmugasundaram, K.; Brahmmananda Rao, C. V. S.; Gopakumar, G.; Choe, Y., Novel Thenil-Based Ionic Small Molecules for Nondoped Light-Emitting Electrochemical Cells for Ultrapure Green Emission. *J. Phys. Chem. C* **2021**, 125 (32), 17993-18001.
90. Rec. 2020. https://en.wikipedia.org/wiki/Rec._2020# (accessed September 2024).
91. John, J. C.; Shanmugasundaram, K.; Gopakumar, G.; Choe, Y., Bright and Efficient Red Light-Emitting Electrochemical Cells with Nondoped Organic Small Molecules: A New Approach. *ACS Photonics* **2022**, 9 (1), 203-210.
92. Puthanveedu, A.; Kanagaraj, S.; Bai, A. A.; Chozhidakath Damodharan, S.; Choe, Y., Blue emitting V-shaped acceptor - donor - acceptor novel ionic organic small molecule for non-doped light-emitting electrochemical cells. *Org. Electron.* **2023**, 122, 106881.
93. Tagare, J.; Yadav, R. A. K.; Swayamprabha, S. S.; Dubey, D. K.; Jou, J.-H.; Vaidyanathan, S., Efficient solution-processed deep-blue CIE $y \in (0.05)$ and pure-white CIE $x, y \in (0.34, 0.32)$ organic light-emitting diodes: experimental and theoretical investigation. *J. Mater. Chem. C* **2021**, 9 (14), 4935-4947.
94. Tagare, J.; Dubey, D. K.; Jou, J.-H.; Vaidyanathan, S., Synthesis, photophysical, theoretical and electroluminescence study of triphenylamine-imidazole based blue fluorophores for solution-processed organic light emitting diodes. *Dyes and Pigments* **2019**, 160, 944-956.

95. Tagare, J.; Ulla, H.; Satyanarayan, M.; Vaidyanathan, S., Synthesis, photophysical and electroluminescence studies of new triphenylamine-phenanthroimidazole based materials for organic light emitting diodes. *Journal of Luminescence* **2018**, *194*, 600-609.
96. Ho, C.-C.; Chen, H.-F.; Ho, Y.-C.; Liao, C.-T.; Su, H.-C.; Wong, K.-T., Phosphorescent sensitized fluorescent solid-state near-infrared light-emitting electrochemical cells. *Physical Chemistry Chemical Physics* **2011**, *13* (39), 17729-17736.
97. Ye, J.; He, Y.; Li, K.; Liu, L.; Xi, C.; Liu, Z.; Ma, Y.; Zhang, B.; Bao, Y.; Wang, W.; Cheng, Y.; Niu, L., Achieving Record Efficiency and Luminance for TADF Light-Emitting Electrochemical Cells by Dopant Engineering. *ACS Applied Materials & Interfaces* **2022**, *14* (15), 17698-17708.
98. Zhou, Z.; Chang, Q.; Chen, R.; Jin, P.; Yin, B.; Zhang, C.; Yao, J., Achieving 9% EQE in Light-Emitting Electrochemical Cells via TADF-Sensitized Fluorescent Strategy. *Physical Chemistry Chemical Physics* **2024**.
99. Chan, C.-Y.; Tanaka, M.; Lee, Y.-T.; Wong, Y.-W.; Nakanotani, H.; Hatakeyama, T.; Adachi, C., Stable pure-blue hyperfluorescence organic light-emitting diodes with high-efficiency and narrow emission. *Nature Photonics* **2021**, *15* (3), 203-207.
100. Zhang, D.; Song, X.; Cai, M.; Duan, L., Blocking energy-loss pathways for ideal fluorescent organic light-emitting diodes with thermally activated delayed fluorescent sensitizers. *Adv. Mater.* **2018**, *30* (6), 1705250.
101. Tanaka, M.; Nagata, R.; Nakanotani, H.; Adachi, C., Understanding degradation of organic light-emitting diodes from magnetic field effects. *Communications Materials* **2020**, *1* (1), 18.
102. Stavrou, K.; Franca, L. G.; Danos, A.; Monkman, A. P., Key requirements for ultraefficient sensitization in hyperfluorescence organic light-emitting diodes. *Nature Photonics* **2024**, 1-8.
103. Mindemark, J.; Edman, L., Illuminating the electrolyte in light-emitting electrochemical cells. *J. Mater. Chem. C* **2016**, *4* (3), 420-432.
104. Edman, L.; Moses, D.; Heeger, A. J., Influence of the anion on the kinetics and stability of a light-emitting electrochemical cell. *Synth. Met.* **2003**, *138* (3), 441-446.
105. Jenatsch, S.; Wang, L.; Bulloni, M.; Véron, A. C.; Ruhstaller, B.; Altazin, S.; Nüesch, F.; Hany, R., Doping Evolution and Junction Formation in Stacked Cyanine Dye Light-Emitting Electrochemical Cells. *ACS Applied Materials & Interfaces* **2016**, *8* (10), 6554-6562.
106. Sunesh, C. D.; Chandran, M.; Ok, S.; Choe, Y., Effect of Smaller Counter Anion, BF₄⁻, on the Electroluminescent Properties of Cationic Iridium Complex Based Light-Emitting Electrochemical Cells. *Molecular Crystals and Liquid Crystals* **2013**, *584* (1), 131-138.
107. Geisberger, G.; Gyenge, E. B.; Hinger, D.; Bösigler, P.; Maake, C.; Patzke, G. R., Synthesis, characterization and bioimaging of fluorescent labeled polyoxometalates. *Dalton Transactions* **2013**, 42 (27), 9914-9920.
108. Odobel, F.; Séverac, M.; Pellegrin, Y.; Blart, E.; Fosse, C.; Cannizzo, C.; Mayer, C. R.; Elliott, K. J.; Harriman, A., Coupled Sensitizer-Catalyst Dyads: Electron-Transfer Reactions in a Perylene-Polyoxometalate Conjugate. *Chem.--Eur. J.* **2009**, *15* (13), 3130-3138.
109. Parrot, A.; Bernard, A.; Jacquart, A.; Serapian, S. A.; Bo, C.; Derat, E.; Oms, O.; Dolbecq, A.; Proust, A.; Métivier, R.; Mialane, P.; Izzet, G., Photochromism and Dual-Color Fluorescence in a Polyoxometalate-Benzospiropyran Molecular Switch. *Angewandte Chemie International Edition* **2017**, *56* (17), 4872-4876.

110. Bolle, P.; Benali, T.; Menet, C.; Puget, M.; Faulques, E.; Marrot, J.; Mialane, P.; Dolbecq, A.; Serier-Braut, H.; Oms, O.; Dessapt, R., Tailoring the Solid-State Fluorescence of BODIPY by Supramolecular Assembly with Polyoxometalates. *Inorg. Chem.* **2021**, *60* (16), 12602-12609.
111. Arumugam, S.; Li, Y.; Pearce, J.; Harrowven, D.; Charlton, M.; Tudor, J.; Beeby, S. In *Spray Coated Light Emitting Electrochemical Cells on Standard Polyester Cotton Woven Textiles*, 2020 IEEE International Conference on Flexible and Printable Sensors and Systems (FLEPS), 16-19 Aug. 2020; 2020; pp 1-4.
112. John, J. C.; Shanmugasundaram, K.; Puthanveedu, A.; Rao, C. V. S. B.; Gopakumar, G.; Choe, Y., Introduction of heterocyclic ring to phenanthroimidazole moiety for efficient blue emitting ionic small molecule LECs. *Org. Electron.* **2020**, *87*, 105939.
113. Madhu, M.; Tseng, W.-B.; Chou, Y.-S.; Krishna Kumar, A. S.; Lu, C.-Y.; Chang, P.-L.; Tseng, W.-L., Peptide-Directed Synthesis of Aggregation-Induced Emission Enhancement-Active Gold Nanoclusters for Single- and Two-Photon Imaging of Lysosome and Expressed $\alpha\beta 3$ Integrin Receptors. *Analytical Chemistry* **2024**, *96* (22), 9007-9015.
114. Klein, J.; Kampermann, L.; Mockenhaupt, B.; Behrens, M.; Strunk, J.; Bacher, G., Limitations of the Tauc Plot Method. *Adv. Funct. Mater.* **2023**, *33* (47), 2304523.
115. Aderne, R. E.; Borges, B. G. A. L.; Ávila, H. C.; von Kieseritzky, F.; Hellberg, J.; Koehler, M.; Cremona, M.; Roman, L. S.; Araujo, C. M.; Rocco, M. L. M.; Marchiori, C. F. N., On the energy gap determination of organic optoelectronic materials: the case of porphyrin derivatives. *Materials Advances* **2022**, *3* (3), 1791-1803.
116. Ravelli, D.; Dondi, D.; Fagnoni, M.; Albini, A.; Bagno, A., Predicting the UV spectrum of polyoxometalates by TD-DFT. *J. Comput. Chem.* **2011**, *32* (14), 2983-2987.
117. Black, F. A.; Jacquart, A.; Toupalas, G.; Alves, S.; Proust, A.; Clark, I. P.; Gibson, E. A.; Izzet, G., Rapid photoinduced charge injection into covalent polyoxometalate–bodipy conjugates. *Chem. Sci. J.* **2018**, *9* (25), 5578-5584.
118. López, X.; Carbó, J. J.; Bo, C.; Poblet, J. M., Structure, properties and reactivity of polyoxometalates: a theoretical perspective. *Chem. Soc. Rev.* **2012**, *41* (22), 7537-7571.
119. Kang, J. S.; Hong, T. R.; Kim, H. J.; Son, Y. H.; Lampande, R.; Kang, B. Y.; Lee, C.; Bin, J.-K.; Lee, B. S.; Yang, J. H.; Kim, J.; Park, S.; Cho, M. J.; Kwon, J. H.; Choi, D. H., High-performance bipolar host materials for blue TADF devices with excellent external quantum efficiencies. *J. Mater. Chem. C.* **2016**, *4* (20), 4512-4520.
120. Li, L.; Han, J.; Nguyen, B.; Burgess, K., Syntheses and Spectral Properties of Functionalized, Water-Soluble BODIPY Derivatives. *J. Org. Chem.* **2008**, *73* (5), 1963-1970.
121. Niu, S.-L.; Massif, C.; Ulrich, G.; Renard, P.-Y.; Romieu, A.; Ziessel, R., Water-Soluble Red-Emitting Distyryl-Borondipyrromethene (BODIPY) Dyes for Biolabeling. *Chem.--Eur. J.* **2012**, *18* (23), 7229-7242.
122. Bacalum, M.; Wang, L.; Boodts, S.; Yuan, P.; Leen, V.; Smisdom, N.; Fron, E.; Knippenberg, S.; Fabre, G.; Trouillas, P.; Beljonne, D.; Dehaen, W.; Boens, N.; Ameloot, M., A Blue-Light-Emitting BODIPY Probe for Lipid Membranes. *Langmuir* **2016**, *32* (14), 3495-3505.
123. Rumyantsev, E. V.; Alyoshin, S. N.; Marfin, Y. S., Kinetic study of Bodipy resistance to acids and alkalis: Stability ranges in aqueous and non-aqueous solutions. *Inorganica Chimica Acta* **2013**, *408*, 181-185.
124. Dagar, M.; Corr, M.; Cook, T. R.; McKone, J. R.; Matson, E. M., Solvent mixtures for improved electron transfer kinetics of titanium-doped polyoxovanadate-alkoxide clusters. *Journal of Materials Chemistry A* **2023**, *11* (25), 13729-13741.

125. Dagar, M.; Dissanyake, D. M. M. M.; Kesler, D. N.; Corr, M.; McPherson, J. D.; Brennessel, W. W.; McKone, J. R.; Matson, E. M., Improved solubility of titanium-doped polyoxovanadate charge carriers for symmetric non-aqueous redox flow batteries. *Dalton Transactions* **2024**, 53 (1), 93-104.
126. Dagar, M.; Brennessel, W. W.; Matson, E. M., Potassium supporting electrolyte enhances stability of Ti-substituted polyoxovanadates for nonaqueous redox flow batteries. *Journal of Materials Chemistry A* **2024**, 12 (3), 1517-1529.
127. Lundberg, P.; Lindh, E. M.; Tang, S.; Edman, L., Toward Efficient and Metal-Free Emissive Devices: A Solution-Processed Host-Guest Light-Emitting Electrochemical Cell Featuring Thermally Activated Delayed Fluorescence. *ACS Applied Materials & Interfaces* **2017**, 9 (34), 28810-28816.
128. Komatsu, R.; Sasabe, H.; Inomata, S.; Pu, Y.-J.; Kido, J., High efficiency solution processed OLEDs using a thermally activated delayed fluorescence emitter. *Synth. Met.* **2015**, 202, 165-168.
129. Seino, Y.; Inomata, S.; Sasabe, H.; Pu, Y.-J.; Kido, J., High-Performance Green OLEDs Using Thermally Activated Delayed Fluorescence with a Power Efficiency of over 100 lm W⁻¹. *Adv. Mater.* **2016**, 28 (13), 2638-2643.
130. Sun, J. W.; Lee, J.-H.; Moon, C.-K.; Kim, K.-H.; Shin, H.; Kim, J.-J., A Fluorescent Organic Light-Emitting Diode with 30% External Quantum Efficiency. *Adv. Mater.* **2014**, 26 (32), 5684-5688.
131. Wang, S.; Zhang, Y.; Chen, W.; Wei, J.; Liu, Y.; Wang, Y., Achieving high power efficiency and low roll-off OLEDs based on energy transfer from thermally activated delayed excitons to fluorescent dopants. *Chem. Commun.* **2015**, 51 (60), 11972-11975.
132. Uoyama, H.; Goushi, K.; Shizu, K.; Nomura, H.; Adachi, C., Highly efficient organic light-emitting diodes from delayed fluorescence. *Nature* **2012**, 492 (7428), 234-238.
133. Feng, H.-T.; Zeng, J.; Yin, P.-A.; Wang, X.-D.; Peng, Q.; Zhao, Z.; Lam, J. W. Y.; Tang, B. Z., Tuning molecular emission of organic emitters from fluorescence to phosphorescence through push-pull electronic effects. *Nat. Commun.* **2020**, 11 (1), 2617.
134. Qiao, S.; Huang, W.; Wei, H.; Wang, T.; Yang, R., Fine tailoring the steric configuration of initial building blocks to construct ultramicroporous polycarbazole networks with high CO₂ uptake and selectivity of CO₂ over N₂. *Polymer* **2015**, 70, 52-58.
135. Rodionov, P. P.; Furin, G. G., Kinetics of nucleophilic substitution reactions of polyfluoroaromatic compounds. *Journal of Fluorine Chemistry* **1990**, 47 (3), 361-434.
136. Steel, P. G., Chapter 3 - Halogenobenzenes. In *Second Supplements to the 2nd Edition of Rodd's Chemistry of Carbon Compounds*, Sainsbury, M., Ed. Elsevier: Amsterdam, 1991; pp 178-224.
137. Jarman, M.; McCague, R., Heptafluoro-p-tolyl and tetrafluoro-4-pyridyl as novel and selective protecting groups for phenolic and alcoholic functions: synthesis and cleavage of perfluoroaryl ethers of steroids. *Journal of the Chemical Society, Chemical Communications* **1984**, (2), 125-127.
138. Levacher, V.; Boussad, N.; Dupas, G.; Bourguignon, J.; Quéguiner, G., Synthesis of annelated NADH models in Benzothieno[2,3-b]pyridine and Pyridol[2,3-b]indole Series. *Tetrahedron* **1992**, 48 (5), 831-840.

139. Usui, S.; Hashimoto, Y.; Morey, J. V.; Wheatley, A. E. H.; Uchiyama, M., Direct ortho Cupration: A New Route to Regioselectively Functionalized Aromatics. *Journal of the American Chemical Society* **2007**, 129 (49), 15102-15103.
140. Krizan, T. D.; Martin, J., In situ trapping of ortho lithiated benzenes containing electrophilic directing groups. *Journal of the American Chemical Society* **1983**, 105 (19), 6155-6157.
141. Omura, S.; Iwai, Y.; Hirano, A.; Nakagawa, A.; Awaya, J.; Tsuchiya, H.; Takahashi, Y.; Asuma, R., A new alkaloid AM-2282 of Streptomyces origin taxonomy, fermentation, isolation and preliminary characterization. *The Journal of Antibiotics* **1977**, 30 (4), 275-282.
142. Omura, S.; Iwai, Y.; Hirano, A. In *Japan Kokai* 78 73, 501, Chem. Abstr, 1978; p 178086b.
143. Funato, N.; Takayanagi, H.; Konda, Y.; Toda, Y.; Harigaya, Y.; Iwai, Y.; Ōmura, S., Absolute Configuration of Staurosporine By X-Ray Analysis. *Tetrahedron Lett.* **1994**, 35 (8), 1251-1254.
144. Tamaoki, T.; Nomoto, H.; Takahashi, I.; Kato, Y.; Morimoto, M.; Tomita, F., Staurosporine, a potent inhibitor of phospholipidCa⁺⁺dependent protein kinase. *Biochemical and Biophysical Research Communications* **1986**, 135 (2), 397-402.
145. Tamaoki, T.; Nakano, H., Potent and Specific Inhibitors of Protein Kinase C of Microbial Origin. *Bio/Technology* **1990**, 8 (8), 732-735.
146. Omura, S.; Yasuharu, S.; Yuzuru, I.; Hideo, T., Staurosporine, a Potentially Important Gift from a Microorganism, The Journal of Antibiotics. *The Journal of Antibiotics* **1995**, 48 (7), 535-548.
147. Nakano, H.; Ōmura, S., Chemical biology of natural indolocarbazole products: 30 years since the discovery of staurosporine. *The Journal of Antibiotics* **2009**, 62 (1), 17-26.
148. Knölker, H.-J.; Reddy, K. R., Isolation and Synthesis of Biologically Active Carbazole Alkaloids. *Chem. Rev.* **2002**, 102 (11), 4303-4428.
149. Bradshaw, D.; Hill, C. H.; Nixon, J. S.; Wilkinson, S. E., Therapeutic potential of protein kinase C inhibitors. *Agents and Actions* **1993**, 38 (1), 135-147.
150. Ōmura, S.; Asami, Y.; Crump, A., Staurosporine: new lease of life for parent compound of today's novel and highly successful anti-cancer drugs. *The Journal of Antibiotics* **2018**, 71 (8), 688-701.
151. Chae, H.-J.; Kang, J.-S.; Byun, J.-O.; Han, K.-S.; Kim, D.-U.; Oh, S.-M.; Kim, H.-M.; Chae, S.-W.; Kim, H.-R., Molecular mechanism of staurosporine-induced apoptosis in osteoblasts. *Pharmacological Research* **2000**, 42 (4), 373-381.
152. Stepczynska, A.; Lauber, K.; Engels, I. H.; Janssen, O.; Kabelitz, D.; Wesselborg, S.; Schulze-Osthoff, K., Staurosporine and conventional anticancer drugs induce overlapping, yet distinct pathways of apoptosis and caspase activation. *Oncogene* **2001**, 20 (10), 1193-1202.
153. Nakano, H.; Kobayashi, E.; Takahashi, I.; Tamaoki, T.; Kuzuu, Y.; Iba, H., Staurosporine Inhibits Tyrosine-Specific Protein Kinase Activity of Rous Sarcoma Virus Transforming Protein. *The Journal of Antibiotics* **1987**, 40 (5), 706-708.
154. Cohen, P., Protein kinases — the major drug targets of the twenty-first century? *Nature Reviews Drug Discovery* **2002**, 1 (4), 309-315.
155. Hantschel, O., Unexpected Off-Targets and Paradoxical Pathway Activation by Kinase Inhibitors. *ACS Chemical Biology* **2015**, 10 (1), 234-245.

156. Rix, U.; Hantschel, O.; Dürnberger, G.; Remsing Rix, L. L.; Planyavsky, M.; Fernbach, N. V.; Kaupe, I.; Bennett, K. L.; Valent, P.; Colinge, J.; Köcher, T.; Superti-Furga, G., Chemical proteomic profiles of the BCR-ABL inhibitors imatinib, nilotinib, and dasatinib reveal novel kinase and nonkinase targets. *Blood* **2007**, *110* (12), 4055-4063.
157. Druker, B. J.; Talpaz, M.; Resta, D. J.; Peng, B.; Buchdunger, E.; Ford, J. M.; Lydon, N. B.; Kantarjian, H.; Capdeville, R.; Ohno-Jones, S.; Sawyers, C. L., Efficacy and Safety of a Specific Inhibitor of the BCR-ABL Tyrosine Kinase in Chronic Myeloid Leukemia. *New England Journal of Medicine* **2001**, *344* (14), 1031-1037.
158. Fabbro, D.; Ruetz, S.; Bodis, S.; Pruschy, M.; Csermak, K.; Man, A.; Campochiaro, P.; Wood, J.; O'Reilly, T.; Meyer, T., PKC412 - a protein kinase inhibitor with a broad therapeutic potential. *Anti-Cancer Drug Design* **2000**, *15* (1), 17-28.
159. Weisberg, E.; Boulton, C.; Kelly, L. M.; Manley, P.; Fabbro, D.; Meyer, T.; Gilliland, D. G.; Griffin, J. D., Inhibition of mutant FLT3 receptors in leukemia cells by the small molecule tyrosine kinase inhibitor PKC412. *Cancer Cell* **2002**, *1* (5), 433-43.
160. Virchis, A.; Ganeshaguru, K.; Hart, S.; Jones, D.; Fletcher, L.; Wright, F.; Wickremasinghe, R.; Man, A.; Csermak, K.; Meyer, T.; Fabbro, D.; Champain, K.; Yap, A.; Prentice, H. G.; Mehta, A., A novel treatment approach for low grade lymphoproliferative disorders using PKC412 (CGP41251), an inhibitor of protein kinase C. *Hematol J* **2002**, *3* (3), 131-136.
161. Hatzimichael, E.; Georgiou, G.; Benetatos, L.; Briasoulis, E., Gene mutations and molecularly targeted therapies in acute myeloid leukemia. *Am J Blood Res* **2013**, *3* (1), 29-51.
162. Clark, A. M.; Hufford, C. D., Chapter 2 Antifungal Alkaloids. In *The Alkaloids: Chemistry and Pharmacology*, Cordell, G. A., Ed. Academic Press: 1992; Vol. 42, pp 117-150.
163. Perfect, J. R., The antifungal pipeline: a reality check. *Nature Reviews Drug Discovery* **2017**, *16* (9), 603-616.
164. Mojicevic, M.; D'Agostino, P. M.; Pavic, A.; Vojnovic, S.; Senthamaraikannan, R.; Vasiljevic, B.; Gulder, T. A. M.; Nikodinovic-Runic, J., Streptomyces sp. BV410 isolate from chamomile rhizosphere soil efficiently produces staurosporine with antifungal and antiangiogenic properties. *MicrobiologyOpen* **2020**, *9* (3), e986.
165. McCarthy, M. W.; Walsh, T. J., Drug development challenges and strategies to address emerging and resistant fungal pathogens. *Expert Review of Anti-infective Therapy* **2017**, *15* (6), 577-584.
166. Baxter, B. K.; DiDone, L.; Ogu, D.; Schor, S.; Krysan, D. J., Identification, in Vitro Activity and Mode of Action of Phosphoinositide-Dependent-1 Kinase Inhibitors as Antifungal Molecules. *ACS Chemical Biology* **2011**, *6* (5), 502-510.
167. Xie, J. L.; O'Meara, T. R.; Polvi, E. J.; Robbins, N.; Cowen, L. E., Staurosporine Induces Filamentation in the Human Fungal Pathogen *Candida albicans* via Signaling through Cyr1 and Protein Kinase A. *mSphere* **2017**, *2* (2), 10.1128/msphere.00056-17.
168. LaFayette, S. L.; Collins, C.; Zaas, A. K.; Schell, W. A.; Betancourt-Quiroz, M.; Gunatilaka, A. A. L.; Perfect, J. R.; Cowen, L. E., PKC Signaling Regulates Drug Resistance of the Fungal Pathogen *Candida albicans* via Circuitry Comprised of Mkc1, Calcineurin, and Hsp90. *PLOS Pathogens* **2010**, *6* (8), e1001069.
169. Xu, L.; Liu, R.; Fang, J.; Zhang, N.; Pu, F.; Lei, Z.; Ding, W.; Jiang, Y., Cytotoxic and Antifungal Staurosporine Derivatives from Marine-Derived Actinomycete *Streptomyces* sp. ZS-A121. *Chemistry & Biodiversity* **2024**, *21* (2), e202301712.

170. Sarstedt, B.; Winterfeldt, E., Reactions with indole derivatives, XLVIII. *Heterocycles* **1983**, *20*, 469.
171. Harris, W.; Hill, C. H.; Keech, E.; Malsher, P., Oxidative cyclisations with palladium acetate. A short synthesis of staurosporine aglycone. *Tetrahedron Lett.* **1993**, *34* (51), 8361-8364.
172. Steglich, W.; Steffan, B.; Kopanski, L.; Eckhardt, G., Indole Pigments from the Fruiting Bodies of the Slime Mold *Arcyria denudata*. *Angewandte Chemie International Edition in English* **1980**, *19* (6), 459-460.
173. Brenner, M.; Rexhausen, H.; Steffan, B.; Steglich, W., Synthesis of arcylarubin b and related bisindolylmaleimides. *Tetrahedron* **1988**, *44* (10), 2887-2892.
174. Joyce, R. P.; Gainor, J. A.; Weinreb, S. M., Synthesis of the aromatic and monosaccharide moieties of staurosporine. *J. Org. Chem.* **1987**, *52* (7), 1177-1185.
175. Faul, M. M.; Sullivan, K. A.; Winneroski, L. L., A General Approach to the Synthesis of Bisindolylmaleimides: Synthesis of Staurosporine Aglycone. *Synthesis* **1995**, *1995* (12), 1511-1516.
176. Faul, M. M.; Winneroski, L. L.; Krumrich, C. A., A new, efficient method for the synthesis of bisindolylmaleimides. *Journal of organic chemistry* **1998**, *63*, 6053-6058.
177. Singh, S.; Samineni, R.; Pabbaraja, S.; Mehta, G., A General Carbazole Synthesis via Stitching of Indole-Ynones with Nitromethanes: Application to Total Synthesis of Carbazomycin A, Calothrixin B, and Staurosporinone. *Organic Letters* **2019**, *21* (9), 3372-3376.
178. Chambers, G. E.; Sayan, A. E.; Brown, R. C. D., The synthesis of biologically active indolocarbazole natural products. *Natural Product Reports* **2021**, *38* (10), 1794-1820.
179. Link, J.; Raghavan, S.; Danishefsky, S. J., First total synthesis of staurosporine and ent-staurosporine. *Journal of the American Chemical Society* **1995**, *117* (1), 552-553.
180. Link, J. T.; Raghavan, S.; Gallant, M.; Danishefsky, S. J.; Chou, T. C.; Ballas, L. M., Staurosporine and ent-Staurosporine: The First Total Syntheses, Prospects for a Regioselective Approach, and Activity Profiles¹. *Journal of the American Chemical Society* **1996**, *118* (12), 2825-2842.
181. Wood, J. L.; Stoltz, B. M.; Dietrich, H.-J., Total Synthesis of (+)- and (-)-K252a. *Journal of the American Chemical Society* **1995**, *117* (41), 10413-10414.
182. Wood, J. L.; Stoltz, B. M.; Goodman, S. N.; Onwueme, K., Design and Implementation of an Efficient Synthetic Approach to Pyranosylated Indolocarbazoles: Total Synthesis of (+)-RK286c, (+)-MLR-52, (+)-Staurosporine, and (-)-TAN-1030a. *Journal of the American Chemical Society* **1997**, *119* (41), 9652-9661.
183. Wood, J. L.; Stoltz, B. M.; Goodman, S. N., Total Synthesis of (+)-RK-286c, (+)-MLR-52, (+)-Staurosporine, and (+)-K252a. *Journal of the American Chemical Society* **1996**, *118* (43), 10656-10657.
184. Seo, K.; Jang, S. H.; Rhee, Y. H., Sequential Metal Catalysis towards 7-Oxostaurosporine and Its Non-Natural Septanose Analogue. *Angewandte Chemie International Edition* **2022**, *61* (3), e202112524.
185. Jang, S. H.; Kim, H. W.; Jeong, W.; Moon, D.; Rhee, Y. H., Palladium-Catalyzed Asymmetric Nitrogen-Selective Addition Reaction of Indoles to Alkoxyallenes. *Organic Letters* **2018**, *20* (4), 1248-1251.

186. Seo, K.; Rhee, Y. H., Ruthenium-Catalyzed Regioselective Olefin Migration of Dihydropyran Acetals: A De Novo Strategy toward β -2,6-Dideoxypyranoglycosides. *Organic Letters* **2020**, 22 (6), 2178-2181.
187. Seo, K.; Kim, Y. j.; Rhee, Y. H., Ru-Catalyzed Chemoselective Olefin Migration Reaction of Cyclic Allylic Acetals to Enol Acetals. *Organic Letters* **2018**, 20 (4), 979-982.
188. Sakander, N.; Hussain, F.; Ahmed, Q. N., An account on pyranosylated and furanosylated indolocarbazole natural products. *Tetrahedron* **2024**, 162, 134116.
189. Chisholm, J. D.; Van Vranken, D. L., Regiocontrolled Synthesis of the Antitumor Antibiotic AT2433-A1. *J. Org. Chem.* **2000**, 65 (22), 7541-7553.
190. Zhang, G.; Shen, J.; Cheng, H.; Zhu, L.; Fang, L.; Luo, S.; Muller, M. T.; Lee, G. E.; Wei, L.; Du, Y.; Sun, D.; Wang, P. G., Syntheses and Biological Activities of Rebeccamycin Analogues with Uncommon Sugars. *Journal of Medicinal Chemistry* **2005**, 48 (7), 2600-2611.
191. Moreau, P.; Anizon, F.; Sancelme, M.; Prudhomme, M.; Bailly, C.; Severe, D.; Riou, J.-F.; Fabbro, D.; Meyer, T.; Aubertin, A.-M., Syntheses and Biological Activities of Rebeccamycin Analogues. Introduction of a Halogenoacetyl Substituent. *Journal of Medicinal Chemistry* **1999**, 42 (4), 584-592.
192. Kaneko, T.; Wong, H.; Okamoto, K. T.; Clardy, J., Two synthetic approaches to rebeccamycin. *Tetrahedron Lett.* **1985**, 26 (34), 4015-4018.
193. Gallant, M.; Link, J. T.; Danishefsky, S. J., A stereoselective synthesis of indole- β -N-glycosides: an application to the synthesis of rebeccamycin. *J. Org. Chem.* **1993**, 58 (2), 343-349.
194. Yoshihisa, K.; Teppei, F.; Tohru, F., Stereocontrolled Total Synthesis of (+)-K252a. *Journal of the American Chemical Society* **1999**, 121 (27), 6501-6502.
195. Chisholm, J. D.; Van Vranken, D. L., Glycosylation of 2,2'-Indolyllindolines. *J. Org. Chem.* **1995**, 60 (21), 6672-6673.
196. Faul, M. M.; Sullivan, K. A.; Grutsch, J. L.; Winneroski, L. L.; Shih, C.; Sanchez-Martinez, C.; Cooper, J. T., Synthesis of indolo[2,3-a]carbazole glycoside analogs of rebeccamycin: inhibitors of cyclin D1-CDK4. *Tetrahedron Lett.* **2004**, 45 (5), 1095-1098.
197. Chambers, G. E. The Total Synthesis of Indolocarbazole Natural Products and towards the Synthesis of (+)-Sparteine. University of Southampton, 2023.
198. Pichon, M. M.; Hazelard, D.; Compain, P., Metal-Free Deoxygenation of α -Hydroxy Carbonyl Compounds and Beyond. *European Journal of Organic Chemistry* **2019**, 2019 (37), 6320-6332.
199. Habib, O. M. A.; Zhao-Karger, Z.; Abdelhamid, I. A.; Wartchow, R.; Butenschön, H., Phthalimide Tricarbonylchromium Complexes: Synthesis, Characterization, Nucleophilic Addition, and Unanticipated syn Adduct Formation upon Addition of Propynyllithium. *European Journal of Organic Chemistry* **2010**, 2010 (31), 6072-6083.
200. Szcześniak, P.; Stecko, S.; Maziarz, E.; Staszewska-Krajewska, O.; Furman, B., Synthesis of Polyhydroxylated Quinolizidine and Indolizidine Scaffolds from Sugar-Derived Lactams via a One-Pot Reduction/Mannich/Michael Sequence. *J. Org. Chem.* **2014**, 79 (21), 10487-10503.
201. Szcześniak, P.; Stecko, S.; Staszewska-Krajewska, O.; Furman, B., Sugar-derived cyclic imines: one-pot synthesis and direct functionalization. *Tetrahedron* **2014**, 70 (10), 1880-1888.

202. Ding, G.; Li, C.; Shen, Y.; Lu, B.; Zhang, Z.; Xie, X., Potassium Hydroxide-Catalyzed Chemoselective Reduction of Cyclic Imides with Hydrosilanes: Synthesis of ω -Hydroxylactams and Lactams. *Advanced Synthesis & Catalysis* **2016**, 358 (8), 1241-1250.
203. Ohkubo, M.; Nishimura, T.; Jona, H.; Honma, T.; Ito, S.; Morishima, H., Synthesis of Dissymmetric Indolocarbazole Glycosides Using the Mitsunobu Reaction at the Glycosylation Step. *Tetrahedron* **1997**, 53 (17), 5937-5950.
204. Mahmoodi, N. O.; Rajabi, A.; Nyaki, H. Y.; Nahzomi, H. T., Synthesis, Characterization, Molecular Docking, and Investigation of Antibacterial Properties of New Derivatives of 1-H-Phenanthro [9,10-d] Imidazole. *Chemistry & Biodiversity* **2024**, 21 (6), e202400325.
205. Górski, K.; Mech-Piskorz, J.; Leśniewska, B.; Pietraszkiewicz, O.; Pietraszkiewicz, M., Toward Soluble 5,10-Diheterotruxenes: Synthesis and Reactivity of 5,10-Dioxatruxenes, 5,10-Dithiatruxenes, and 5,10-Diazatruxenes. *J. Org. Chem.* **2020**, 85 (7), 4672-4681.
206. Minkkilä, A.; Saario, S. M.; Käsänen, H.; Leppänen, J.; Poso, A.; Nevalainen, T., Discovery of Boronic Acids as Novel and Potent Inhibitors of Fatty Acid Amide Hydrolase. *Journal of Medicinal Chemistry* **2008**, 51 (22), 7057-7060.
207. Tang, X.; Shan, T.; Bai, Q.; Ma, H.; He, X.; Lu, P., Efficient Deep-Blue Electroluminescence Based on Phenanthroimidazole-Dibenzothiophene Derivatives with Different Oxidation States of the Sulfur Atom. *Asian J. Chem.* **2017**, 12 (5), 552-560.
208. Sperátová, M.; Jedyrka, J.; Pytela, O.; Kityk, I. V.; Reshak, A. H.; Bureš, F.; Klikar, M., Novel dibenzothiophene chromophores with peripheral barbituric acceptors. *Tetrahedron* **2019**, 75 (34), 130459.
209. Gilman, H.; Cook, T. H.; Hogg, J. A.; Swiss, J.; Johnson, R. G., Some 1,2-, 2,3- and 3,4-Disubstituted Dibenzofurans. *Journal of the American Chemical Society* **1954**, 76 (22), 5783-5786.
210. Meng, G.; Liu, C.; Qin, S.; Dong, M.; Wei, X.; Zheng, M.; Qin, L.; Wang, H.; He, X.; Zhang, Z., An improved synthesis of sunitinib malate via a solvent-free decarboxylation process. *Research on Chemical Intermediates* **2015**, 41 (11), 8941-8954.
211. He, Y.; Lin, M.; Li, Z.; Liang, X.; Li, G.; Antilla, J. C., Direct synthesis of chiral 1, 2, 3, 4-tetrahydropyrrolo [1, 2-a] pyrazines via a catalytic asymmetric intramolecular aza-Friedel-Crafts reaction. *Organic Letters* **2011**, 13 (17), 4490-4493.
212. Wang, J.-L.; Zhang, L.; Gao, L.-X.; Chen, J.-L.; Zhou, T.; Liu, Y.; Jiang, F.-L., A bright, red-emitting water-soluble BODIPY fluorophore as an alternative to the commercial Mito Tracker Red for high-resolution mitochondrial imaging. *Journal of Materials Chemistry B* **2021**, 9 (41), 8639-8645.
213. Gagandeep; Kumar, P.; Kandi, S. K.; Mukhopadhyay, K.; Rawat, D. S., Synthesis of novel monocarbonyl curcuminoids, evaluation of their efficacy against MRSA, including ex vivo infection model and their mechanistic studies. *European Journal of Medicinal Chemistry* **2020**, 195, 112276.
214. Durantini, E. N.; Silber, J. J., Synthesis of 5-(4-Acetamidophenyl)-10,15,20-tris(4-Substituted Phenyl) Porphyrins using Dipyrromethanes. *Synthetic Communications* **1999**, 29 (19), 3353-3368.
215. Xie, W.-J.; Chen, J.-M.; Yang, Z.-W.; He, L.-N., Cobalt macrocyclic complex-catalyzed selective electroreduction of CO₂ to CO. *Green Chemistry* **2023**, 25 (24), 10366-10371.

216. Siwawannapong, K.; Nemeth, A. M.; Melander, R. J.; Rong, J.; Davis, J. R.; Taniguchi, M.; Carpenter, M. E.; Lindsey, J. S.; Melander, C., Simple Dipyrin Analogues of Prodigiosin for Use as Colistin Adjuvants. *ChemMedChem* **2022**, *17* (16), e202200286.
217. Steingruber, H. S.; Mendioroz, P.; Volpe, M. A.; Gerbino, D. C., Convenient One-Pot Synthesis of 9H-Carbazoles by Microwave Irradiation Employing a Green Palladium-Based Nanocatalyst. *Synthesis* **2021**, *53* (21), 4048-4058.
218. Shi, L.; Tian, G.; Ye, H.; Qi, S.; Wu, D., Volatile static random access memory behavior of an aromatic polyimide bearing carbazole-tethered triphenylamine moieties. *Polymer* **2014**, *55* (5), 1150-1159.
219. Liu, Y.; Chao, D.; Yao, H., New triphenylamine-based poly(amine-imide)s with carbazole-substituents for electrochromic applications. *Org. Electron.* **2014**, *15* (7), 1422-1431.
220. Nazarpak-Kandlousy, N.; Nelen, M. I.; Goral, V.; Eliseev, A. V., Synthesis and mass spectrometry studies of branched oxime ether libraries. Mapping the substitution motif via linker stability and fragmentation pattern. *J. Org. Chem.* **2002**, *67* (1), 59-65.
221. Ye, Q.; Li, M.; Zhou, Y.; Pang, T.; Xu, L.; Cao, J.; Han, L.; Li, Y.; Wang, W.; Gao, J.; Li, J., Synthesis and Biological Evaluation of 3-Benzisoxazolyl-4-indolylmaleimides as Potent, Selective Inhibitors of Glycogen Synthase Kinase-3 β . *Molecules* **2013**, *18* (5), 5498-5516.
222. Ye, Q.; Li, M.; Zhou, Y.; Pang, T.; Xu, L.; Cao, J.; Han, L.; Li, Y.; Wang, W.; Gao, J., Synthesis and biological evaluation of 3-benzisoxazolyl-4-indolylmaleimides as potent, selective inhibitors of glycogen synthase kinase-3 β . *Molecules* **2013**, *18* (5), 5498-5516.
223. Keshipour, S.; Shaabani, A., Selective aerobic hydrolysis of nitriles to amides using cobalt(II)/zinc. *Research on Chemical Intermediates* **2015**, *41* (8), 5071-5078.
224. An, Y.-L.; Yang, Z.-H.; Zhang, H.-H.; Zhao, S.-Y., Palladium-Catalyzed Tandem Regioselective Oxidative Coupling from Indoles and Maleimides: One-Pot Synthesis of Indolopyrrolocarbazoles and Related Indolylmaleimides. *Organic Letters* **2016**, *18* (2), 152-155.
225. Davis, P. D.; Hill, C. H.; Lawton, G.; Nixon, J. S.; Wilkinson, S. E.; Hurst, S. A.; Keech, E.; Turner, S. E., Inhibitors of protein kinase C. 1. 2, 3-Bisarylmaleimides. *Journal of medicinal chemistry* **1992**, *35* (1), 177-184.
226. Davis, P. D.; Hill, C. H.; Lawton, G.; Nixon, J. S.; Wilkinson, S. E.; Hurst, S. A.; Keech, E.; Turner, S. E., Inhibitors of protein kinase C. 1. 2,3-bisarylmaleimides. *Journal of Medicinal Chemistry* **1992**, *35* (1), 177-184.
227. Rajeshwaran, G. G.; Mohanakrishnan, A. K., Synthetic Studies on Indolocarbazoles: Total Synthesis of Staurosporine Aglycon. *Organic Letters* **2011**, *13* (6), 1418-1421.
228. YASUZAWA, T.; IIDA, T.; YOSHIDA, M.; HIRAYAMA, N.; TAKAHASHI, M.; SHIRAHATA, K.; SANO, H., The structures of the novel protein kinase C inhibitors K-252a, b, c and d. *The Journal of Antibiotics* **1986**, *39* (8), 1072-1078.